AD-A041 877 AIR WEATHER SERVICE SCOTT AFB ILL F/G 17/9
ESTIMATING METEOROLOGICAL EFFECTS ON RADAR PROPAGATION. VOLUME --ETC(U)
DEC 76 W B MORELAND
UNCLASSIFIED AWS-TR-183-VOL-1 NL

1 OF 3
ADA041 877

TECHNICAL REPORT 183
VOLUME I

(REPRINTED DECEMBER 1976 WITH
CHANGE 1, JUNE 1965 INCORPORATED)

1

ESTIMATING METEOROLOGICAL EFFECTS ON RADAR PROPAGATION

VOLUME I
TEXT

By
W. B. Moreland

Published By
AIR WEATHER SERVICE (MATS)
UNITED STATES AIR FORCE
JANUARY 1965

CHANGE

Technical Report 183
Vol. I

June 1965

ESTIMATING METEOROLOGICAL EFFECTS ON RADAR PROPAGATION
VOLUME I: TEXT

Technical Report 183, Volume I, January 1965, is changed as follows:

1. Make the following changes by pen and ink:

Page	Line	Action to be Taken
vi	11	Figure 48 legend, change "B-Deficit" to read "N-Deficit."
4	8	Delete "P_t."
14	29	Change "reflactor" to read "reflector."
16	34	Change "ϵ" to read "ϵ_a."
83	30	Change "10" to read "12."
104		Second equation from top of page, change "h_R" in the numerator to read "h_r."
105		Second equation, Example 3, change "0.044" to read "-0.044."
108	1	Figure 48 legend, change "B-Deficit" to read "N-Deficit."
126	2	Delete the words "superrefractive or."
126	3	Delete the words "subrefractive or."
127	1	Change "Tropical" to read "Typical."
177	31	Change "-24B/1000 feet" to read "-12B/1000 feet."
177	33	Change "-24B/1000 feet" to read "-12B/1000 feet."
181	8	Change "The" to read "That."
188	4	Change "average weather" to read "average weather conditions."

2. After necessary action, file this change in front of page 1, PREFACE.

WILLIAM B. MORELAND
Consultant, AWS Aerospace Sciences
Scott AFB, Illinois 62226
3 June 1965

DISTRIBUTION:

HQ AWS	46
Wings and Groups	5
except 8 Wea Gp	17
Squadrons	2
except 1210th	10
Forecasting Detachments	1
Special	

UNCLASSIFIED

SECURITY CLASSIFICATION OF THIS PAGE *(When Data Entered)*

REPORT DOCUMENTATION PAGE		READ INSTRUCTIONS BEFORE COMPLETING FORM
1. REPORT NUMBER Technical Report 183, Vol. I.	2. GOVT ACCESSION NO.	3. RECIPIENT'S CATALOG NUMBER
4. TITLE *(and Subtitle)* Estimating Meteorological Effects on Radar Propagation Volume I: Text		5. TYPE OF REPORT & PERIOD COVERED 6. PERFORMING ORG. REPORT NUMBER
7. AUTHOR(s) W. B. Moreland		8. CONTRACT OR GRANT NUMBER(s)
9. PERFORMING ORGANIZATION NAME AND ADDRESS Hq, Air Weather Service (MAC) Scott Air Force Base, Illinois 62225		10. PROGRAM ELEMENT, PROJECT, TASK AREA & WORK UNIT NUMBERS
11. CONTROLLING OFFICE NAME AND ADDRESS Hq, Air Weather Service (MAC) Scott Air Force Base, Illinois 62225		12. REPORT DATE January 1965 13. NUMBER OF PAGES 212
14. MONITORING AGENCY NAME & ADDRESS*(if different from Controlling Office)*		15. SECURITY CLASS. *(of this report)* Unclassified 15a. DECLASSIFICATION/DOWNGRADING SCHEDULE

16. DISTRIBUTION STATEMENT *(of this Report)*

Approved for public release; distribution unlimited.

17. DISTRIBUTION STATEMENT *(of the abstract entered in Block 20, if different from Report)*

18. SUPPLEMENTARY NOTES

Reprinted December 1976 with Change 1, June 1965 incorporated.

This reprint supercedes AD-459466.

19. KEY WORDS *(Continue on reverse side if necessary and identify by block number)*

Absorption, atmospheric models, atmospheric refraction, climate, data, ducts, electromagnetic radiation, interference, meteorological phenomena, meteorological radar, propagation, radio transmission, refraction, refractive index, refractive index climatology, tables (data), weather forecasting.

20. ABSTRACT *(Continue on reverse side if necessary and identify by block number)*

The report discusses in detail the meteorological effects on radar propagation. Topics covered include: the theory of atmospheric refraction, the atmosphere, radio refractive index, models and actual behavior of the refractive index in the atmosphere, and related subjects. A discussion is included which covers the behavior of the refractive index in various air masses as well as under differing meteorological conditions, e.g., thunderstorms, fog, precipitation, and others. There is also a discussion (over)

DD FORM 1 JAN 73 1473 EDITION OF 1 NOV 65 IS OBSOLETE

UNCLASSIFIED

20. ABSTRACT (Continued)

on forecasting the refractive index, ducting, and related phenomena. See also Volume II (ADA-) for appendices.

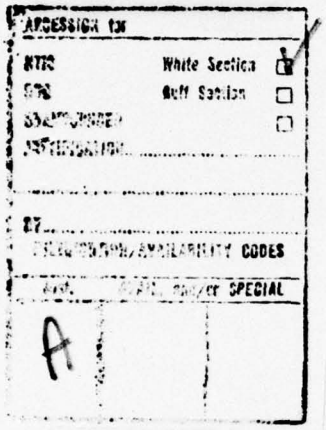

REVIEW AND APPROVAL STATEMENT

This report is approved for public release. There is no objection to unlimited distribution of this report to the public at large, or by DDC to the National Technical Information Service (NTIS).

This technical report has been reviewed and is approved for publication.

Gary D. Atkinson

GARY D. ATKINSON, Colonel, USAF
Director, Aerospace Sciences
DCS/Aerospace Sciences
Reviewing Officer

FOR THE COMMANDER

Walter S. Burgmann

WALTER S. BURGMANN
Scientific and Technical
Information Officer (STINFO)

PREFACE

This report is intended to serve as a comprehensive reference in radio-radar meteorology for Air Weather Service personnel. It does not attempt to establish set procedures for a problem, but more often than not, suggests several solutions without prescribing the "best one." The objective has been to give the AWS meteorologist sufficient background information on the subject so that he can find the best solution for both routine and new problems as they arise in the field.

The material presented herein is for the most part not new, but consists of updating and expanding on material obtained from earlier publications. The basic references from which material was taken were:

a. NAVWEPS 50-1P-550, "Meteorological Aspects of Radio-Radar Propagation," US Navy.

b. Technical Papers 1, 2, and 3, 3d Weather Group (now 4th Weather Wing) Air Weather Service, prepared by Major L. W. Cowan, and material updating thereto furnished by Captain Eugene T. Gray, 4th Weather Wing, and by Lt. Colonel A. Carpenter, Staff Meteorologist to AFCRL and ESD.

c. Technical reports prepared by Dr. B. R. Bean and associates at the Boulder Laboratories of the National Bureau of Standards.

d. US Navy Electronics Laboratory Paper No. 243, "Refractive Properties of Air Masses," by V. G. Plank.

Other publications employed are included in the list of references. A bibliography is also included for those who wish to study the subject in greater depth.

This report is being issued in two volumes. Volume I contains all the text with explanation of principles and procedures. Volume II contains three Appendices which consist of tables and charts that are to be used as tools in the routine of operational analysis and forecasting. The forecaster will wish to have Volume II conveniently available for daily use. Additional separate copies of Volume II may be requisitioned, if needed, for operational convenience.

Technical Report 183
Vol. I

January 1965

WILLIAM B. MORELAND
Consultant, AWS Aerospace Sciences
Scott AFB, Illinois
19 January 1965

DISTRIBUTION:

Hq AWS	46
Wings and Groups	5
except 8 Wea Gp.	17
Squadrons.	2
except 1210th.	10
Forecasting Detachments.	1
Special	

TABLE OF CONTENTS

LIST OF ILLUSTRATIONS

LIST OF TABLES

LIST OF SYMBOLS

A, B, K_p, M = Modified refractive indices.

a = Earth's radius.

a_e = Effective earth's radius.

C_1, C_2 = Parameters employed in computing location of radar holes when radar is above elevated N-layer.

c = Propagation speed of electromagnetic energy in a vacuum.

c_d = Exponential coefficient employed in standard refractivity profile.

c_e = Exponential coefficient employed in the CRPL exponential reference atmosphere.

D_1, D_2 = Parameters employed in computing location of radar holes when radar is below elevated N-layer.

d = Expression for distance in various equations. Refer to appropriate figure for definition.

E_A, E_B = Component waves of electromagnetic field strength E_R.

E_R = Electromagnetic field strength.

e = Vapor pressure.

e_s = Saturation vapor pressure.

G = Antenna gain.

H = Height of HIRAN aircraft above earth's surface.

H' = Height of HIRAN aircraft above sea level.

H_R = Height of transmitter above reflection plane.

H_T = Height of target above reflection plane.

h = Arbitrary height above earth's surface.

h' = Height of HIRAN ray path above sea level.

h_B = Height of bottom of elevated N-layer.

h_T = Height of top of elevated N-layer.

h_a = Apparent height of target above sea level.

h_o = Height of HIRAN ray path above earth's surface.

h_r = Height of transmitter above sea level.

h_s = Height of earth's surface above sea level.

h_t = Height of target above sea level.

K = Refractive correction factor (K-function) for AN/FPS-26 radar-height finder.

k = Effective earth's radius factor.

M_o = Map distance.

M_1 = Geodetic distance.

N = Refractivity.

N_B = Refractivity at base of elevated N-layer.

N_D = Dry term in the refractivity equation.

N_h = Refractivity at height h.

N_r = Refractivity at height of transmitter.

N_s = Refractivity at earth's surface.

N_s^* = Value of N_s specified by the CRPL exponential reference atmosphere when the N-difference between the surface and 100 meters is equivalent to δN.

N_T = Refractivity at top of elevated layer.

N_W = Wet term in the refractivity equation.

δN = Approximation for $\delta N'$.

$\delta N'$ = Initial gradient of N in ground-based layer 100 meters thick.

ΔN_L = Refractivity difference through elevated N-layer of thickness $\Delta h = h_T - h_B$.

n = Index of refraction of a medium.

n_s = Index of refraction of earth's surface.

Δn_L = Refractive-index difference through elevated n-layer of thickness Δh.

P = Atmospheric pressure.

P_r = Power received at receiver antenna.

P_t = Power emitted by isotropic radiating source.

R = Geometric range.

R' = Range to near edge of radar hole.

R'' = Range to far edge of radar hole.

R_H = Uncorrected range from HIRAN aircraft to ground station.

R_L = Optical or radio range.

R_o = True slant range.

R_1 = Uncorrected range from ground station to point on HIRAN ray path.

RH = Relative humidity.

ΔR = Range error.

r = Radial coordinate in cylindrical or spherical coordinate system.

r' = Radius of curvature of the ray path.

r_o = Value of r at the transmitter.

T = Absolute temperature.

t = Time.

v = Propagation speed of electromagnetic energy in the medium in question.

$\bar{v}$ = Mean speed of electromagnetic energy over HIRAN ray path.

v_h = Design speed of electromagnetic energy for HIRAN equipment.

W = Width of radar hole.

W_t = Width of radar hole at a height h_t.

w = Mixing ratio.

α_o = Ray inclination angle at transmitter, i.e., elevation angle indicated by radar.

β_i, β_r, β_f = Angle of incidence, angle of reflection, and angle of refraction.

γ = Change of refraction index with height.

δ = Path difference length of direct and reflected waves.

ϵ_a = Radar elevation angle error.

ϵ_h = Height error.

η = Constant employed in derivation of equations for CRPL exponential reference atmosphere.

θ = Inclination angle of ray at height h.

κ = Constant in Snell's Law.

λ = Wavelength.

ν = Central angle formed by radii of curvature of ray path.

ξ = True elevation angle.

ρ = Curvature of ray path.

τ = Total bending of ray.

τ_E = Total bending of ray determined from the CRPL exponential reference atmosphere.

$\delta\tau_E$ = Bending correction factor for initial N-gradient $\delta N'$.

ϕ = Central angle subtended by ray path from the earth's center.

ψ = Any rectangular component of electric or magnetic field strength in scaler wave equation.

ω = Magnitude of propagation vector in scaler wave equation.

Chapter 1

FACTORS IN RADIO-RADAR WAVE PROPAGATION

1.1. Introduction.

That portion of the electromagnetic spectrum utilized for communication extends from millimeter wavelengths to those thousands of meters long. This broad zone covers all the frequencies of radio and radar transmission (see Figure 1). Because the effect of meteorological variables (troposphere and stratosphere) is most pronounced on the shorter wavelengths, our primary interest in this report will be focused on the short-wave end of the radio-radar spectrum from about 1 centimeter to 10 meters. At longer wavelengths, the ionosphere becomes the controlling influence, rather than the comparatively shallow layer encompassing the troposphere and stratosphere. At wavelengths shorter than 1 centimeter, on the other hand, the atmosphere becomes relatively opaque for at least two decades of wavelength, and long-distance propagation is impractical.

When Marconi demonstrated in 1901 that radio signals could be transmitted across the Atlantic Ocean, investigations were soon initiated to account for the presence of signals beyond the horizon. Four principal mechanisms were proposed; diffraction, atmospheric refraction, atmospheric scattering, and reflection from an elevated layer of ionized gases. The reflecting-layer hypothesis, proposed by Kennelly [24] and Heaviside [21] in 1902 and proven by Watson [36] in 1919, is generally accepted as the primary mechanism which permits extended range transmission at wavelengths greater than about 10 meters. Although communication at these longer wavelengths is subject to various anomalies (fading, holes, etc.) which may become serious problems in practice, the principles of ionospheric transmission lie outside the scope of this report.

In the 1930's new developments in electronic oscillators made shorter wavelengths useable for practical communication. It was soon observed that signals shorter than about 10 meters were often not received at ranges greatly exceeding the horizon distance. The shorter the wavelength the more transparent the Kennelly-Heaviside layer becomes to incident radiation, and the ionospheric reflection mechanism becomes relatively unimportant in explaining transmission beyond the horizon. Once again the attention of researchers was focused on the phenomena of diffraction, refraction, and scattering as the mechanisms which might explain extended-range, short-wave (<10 m) communication.

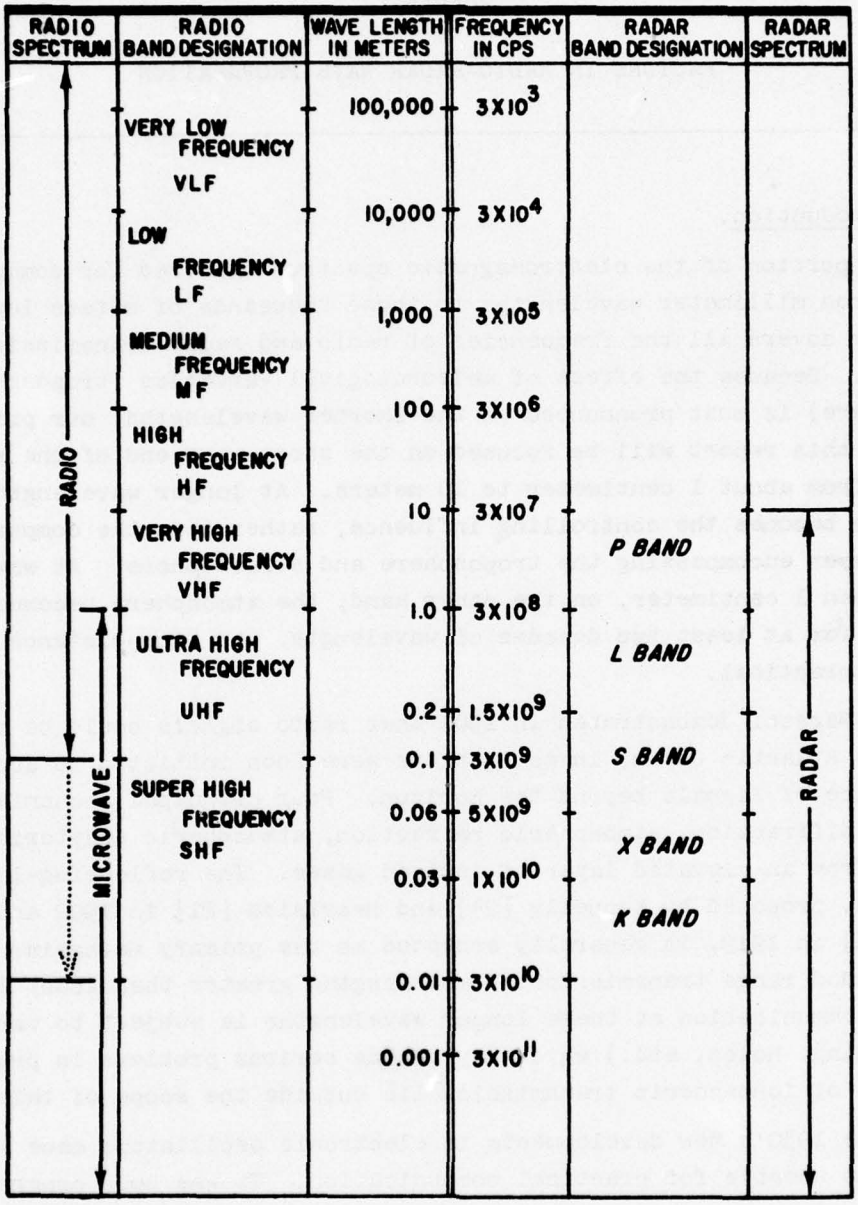

Figure 1. The Radio-Radar Spectrum.

With the development of radar in the 1940's (on even shorter wavelengths), it was found that the shorter the wavelength in use the more frequent were

occurrences of propagation well beyond the radio horizon. Surface objects were often observed at distances many times greater than the visual range, and these occurrences were found to be associated with unusual distributions of temperature and relative humidity in the layers near the earth's surface. This phenomenon is known as ducting or trapping. It is, in effect, an extreme case of superrefraction, or atmospheric refraction greater than normal.

The phenomenon of superrefraction was observed even prior to 1940 for radio propagation in the range of 1.6 to 5 meters; comprehensive studies of superrefraction have been principally stimulated, however, by the development of radar during and after World War II. The 7-meter and 1.5-meter radar sets established at coastal sites along the Mediterranean reported superrefraction effects much more intense than those reported on the same wavelengths around the British Isles. The entire coast of Sicily, for example, could frequently be seen with 1.5-meter radars on Malta, and from time to time echoes from Greece and Sardinia at ranges on the order of 650 kilometers were obtained. Ships were sometimes plotted to a range of 300 kilometers in locations where the geometrical horizon was less than 30 kilometers away. Perhaps the most distant targets ever observed were seen on a 1.5-meter radar at Bombay, India [18], which received echoes from points in Arabia at a distance of 2700 kilometers. Although meteorological effects usually act to extend surface radar coverage, it should be mentioned here that subrefraction also does occur. On several occasions, radar equipment on Fisher's Island, New York [25], was unable for many hours to pick up Block Island despite the fact that it is only 35 kilometers away and visible to the naked eye.

In the years following World War II with the continuously increasing application of airborne radar, an even more disturbing phenomenon has been frequently observed, the radar hole. This effect, produced by the presence of superrefractive layers aloft, may at times drastically reduce the effectiveness of airborne search radar.

More recently, with the advent of high precision, long-range radar techniques, the need for rectification of range- and elevation-angle errors resulting from refraction has become more acute. Today the primary limiting factor to the accuracy attainable by a position-fixing system is not the engineering or operational aspect of the instruments, but the residual error resulting from improperly accounting for the effects of the atmosphere on the electromagnetic signal utilized by the tracking device.

1.2. Propagation Factors in Free Space.

It is convenient to begin our discussion of electromagnetic propagation

characteristics with a consideration of the behavior of electromagnetic waves in free space; i.e., in a vacuum and without the presence of discrete bodies.

1.2.1. Free-Space Fields. A fundamental factor governing the behavior of electromagnetic waves is the inverse distance spreading of energy. If an isotropic source emits a given amount of energy per second, P_t, when one is at distance r from the transmitter this energy is spread out over the surface of a sphere of radius r and area $4\pi r^2$ (see Figure 2). Thus, the power received P_r (watts per unit area) at distance r from a point source is

$$P_r = \frac{P_t}{4\pi r^2} \tag{1}$$

The power decreases as the square of the distance from the source (or transmitter), and the electromagnetic field strength, which is proportional to the square root of power, decreases as the first power of the distance. This decrease is known as the free-space attenuation of the field, since it occurs even in a vacuum and without the earth present. It is a direct consequence of the fundamental law of the conservation of energy, and applies both in free space and in the terrestrial environment.

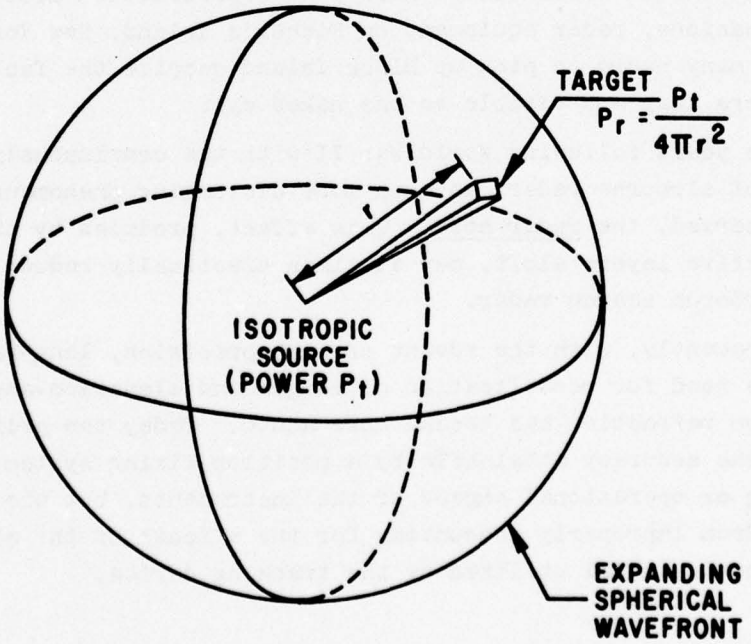

Figure 2. Free-Space Attenuation.

1.2.2. Interference. Whenever two (or more) wave trains traveling over different paths impinge (intersect) at a point in space, the phenomenon known as interference occurs. If the two waves arrive at the point in question in phase, they reinforce one another and produce a resultant field strength greater than either of the two component waves taken alone. If the two waves arrive at the point in question out of phase, they partially cancel one another and produce a weaker resultant field strength. This phenomenon is fundamental to all wave motion and occurs both in free space and in the terrestrial environment. Figure 3 illustrates the phenomenon of interference for two simple sine waves of the same frequency (or wavelength). The figure shows the time variation of the electromagnetic field strength, E_R, at a point in space, which results from the interference of two waves of equal frequency and with field strengths E_A and E_B. The component waves E_A and E_B are shown in phase, 90° out of phase, and 180° out of phase.

1.3. Propagation Factors in the Troposphere.

In order to find an explanation for the anomalies described in the foregoing paragraphs we shall consider in some detail those phenomena which control propagation in the troposphere; (a) the absorption of radiant energy, (b) the interference of waves, resulting in regions where two waves enhance and in adjacent regions where they cancel each other, (c) the diffraction of waves around the earth and other objects, and (d) the variations in propagation velocity caused by changes in pressure, temperature, and humidity; which give rise to refractive, reflective, and scattering effects.

1.3.1. Absorption. Whenever electromagnetic radiation propagates through a real medium (be it solid, liquid, or gaseous), a fraction of the incident energy is absorbed in passing through each increment of the medium. The energy absorbed is imparted to the atomic or molecular structure of the medium and, in most cases, is eventually given up as heat. The effect may be thought of as a kind of frictional loss.

Any particular substance does not absorb radiation of different wavelengths equally, nor do different substances absorb radiation of one particular wavelength equally—as anyone familiar with the spectrograph will know. The particular absorption characteristics of the medium (e.g., air), therefore, depend upon its composition, upon the atomic and molecular structure of each constituent, and upon the physical characteristics of the incident radiation.

Fortunately, in practice the absorption mechanism does not often produce serious performance anomalies in the operation of radio or radar equipment.

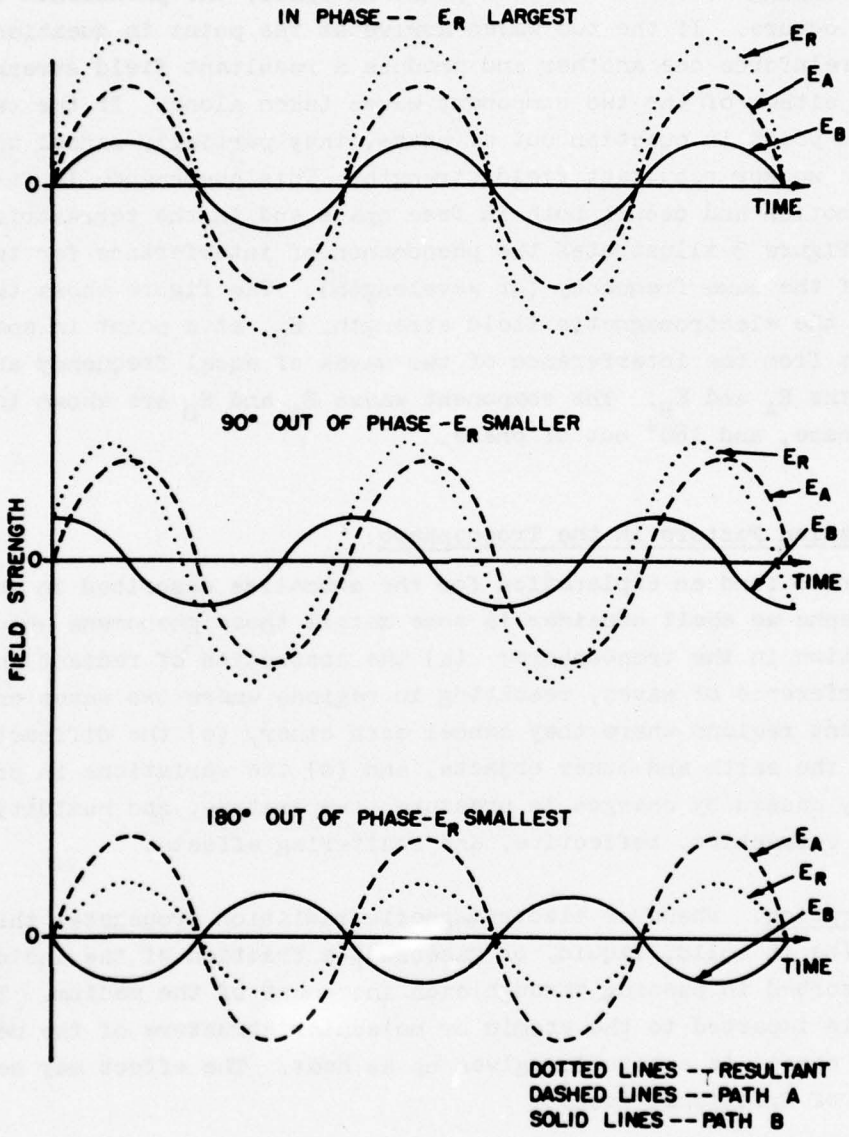

Figure 3. The Interference of Two Wave Trains.

Absorption may, however, become an important design consideration in selecting the wavelength to be used in a radar system; e.g., for air-search radar one would avoid selecting a wavelength close to one of the water-vapor absorption bands, since water vapor is present in the natural atmosphere.

1.3.2. Interference. In the radio-radar spectrum interference produces very pronounced fluctuations in signal strength (see Figure 3). These are not only produced by electromagnetic wave trains from two or more sources (transmitters) arriving at a particular point in space (receiver), but also by wave trains from a single source arriving at a particular point, having traveled over different transmission paths. For example, two different ray paths from source to receiver might be the direct, line-of-sight ray and a reflected ray from the transmitting antenna to the earth's surface and thence to the receiving antenna (refer to Figure 5).

Interference between signals of different wavelengths from two or more sources is eliminated by the "tuning section" of the receiver which is nothing more than a sharply tuned bypass filter. The filter rejects all signals except those having frequencies within a very narrow band centered on the frequency to which the receiver is "tuned." Any electromagnetic wave (signal) having a frequency within the bypass band will be "passed" on through the amplification and detection stages of the receiver; waves having other frequencies are rejected.

Signals of the same (or nearly the same) frequency, whether from several sources or from a single source, produce interference which cannot be eliminated by a filter (tuner). The case of two or more sources is of practical importance in connection with electronic countermeasures (ECM) but will not be discussed further here. The case of interference produced by surface reflections from a single source will be developed more fully in the following paragraphs.

A spherical earth enveloped by a homogeneous atmosphere is shown in Figure 4. In this figure, as in all others depicting curved-earth geometry, the height scale has been greatly exaggerated compared to the horizontal distance scale. Assume that a radio transmitter is located at R at height h_r above the earth. Since the atmosphere is homogeneous, energy will leave the antenna in straight rays. If one now draws a straight ray from R tangent to the earth's surface, this line defines the horizon distance d_h and the horizon height h at point P which is at a distance d beyond the tangent point. Referring to Figure 4,

$$a^2 + d_h^2 = (a + h_r)^2 \tag{2}$$

expanding, we have

$$d_h^2 = 2ah_r + h_r^2 \tag{3}$$

Since h_r is much smaller than 2a, the second order term in the above equation may be neglected. Therefore,

(4) $d_h \cong \sqrt{2ah_r}$

and similarly

(5) $d \cong \sqrt{2ah}$

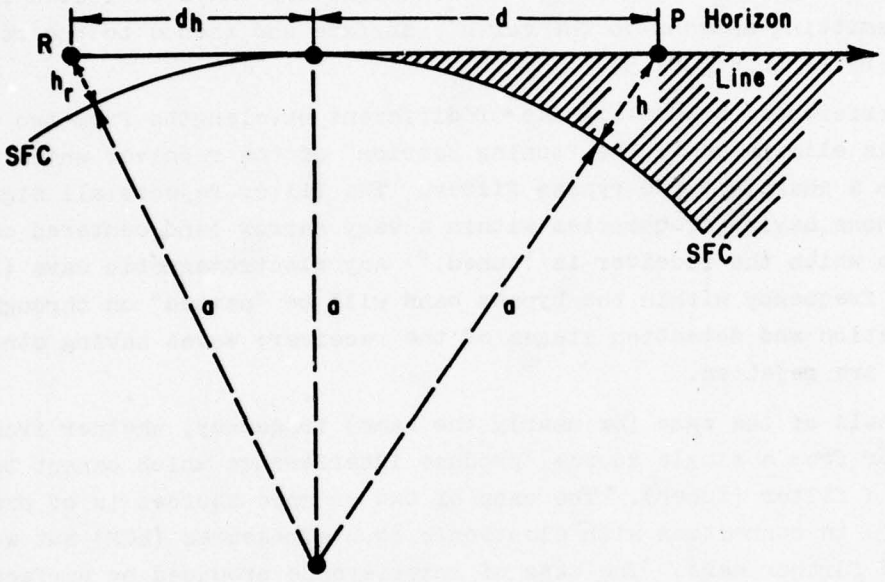

Figure 4. Ray Geometry for Spherical Earth—Homogeneous Atmosphere.

The horizon line beyond the tangent point divides radio space into two regions. The region above the line is always illuminated directly by the transmitter and is called the interference region; the region below the line is not directly illuminated and is generally called the diffraction region (shaded in Figure 4). The illuminated region is referred to as the interference region because the radio field strength at a given point above the horizon line is determined by the interference between two rays, as described in section 1.3.2. One is the direct ray from the transmitter to the point; the other is a ray reflected from the earth's surface to the point. Since the reflected ray path is somewhat longer, the reflected ray arrives at the point somewhat later than the direct ray. If it arrives half a wavelength behind (180° out of phase) the two waves will tend to cancel each other, and if they

are of equal strength the resultant field at the point will be zero. On the other hand, if the point is higher, so that the reflected wave arrives a full wavelength behind the direct wave, the two will be in phase, and the field strength will be intensified. This alternate cancellation and enhancement in the field strength as the path-length differences are increased, gives rise to a vertical interference pattern, consisting of a series of narrow fingers or lobes of strong field strength with weaker fields in between (see Figure 6).

In Figure 5, showing a spherical earth surrounded by a homogeneous atmosphere, the path difference, δ, between the direct and reflected waves may be shown to be

$$(6) \qquad \delta \cong \frac{2H_R H_T}{d}$$

where H_R and H_T are the heights of the transmitter at point R and of the target at point P above the reflecting plane and d is the direct path distance. The reflection plane is tangent to the earth at the point of reflection, such that the angle of incidence β_i, equals the angle of reflection β_r.

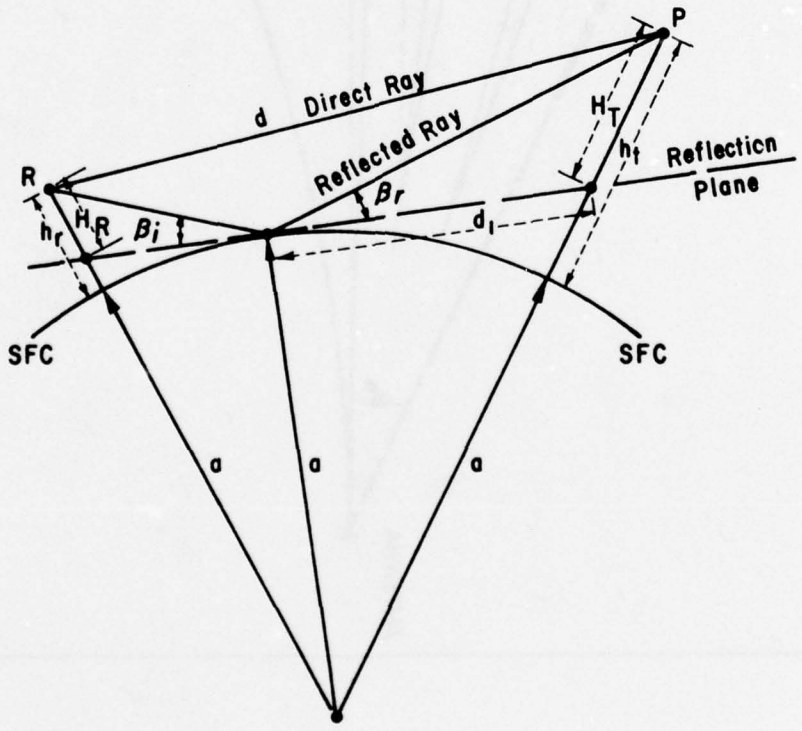

Figure 5. Path-Difference Geometry—Spherical Earth.

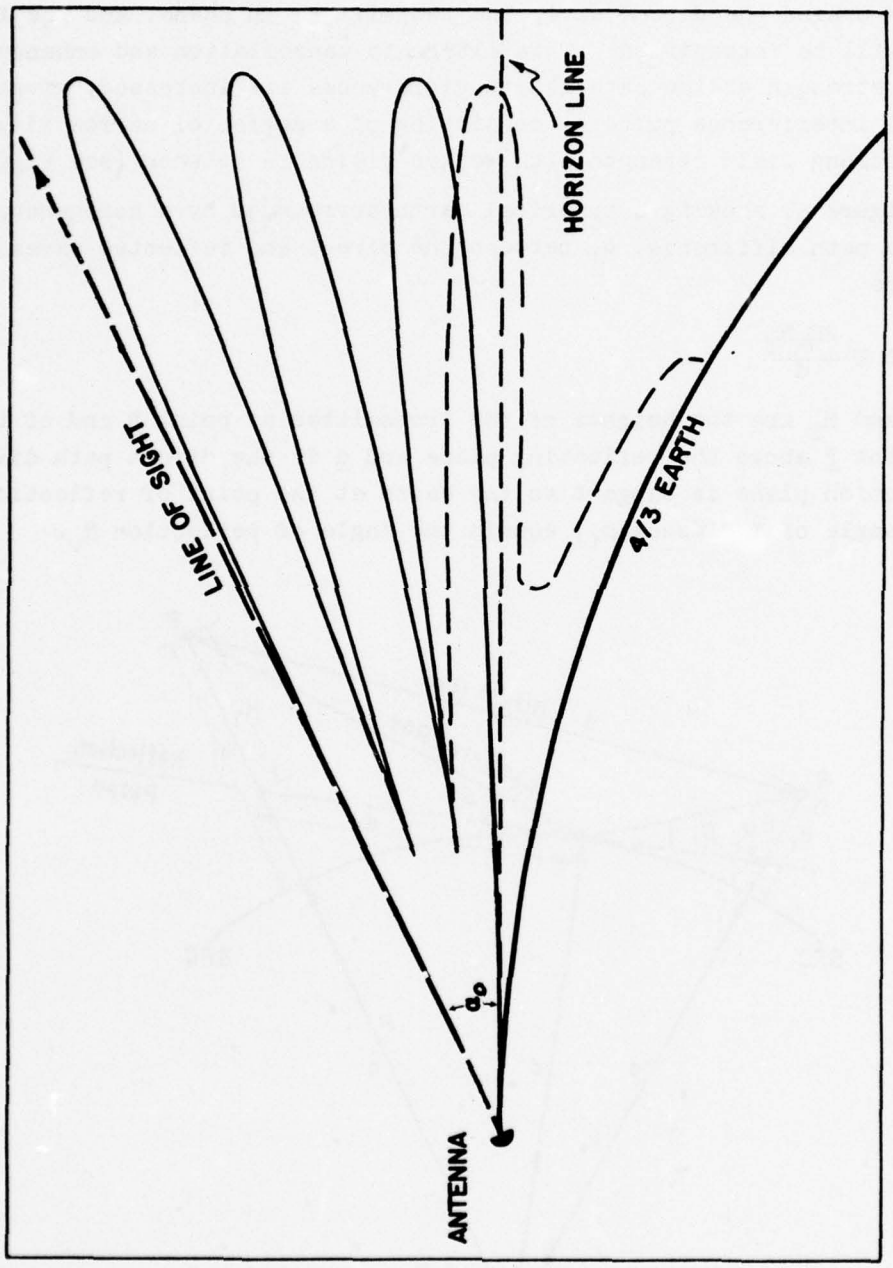

Figure 6. Vertical Coverage Pattern—Surface Radar.

On a spherical earth, H_R and H_T are not the actual heights above the surface. Referring to Figure 5, it may be shown that

$$(7) \qquad H_R \cong h_r - \frac{(d - d_1)^2}{2a}$$

and

$$(8) \qquad H_T \cong h_t - \left(\frac{d_1^2}{2a}\right)$$

where h_r and h_t are the heights of the transmitter and target above the earth's surface and d_1 is the distance from the reflection point to the projection of the target on the reflection plane. Since the angle of incidence is equal to the angle of reflection, we also have

$$(9) \qquad \frac{d_1}{d - d_1} = \frac{H_T}{H_R}$$

One can eliminate H_T, H_R, and d_1 from the above four expressions, and solve for δ in terms of h_r, h_t, and $\underline{d}$. The resulting expression, however, is too complicated to warrant further discussion in this report. Domb and Pryce [17] have developed a convenient means of plotting interference patterns, to which the reader is referred for practical assistance.

The picture just described is further complicated in that the reflected ray undergoes a sudden phase shift of one-half wavelength (180°) on reflection; minimum fields, therefore, occur when the path difference is an integral number of wavelengths (1, 2, 3, ... etc.), and maxima are centered at those points having 1/2, 1-1/2, 2-1/2 ... etc. wavelength path differences. Furthermore, the strength of the reflected wave is reduced by scattering if the reflecting surface is rough and by divergence if it is smooth, so that the direct and reflected waves are not of equal strength. These factors modify, but do not invalidate, the general characteristics of the interference pattern as described above.

In practice, interference patterns for a given antenna are computed for various angles of elevation of the antenna (tilt); these computed values are checked and corrected with observational data whenever possible. The weather officer should consult the radar controller or electronics officer for further information concerning the characteristics of a particular antenna array. The phenomenon of interference is not affected per se by changing meteorological conditions, except that, as we shall see, refractive effects may produce path length changes.

1.3.3. Diffraction. In a homogeneous atmosphere, the only way in which

energy can penetrate the region below the horizon line is by the process of diffraction (see Figure 4). This process results from the wave nature of the transmitted energy and is similar to simple diffraction over a knife edge. The mathematics of diffraction over a spherical obstacle is quite formidable and will not be attempted here. It turns out, however, that the depth of penetration of energy below the horizon line is proportional to the wavelength, and, at a constant height above the surface, it falls off exponentially with distance beyond the horizon point. Domb and Pryce [17] have developed relatively simple methods for computing diffraction fields, and the reader is referred to their paper for a discussion of practical computational techniques.

As was the case with interference, the mechanism of diffraction is not primarily weather-dependent, and as such its effect upon radio-radar performance is more properly a problem for the electronics engineer.

1.3.4. Reflection and Refraction. We now can complicate the simple case of Figures 4 and 5 by surrounding our spherical earth with a nonhomogeneous atmosphere (such as the earth's real atmosphere). Inhomogeneties produce changes in the speed of propagation of electromagnetic energy through different portions of the atmospheric envelope, giving rise to the phenomena of reflection, refraction, and scattering.

The index of refraction, n, of a medium is defined as

$$n = \frac{c}{v} \tag{10}$$

where c is the propagation velocity of electromagnetic energy in a vacuum, and v is the propagation velocity in the medium in question. The index of refraction of a medium is therefore a measure of the propagation speed (relative to the velocity of light) of an electromagnetic wave through the medium.

a. Reflection and Refraction at a Discontinuity. Whenever an electromagnetic wave strikes a surface of discontinuity in n (i.e., a surface across which there is an abrupt change in propagation speed) the incident wave, in general, is partially reflected and partially refracted (see Figure 7). The law of refraction at a discontinuity may be derived from a consideration of propagation speeds in the two media. In Figure 7 we assume electromagnetic energy strikes the boundary between two media with indices of refraction of n_1 and n_2, where n_1 is associated with the initial medium and n_2 is greater than n_1; i.e., the propagation speed is greater in the initial than in the final medium. In a certain length of time, t, the wave front travels from position 1-2 to position 4-3, and

$$d_{2-3} = v_1 t \tag{11}$$

(12) $d_{1-4} = v_2 t$

where d_{2-3} is the distance traveled and v_1 is the speed of propagation in medium 1, and d_{1-4} and v_2 are the corresponding distance and speed in medium 2.

Also, we have

(13) $$\sin \beta_i = \cos \angle 132 = \frac{d_{2-3}}{d_{1-3}}$$

and

(14) $$\sin \beta_f = \cos \angle 413 = \frac{d_{1-4}}{d_{1-3}}$$

Therefore,

(15) $$\frac{\sin \beta_i}{\sin \beta_f} = \frac{d_{2-3}}{d_{1-4}} = \frac{v_1 t}{v_2 t} = \frac{v_1}{v_2}$$

and, since $n = c/v$, we may write the law of refraction (Snell's Law)

(16) $$\frac{\sin \beta_i}{\sin \beta_f} = \frac{n_2}{n_1}$$

where β_i is the angle of incidence and β_f is the angle of refraction.

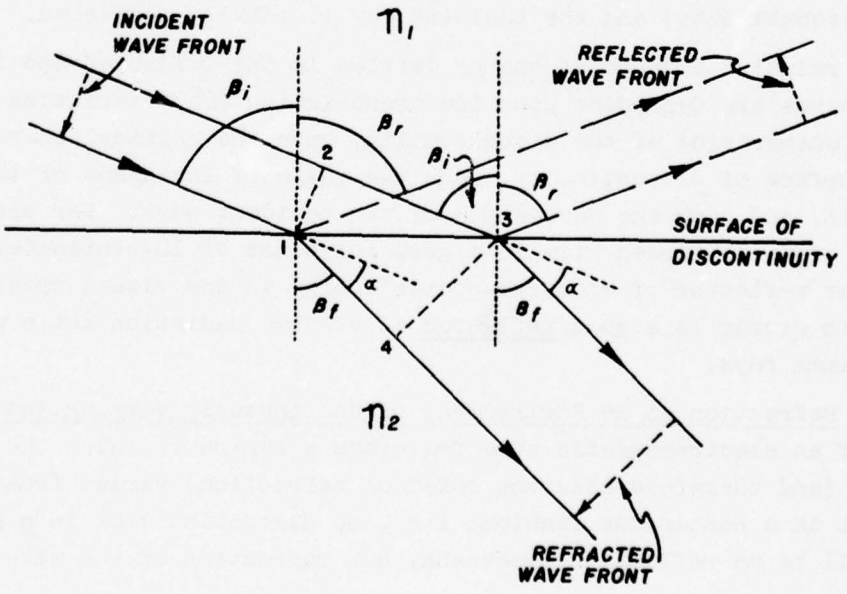

Figure 7. Refraction and Reflection at a Surface of Discontinuity.

It is well to note that in Figure 7 the direction of propagation may be reversed without invalidating the conclusions just reached so long as we interchange the designation of incident and refracted wave fronts and the angles of incidence and refraction. The incident and refracted rays lie in the same plane, and the incident rays are always bent toward the medium of higher index of refraction (i.e., lower propagation speed) in passing through a surface of discontinuity.

With the aid of Huyghens' principle one may derive the law of reflection which states that the incident and reflected rays lie in the same plane and the angle of incidence is equal to the angle of reflection; i.e., $\beta_i = B_r$ in Figure 7. It will be noted that the incident wave front is inverted by reflection (the incident wave is shifted in phase 180°), as has been mentioned previously; in refraction there is no corresponding phase shift.

Whenever energy is passing through a discontinuity between a medium of higher to a medium of lower index of refraction, the phenomenon of total reflection will occur when the angle of incidence exceeds a certain critical value given by

$$(17) \qquad \beta_i = \sin^{-1} \frac{n_1}{n_2}$$

where $n_2 > n_1$ (see Figure 7). At angles of incidence greater than this critical value, the refracted ray is suppressed (does not emerge above the surface of the discontinuity) and the incident ray is totally reflected.

The relative amounts of energy carried in the reflected and in the refracted waves are dependent upon the transmission characteristics of the two media on either side of the discontinuity, upon the physical characteristics of the surface of discontinuity, upon the angle of incidence of the initial wave train, and upon the wavelength of the incident wave. For example, a sheet of ordinary screen wire is a good reflector of 10-centimeter radar waves but a poor reflector of electromagnetic energy in the visual spectrum; whereas, a silvered mirror is a good reflector of visible radiation but a poor reflector of gamma rays.

b. Refraction in an Environment of Continuously Varying Index of Refraction. If an electromagnetic wave traverses a region in which the propagation velocity (and therefore also the index of refraction) varies from point to point but in a continuous fashion; i.e., no discontinuities in n present, there will be no reflection phenomena, but refraction of the wave will occur.

In Figure 8 the dashed vertical line at the left represents a wave front at time $t = 0$. The wave is traveling horizontally toward the right. Assume that the refractive index is n_o at the bottom of the wave front and is $n_o - \Delta n$

at the top. As the wave proceeds along, the top part will travel faster than the bottom part, because the refractive index at the top is less than at the bottom. After time Δt, the top end of the wave will have traveled

$$(18) \qquad d_o + \Delta d = v_{top}\Delta t = \frac{c\Delta t}{n_o - \Delta n}$$

where c is the propagation velocity in vacuum. The bottom end will have traveled

$$(19) \qquad d_o = v_{bottom}\Delta t = \frac{c\Delta t}{n_o}$$

and, thus

$$(20) \qquad \Delta d = c\Delta t\left(\frac{1}{n_o - \Delta n} - \frac{1}{n_o} \right) = \frac{d_o \Delta n}{n_o - \Delta n}$$

Since $(n_o - \Delta n)$ is very close to unity we may disregard it and write

$$(21) \qquad \Delta d \cong d_o \Delta n$$

Since the top of the wave has traveled Δd farther than the bottom, the wave front is now tipped downward by an angle $\tau = \Delta d/\Delta h$, where Δh is the distance increment between the top and bottom of the wave front. Substituting $\Delta d = d_o \Delta n$, one obtains the expression

$$(22) \qquad \tau = d_o \frac{\Delta n}{\Delta h}$$

for the angle through which the ray is bent.

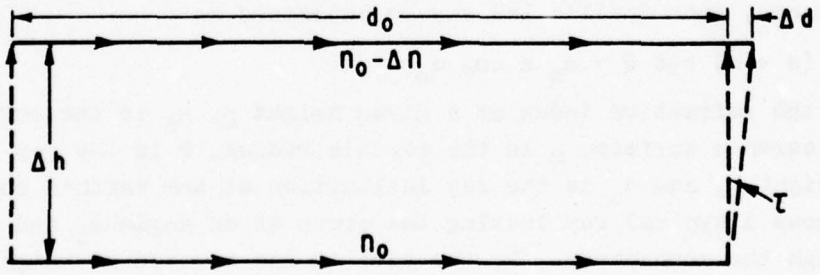

Figure 8. Refraction in an Environment of Continuously Varying Index of Refraction.

But τ/d_o is simply the curvature, ρ, of the ray and since the bending is proportional to distance, the ray path is an arc of a circle of radius

$r' = d_\alpha/\tau$, so long as the n-gradient, $\Delta n/\Delta n$, remains constant. Thus, one can say that,

$$(23) \qquad \rho = \frac{1}{r'} = \frac{\Delta n}{\Delta h}$$

This is a very important expression in radio-wave refraction: the curvature of a ray is equal to the gradient of the refractive index normal to the ray path. Stated another way, the angle through which a ray will be bent in passing through a refractive-index gradient is equal numerically to the gradient normal to the path, times the distance traveled.

In the natural atmosphere the index of refraction becomes smaller as one proceeds to higher and higher altitudes, but abrupt changes (discontinuities) in n are not infrequently observed. For this reason refractive effects in the earth's atmosphere are generally more important in the study of anomalous radio-radar performance than are reflective effects. As has already been implied, however, the surface of the earth acts as a good reflector of electromagnetic waves in the radio-radar spectrum.

c. Snell's Law. One is frequently interested in tracing the trajectory of a ray as it travels through a medium such as the atmosphere in which the refractive index changes with height. Theory indicates that the ray will follow a trajectory having the shortest optical path. This principle is expressed in a simple mathematical form known as Snell's Law. It was originally applied to ray tracing through lenses and prisms, but applies equally well in the radio-radar case. If one assumes that the refractive index in the atmosphere changes only with height above the spherical earth, and not with horizontal distance, then Snell's Law may be expressed as

$$(24) \qquad n\,(a + h)\cos\theta = n_s\, a \cos\alpha_o$$

where n is the refractive index at a given height h, n_s is the refractive index at the earth's surface, a is the earth's radius, θ is the ray inclination angle at height h, and α_o is the ray inclination at the earth's surface. Figure 9 shows a typical ray leaving the earth at an angle α_o and passing upwards through the atmosphere. By the time it has arrived at height h, it has been bent downward by a total angle τ, which can be calculated if one knows the way in which n changes with height. This figure will be referred to later when the method for computing total bending, τ, and the associated radar elevation angle error, ϵ_a, is developed.

1.3.5. Scattering. The presence of neighboring thermodynamically dissimilar parcels of air in the atmosphere is responsible for a propagation mechanism which has not been considered previously and which is known as scattering. It has been found experimentally that when one proceeds away from a transmitter

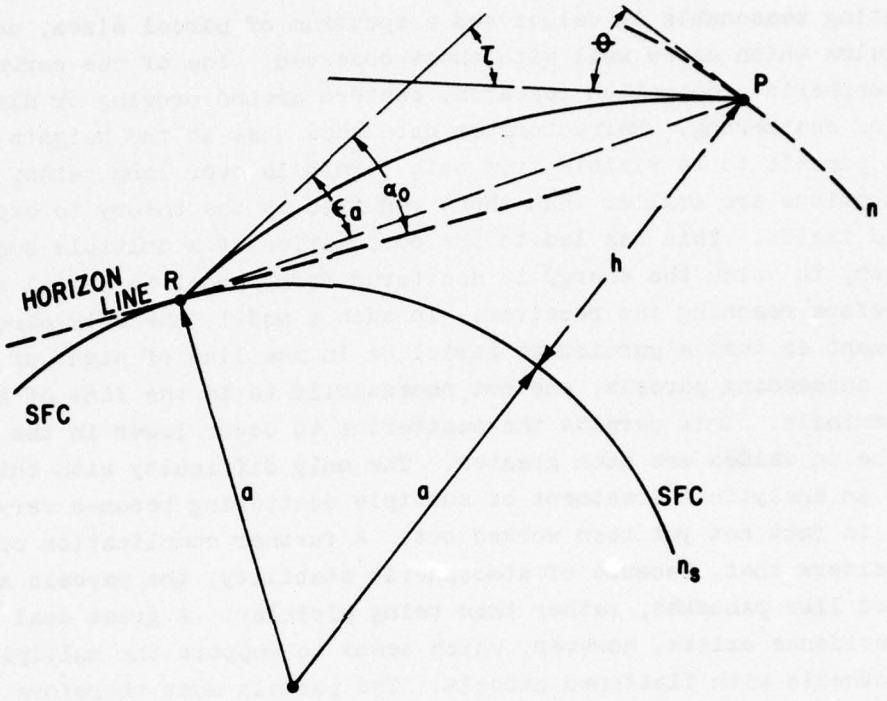

Figure 9. The Geometry of Ray Bending.

with a receiver near the surface, the fields beyond the horizon decrease exponentially at a rate which agrees with diffraction theory for quite some distance. As one proceeds further away from the transmitter, however, the attenuation rate suddenly decreases (the fields decrease with distance at a much slower rate). In other words, beyond a certain critical distance, the received fields are much stronger than can be accounted for by diffraction theory. The mechanism by which these fields are produced is called scattering. Each parcel above the horizon, which is illuminated by the transmitter, scatters a small part of the incident energy in directions other than along the straight-line path from the transmitter through the parcel. Most of the energy, of course, continues straight through. If a particular parcel is above the horizon for both the transmitter and the receiver, part of the scattered energy will be directed toward the receiver. The scattered field at any point may be regarded as the sum of the energies scattered by a multitude of such parcels and directed toward the point in question. Theories have been

developed for computing the fields to be expected by such a mechanism; by postulating reasonable Δn values and a spectrum of parcel sizes, one can compute fields which agree well with those observed. One of the current problems in tropospheric propagation research, centers around proving or disproving this theory of scattering. Refractometer data show that at the heights required for the parcels to be visible from both terminals over long paths, the actual n fluctuations are smaller than those required by the theory to explain the observed fields. This has led to the postulation of a multiple scattering mechanism, in which the energy is scattered from parcel to parcel several times before reaching the receiver. In such a model, the only parcel-height requirement is that a particular parcel be in the line of sight of the previous and the succeeding parcels, and not necessarily be in the line of sight of both terminals. This permits the scattering to occur lower in the atmosphere where the Δn values are much greater. The only difficulty with this proposal is that an analytical treatment of multiple scattering becomes very complex and has in fact not yet been worked out. A further complication occurs when one considers that, because of atmospheric stability, the parcels are probably flattened like pancakes, rather than being globular. A great deal of experimental evidence exists, however, which seems to support the multiple scattering hypothesis with flattened parcels. The parcels must therefore be related to small non-isotropic turbulence eddies.

In any case, scatter fields do exist; they are stronger at night than in mid-afternoon, and are stronger in summer than in winter. Even at their weakest, they are much stronger than diffraction fields over paths greater than a few hundred miles in length.

1.4. Summary.

In this chapter we have described briefly some of the operational anomalies actually observed in the performance of radio-radar equipment and have discussed the physical phenomena which are important in producing the anomalous performance observed. Of these phenomena, absorption, interference, and diffraction are not significantly affected by varying atmospheric parameters and do not, therefore, produce critical weather problems in the field.

On the other hand, refraction, reflection, and scattering are most commonly (except in the case of reflection) produced by inhomogeneities in the atmosphere which in turn are attributable to variations in meteorological parameters. Of these, by far the most important in explaining or predicting the anomalous performance of radio-radar equipment is refraction. It is for this reason that the remaining portion of this report is devoted principally to a detailed discussion of atmospheric refraction.

Chapter 2

THEORY OF ATMOSPHERIC REFRACTION

2.1. Ray Theory Concepts on Geometric Optics.

For a complete study of microwave[1] propagation, both physical and geometrical optics are necessary. Geometrical optics, in general, is the simpler of the two, as it predicts propagation of waves along "rays" according to simple geometrical laws without regard to wavelength or phase. Physical optics, on the other hand, result from a solution of Maxwell's wave equations and thus automatically introduce wavelength, phases, and penetration of waves into shadow regions in which geometrical optics give no information. Thus, to explain completely the effects such as diffraction and interference, it is necessary to employ physical optics. However, the general problem of following the propagation of electromagnetic waves is far too complicated to allow a complete analysis in this report. For more complete discussions of the subject, the reader is referred to general textbooks on optics and radio-propagation theory [11] [25]. The following discussion of atmospheric refraction will employ only principles of geometric optics. Fortunately, experimental results indicate that ray theory is adequate for most purposes at the frequencies encountered in the microwave region.

2.1.1. Foundations of Geometric Optics. The mathematical formulation of ray theory may be obtained by an approximate solution of the scalar-wave equation

$$\nabla^2\psi + \omega^2 n^2\psi = 0$$

where ψ denotes any rectangular component of the electric or magnetic field strength, $\omega = 2\pi/\lambda$ is the magnitude of the propagation vector [11], and λ is the wavelength. The following physical concepts which are the foundation of geometric optics are obtained from the solution:

a. Fermat's Principle of least path or least time which states that the energy in an electromagnetic wave travels along ray paths such that the time of travel between any two points (A_1, A_2) is minimum and the velocity of propagation at each point is inversely proportional to the refractive index at that point. That is, the line integral $\int_C n\, ds$, where ds is the differential

[1] The range of wavelengths below about 1 meter for the purpose of this report is defined as the microwave region.

distance along the path, C, is less for the actual ray path than for neighboring paths. This line integral is called the optical or effective radio-path length. A consequence of Fermat's Principle is that the ray paths must obey Snell's Law of refraction (see paragraph 1.3.4).

b. The ray paths are everywhere perpendicular to the surfaces of constant phase of the wavefronts.

c. The energy confined within a given bundle or pencil of rays is constant. Thus, if a small bundle of rays is considered, the energy density at any point along this bundle is inversely proportional to the cross-sectional area of the bundle at that point.

d. The relative phase at point A_2 to that at point A_1 on the same ray is given by $\omega \int_C n\, ds$, the integration being along the ray paths.

2.1.2. Limitations of Ray Methods. The mathematical development also indicates that two conditions must be placed on ray methods in order for these results to be valid. The first condition states that the fractional change in refractive index within one wavelength is small compared to unity, i.e., the refractive index does not change appreciably in a wavelength. The second condition states that the fractional change in spacing between adjacent rays within one wavelength be small compared to unity. A ray pattern, therefore, leads to questionable results in regions where rays either diverge or converge rapidly, and especially where neighboring rays cross to form foci or caustics[2]. Thus, ray theory fails in the diffraction region and in the neighborhood of caustics such as are present under atmospheric trapping conditions. Caustics are formed at heights where the rays are turned back toward the earth's surface (see Case #56, Part 6, Appendix B, Volume II).

2.2. Ray Bending.

The object of atmospheric radar-radio wave bending studies usually is to find a convenient method of correcting the electromagnetic field strength equation for this effect. This final step will not be taken in this report (not being a forecaster's function) but equations for elevation angle, height and range errors will be derived. The general procedure in the ray theory approach is to trace rays through the medium, requiring the rays to obey Snell's refractive law, and then deduce from the ray paths the direction of wavefront propagation. In many cases, the actual ray paths do not have to be

[2] In optics a caustic is a curve or surface to which the rays of light are tangent after reflection or refraction by another curve or surface.

determined, the results being obtainable by expressing the general ray path by a suitable (usually integral) equation and deriving the desired quantities by manipulation of this equation. This type of approach will be used in this chapter to derive relatively simple approximate expressions for the elevation angle, height and range errors.

2.2.1. Snell's Law for Spherical Surfaces. In order to apply Snell's Law of refraction to atmospheric ray tracing, it is usually assumed that the surfaces of constant index of refraction are spherically stratified about a spherical earth. This assumption greatly simplifies the mathematics of the problem and, as will be shown later, does not usually introduce a large error in the computations of elevation angle, height, and range.

As was shown in paragraph 1.3.4, the ordinary law of refraction known as Snell's Law may be expressed as

$$n_o \sin \beta_i = n_1 \sin \beta_f \tag{25}$$

where β_i and β_f are the angles which the ray makes with the perpendicular to the boundary (see Figure 10). Here it is more convenient to take the angle θ between the ray and the boundary surface. Snell's Law then reads

$$n_o \cos \theta_o = n_1 \cos \theta_1 \tag{26}$$

The refraction at a sharp boundary is shown in Figure 10a. If there are several boundaries, it is readily seen that Snell's Law generalizes (Figure 10b) to

$$n_o \cos \theta_o = n_1 \cos \theta_1 = n_2 \cos \theta_2 = \ldots \tag{27}$$

and for a continuously variable layer it becomes

$$n \cos \theta = n_o \cos \theta_o \tag{28}$$

where n and θ are continuous variables which are functions of the height and the index o designates an arbitrary reference level.

Snell's Law for a curved earth may be derived from Figure 10c. For successive boundaries it is found

$$n_o \sin \beta_o = n_1 \sin \beta_o'$$

$$n_1 \sin \beta_1 = n_2 \sin \beta_1' \text{ , etc.}$$

Multiply the first equation by r_o and the second by r_1, etc. (see Figure 10c). Then

$$n_o r_o \sin \beta_o = n_1 r_o \sin \beta_o'$$

$$n_1 r_1 \sin \beta_1 = n_2 r_1 \sin \beta_1' \text{ , etc.}$$

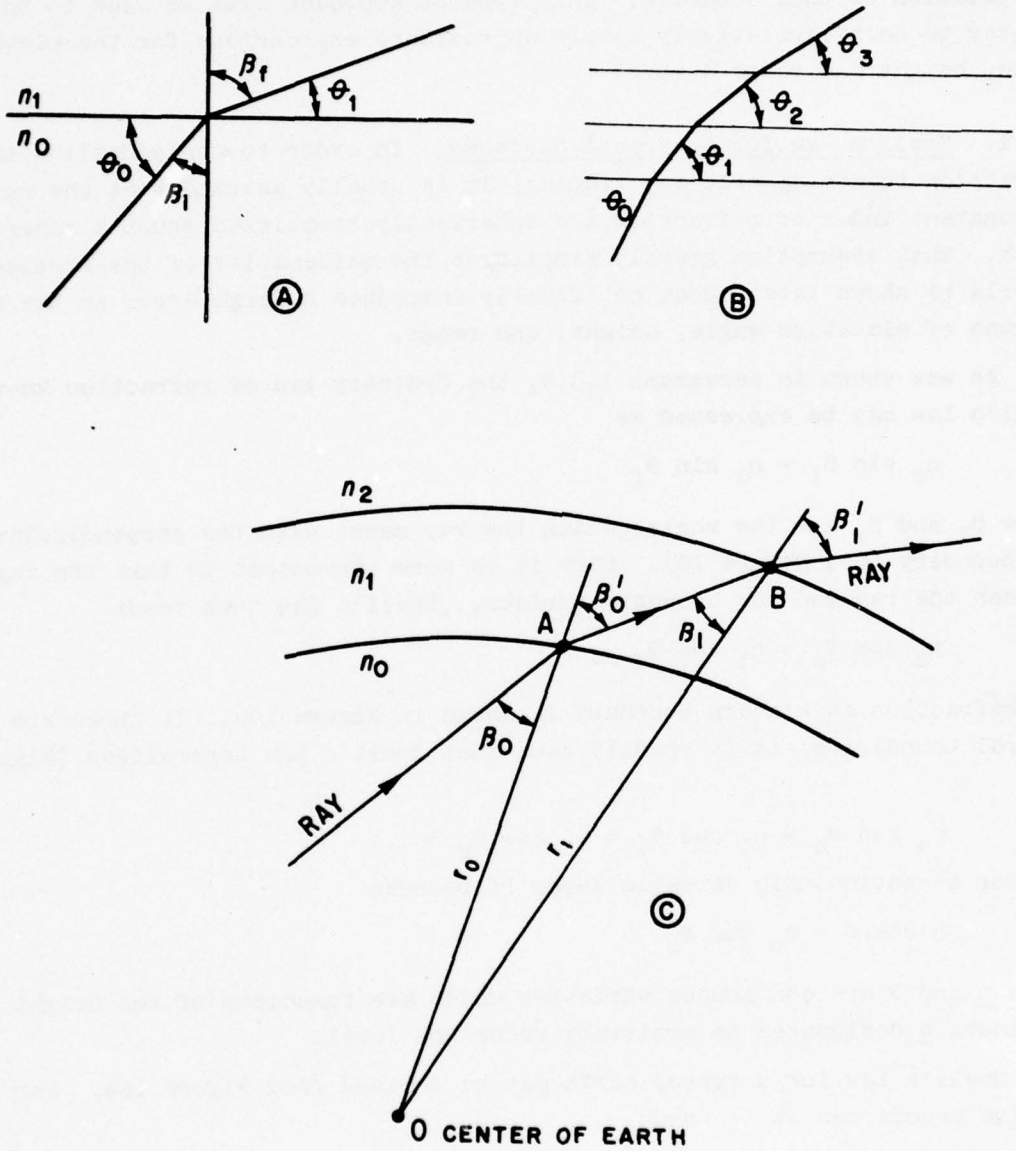

Figure 10. Snell's Law for Spherical Surfaces.

But from triangle OAB the law of sines gives

$$\frac{\sin \beta_o'}{r_1} = \frac{\sin \beta_1}{r_o} \text{ , etc.}$$

so that

$$n_o r_o \sin \beta_o = n_1 r_1 \sin \beta_1 = n_2 r_2 \sin \beta_2 = \ldots$$

Again introducing the angle θ with the horizontal and making the transition to a continuously variable refractive index gives

(29) $$nr \cos \theta = n_o r_o \cos \theta_o = \kappa$$

which is the generalization of Snell's Law for a curved earth. r_o may be chosen as any convenient height, say at the earth's surface or $r_o + h$ for the height of the transmitter, and n_o is the corresponding value of $\underline{n}$.

2.2.2. Development of Differential Ray Bending Equation. The derivation of the classic expression for the bending of a radio ray assumes the refractive index spherically stratified with respect to the earth. With this assumption, *Snell's Law, equation (29), may be used to calculate the local elevation* angle, θ, at any point along the ray and thus affords a complete description of the ray path. The geometry of the problem is illustrated in Figure 11.

Differentiating equation (29) with respect to height, $\underline{h}$, and dividing by nr, we obtain:

(30) $$\sin \theta \frac{d\theta}{dh} - \frac{1}{r} \cos \theta = \frac{1}{n} \cos \theta \frac{dn}{dh}$$

From the infinitesimal section of the ray path in Figure 12, we have:

$$ds^2 = (r d\phi)^2 + dr^2$$

$$r \frac{d\phi}{ds} = \cos \theta$$

and

$$\frac{dr}{ds} = \sin \theta = \frac{dh}{ds}$$

Substituting into equation (30) for cos θ and sin θ, we have:

(31) $$\frac{d\phi}{ds} - \frac{d\theta}{ds} = - \frac{1}{n} \cos \theta \frac{dn}{dh}$$

From Figure 12, we obtain:

$$(90° + \theta) + d\phi + 90° - d\tau - (\theta + d\theta) = 180°$$

$$d\phi - d\theta = d\tau$$

and

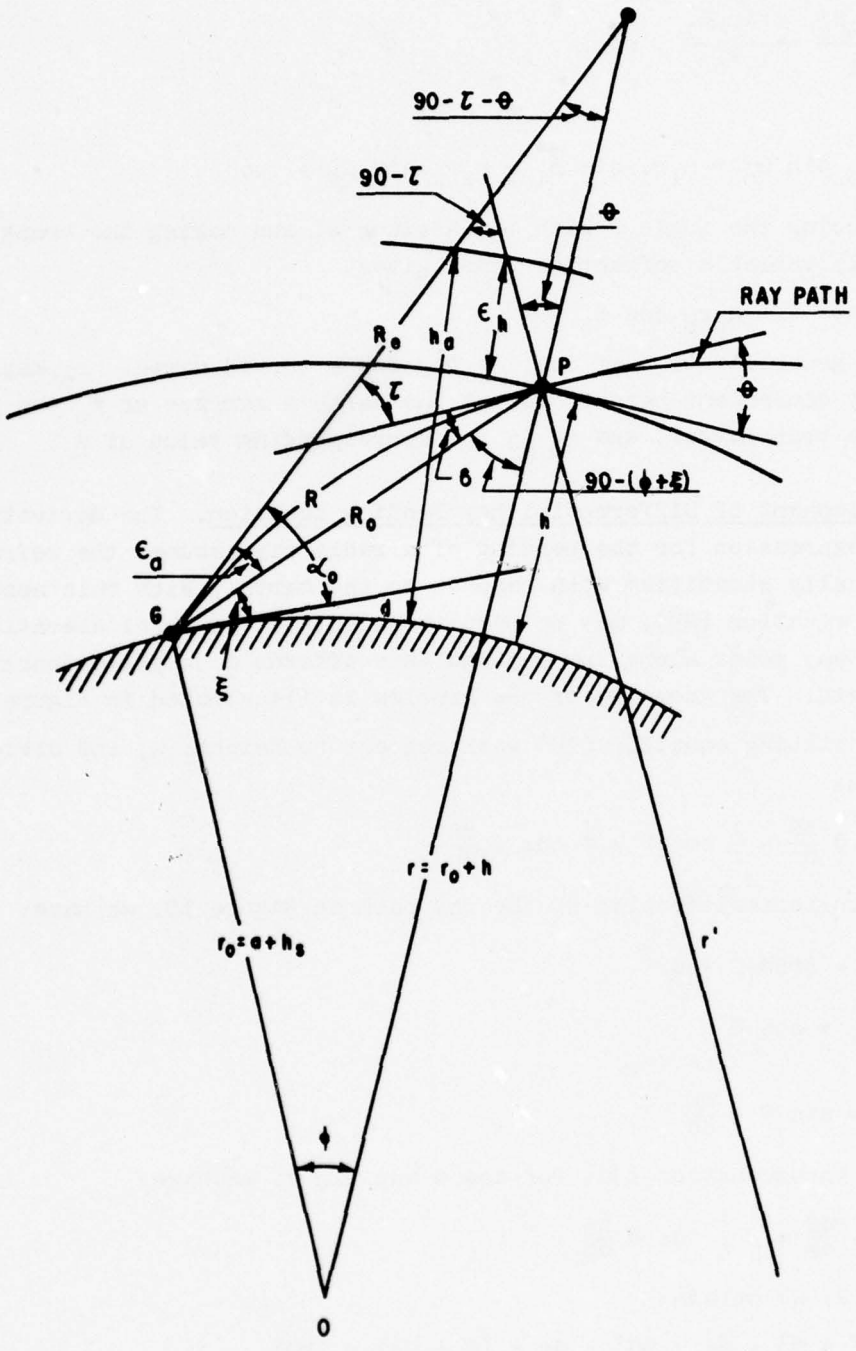

Figure 11. Geometry of Radio-Ray Refraction.

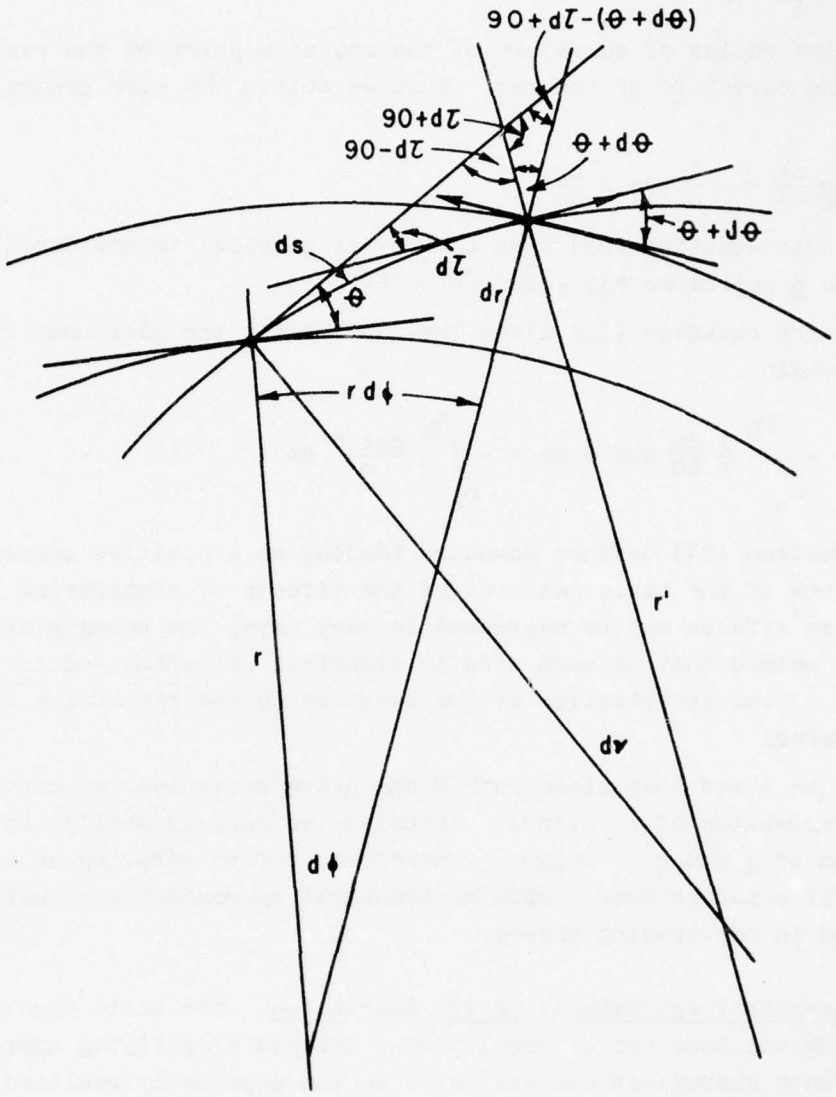

Figure 12. Infinitesimal Section of Ray Path.

$$(32) \qquad \frac{d\phi}{ds} - \frac{d\theta}{ds} = \frac{d\tau}{ds} = -\frac{1}{n}\cos\theta\,\frac{dn}{dh}$$

Also from Figure 12

$$d\tau = d\nu$$

$$ds = r'd\nu = r'd\tau$$

and

$$\frac{d\tau}{ds} = \frac{1}{r'} = \rho$$

where r' is the radius of curvature of the ray at a point on the ray and ρ is defined as the curvature of the ray. Thus we obtain the more general formula:

$$(33) \qquad \frac{1}{r'} = \frac{d\tau}{ds} = -\frac{1}{n} \cos\theta \frac{dn}{dh}$$

which reduces to equation (23) when the ray is parallel to the earth's surface and we assume n approximately equal to unity.

Integrating equation (33) along the ray between the altitudes r_o and $r_o + h$, we obtain

$$(34) \qquad \tau = -\int_{n_o}^{n_h} \frac{1}{n} \frac{dn}{dh} \cos\theta \, ds = -\int_{n_o}^{n_h} \frac{\cot\theta}{n} \, dn$$

Note that equation (34) defines downward bending as a positive quantity. This equation is one of the basic measures of the effects of atmospheric refraction. Although these effects may be expressed in many ways, the bending often offers a convenient method that is much used in classical astronomy and is simply the angle formed by the intersection of the tangents to the ray at the two points being considered.

It will be noted that since both θ and n are variables, we cannot integrate this expression as it stands. Actually, we know by Snell's Law that θ is a function of n and r or height. Therefore, before deriving an expression for τ, we will consider some useful mathematical approximations that are usually employed in ray-tracing theory.

2.2.3. Mathematical Approximations for Refraction. The basic equation for bending yields the most useful results when certain simplifying approximations are made. These approximations are based on the physically realized properties of the troposphere and the geometry of the tropospheric propagation problem. As is always the case, the validity of the approximations depends on the accuracy required.

Two approximations are almost always employed in all workable solutions to the tropospheric refraction problem, and are generally very well satisfied in the troposphere. These two approximations are:

$$(35) \qquad \begin{aligned} n &\cong 1.0 \\ r &\cong r_o \end{aligned}$$

where

n = the index of refraction.

r = the radial coordinate in the cylindrical coordinate system.

r_o = the value of r at the transmitter.

Another assumption based on the second approximation is obtained from the expression

$$r = r_o + h = r_o \left(1 + \frac{h}{r_o}\right)$$

and states $h/r_o \ll 1$.

For heights of 100,000 feet or less h/r_o never exceeds 5×10^{-3}, but still includes almost all cases of interest in the troposphere.

A quantity of the form

$$(1 + b)^m , \quad b \ll 1$$

appears frequently in tropospheric refraction problems and may be approximated through the binomial expansion by discarding all but the first two terms in

$$(1 \pm b)^m = 1 \pm mb + \frac{m\,(m - 1)}{2!}$$

$$(36) \qquad (1 \pm b)^m \cong 1 \pm mb , \quad b \ll 1$$

where m need not be an integer. Furthermore, products of the form

$$(1 + b_1)\ (1 + b_2) \ldots$$

may often be approximated by

$$(37) \qquad (1 + b_1)\ (1 + b_2) \ldots \cong 1 + b_1 + b_2 \ldots$$

when the higher ordered terms are neglected. For example:

$$(1 + b_1)\ (1 + b_2) = 1 + b_1 + b_2 + b_1 b_2 \cong 1 + b_1 + b_2$$

2.2.4. Solution of Differential Equation for Ray Bending. We may now obtain a solution to the differential ray equation (34) derived in section 2.2.2 by employing the approximations discussed in section 2.2.3. Equation (34) may be written as follows:

$$(38) \qquad \tau_{o,1} = \int_{h_o}^{h_1} \frac{1}{n} \frac{dn}{dh} \frac{\cos\theta}{\sin\theta}\, dh$$

where $h = r - r_o$; $h_o = 0$; $\theta_o = \alpha_o$; and $h_1 = r_1 - r_o$. From Snell's Law [equation (29)] we have

$$\sin\theta = \frac{\cos\theta}{\cos\alpha_o}\left[\left(\frac{nr}{n_o r_o}\right)^2 - \cos^2\alpha_o\right]^{-1/2} \tag{39}$$

Equation (39) can be substituted in (38) to give the general equation for refractive bending

$$\tau_{o,1} = -\int_{h_o}^{h_1} \frac{1}{n}\frac{dn}{dh}\frac{\cos\alpha_o\, dh}{\left[\left(\frac{nr}{n_o r_o}\right)^2 - \cos^2\alpha_o\right]^{1/2}} \tag{40}$$

We now assume that (a) $dn/dh = -\gamma$ = constant, (b) $h/r_o \ll 1$, and (c) index of refraction n is very nearly unity, i.e., $n = 1 + \Delta n$. On the basis of these assumptions we can write:

$$\gamma = \frac{n_o - n}{r - r_o} = \frac{n_o - n}{h} \tag{41}$$

and

$$\left(\frac{nr}{n_o r_o}\right)^2 = \left[\frac{1 + \Delta n}{1 + \Delta n_o}\right]^{-2}\left[1 + \frac{h}{r_o}\right]^{-2} \tag{42}$$

Employing the approximation formulas (36) and (37), equation (42) can be approximated by

$$\left(\frac{nr}{n_o r_o}\right)^2 \cong \left[1 + 2h\left(\frac{1 - \gamma r_o}{r_o}\right)\right] \tag{43}$$

and, substituting into (40), we get:

$$\tau_{o,1} = \gamma\cos\alpha_o \int_{h_o=0}^{h_1} \frac{dh}{\left[\sin^2\alpha_o + 2h\left(\frac{1 - \gamma r_o}{r_o}\right)\right]^{1/2}} \tag{44}$$

$$= \frac{\gamma r_o \cos\alpha_o}{1 - \gamma r_o}\left\{\left[\sin^2\alpha_o + 2h_1\left(\frac{1 - \gamma r_o}{r_o}\right)\right]^{1/2} - \sin\alpha_o\right\}$$

From equations (39) and (43), we obtain:

$$\sin\theta_1 = \frac{\cos\theta_1}{\cos\alpha_o}\left[\sin^2\alpha_o + 2h_1\left(\frac{1 - \gamma r_o}{r_o}\right)\right]^{-1/2}$$

Combining with (44), we have

$$\tau_{o,1} = \frac{\gamma r_o \cos\alpha_o}{1 - \gamma r_o}\left(\frac{\sin\theta_1}{\cos\theta_1}\cos\alpha_o - \sin\alpha_o\right)$$

and after factoring $\cos\alpha_o$, obtain

$$(45) \qquad \tau_{o,1} = \frac{\gamma r_o \cos^2 \alpha_o}{1 - \gamma r_o} (\tan \theta_1 - \tan \alpha_o)$$

From (43) and (41) we obtain:

$$(46) \qquad \frac{\gamma r_o}{1 - \gamma r_o} = \frac{2(n_o - n_1)}{\left(\frac{nr}{n_o r_o}\right)^2 - 1} = \frac{2(n_o - n_1)\sec^2 \alpha_o}{\tan^2 \theta_1 - \tan^2 \alpha_o}$$

where

$$\left(\frac{n_1 r_1}{n_o r_o}\right)^2 = \frac{\cos^2 \alpha_o}{\cos^2 \theta_1} = \frac{\sec^2 \theta_1}{\sec^2 \alpha_o} = \frac{1 + \tan^2 \theta_1}{1 + \tan^2 \alpha_o}$$

which, substituted into (45) gives the desired expression for $\tau_{o,1}$

$$(47) \qquad \tau_{o,1} = \frac{n_o - n_1}{\frac{1}{2}(\tan \theta_1 + \tan \alpha_o)} \text{ radians}$$

Total bending through the atmosphere is simply the sum of individual contributions

$$(48) \qquad \tau_{total} = \sum_{j=o}^{m-1} \frac{(n_j - n_{j+1})}{\frac{1}{2}(\tan \theta_j + \tan \theta_{j+1})} \text{ radians}$$

where $\underline{m}$ is the number of atmospheric layers through which dn/dh = constant, and θ_j at the surface is α_o.

2.3. Elevation-Angle Errors.

The objective of this section is to employ ray theory concepts to derive approximate expressions appropriate for the computation of the radar elevation-angle error. The geometry of the problem is indicated in Figure 11. Since the ray path is curved, rather than straight, the apparent position of the target is displaced from the true position. In general, both the apparent elevation angle, α_o (as seen by the radar), and the apparent range are in error but only the former will be considered in this section.

The elevation-angle error denoted by ϵ_a can be obtained from Figure 11 by the use of the law of sines.

$$(49) \qquad \frac{\sin (90° + \xi)}{r} = \frac{\sin [90° - (\phi + \xi)]}{r_o}$$

Employing the relationships from Figure 11,

$$\xi = \alpha_o - \epsilon_a$$

$$\phi + \xi = \tau + \theta - \epsilon_a$$

Snell's Law,

$$r_o = \frac{nr \cos \theta}{n_o \cos \alpha_o}$$

and substituting into equation (49) we obtain:

$$\cos \alpha_o + \sin \alpha_o \tan \epsilon_a = \frac{(\cos \tau \cos \theta - \sin \tau \sin \theta)\, n_o \cos \alpha_o}{n \cos \theta} + \frac{(\sin \tau \cos \theta + \cos \tau \sin \theta)\, n_o \cos \alpha_o \tan \epsilon_a}{n \cos \theta}$$

Solving for $\tan \epsilon_a$ we obtain

$$\tan \epsilon_a = \frac{\frac{n}{n_o} + \sin \tau \tan \theta - \cos \tau}{\sin \tau + \cos \tau \tan \theta - \frac{n}{n_o} \tan \alpha_o} \tag{50}$$

Application of small-angle approximations and the relationship

$$\frac{n}{n_o} = \frac{1 + \Delta n}{1 + \Delta n_o} \cong 1 + \Delta n - \Delta n_o = 1 + n - n_o$$

to formula (50) results in

$$\epsilon_a = \frac{\tau \tan \theta - (n_o - n) + \frac{\tau^2}{2}}{\tau + \tan \theta - \tan \alpha_o + (n_o - n) \tan \alpha_o}$$

$$\epsilon_a \cong \frac{\tau \tan \theta - (n_o - n) + \frac{\tau^2}{2}}{\tau + \tan \theta - \tan \alpha_o} \tag{51}$$

The true elevation angle ξ is then found from

$$\xi = \alpha_o - \epsilon_a$$

To determine the various θ's in terms of the angle of elevation α_o and height $\underline{h}$, we use Snell's Law [equation (29)] and the approximations (35) and (37) to obtain

$$\cos \theta = \frac{\cos \alpha_o}{(1 + h/r_o)\,[1 - (n_o - n)]} \cong [1 + (n_o - n) - \frac{h}{r_o}] \cos \alpha_o \tag{52}$$

We note that θ, the ray inclination angle, is a function only of height $\underline{h}$ and the difference in the refractive index between the surface and $\underline{h}$. It is independent of the shape of the refractive profile. This fact allows us to determine θ at each significant level independently of other levels. Thus, it is not necessary to start at the surface and work up layer by layer as is required in many other computational methods.

2.4. Range Errors.

A radar determines range by actually measuring the time of travel required for a radiated pulse to travel from the radar to the target and applying a multiplying factor to convert to distance. An error is introduced into the apparent radar range by the velocity of propagation along the path differing from the value for which the radar (or other electronic instrument) is calibrated. The increased path length due to the curvature of the ray is a much smaller contribution to the range error and may be neglected for most applications. The following development neglects the effects of curvature.

For the development of a formula for computing range error, consider Figures 11 and 12. From Figure 11:

$$\Delta R = (R_L - R) + (R - R_o)$$

$$\Delta R \cong R_L - R \tag{53}$$

where

$$R_L = nR \quad \text{and} \quad R \cong R_o$$

and from Figure 12

$$R = \int_{h_o}^{h_1} ds \quad \text{and} \quad R_L = \int_{h_o}^{h_1} nds \tag{54}$$

where

$$ds = \frac{dh}{\sin \theta} \tag{55}$$

Substituting equations (54) and (55) into equation (53) we obtain:

$$\Delta R_{o,1} = \int_{h_o}^{h_1} \frac{(n - 1)\, dh}{\sin \theta} \tag{56}$$

In evaluating τ, refractive ray bending, we found

$$\tau_{o,1} = -\int_{h_o}^{h_1} \frac{1}{n} \frac{dn}{dh} \frac{dh}{\tan \theta} = \int_{h_o}^{h_1} \frac{dn}{\tan \theta} = \frac{n_o - n_1}{\frac{1}{2}(\tan \alpha_o + \tan \theta_1)}$$

In other words, the value of the integral for the case of a constant radial gradient was found to be very nearly equal to the one that would have been obtained had we taken the average value of the denominator of the integrand and treated it as a constant. We are, therefore, tempted to treat the integral of (56) in a similar manner. Furthermore, we can argue that at low angles sine

and tangent are nearly the same and at high angles the rate of change of sin θ is so slow that such procedure is certainly justifiable.

Thus, we evaluate (56) by setting

$$(57) \qquad \Delta R_{o,1} = \int_{h_o}^{h_1} \frac{(n-1)\,dh}{\sin\theta} = \frac{2}{\sin\alpha + \sin\theta_1} \int_{h_o}^{h_1} (n-1)\,dh$$

but from (41)

$$\int_{h_o}^{h_1} (n-1)\,dh = \int_{h_o}^{h_1} (n_o - 1)\,dh - \int_{h_o}^{h_1} \gamma h\,dh$$

$$= (n_o - 1)\,h_1 - \tfrac{1}{2}(n_o - n)\,h_1$$

$$= \left[\frac{n_o + n}{2} - 1\right] h_1$$

Substituting into (57) we get

$$(58) \qquad \Delta R_{o,1} = \frac{[(n_o - 1) + (n - 1)]\,[h_1]}{\sin\alpha_o + \sin\theta_1}$$

To compute retardation for a double passage through the layer (58) must be doubled

$$(59) \qquad \Delta R_{total} = 2 \sum_{j=o}^{m-1} \frac{[(n_j - 1) + (n_{j+1} - 1)]\,[h_{j+1} - h_j]}{\sin\theta_j + \sin\theta_{j+1}}$$

The integral (56) can be evaluated exactly. The resulting expression, however, is quite involved. Comparison of the exact solution with (58) indicates an error of a few hundreths of one percent for tropospheric propagation [37].

2.5. Height Errors.

In section 2.3.1, a formula was developed which can be employed in computing the elevation-angle error. This correction when applied to the apparent elevation angle will give the true elevation angle ξ. Employing this angle and the corrected range $\underline{R}$, it is possible to compute the true height. However, for certain purposes it is desirable to have a formula which will give the height error directly.

The apparent height of the target, in Figure 13, is obtained by solving:

$$(60) \qquad (r_o + h_a)^2 = r_o^2 + R^2 + 2r_o R \sin\alpha_o$$

for h_a. Because the difference between $\underline{R}$ and the true slant range, R_o is extremely small compared to the height error, we again assume that $R \cong R_o$. The following form of the solution for h_a is useful for numerical calculations:

$$(61) \qquad h_a = \frac{R\,(R + 2r_o \sin \alpha_o)}{r_o + [r_o^2 + R\,(R + 2r_o \sin \alpha_o)]^{1/2}}$$

The height error for a target at height $\underline{h}$ is found by

$$(62) \qquad \epsilon_h = h_a - h$$

which will always be positive if $\underline{n}$ decreases with height.

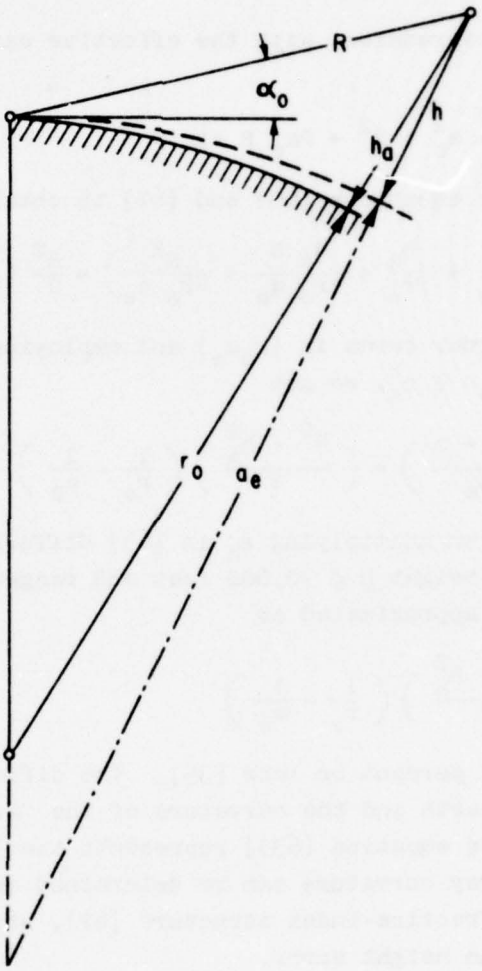

Figure 13. Effective Earth's Radius Geometry.

If the refractive index is known as a function of height the foregoing procedure is useful for determining the height error when the true height and the arrival angle of the ray are hypothesized. Unfortunately, it is not applicable for obtaining the height error from the apparent positions of the target.

In order to eliminate $\underline{h}$ from equation (62) we define a new parameter, a_e, the effective earth's radius (see Figure 13) where

$$(63) \qquad \frac{1}{r_o} - \frac{1}{r'} = \frac{1}{a_e}$$

and $1/r'$ = curvature of ray. Thus, by subtracting the curvature of the ray from the earth's curvature, we obtain a new earth's radius which makes the ray path a straight line.

The following expression, with the effective earth's radius denoted by a_e in Figure 13

$$(64) \qquad (a_e + h)^2 = a_e^2 + R^2 + 2a_e R \sin\theta$$

can be combined with equations (60) and (62) to obtain

$$(65) \qquad \epsilon_h \left(1 + \frac{h}{2a_e} + \frac{h_a}{2r_o} + \frac{h_a h}{4r_o a_e} + \frac{R^2}{4r_o a_e}\right) = \frac{R^2}{2}\left(\frac{1}{r_o} - \frac{1}{a_e}\right) + \frac{h_a h}{2a_e} - \frac{h_a^2}{2r_o}$$

Neglecting higher order terms in $(r_o a_e)$ and employing approximations $h_a/r_o \cong h_a/a_e$ and $h_a h \cong h_a^2$, we get

$$(66) \qquad \epsilon_h \left(1 + \frac{h_a + h}{2a_e}\right) = \left(\frac{R^2 - h_a^2}{2}\right)\left(\frac{1}{r_o} - \frac{1}{a_e}\right)$$

Because the expression multiplying ϵ_h in (65) differs from unity by less than 4×10^{-3} for target height $\underline{h} \leqslant 70{,}000$ feet and ranges $\underline{R} \leqslant 155$ miles, the height error can be approximated as

$$(67) \qquad \epsilon_h \cong \left(\frac{R^2 - h_a^2}{2}\right)\left(\frac{1}{r_o} - \frac{1}{a_e}\right)$$

with an error of 0.4 percent or less [35]. The difference between the curvature of the actual earth and the curvature of the "average" effective earth for the ray path [see equation (63)] represents the "average" curvature of the ray. Thus, if the ray curvature can be determined as a function of the target position and the refractive-index structure (67), provides a simple formula for approximating the height error.

From Figures 11 and 12, we obtain:

(68) $$\frac{1}{r'} = \frac{\tau}{R}$$

Substituting (68) and (63) into (67), we obtain:

(69) $$\epsilon_h \cong \left(\frac{R^2 - h_a^2}{2} \right) \left(\frac{1}{r'} \right) = \frac{(R^2 - h_a^2)\,\tau}{2R}$$

combining equations (48) and (69), we have

(70) $$\epsilon_h = \left(\frac{R^2 - h_a^2}{2R} \right) \sum_{j=o}^{m-1} \frac{(n_j - n_{j+1})}{(0.5)\,(\tan \theta_j + \tan \theta_{j+1})}$$

2.6. Formula Summary.

Given below is a summary of the important formulas developed in this chapter. The formulas are also expressed in terms of refractivity, N, a parameter defined in the next chapter (section 3.1).

a. Total Bending.

(71) $$\tau_{total} = \sum_{j=o}^{m-1} \frac{(n_j - n_{j+1})}{0.5\,(\tan \theta_j + \tan \theta_{j+1})} \text{ radians}$$

$$= \sum_{j=o}^{m-1} \frac{(N_j - N_{j+1})}{500\,(\tan \theta_j + \tan \theta_{j+1})} \text{ milliradians}$$

where $\theta_j = \alpha_o$ when $j = o$.

b. Elevation-Angle Error.

(72) $$\epsilon_a = \frac{\tau \tan \theta - (n_o - n) + \frac{\tau^2}{2}}{\tau + \tan \theta - \tan \alpha_o} \text{ radians}$$

$$= \frac{1000\,\tau \tan \theta - (N_o - N) + \frac{\tau^2}{2}}{\tau + 1000 \tan \theta - 1000 \tan \alpha_o} \text{ milliradians}$$

where τ is in milliradians.

c. Range Error.

(73) $$\Delta R_{o,1} = \frac{[(n_o - 1) + (n - 1)]\,[h_1]}{\sin \alpha_o + \sin \theta_1} = \frac{(N_o + N)\,(h_1)\,10^{-6}}{\sin \alpha_o + \sin \theta_1}$$

$$(74) \qquad \Delta R_{total} = 2 \sum_{j=o}^{m-1} \frac{(N_j + N_{j+1})\,(h_{j+1} - h_j)\,10^{-6}}{\sin \theta_j + \sin \theta_{j+1}} \quad \text{(Double Passage)}$$

d. Height Error.

$$(75) \qquad \epsilon_h = \frac{(R^2 - h_a^2)\,\tau_h}{2R}$$

where τ_h = total bending at height h.

Chapter 3

THE ATMOSPHERIC RADIO REFRACTIVE INDEX

3.1. Definition.

It was mentioned previously that the propagation velocity of all electromagnetic energy in a vacuum is a constant ($c = 3.0 \times 10^{10}$ cm/sec). In atmospheric gases this velocity is reduced slightly. The ratio of the velocity of propagation of electromagnetic energy in a vacuum to that in a particular medium, is defined as the refractive index of the medium as was described in section 1.3.4. This quantity, designated as n, generally varies with wavelength and, of course, from medium to medium. In tropospheric air (within the wavelength band from 1 cm to 10 m) the refractive index is, for all practical purposes, independent of wavelength and has a value slightly greater than unity. At sea level, values range from approximately 1.000250 to 1.000450, with values near 1.000350 frequently found over an ocean surface.

To facilitate numerical computation it is more convenient to define a derived index, called the refractivity, as follows

$$(76) \qquad N = (n - 1) \times 10^6$$

The atmospheric refractivity ranges from 250 to 450 N-units at sea level. It is also possible to express N as a function of total atmospheric pressure, temperature, and water-vapor pressure, as follows

$$(77) \qquad N = \frac{D}{T}\left(P + \frac{Ee}{T}\right)$$

where P and e are in millibars and T is in degrees absolute. The constants, D and E, have been determined experimentally by a number of investigators; D is the dielectric constant for dry air and E is the water-vapor dipole-moment constant. Smith and Weintraub [33] have evaluated the results obtained by numerous investigators and have recommended the value of 77.6 for D and the value of 4810 for E, which has been internationally adopted by IRCC. Equation (77) is frequently written in the following form:

$$(78) \qquad N = 77.6\left(\frac{P}{T}\right) + 3.73 \times 10^5\left(\frac{e}{T^2}\right)$$

where the first and second terms are called the "dry" and the "wet" terms, respectively. Since both P and e normally decrease with height above sea level, N also decreases with height. The exact way in which N varies with height is, of course, determined by meteorological processes and has a

profound effect upon radio-radar propagation.

In the event that available moisture data are expressed as relative humidities, equation (78) may be written as follows:

$$(79) \qquad N = 77.6 \left(\frac{P}{T} \right) + 3.73 \times 10^5 \left(\frac{e_s RH}{T^2} \right)$$

where e_s is the saturation vapor pressure in millibars and RH is the relative humidity in percent. Since they depend on meteorological variables, both n and N are functions which in general vary from place to place in the atmosphere and with time at a particular point. The preceding formulas permit one to determine the refractivity for one particular place and time; namely, the place and time represented by the values of pressure, temperature, and humidity used. In general, the path which a radio-radar ray will follow is primarily determined by the gradient of N rather than by N itself, as was discussed in section 1.3.4(b). N-gradients may be determined from a series of discrete values of N in the region of interest, or the gradients may be determined by direct measurement with suitable equipment.

3.2. Methods of Measurement and Computation.

Direct measurements of the propagation velocity of electromagnetic energy in a particular medium can be made and, when compared with the speed of light, give a direct measure of the refractive index or refractivity. Because of the complexity of the equipment needed, this approach is impractical for operational use.

3.2.1. Refractometer. A more practical way to measure the atmospheric refractive index, an indirect method, was developed in the 1940's by Birnbaum [10] at the National Bureau of Standards and, somewhat later, in a slightly different form by Crain and Deam [14] at the University of Texas. The refractometer, as the instrument is called, essentially measures changes in the dielectric constant of the air inside a perforated cylindrical cavity. This is done by feeding electromagnetic energy of about a 3-centimeter wavelength into a cavity which has been machined to resonate over a very narrow band of wavelengths. Changes in the dielectric constant of the air inside the cavity cause the resonant frequency of the cavity to change proportionally. By using two cavities (one being hermetically sealed and containing either dry air or vacuum and the other being perforated to allow passage of outside air) one can detect very small changes in the resonant frequency of the perforated cavity. Since the refractive index in this case is simply the square root of the dielectric constant, these changes can be recorded as changes in N. The sensing lag of

the device is limited only by the time needed to introduce new air into the cavity. Since the volume of air contained in the cavity is very small, the speed of response may be reduced to a fraction of a second by careful design of the ventilating ducts or ports.

In spite of various simplifications which have been made in recent years, the airborne refractometer is a relatively complex and heavy instrument which is not suitable for use on balloons. However, expendable light-weight balloon-borne refractometers are under development. Aboard aircraft, many hundreds of vertical and horizontal profiles of refractive index have been recorded, particularly over the continental United States and Alaska. In the future refractometer data may be expected to become available to weather detachments supporting units concerned with radio-radar propagation. It should always be used in preference to derived N-data, whenever there is a choice, because of its greater precision and because it reproduces the "fine" structure of atmospheric refractivity.

3.2.2. Temperature, Pressure, and Humidity Method. Since N is a function of P, T, and e, it follows that whenever measurements of these quantities are available they also serve to define N. At the surface the conventional barometer, thermometer, and hygrometer may be used to determine N; aloft the radiosonde provides the necessary measurements. From values of P, T, and e, N may be computed using equations (78) or (79). The particular features of the radiosonde which make it useful for propagation purposes are that it measures the required quantities as functions of height, and that record data are available which have been obtained over periods of many years and from hundreds of stations having a wide geographic distribution.

All meteorologists recognize that the radiosonde has certain deficiencies which make it somewhat less than ideal, particularly in the measurement of humidity. The high lag coefficient of the humidity-sensing element, particularly at low temperatures, causes the resulting N (namely, the height profile) to deviate from its true shape. The effect of these deviations on radio propagation perhaps is not as serious as it may be for other purposes. The reason for this is that, as will be shown later, anomalous propagation effects are principally conditioned by the gross features of the N-profile; the fine structure is not of first order importance. This does not mean that for propagation work, improvements in the radiosonde are unnecessary; rather, they are greatly desired (see section 3.3.4). It does mean, however, that record radiosonde data can be used to good advantage in spite of its shortcomings.

Comparisons between N-values obtained from refractometer measurements and those computed from radiosonde data are in good agreement as to the gross

structure present, but, of course, the fine details are largely missed in the computed radiosonde values. Figure 14 is an example of such a comparison. Where appreciable deviations occur, it has been found that these were caused by pronounced humidity fluctuations, as would be expected.

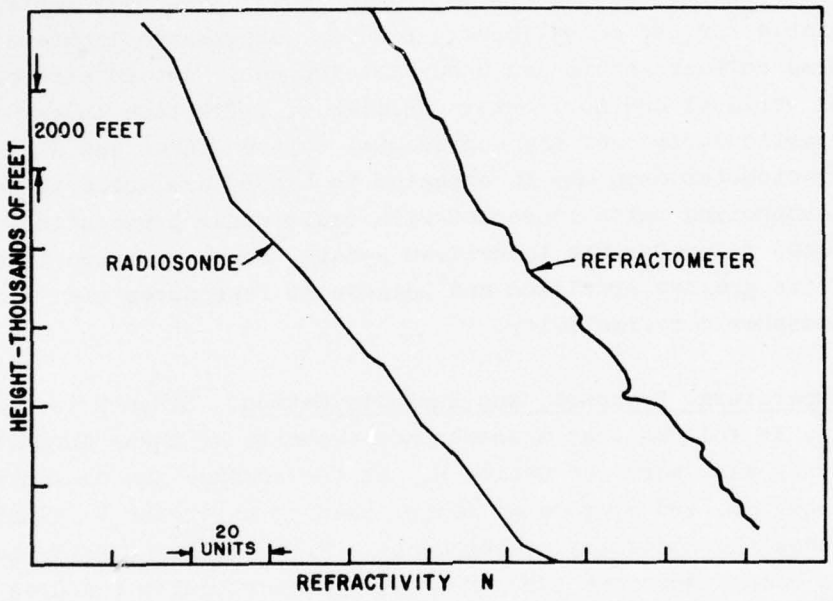

Figure 14. Comparison of Radiosonde and Refractometer N-Profiles.

In propagation problems, one is continually faced with the problem of reducing P-, T-, and e-data to N-values at numerous heights. Over the years, various methods have been devised for computing N. These take the form of tables, slide rules, analogue computers, and nomograms.

a. Refractive-Index Nomogram. Perhaps the most convenient of these, for use when great precision is not required, is the nomogram shown in Figure 15. Pressure, temperature, and humidity are shown in the units commonly used in radiosonde data tabulations; i.e., pressure in millibars, temperature in °C, and dew point in °C. It is particularly convenient in that the nomogram and a straight edge are all that is required. Assuming no error in entry data, the accuracy of the N-values so derived is ±1 N-unit, which is compatible with the accuracy of radiosonde data. A larger, full-size version of the refractive-index nomogram (Figure 15) is provided as a fold-in inclusion to Volume II of this report and is marked as Chart I; local reproduction of this chart

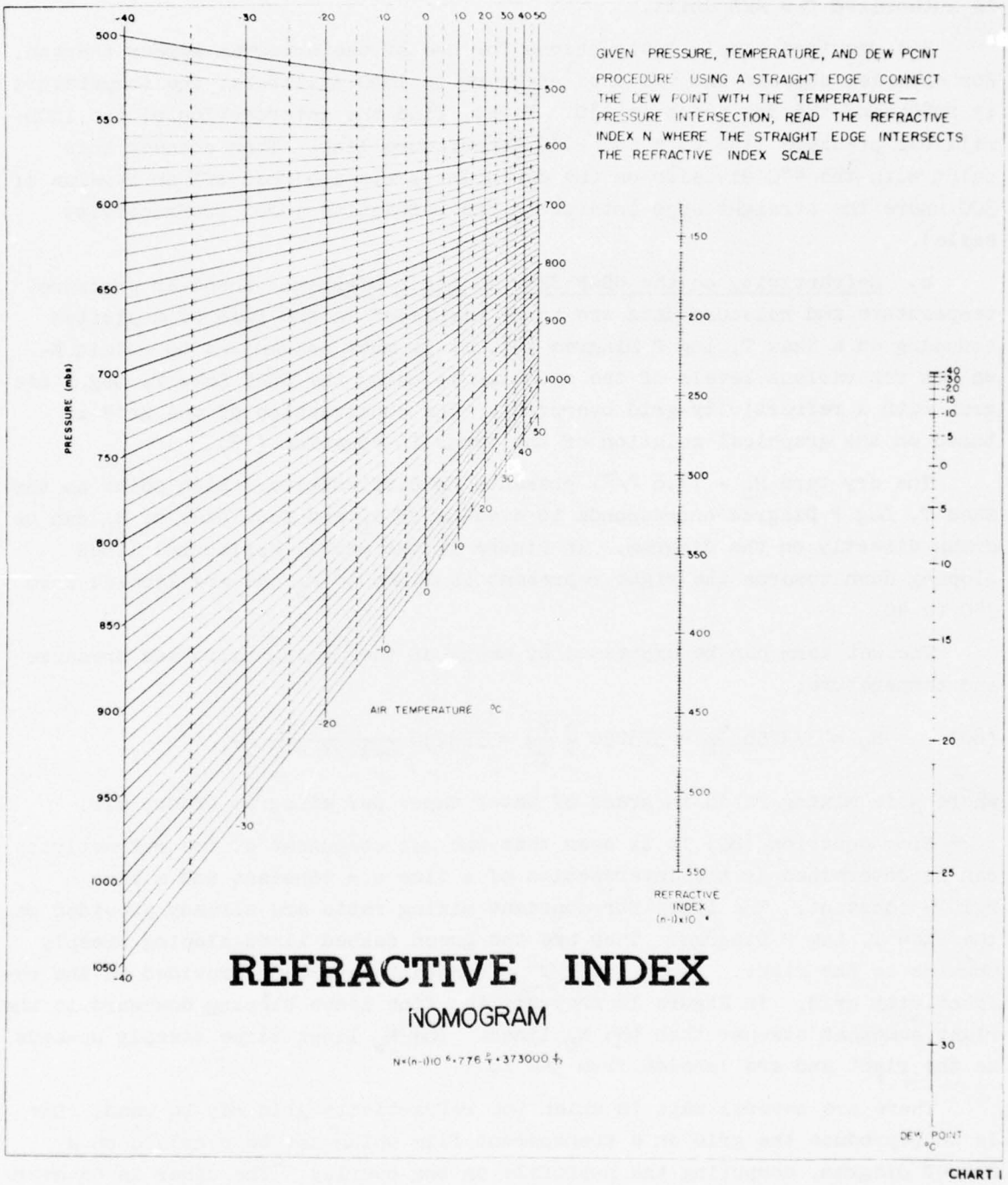

Figure 15. Refractive-Index Nomogram (Chart I).

is authorized for AWS units.

The required simple instructions for use of the nomogram appear thereon. For example, suppose the value of pressure is 1000 millibars, the temperature is 20°C, and the dew point is 4°C. First find the intersection of the 1000-millibar pressure line with the 20°C temperature line. Then connect this point with the 4°C division on the dew-point scale and read off an N-value of 300 where the straight edge intersects the refractive index (refractivity scale).

b. Refractivity on the USAF Skew T, Log P Diagram. Whenever pressure, temperature and moisture data are to be displayed in the form of a plotted sounding on a Skew T, Log P Diagram [4], it is most convenient to obtain N-values for various levels of the sounding by using the USAF Skew T, Log P diagram with a refractivity grid overprint. The construction of the grid is based on the graphical solution of the terms in equation (78).

The dry term $N_D = 77.6\ P/T$, presents no difficulties. Each point on the Skew T, Log P Diagram corresponds to a value of N_D and isopleths of N_D can be drawn directly on the diagram. In Figure 16 the nearly horizontal lines sloping down towards the right represent isolines of N_D and are labeled from 340 to 40.

The wet term can be expressed by means of the mixing ratio and pressure and temperature:

$$(80) \qquad N_W = 373256\ \frac{e}{T^2} = 373256\ \frac{e}{P}\ \frac{P}{T^2} = 373256\ \frac{w}{621.97 + r}\ \frac{P}{T^2}$$

where w is mixing ratio in grams of water vapor per kilogram of dry air.

From equation (80) it is seen that the wet component of the refractivity can be determined at the intersection of a line w = constant and a line P/T^2 = constant. The lines for constant mixing ratio are already provided on the Skew T, Log P Diagram. They are the green dashed lines sloping steeply upwards to the right. Lines for P/T^2 = constant have been provided in the refractivity grid. In Figure 16 they are the fine lines sloping downward to the right somewhat steeper than the N_D lines. The N_W lines slope steeply upwards to the right and are labeled from 340 to 1.

There are several ways in which the refractivity grid may be used. One is to reproduce the grid on a transparent film which can be overlaid on a Skew-T diagram, computing the N-profile on the overlay. The other is to overprint the grid on the Skew-T diagram, which is then used as an expendable plotting chart. It is believed the latter method will be generally preferable, and a special edition of the USAF Skew T, Log P Diagram has been issued, designated DOD-WPC 9-16-2, which AWS activities can requisition by the same

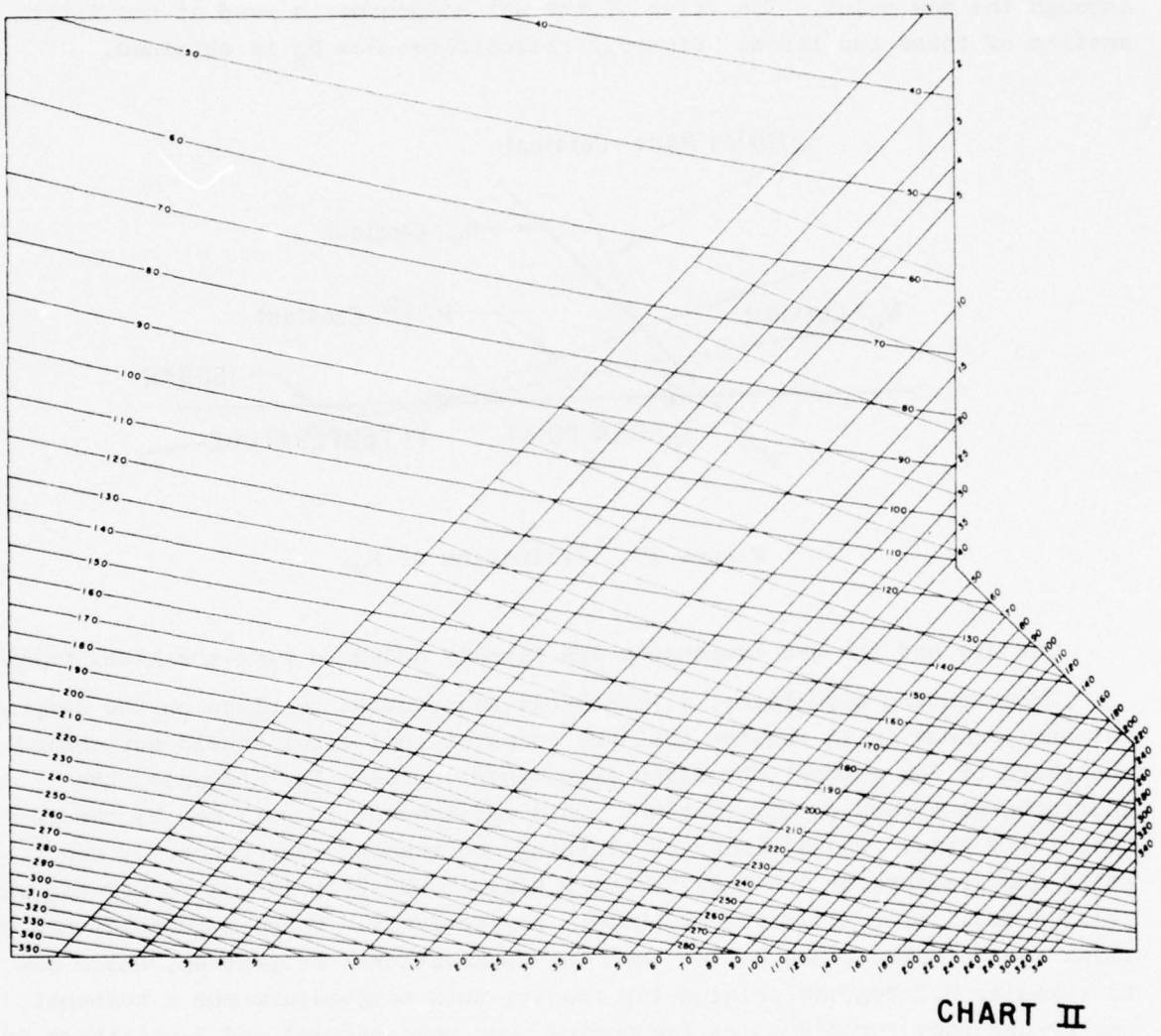

Figure 16. Refractivity Grid for USAF Skew T, Log P Diagram (Chart II).

channels as other DOD-WPC charts. A sample of this chart is included in Volume II of this report and is marked as Chart II.

In preparing a refractivity profile from a sounding, the dry component and the wet component are evaluated separately at each level which contains a significant point.

The dry component is read directly point by point on the temperature trace.

The wet component is obtained by following the thin lines sloping upwards left from the temperature point to intersection with the mixing-ratio line

through the dew point. The value of the wet component is read at the intersection of these two lines. Figure 17 illustrates how N_W is obtained.

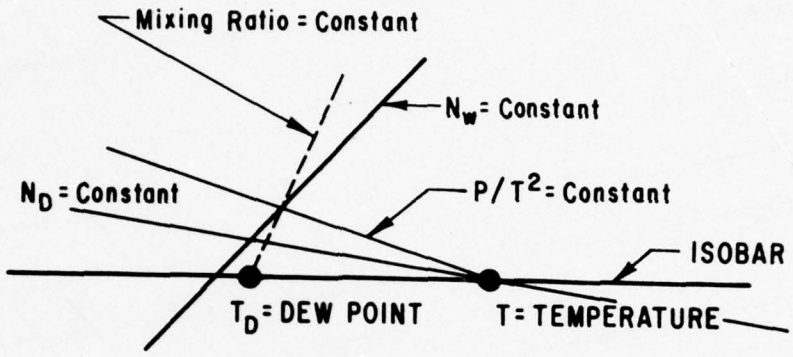

Figure 17. Evaluation of N_W.

The dry and the wet components are finally added to give the total value.

In computing quantities, a reasonable restriction to place on the computational scheme is to require that the computational error should not exceed one-third of the errors introduced from other sources, for instance, the instrumental errors of observation. This requirement is well met by the refractivity grid. The accuracy of plotting and reading temperature or dew point and pressure on the Skew T, Log P Diagram WPC 9-16 is 0.1 to 0.2 degrees Celsius and 1 or 2 millibars or better, respectively. These accuracies are at least two to three times better than the observational accuracies, which may be taken as 0.7 degrees Celsius for the dry-bulb temperature and a somewhat poorer accuracy for dew point (depending upon temperature) and 3 millibars for pressure. (Root-mean-square accuracies are used throughout this discussion.) Correspondingly, the grid will give the refractivity with a computational error which is at most one-third of the error introduced by the radiosonde on the average.

The resulting computational accuracy is about one N-unit or better for the values of temperature and dew point which occur in practice.

3.3. Refractivity Gradients.

Most tropospheric propagation anomalies are caused by the bending (refraction) of radio-radar waves and such bending is, in turn, caused by gradients in the refractive index, rather than by the absolute value of N itself.

In fact, in an atmosphere of constant N no refraction occurs irrespective of the value of N. Since gradients in pressure, temperature, and humidity prevail in the atmosphere, refractivity gradients must also generally occur.

By far the strongest and most persistent gradients in refractivity are observed in the vertical plane. The largest and most persistent contribution to the decrease in refractivity with height is the pressure gradient, which amounts to about 35 millibars in the first 1000 feet above sea level. For a similar pressure change to take place in the horizontal plane, even in association with a deep low-pressure center, would require a distance of many hundreds of miles. Similarly, vertical gradients of temperature and humidity are usually much stronger than those in the horizontal plane. For these reasons, in the study of propagation anomalies we are primarily concerned with gradients in the vertical plane. As will be apparent to the meteorologist, these vertical gradients are strongly affected by meteorological processes such as advection, subsidence, turbulence, radiation, and evaporation.

3.3.1. Validity of Horizontal Stratification Approximation. The assumption of a horizontally homogeneous atmosphere has been made in the previous theoretical derivations of refraction-correction expressions. The reasons for the assumptions have been twofold: It is a very good approximation and it is about the only procedure possible with the meteorological data which are generally available.

A study by Bean and Cahoon [6] indicated that the horizontal variations of n near the earth's surface produce the most marked deviations from the ray paths obtained by assuming horizontal stratification of n. The horizontal changes occurring more than a kilometer above the surface appear to have little effect. Further, the effects of horizontal changes appear to be most pronounced in the presence of surface ducts and at small elevation angles. The authors concluded that the effect of horizontal n change is normally small since ducting will occur less than 15 percent of the time.

3.3.2. Standard Refractivity Profile. If one averages out in time the local variations in refractivity at various heights, there results what is defined as the standard refractivity profile, such as that shown in Figure 18. In the troposphere, the vertical decrease in N is exponential, reaching a certain constant value of N at the tropopause, regardless of the surface value. In the stratosphere a single exponential curve is sufficient to describe the average profile. The mathematical form of each of the two segments of this profile may be written as

$$N_h = N_s \exp(-c_d h) \tag{81}$$

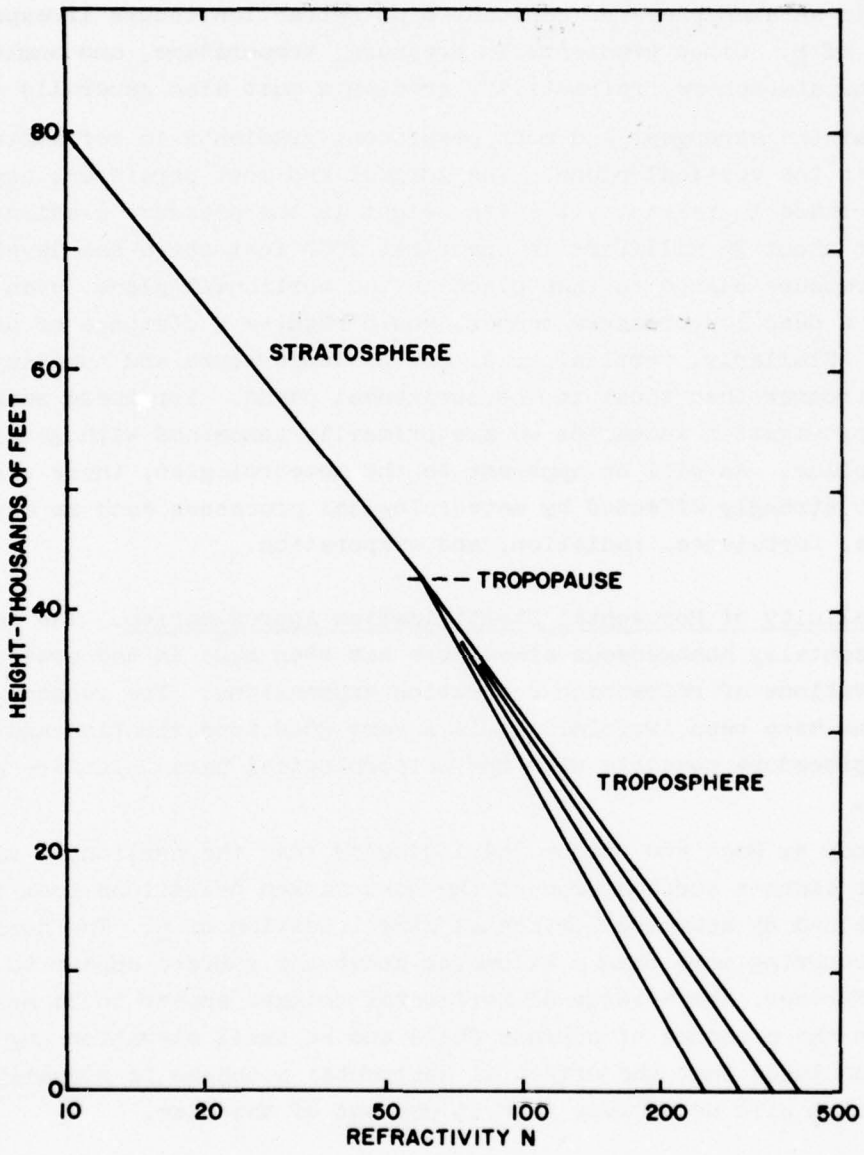

Figure 18. Standard Refractivity Profile.

where N_h is the refractivity at height $\underline{h}$, N_s is the refractivity at the earth's surface, $\underline{h}$ is height in thousands of feet, and c_d is a constant which depends upon N_s. If one assumes a constant value of $\underline{N}$ at the tropopause of 61.0 units at a height of 42,500 feet, the constant c_d, in the troposphere, may be expressed as the following function of N_s,

$$(82) \qquad c_d = \frac{\ln N_s}{42.5} - 0.0968$$

Values of c_d corresponding to several values of N_s are given in Table 1. The stratospheric segment of the standard refractivity profile may be expressed as

$$(83) \qquad N_h = 465 \exp(-0.0478h)$$

where $\underline{h}$ is the height in thousands of feet.

TABLE 1

Values of the Exponential Coefficient (c_d) for Various Values of Surface Refractivity (N_s).

N_s	c_d
N-Units	Per Thousand Feet
465	0.0478
400	0.0442
350	0.0411
318	0.0388
300	0.0375
273	0.0351
250	0.0331

This two-segment form of the standard refractivity profile was derived from data presented by Schulkin [32] and has been found to fit observations quite adequately. It should perhaps be noted that the standard refractivity profile here defined is not necessarily identical with either the US or the ICAO Standard Atmospheres. By selecting N_s equal to the value computed from the US Standard Atmosphere (1959-1962) surface values (US Standard Dry, N_s = 273 and US Standard 60% RH, N_s = 318), an N-profile is obtained which agrees, in the troposphere, with that obtained by calculating N-values from US Standard Atmosphere pressure, temperature, and humidity data [using equation (78) or (79)].

It should be realized that the structure depicted in Figure 18 is a long-term average, and that significant departures, particularly at low altitudes, are to be expected. Furthermore, the height of the tropopause varies seasonally and with latitude, but these departures will not cause serious deviations from the N-profile as described above. The behavior of radio propagation in a

standard atmosphere will be discussed in detail in the next chapter.

The gradient of refractivity, N, in a standard atmosphere, may be obtained from the general equation of the standard refractivity profile by differentiation [of equation (81)] with respect to h as follows:

$$\frac{dN}{dh} = \frac{d}{dh}\left[N_s \exp(-c_d h)\right]$$

(84) or

$$\frac{dN}{dh} = -c_d N_s \exp(-c_d h)$$

where dN/dh is given in N-units per thousand feet, N_s is the surface refractivity, c_d is the coefficient given in Table 1, and h is the height expressed in thousands of feet.

We see that the N-gradient is negative in the standard atmosphere; i.e., the value of N decreases with height, and that the magnitude of the gradient also decreases with height. Values of N-gradient for several altitudes in the standard troposphere are given in Table 2; surface values for pressure and temperature were taken from US Standard Atmosphere with 60 percent RH; i.e., $N_s = 318$. It will be noted that the N-gradient in the standard atmosphere falls from an average value of about minus 12 units per thousand feet in the lowest layers to an average value of about minus 6 units per thousand feet in the midtroposphere.

TABLE 2

Values of N-Gradient in the Standard Atmosphere ($N_s = 318$) for Several Altitudes in the Troposphere.

h	dN/dh
Feet	N-Units/Thousand Feet
Surface	-12.3
1,000	-11.9
10,000	-8.4
20,000	-5.6
30,000	-3.8

3.3.3. Actual Atmosphere. In order to evaluate N-gradients in the actual atmosphere it is recommended that a plot of N versus height be constructed.

The height scale may be constructed in terms of geometric height, pressure altitude, pressure, etc., depending upon the application intended. For most purposes a simple linear plot of N versus geometric height or pressure altitude will suffice. It is recommended the ordinary 10 × 10 per inch graph paper be ruled off with height (2000 feet to the inch) as the ordinate and with refractivity (50 N-units to the inch) as the abscissa. Such an N-profile is shown diagramatically in Figure 19. In order to evaluate rapidly the N-gradient in the various layers of the profile an N-gradient overlay has been prepared and is shown in Figure 20. This overlay has been designed for use with N-profiles constructed as shown in Figure 19; it may be used on any N-profile chart having linear h- and N-scales with a ratio $\Delta h/\Delta N$ equal to 40. It is suggested that working copies of this Figure be made locally on transparencies.

The overlay is used by matching one of the sloping lines on the overlay with the slope of a section of the plotted N-profile (the N- and h-reference lines on the overlay must be parallel with the vertical and horizontal lines on the graph paper). The value of the selected sloping line is the estimated N-gradient for the section of the profile concerned. This process can be repeated until the gradients of all layers are determined.

In order to classify the refractive properties of layers conveniently, four zones are defined as follows:

Zone 1. Subrefractive ($\Delta N/\Delta h > 0$); N increases with height. Rays curve upward with reference to a straight line (opposite in sense to the curvature of the earth's surface). Radio-radar ranges are significantly reduced; occurrence quite rare.

Zone 2. Normal ($0 > \Delta N/\Delta h > -24/1000$); N decreases with height. Rays curve downward (in the same sense as the curvature of the earth's surface) but not as sharply as in Zone 3. Radio-radar performance is generally undisturbed.

Zone 3. Superrefractive ($-24/1000 > \Delta N/\Delta h > -48/1000$); N decreases with height. Rays curve downward (in the same sense as the curvature of the earth's surface) more sharply than Zone 2 but not as much as the curvature of the earth's surface. Radio-radar ranges are significantly extended; occurrence frequent.

Zone 4. Trapping ($-48/1000 > \Delta N/\Delta h$); N decreases with height. Rays curve downward more sharply than, and in the same sense as, the curvature of the earth's surface. Radio-radar performance is greatly disturbed; ranges extended greatly, appearance of radar holes, etc.; occurrence not frequent.

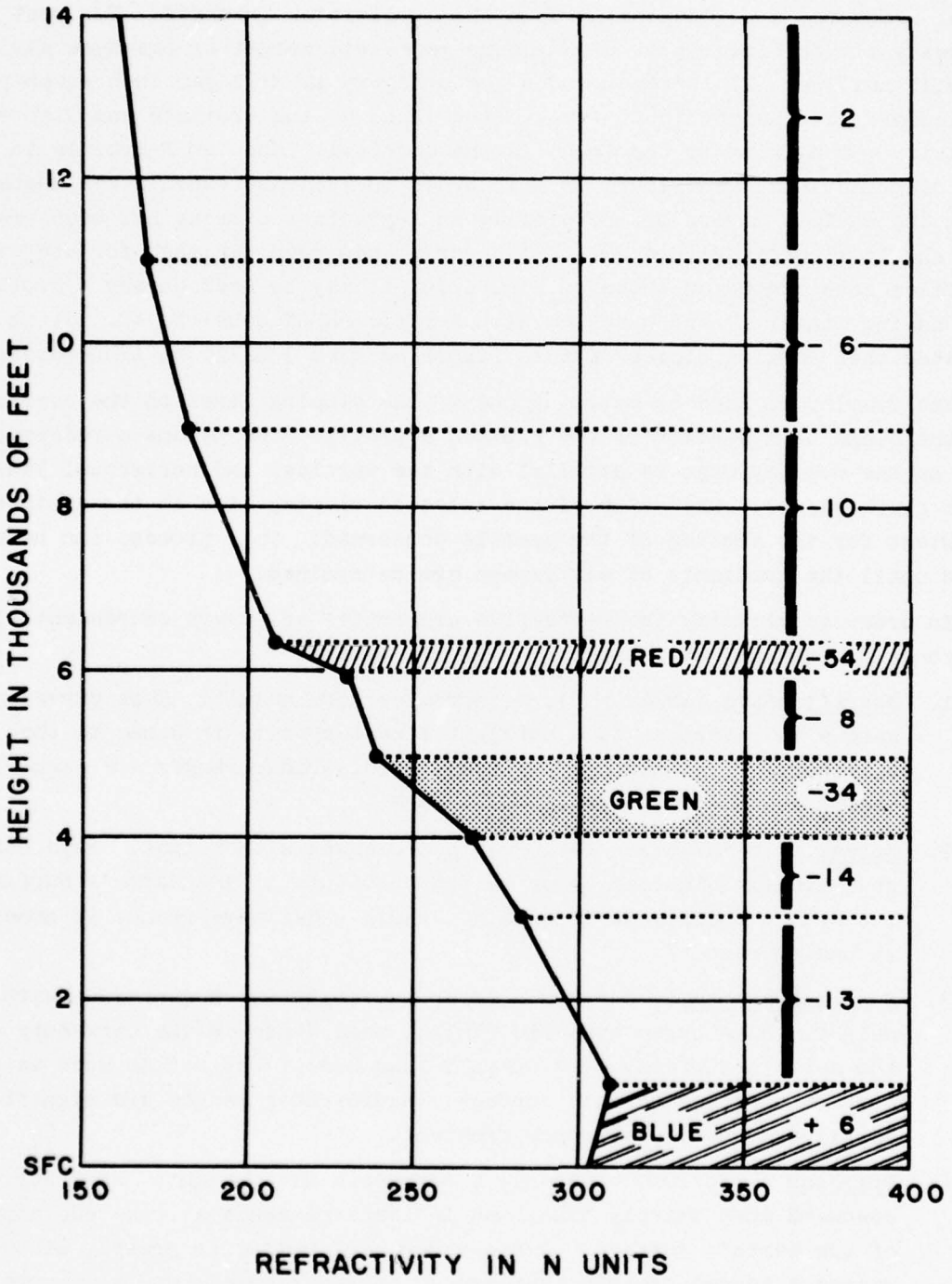

Figure 19. Analyzed N-Profile.

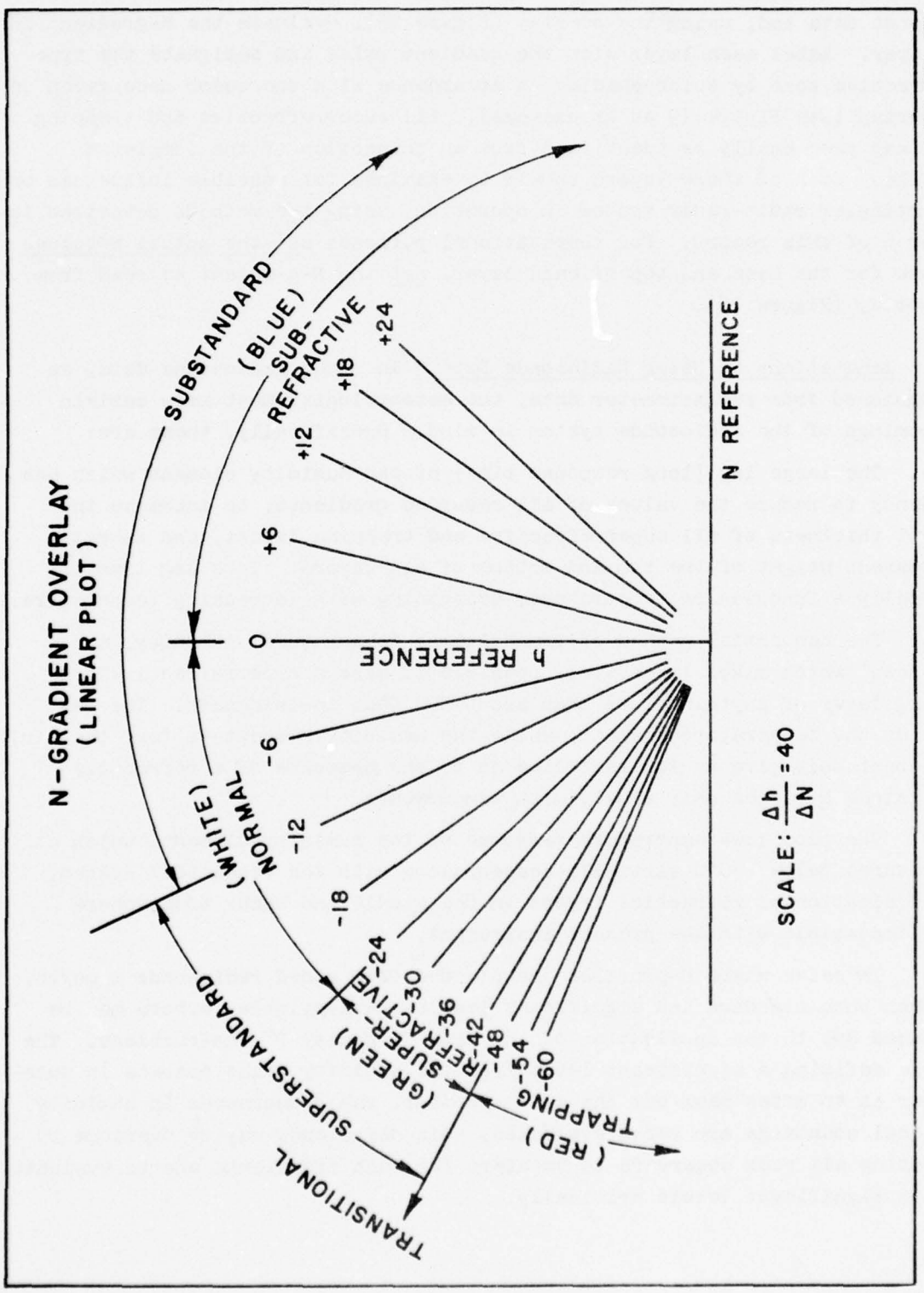

Figure 20. N-Gradient Overlay (Linear Plot).

In practice construct the N-profile from refractometer values or from radiosonde data and, using the overlay (Figure 20), evaluate the N-gradient in each layer. Label each layer with the gradient value and designate the type of refractive zone by color shading in accordance with the color code given on the overlay (see Figure 19 as an example). All superrefractive and trapping layers may then easily be identified from an inspection of the completed N-profile. Each of these layers should be examined for possible influences on the particular radio-radar system in operation, using the methods described in Chapter 6 of this report. For computational purposes use the actual N-values obtained for the base and top of each layer, not the N-gradient as read from the overlay (Figure 20).

3.3.4. Limitations in Using Radiosonde Data. In using radiosonde data, as distinguished from refractometer data, the meteorologist must keep certain shortcomings of the radiosonde system in mind. Specifically, these are:

a. The large lag (long response time) of the humidity element which has a tendency to reduce the values of all recorded gradients, to increase the apparent thickness of all superrefractive and trapping layers, and to raise the apparent height of the top and bottom of all layers. This lag time is principally a function of temperature; decreasing with increasing temperature.

b. The sequential method of transmitting temperature, humidity, and references, which makes it entirely possible to miss a superrefractive or trapping layer of anything less than about 300 feet in thickness. The response of the temperature element, while the humidity element is "off the air," can at best only give an indirect clue as to the presence of a refractive layer, since N varies only slowly with temperature.

c. The poor low-temperature response of the humidity element, which at temperatures below -40°C virtually ceases, along with the sequential system, makes evaluation of refractive layers in the middle and upper troposphere nearly impossible with the present instrument.

d. In cases where N-profiles are plotted from coded radiosonde reports, even when both standard and significant levels are available, errors may be introduced due to the application of the WBAN "Circular P" instructions. The criteria defining a significant level from the humidity trace operate in such a manner as to often mask out the all-important, rapid decreases in humidity. When local soundings are being evaluated, this deficiency may be overcome by instructing all raob observers to be alert for such transients and to evaluate humidity significant levels critically.

3.4. Modified Refractive Indices.

The B-, M-, A-, and K_p-modifications of refractivity are useful, particularly in ray tracing problems and in synoptic studies of refractivity. Each results in simplifications in ray geometry in certain situations, not only in plotting ray trajectories but also in the mathematical relationships describing various propagation mechanisms and in the study of climatic and synoptic relationships. There is much to be said, however, for retaining the unmodified refractivity N itself. It is a basic physical quantity, and as such is more easily understood than are B, M, A, or K_p. For the purposes of uniformity and initial simplicity, N-units are therefore the principal refractive index units employed in this report (except in Chapters 7 and 8). For reference purposes, however, a description of each of the modified indices is given in the following four subparagraphs.

3.4.1. B-Units. It is shown in section 4.2 that one can compensate for a linear refractive index gradient merely by changing the effective radius of the earth. The most convenient way to represent departures of a given refractivity-profile from the standard atmosphere (at least in the lowest layers where the departure of the N-gradient from the assumed constant value is negligible) is to add 12 N-units per 1000 feet to all N-values. This modified index, B, is defined as

$$B = N_h + 0.012h \tag{85}$$

where N_h is the value of refractivity at any height h in feet. A B-profile will have zero gradient in the lower layers of a standard atmosphere. The B-modification, therefore, is a logical consequence of the four-thirds earth radius concept described in section 4.2 because the B-gradient is zero for the same situation where the ray curvature is zero. A standard atmosphere B-profile is compared with standard N-, A-, and M-profiles in Figures 21 and 22. Note that in the lowest few thousand feet B has a zero gradient but at higher levels (where the departure of $\Delta N/\Delta h$ from an assumed constant surface value of minus 12 N-units per 1000 feet has become appreciable) B shows a small positive gradient.

3.4.2. M-Units. Another form of modified refractive index has been widely used, and is associated with the flat-earth concept of section 4.3. In this case, one adds 48 N-units per 1000 feet to all N-values. This modified index, M, is defined as:

$$M = N_h + 0.048h \tag{86}$$

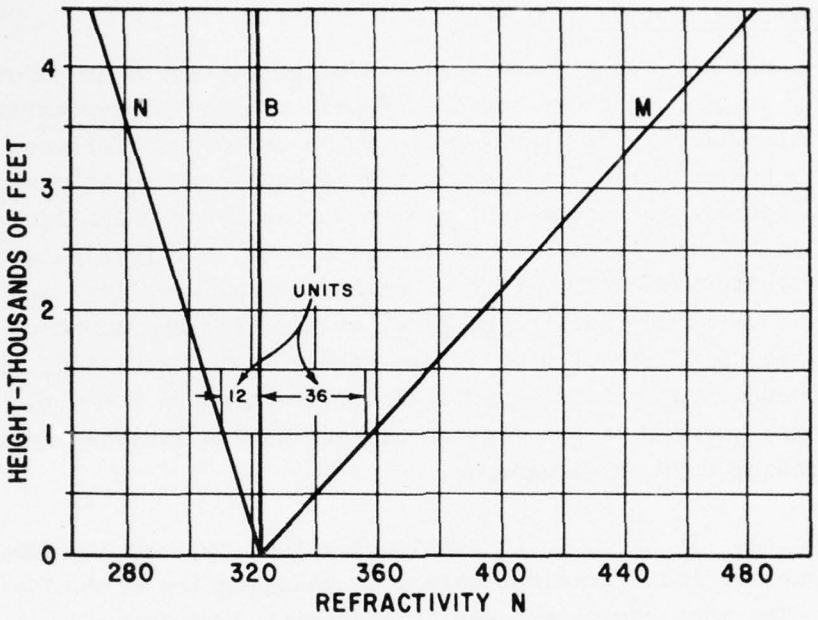

Figure 21. N-, B-, and M-Profiles for a Standard Atmosphere.

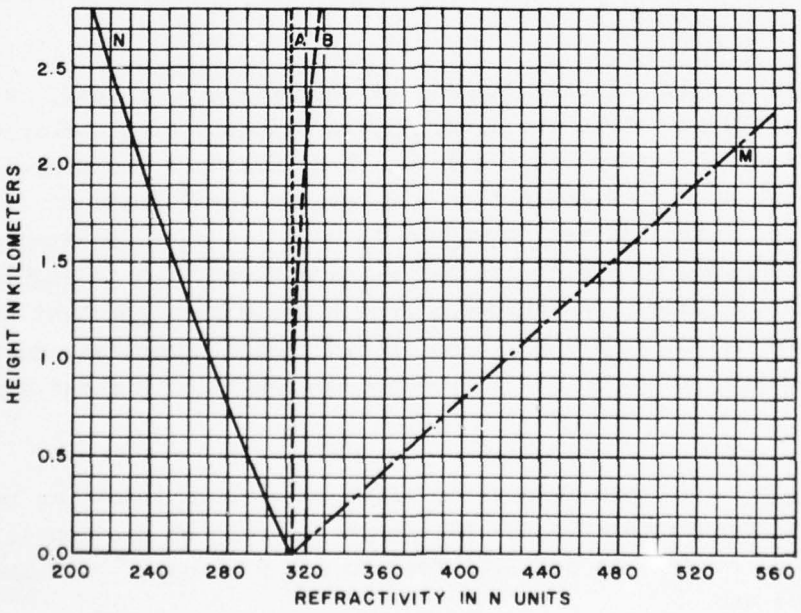

Figure 22. N-, A-, B-, and M-Profiles for a Standard Atmosphere.

where N_h is the value of refractivity at any height h in feet. When the M-gradient is zero the ray curvature is zero in the flat-earth case. This is another way of saying that when the N-gradient is minus 48 units per 1000 feet, the ray has the same curvature as the earth. Thus, if the earth's surface is represented as a straight line, the ray will also be straight. Figures 21 and 22 show a standard atmosphere profile, expressed in terms of N-, A-, B-, and M-units for comparison purposes.

3.4.3. A-Units. As we have seen the B-unit modified index overcorrects for the decrease in N with height in the standard atmosphere, as shown in Figure 22 by the increase of B with height. This overcorrection results from the assumption of a constant N-gradient (i.e., linear N-profile) having a value representative of the lowest few thousand feet of the standard atmosphere. A modified refractive index (potential refractivity) expressed in A-units has been defined by Bean, Riggs, and Horn [8] in order to eliminate this overcorrection. The expression for A, which is written in terms of an exponential height function, is given by

$$A = N_h + N_s [1 - \exp(c_e h)]$$

(87) or

$$A = N_h + 313 [1 - \exp(-0.144h)]$$

where N_h is the refractivity at height h, in kilometers. The decay coefficient $c_e = -0.144$ was determined so as to correspond best with the average station value of $N_s = 313$ for the United States (see Table 3, Chapter 4). Figure 22 shows a comparison between the standard atmosphere profile expressed in terms of N-, A-, B-, and M-units.

To facilitate the transformation of N-units to A-units, a potential refractivity chart was prepared and is given in Figure 23. This chart eliminates the necessity of using exponential tables in each individual calculation of A and thus lends considerable ease to the preparation of charts of the new parameter.

3.4.4. K_p-Units. In order to remove the height-dependent variations of refractivity in homogeneous air (the problem for which Bean proposed the A-unit modification) and to develop a modified index of fundamental meteorological relationships (rather than from essentially empirical considerations as Bean has done), a modified index (potential-refractive index) expressed in K_p-units has been defined by Jehn [23]. The expression for K_p is given by

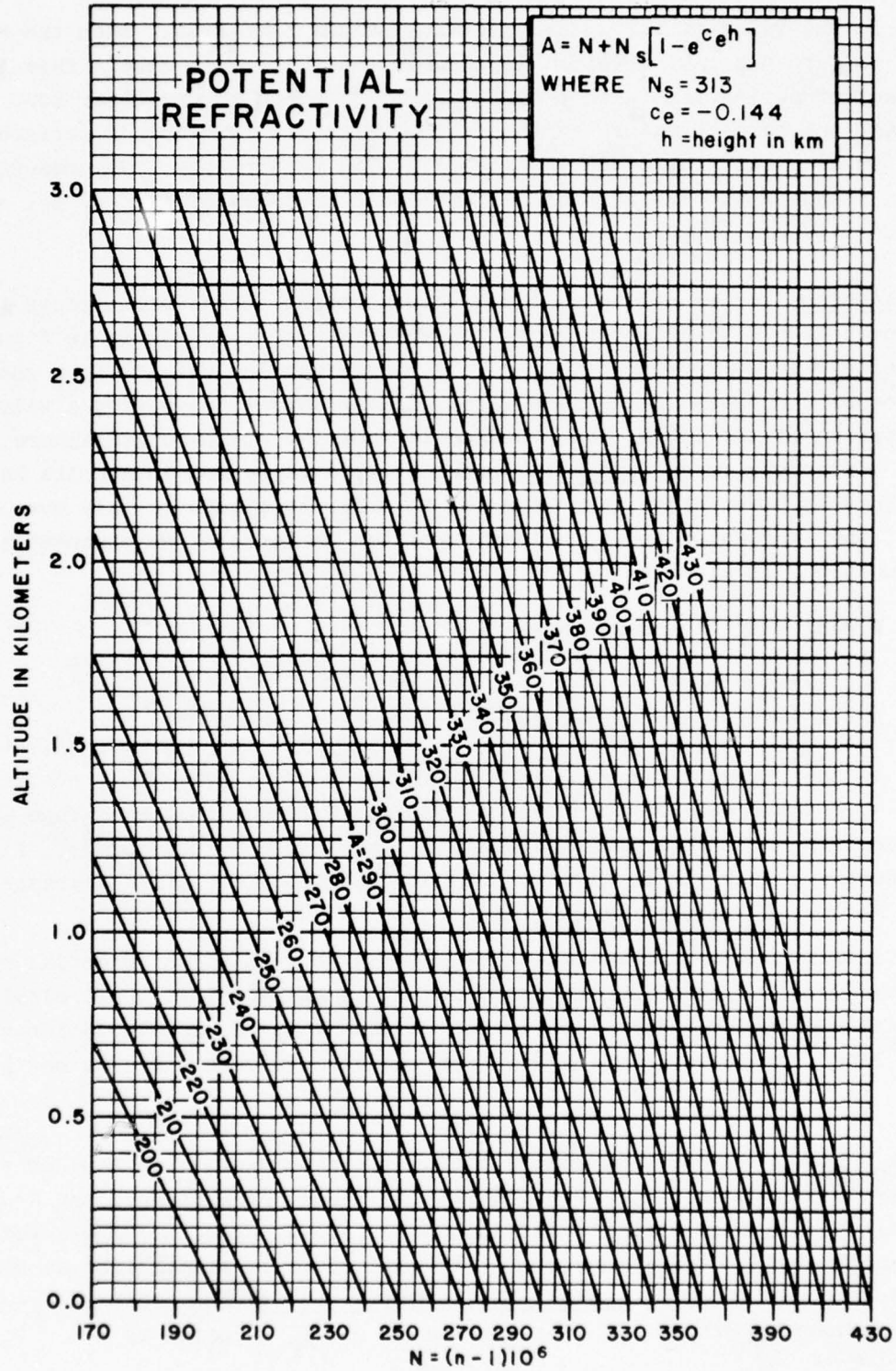

Figure 23. Potential-Refractivity Chart.

$$(88) \qquad K_p = \left(\frac{1000}{P} \right)^{0.714} \left[N_D + \left(\frac{P}{1000} \right)^{0.286} N_W \right]$$

where N_D is the conventional "dry" term and N_W the conventional "wet" term in the refractivity equation and P is the pressure in millibars at the point in question. Tables or graphs of the two multipliers could be prepared to facilitate the conversion from N-units to K_p-units, but as yet these are not available.

It should be noted that K_p-values are referred to the 1000-millibar pressure surface, and as a result the station-to-station variability of refractivity occasioned by differences in station elevation are strongly suppressed. In synoptic radio-meteorology this becomes an important factor.

Chapter 4

MODELS OF THE ATMOSPHERIC RADIO REFRACTIVE INDEX

In the preceeding chapter we have defined a standard refractivity profile in a standard atmosphere and have discussed the computation of N-gradient values in both the standard and the actual atmosphere. The various "modified" refractive indexes in current use were also described. In this chapter we shall discuss other atmospheric models and the effect of refractive gradients in these models upon propagation.

4.1. Refraction in a Standard Atmosphere.

We have seen that N decreases exponentially with height in the standard atmosphere and that, as a consequence, electromagnetic rays are bent downward by refraction in such an atmosphere. Figure 24 shows a radio frequency source of electromagnetic radiation above the surface of the earth. The lit zone (or interference zone) forms the locus of all direct paths, while the cross-hatched area below the grazing path is the diffraction region. Note that the radio horizon, C, lies beyond the geometric horizon, A, and the optical horizon, B. In a standard atmosphere the curvature of a radio ray is about one-fourth the curvature of the earth so that the radio horizon extends beyond the geometric horizon by about 15 percent. Tables have been calculated for radio horizon distance versus transmitter height in a standard atmosphere for several values of surface refractivity, N_s. The results of such a calculation are plotted in graphical form in Figure 25.

4.2. The Four-Thirds Earth Radius Concept.

In the first few thousand feet above the surface, the exponential decrease of N with height (in the standard atmosphere) may be closely approximated by a linear decrease. The upper sketch in Figure 26 shows the earth's surface and a tangent ray having a curvature equal to one-fourth the earth's curvature. At a given distance beyond the tangent point, a straight tangent line will be $d^2/2a$ above the surface, if we neglect second order terms (see Figure 4). At the same distance away, the straight line will be $d^2/2\ (\Delta n/\Delta h)$ above the curved ray. Assuming $\Delta n/\Delta h$ is constant and equal to $1/4a$, it follows that the ray will be $d^2/2\ (1/a - 1/4a)$ above the earth at the distance, d. The same height-distance relationship between ray and surface may be

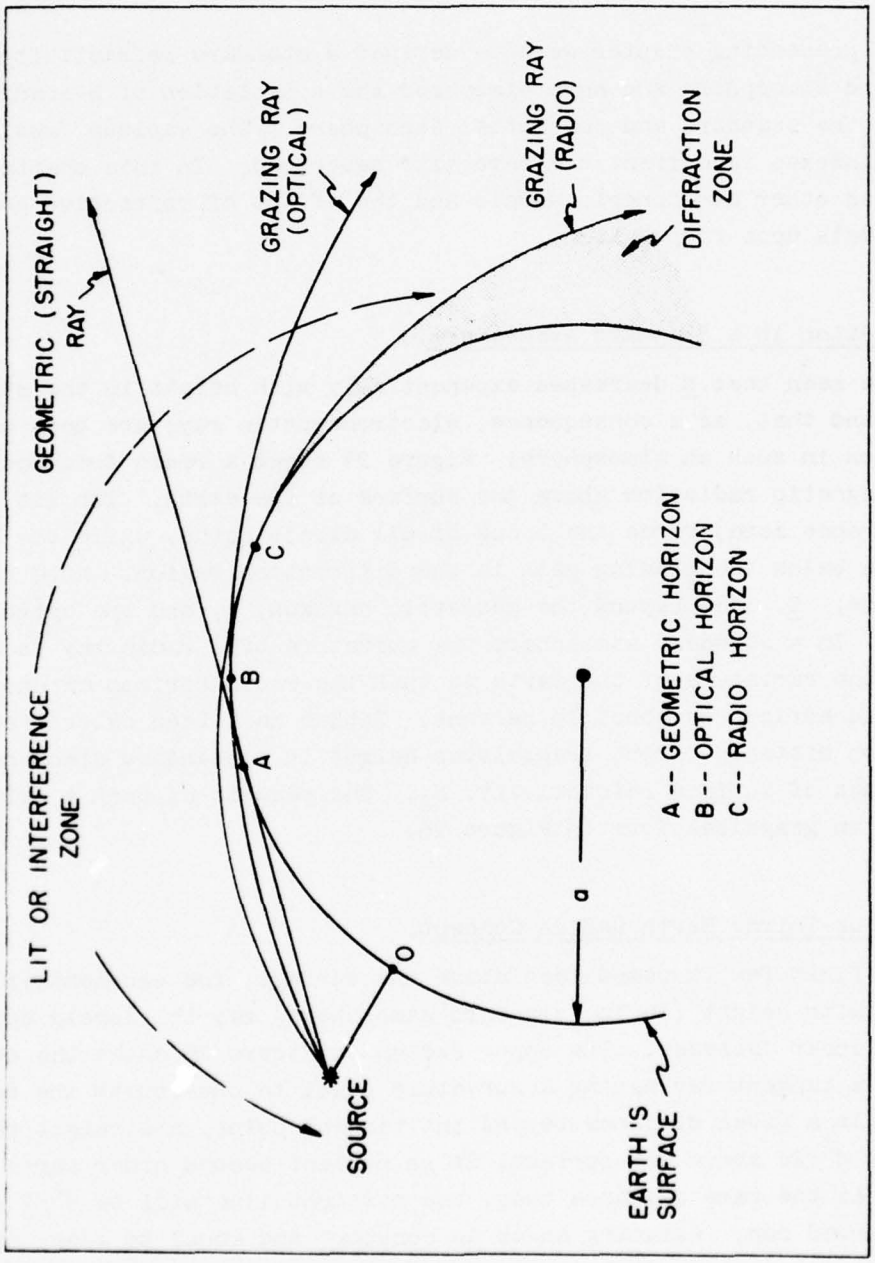

Figure 24. Ray Geometry for Spherical Earth—Standard Atmosphere.

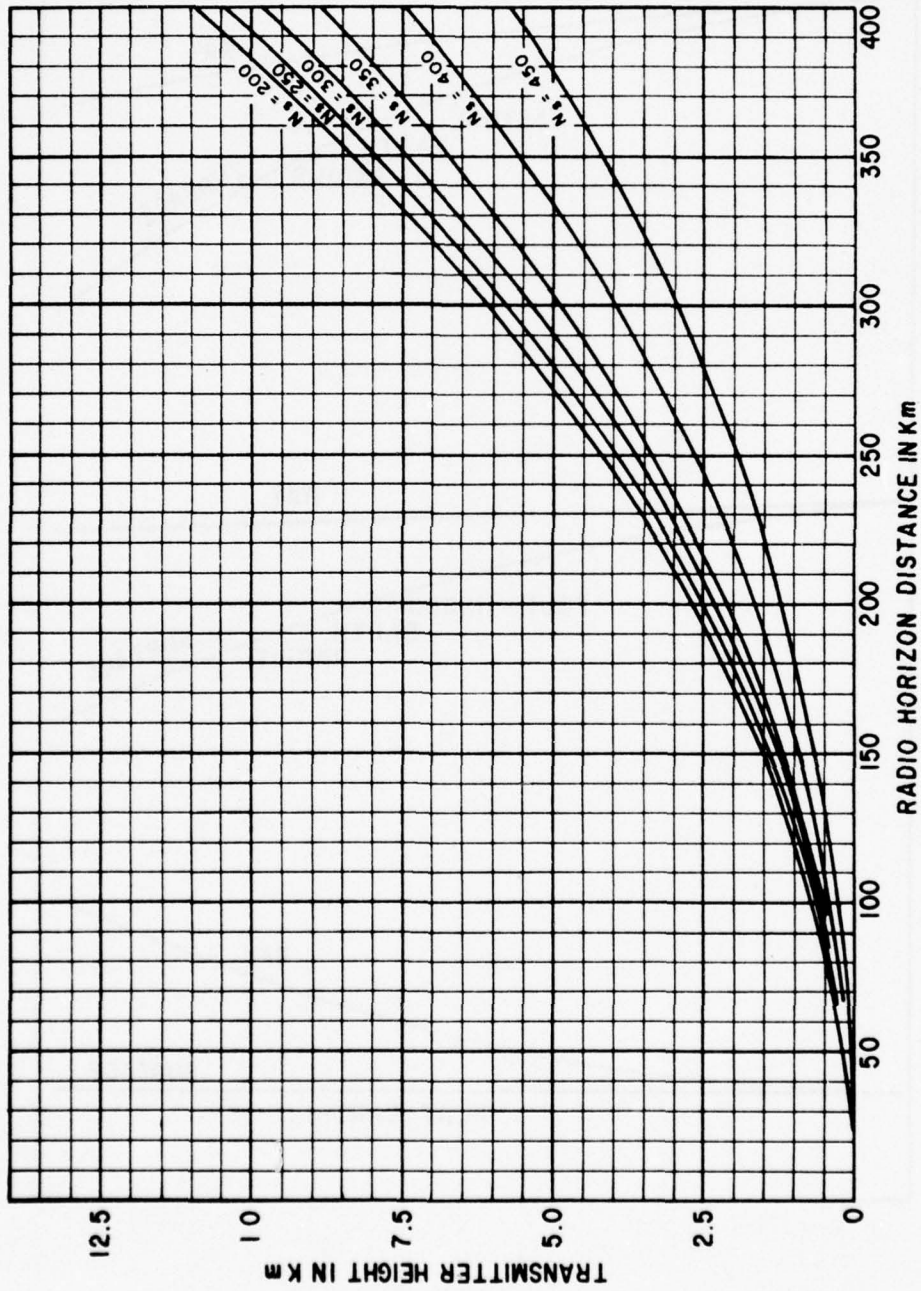

Figure 25. Radio Range versus Transmitter Height.

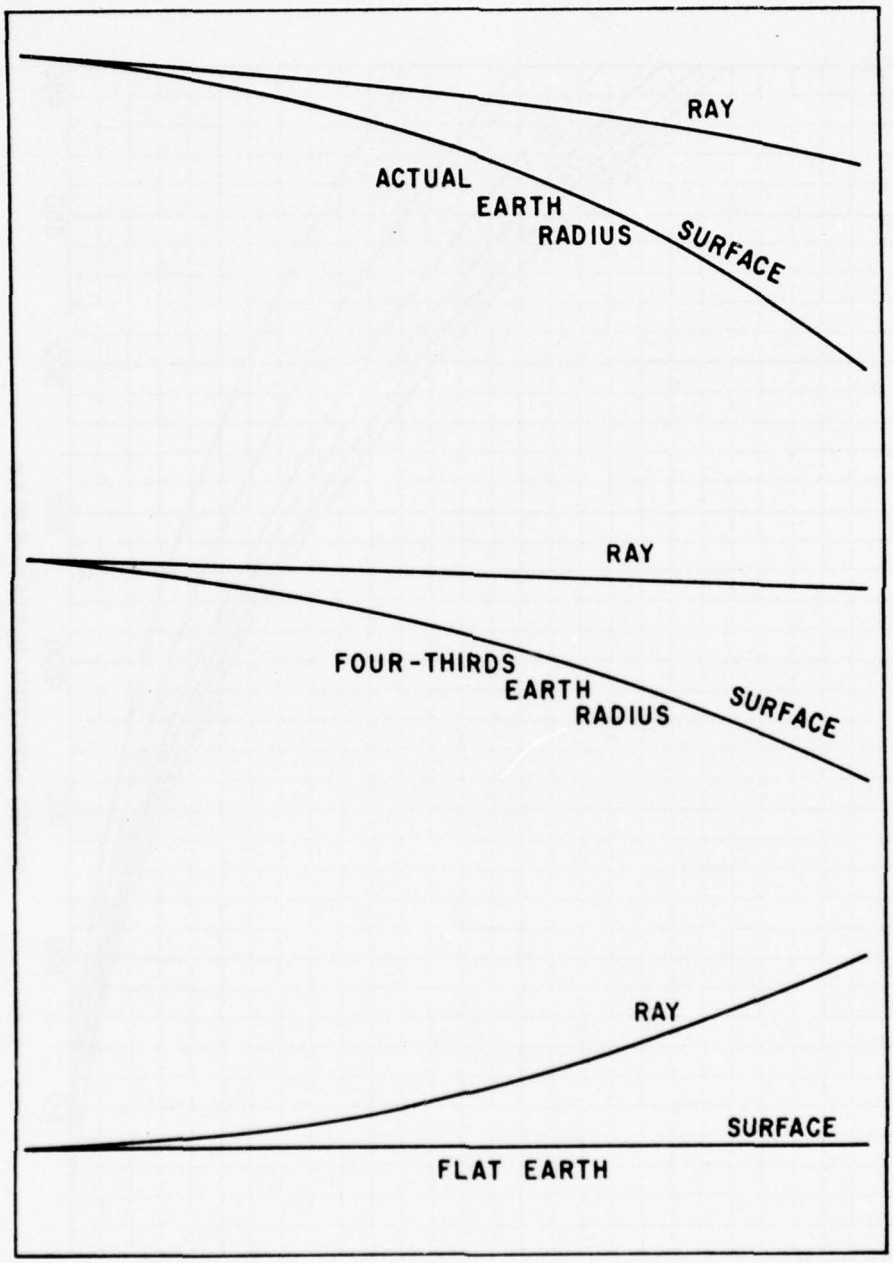

Figure 26. Comparative Ray Geometry.

obtained if one makes the ray straight and modifies the earth's radius to a new value a_e, such that

$$\frac{1}{a} - \frac{1}{4a} = \frac{1}{a_e}$$

or

$$a_e = \frac{4}{3} a \tag{89}$$

Thus, by making the effective earth's radius four-thirds as great as the true radius, the situation has been restored to that of the homogeneous atmospheric case (straight ray and curved earth)—see middle sketch in Figure 26. This method, advanced by Schelleng, Burrows, and Ferrell [31], assumes an earth suitably larger than the actual earth and allows radio rays to be drawn as straight lines over this earth rather than as curved rays over an earth with true radius a.

In general, the effective earth's radius $a_e = ka$, where k is the effective earth's radius factor and a is the true radius of the earth. The value of k is usually assumed to be four-thirds in the United States. It is desirable, however, in some geographic areas to use a somewhat different value of k, for example in desert areas it is more nearly six-fifths. One may write in general

$$k = \frac{1}{1 + a \frac{\Delta n}{\Delta h}} \tag{90}$$

where $\Delta n/\Delta h$ is the assumed linear gradient of the index of refraction (usually negative), applying to a particular area or season and a is the sea-level radius of the earth.

In the four-thirds atmosphere concept the refractivity gradient $\Delta N/\Delta h$ is -12N/1000 feet. This gradient is frequently called the standard gradient. Propagation conditions for gradients less than standard (larger negative values) are called superstandard (superrefractive) and those greater than standard (smaller negative values) are called substandard (subrefractive). When the rate of change of refractivity with height is equal to -48N/1000 feet, the curvature of the rays will be the same as that of the earth's surface and is called transitional (see Figure 20).

This method of accounting for atmospheric refraction permits a tremendous simplification in the computation of radio field strengths even though the distribution of refractive index (linear with height) implied by this method is realistic only in the lowest few thousand feet of the atmosphere.

4.3. The Flat-Earth Concept.

For some purposes, it is desirable to portray the earth as being flat with upward curving rays. This is done by subtracting the earth's curvature from both ray and earth. This results in an upward ray curvature equal to the downward curvature given to the earth in the situation described in section 4.2 (see bottom sketch in Figure 26). This representation is not now widely used because of its unrealistic portrayal of the earth-ray relationship. However, there are instances, such as ray plotting by analogue computers, where it is advantageous to use the flat-earth type of presentation.

4.4. Central Radio Propagation Laboratory (CRPL) Exponential Reference Atmosphere.

Evaluation of atmospheric refraction effects on UHF-VHF radio propagation has long been accomplished with the convenient four-thirds earth concept described in section 4.2. However, long-range radar applications have demanded a model of atmospheric radio-refractive index more representative of observed refractive index profiles than the simple linear decay inherent in the four-thirds earth approach.

4.4.1. Development of Model. A simple and more accurate model has been proposed and adopted by the CRPL of the National Bureau of Standards for use in the prediction of refraction phenomena. This model assumes an exponential decrease of $\underline{N}$ with height defined by equation (81) and the gradient of $\underline{N}$ defined by equation (84) which may be written as

$$\frac{\Delta N}{\Delta h} = \eta_1 \exp(-\eta_2 h) \tag{91}$$

The most extensive source of data with which to evaluate the coefficients in equation (91) is that of ΔN which is the difference between $\underline{N}$ at one kilometer above the earth's surface and the surface value N_s ($\Delta N = N_{1\ km} - N_s$). Thus, equation (91) takes the form

$$\Delta N = \eta_1 \exp(-\eta_2) \tag{92}$$

for the special case of $\Delta h = h = 1$ km. Examination of the ΔN data revealed that η_2 was dependent upon N_s, i.e., the higher the surface value of $\underline{N}$ the greater the expected drop in $\underline{N}$ over 1 kilometer. Examination of the data indicated that

$$\eta_2 = \eta_3 N_s$$

and the resultant equation

(93) $\Delta N = \eta_1 \exp(-\eta_3 N_s)$

was solved by least squares. The least squares determination was facilitated by converting (93) to the form

(94) $\ln |\Delta N| = - \eta_3 N_s + \ln \eta_1$

or, in words, expressing the natural logarithm of ΔN as a linear function of N_s. The values of η_1 and η_3 were established from some 888 sets of 8-year means of ΔN and N_s from 45 US Weather Bureau stations. The results of this study [9] are shown graphically in Figure 27 where the least squares exponential fit of $\overline{\Delta N}$ and $\overline{N}_s$ is given by

(95) $-\overline{\Delta N} = 7.32 \exp(0.005577 \overline{N}_s)$

From this equation the CRPL Exponential Reference Atmosphere was determined, the profiles being defined by the following equations:

(96) $N = N_s \exp(-c_e h)$

(97) $c_e = \ln \left(\frac{N_s}{N_s + \overline{\Delta N}} \right)$

This model is a close representation of the average refractivity structure within the first three kilometers. It also has the advantage of being a continuous function and therefore may be used for theoretical studies. The specific values of the constants employed in equations (96) and (97) are given in Table 3. In Figure 28 the bending in the four-thirds earth atmosphere is compared with that in the CRPL exponential reference atmosphere. The bending in an "average" atmosphere is also given. This "average" atmosphere is a composite of the 5-year mean profiles for both summer and winter at eleven US radiosonde stations and was used as a readily available measure of average conditions. The important point made in Figure 28 is that the four-thirds earth model is systematically in disagreement with average bending; at low heights it gives too little bending while at high altitudes it gives too much bending. The exponential reference atmosphere does not appear to be systematically biased, and deviates less than 5 percent from the average atmosphere. It is significant that the exponential reference and the average atmosphere are in essential agreement as to the shape of the bending-height curve.

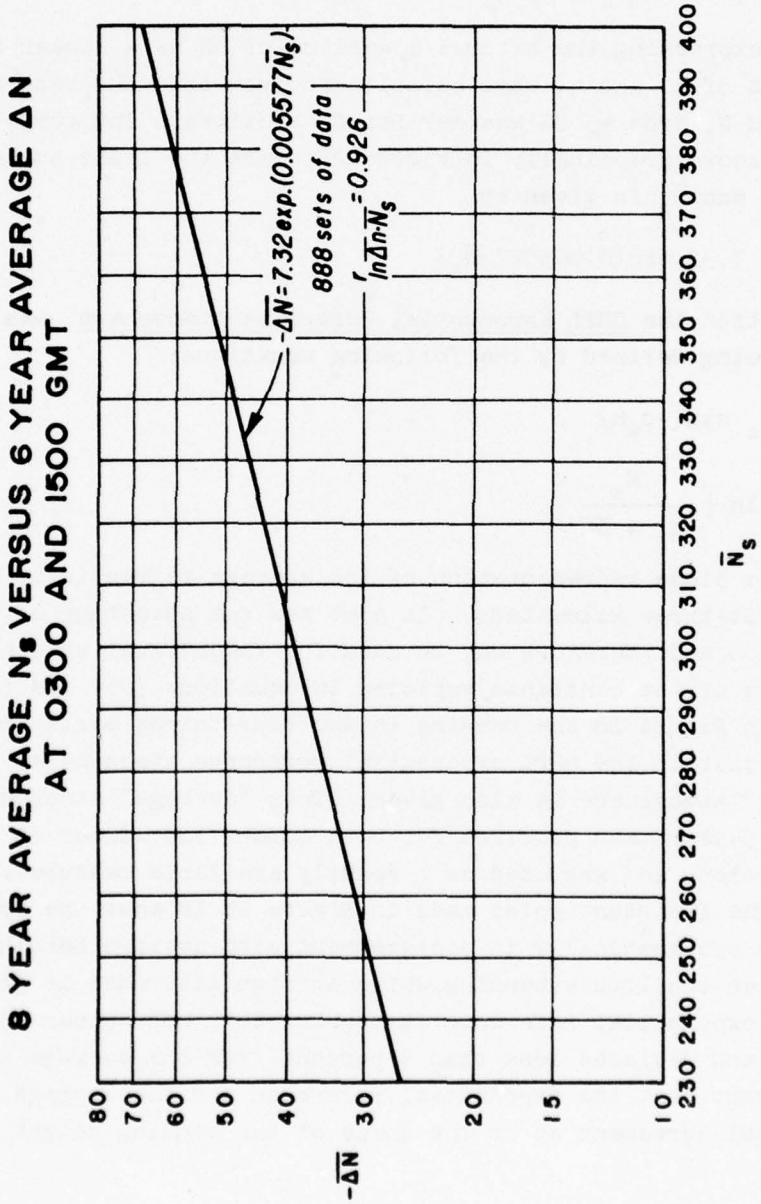

Figure 27. Regression of ln $|\overline{\Delta N}|$ upon $\overline{N}_s$.

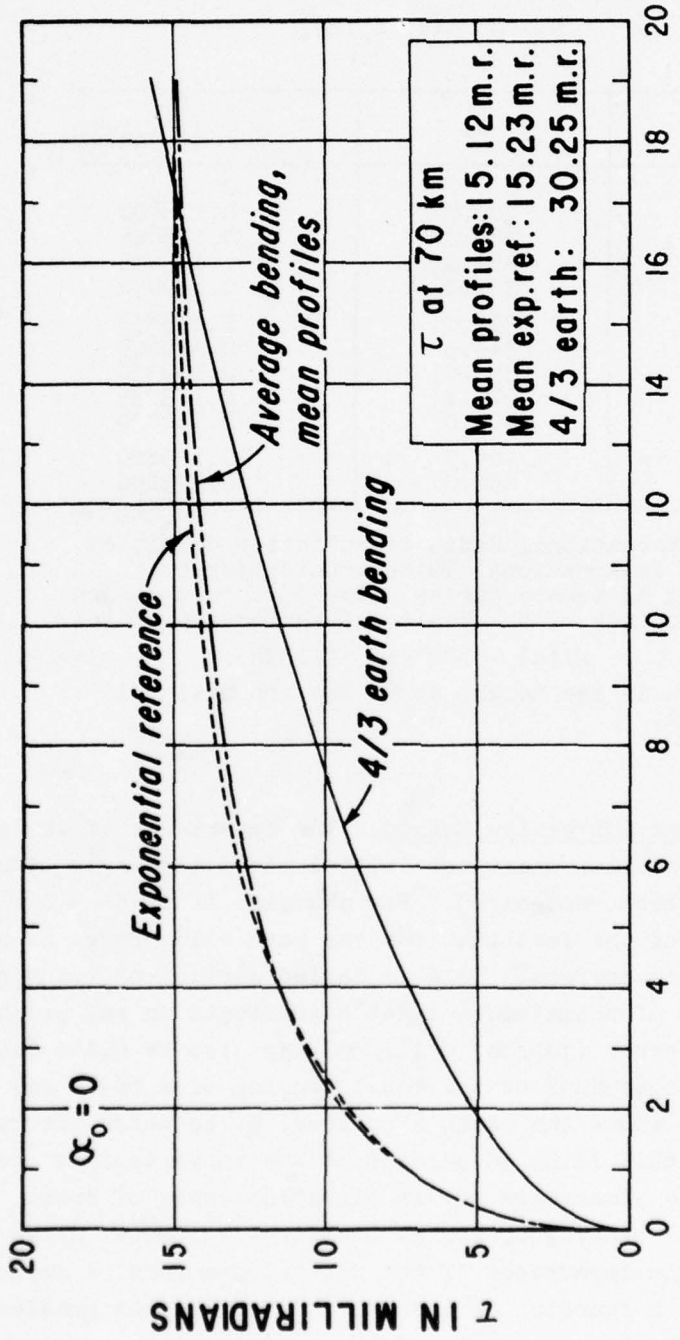

Figure 28. τ Versus Height.

TABLE 3

Table of the Constant c_e for the CRPL Exponential Radio Refractivity Atmospheres*

$$N = N_s \exp[-c_e(h)]$$

ΔN	N_s	c_e per kilometer
0	0	0
22.3318	200.0	0.118400
29.5124	250.0	0.125625
30.0000	252.9	0.126255
39.2320	301.0	0.139632
41.9388	313.0	0.143859
50.0000	344.5	0.156805
51.5530	350.0	0.159336
60.0000	377.2	0.173233
68.1295	400.0	0.186720
70.0000	404.9	0.189829
90.0406	450.0	0.223256

* The International Radio Consultative Committee of the International Telecommunication Union meeting in Geneva during July 1958, recommended the adoption of the basic reference atmosphere:

$$N(h) = 300 \exp(-0.139h)$$

where h is the height above the ground in kilometers.

4.4.2. Initial-Gradient Correction Method. The importance of the initial gradient in radio propagation where the initial elevation angle of a ray path is near zero has long been recognized. For example, if $dN/dh = 1/r_o$ then $\Delta\tau = \infty$, an expression of the fact that the ray path will travel at a constant height above the earth's surface. This is called ducting or trapping of the radio ray. The effect of anomalous initial N-gradients on ray propagation at elevation angles near zero, ($|dN/dh| < 157/km$) may also be quite large. In Figure 29, where the percentage of the total bending of a radio ray is given in terms of the height above the earth's surface, h, to which the radio ray has traveled, we note that fully 30 percent of the total bending occurs in the first 100 meters of the atmosphere for an elevation angle of zero. Similarly, 60 percent of the total bending occurs in the first kilometer above the earth's surface. In view of the importance of the initial gradient, a method was devised to estimate τ as a function of both N_s and the initial gradient of N, which will be denoted by $\delta N'$.

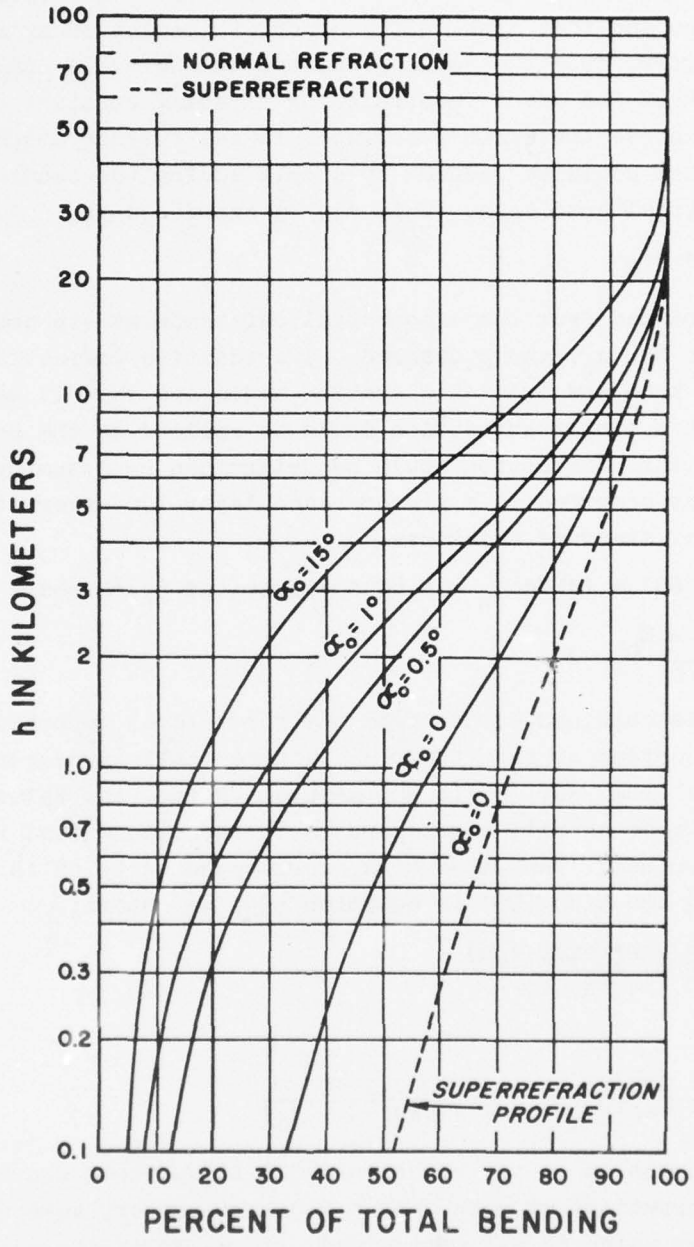

Figure 29. Percent of Total Bending.

For the development of this method it was assumed that the exponential reference atmosphere defined the expected bending under any refractive-index profile conditions and that most of the error of prediction arises from the fact that $\delta N'$ differs from the value predicted by the model atmosphere. Since it was observed that the error in predicting τ became constant after the first 100 meters or so above the earth's surface, it was further assumed that this error of prediction could be reduced by simply adding the bending due to the difference in initial gradients. This may be expressed as:

$$\tau = \tau_E + \delta\tau_E \tag{98}$$

where τ_E is determined from the exponential reference atmosphere for the particular values of N_s, α_o, and $\underline{h}$ desired. The additive correction factor, $\delta\tau_E$, is a function of both the initial elevation angle and δN. It was assumed, arbitrarily, that a single correction could be applied to the bending at all heights and that this correction could be determined by assuming that the initial N-gradient occurred in a ground-based layer 100 meters thick, regardless of the actual observed thickness.

In practice $\delta N' \equiv (dN/dh)_h$ may be approximated by δN where

$$\delta N \equiv \frac{N_s - N_h}{h} \tag{99}$$

The value of N_h is obtained either from the first level reported by the radiosonde above the surface or from tower or tethered balloon measurements, $\underline{h}$ will range in practice from, say, 30 to 300 meters. First, the value of N_s, which the observed value of δN will correspond to in the exponential reference atmosphere is determined. The value of N_s corresponding to δN is designated as N_s^*. Substituting equation (96) in equation (99) we obtain:

$$-\delta N = \frac{N_s^* - N_s^* \exp(-c_e h)}{h} \tag{100}$$

or

$$N_s^* = \frac{-\delta N\,(h)}{1 - \exp(-c_e h)} = \frac{-0.1\,\delta N}{1 - \exp(-0.1\,c_e)} \tag{101}$$

In the second expression on the right in (101) it has been assumed for the purpose of the correction process that $h = 0.1$ kilometer, regardless of the actual height over which δN was determined. Thus, N_s^* is the value of N_s specified by the exponential reference atmosphere when the $\underline{N}$ difference between the surface and 100 meters is equivalent to δN.

The additive correction factor is then the simple difference between the 100-meter layer bendings as determined by N_s and N_s^* which may be obtained from Figure 30. This may be expressed as:

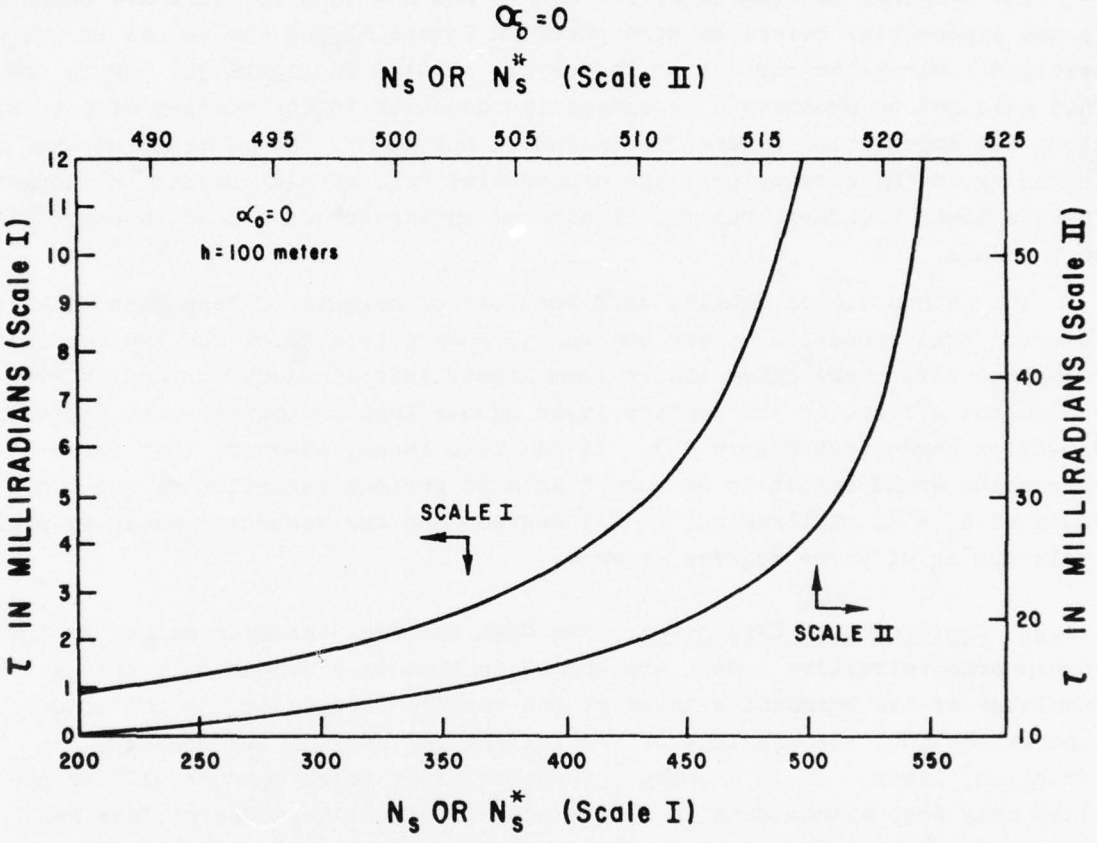

Figure 30. τ Versus N_S Exponential Reference Atmosphere Height Increment 0 to 100 Meters.

(102) $$\delta\tau_E = \tau_{0.1}(N_S^*) - \tau_{0.1}(N_S)$$

where the subscript 0.1 refers to the bending in the initial 100 meters above the surface.

This method of prediction was tested by comparison with bending data obtained from 22 different N-profiles typical of long-term mean conditions as well as 67 individual N-profiles typical of superrefraction and elevated-layer conditions. The superrefractive profiles, which comprised 32 of the 89 profiles, were those with an initial layer in which N decreased more rapidly than -100 N-units/kilometer as compared to the normal decrease of about -45 N-units/kilometer.

The original bending data, for $\alpha_o = 0$ and h = 70 kilometers are compared to the exponential reference atmosphere in Figure 31 and the values of the observed τ minus the correction factor are plotted in Figure 32. It is seen that this method produces a considerable reduction in the scatter of points about the exponential reference atmosphere curve. By the addition of the initial-gradient corrections, the exponential reference atmosphere no longer forms a lower boundary, but rather has the appearance of a least squares fit to the data.

The method yields equally good results for heights of less than 70 kilometers. Some reduction of the scatter of data points about the exponential reference atmosphere curve occurs from higher initial elevation angles even though the effects of the surface layer become less pronounced with increasing elevation angle (see Figure 29). It has been found, however, that the $\delta\tau_E$ correction would result in no more than a 50 percent reduction of the r.m.s. error at α_o = 10 milliradians ($\sim$ 0.5 degree) and the reduction would be negligible for α_o of three degrees or more.

4.4.3. Employment of CRPL Model. The CRPL methods, based on models of the atmospheric refractive index, are unique in that they depend only upon a knowledge of the refractive index at the earth's surface or, in the case of superrefraction, the gradient of the refractive index in the boundary (friction) layer. It is assumed, of course, that these methods will be applied only when either details of the actual refractive-index profile are unknown or it is impractical to obtain these details. If details of the refractive-index profile are available from either refractometer or radiosonde ascents, then one can evaluate refraction effects with the aid of an electronic computer or with simplified graphical techniques discussed in Chapter 6. However, if one wishes to obtain a quick evaluation of some refractive effect, he may consult the rather extensive tables of the CRPL Experimental Reference Atmosphere (see Vol. II, Appendix A). These tables make possible, for instance, the determination of the elevation-angle error as a function of α_o, N at the earth's surface, and the radar range.

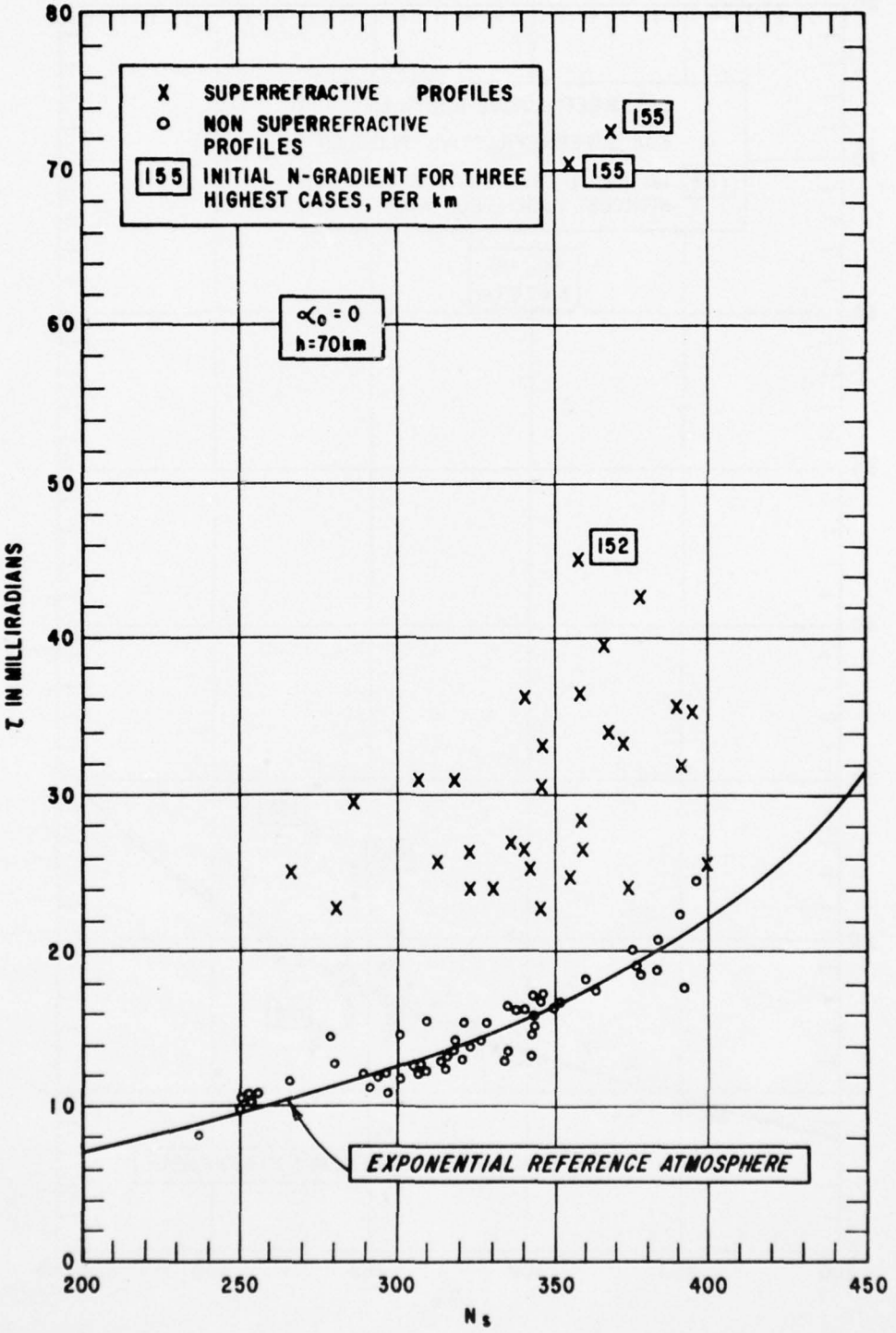

Figure 31. τ Versus N_s from 89 Profiles Compared with Values Predicted by the Exponential Reference Atmosphere.

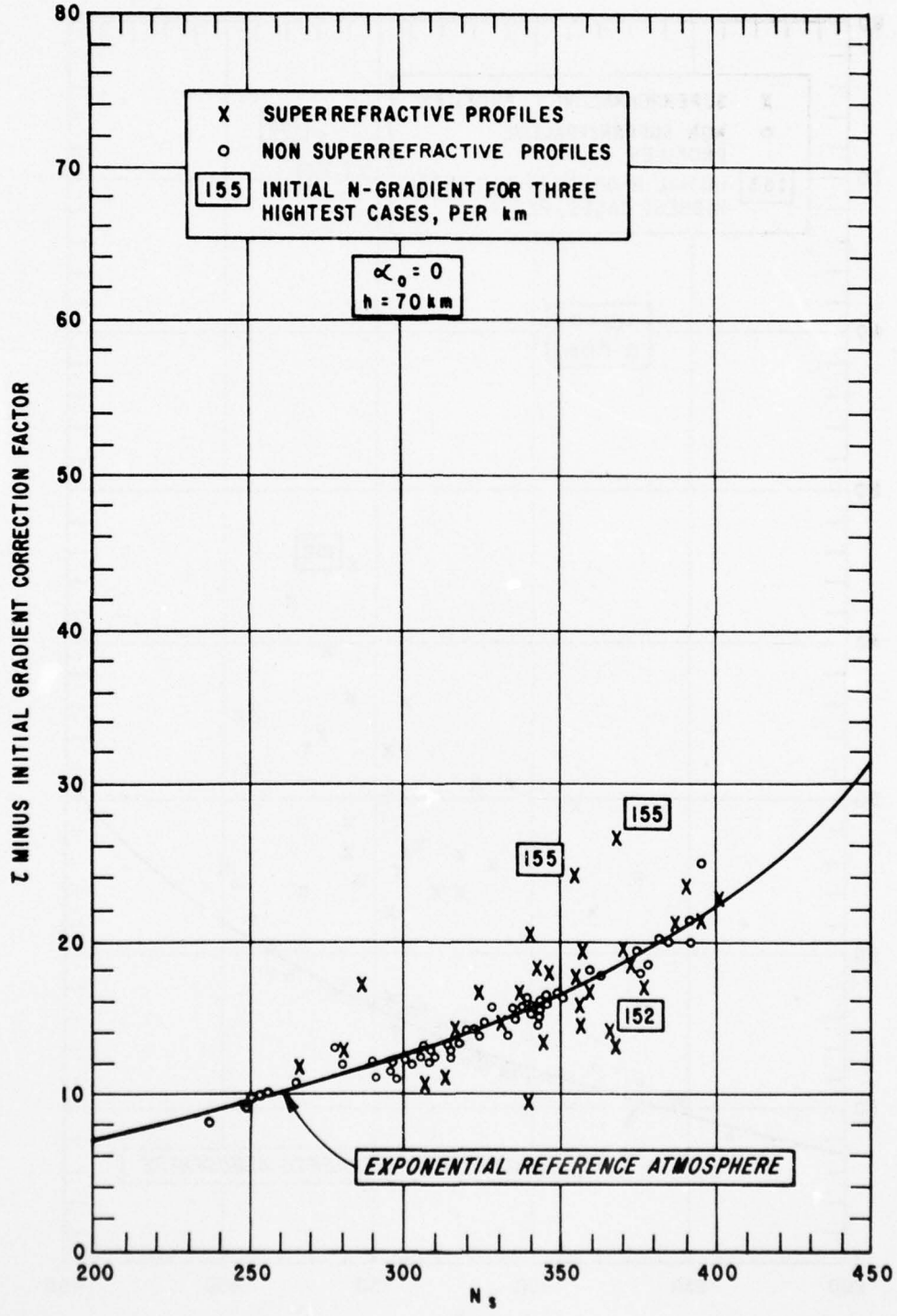

Figure 32. Corrected τ Versus N_s from 89 Profiles and the Values Predicted by the Exponential Reference Atmosphere.

Chapter 5

REFRACTION IN THE ACTUAL ATMOSPHERE

Thus far, the discussion has been concerned with the propagation of radio waves under artificial situations; an earth enveloped by a homogeneous atmosphere, and one with an atmosphere in which refractivity decreases smoothly (linearly or exponentially) with height. As a final step, it is now in order to consider the actual atmosphere and its effects on propagation.

There are numerous ways in which the troposphere departs from the simple linear or exponential gradient model. In a well mixed troposphere, for example, there are a myriad of small random variations in N, both in vertical and horizontal planes. Even at a fixed point, N is found to vary in a random way about some mean value. These fluctuations are caused by parcels of air with different temperatures and/or vapor pressures than those of their surroundings. Most parcels are caused by unequal heating, during the daytime, of air in contact with the ground. The warmer parcels rise convectively and drift with the wind until they are broken up and eventually lose their identity through turbulent mixing with the surrounding air. Similarly, air overlying lakes, rivers, and oceans becomes more moist than its surroundings and rises because of its lower density. Refractometer measurements show that the root-mean-square value of the N fluctuations decreases exponentially with height in a well mixed atmosphere. This is a priori evidence that the source of the small-scale variability of N is mainly at the surface.

5.1. Anomalous Propagation.

In some cases the actual refractive-index profile in the atmosphere departs from the linear and exponential models enough to cause radio and radar fields to be much stronger well beyond the horizon than would be expected from standard refraction and diffraction. These situations are generally caused by the presence of steep, negative, vertical gradients of refractivity in layers, which in turn cause the radio waves to be bent downward sufficiently to continue some distance on around the figure of the earth. A discussion follows of the development and of the characteristics of these so-called trapping or ducting layers.

5.1.1. Surface Layers. The actual troposphere departs most frequently from standard in the lowest few hundred feet. These surface layers, in which the

N-gradient is much steeper than minus 12 units per 1000 feet, are caused by nocturnal radiational cooling, by evaporation, or by advection. Frequently the N-gradient, particularly just above the ground, is considerably stronger than minus 48 units per 1000 feet, such that a ray actually has a downward curvature greater than the earth's curvature. If the layer is thick enough compared to the propagation wavelength, energy is guided around the figure of the earth in the layer, causing fields beyond the horizon to be very much stronger than normal. Because of the wave nature of radio energy, it turns out that the layer thickness must exceed a certain critical value, which is a function of wavelength and of the shape of the N-profile, before guiding or ducting of the wave can occur.

When the layer becomes particularly intense, the horizontally directed energy from a transmitter located within the layer will be completely contained in the layer; in this instance the fields will decrease as the square root of distance rather than as the first power of distance. At some distance beyond the horizon, these fields would then theoretically not only be stronger than the diffracted fields, but would even be stronger than the free space fields. Such intense layers have not actually been found in the atmosphere. The strongest fields observed in surface ducts have been about equal to the free space fields. When the fields approach this level, the energy is said to be trapped. The refractivity profile requirements for trapping radio energy of various wavelengths are described in more detail in section 6.1.

a. Radiation Ducts. Nocturnal radiational cooling of the ground surface may produce radiation ducts. They are particularly intense over dry or desert areas, where there is little water vapor in the air to intercept and return outgoing, long-wave radiation back to the ground. Calm nights tend to intensify duct formation because there is little mechanical turbulence to mix the cool lower layers with the warmer air above. The typical N-profile is exponential in shape, merging with the standard gradient at heights of a few hundred feet. Measurements in southwestern Arizona by Day and Trolese [15] showed that usually the profile is standard at sunset, with the surface N-value increasing as the night progresses. At sunrise, the surface N-value has typically increased by about 15 units while the values above 500 feet have increased by only 2 or 3 units. Usually the top of the duct is arbitrarily taken to be the height where the gradient is minus 48 units per 1000 feet. A typical value of this height at sunrise in Arizona is about 50 feet. Such a duct would be expected to trap wavelengths shorter than about 30 centimeters, and experimental results [15] show this to have been the case.

b. Evaporation Ducts. Over the ocean, surface refracting layers are caused by a different process than that described in (a) above. Diurnal

temperature changes over large bodies of water are usually quite small. This is because solar energy penetrates well beneath the sea surface. Therefore, a relatively large amount of heating is required to change the sea surface temperature. Radiational cooling, which does occur, makes the surface water heavier than the underlying water, so it sinks, bringing up warmer water from below. The surface temperature, therefore, remains practically constant ($< 1°C$) night and day. Daytime heating can cause a thin surface layer of higher temperature, but wave action usually rapidly mixes this layer with the cooler water below.

Evaporation from the sea surface, on the other hand, causes air parcels to be carried aloft by buoyancy, and thus gives rise to a steep gradient of water vapor pressure (and hence of N) in the first few hundred feet above the sea. While instantaneous N-profiles show wide fluctuations, the average over several minutes shows a profile which is exponential in shape when the air and sea are the same temperature. When the air is warmer than the sea the profile is more nearly linear; i.e., the N-gradient changes more slowly with height. In the unstable case (sea warmer than air), the gradient decreases more rapidly with height than in the neutral case (sea and air temperature the same). An interesting consequence of the physical processes which take place in the formation of an evaporation duct, is that in the stable case, low wind speeds favor strong duct formation; while in the unstable case, high wind speeds favor strong ducts. These hypotheses have been verified in data taken over the Irish Sea by Anderson and Gossard [2].

c. Advection Ducts. Another process by which surface layers with superstandard N-gradients can be formed, is the advection of dry air over the sea. If the air is colder than the sea, vertical convection takes place which tends to disperse air parcels with high refractivity upward, thus producing a weak but thick surface layer which does not usually affect propagation appreciably.

However, if the air is warmer than the sea, stability will keep the cool, moist (high N) air confined to a thinner layer. This gives rise to surface layers in which the N-gradient can be strong enough for trapping and at the same time be thick enough to affect longer wavelength energy than is the case with evaporation ducts. This situation is prevalent over the Mediterranean, Red Sea, and Gulf of Arabia.

5.1.2. Elevated Layers. Thus far, processes which cause persistent departures of N in atmospheric layers close to the earth or sea surface have been considered. These layers are caused by processes taking place at the surface itself. There is another class of phenomena which gives rise to strong N-gradients at some height above the surface. Refractometer studies have shown that

these elevated layers exist to some extent over wide geographic areas. In fact, very few refractometer profiles have been taken which do not show the presence of at least one elevated layer within 10,000 feet of the earth's surface.

Most of these layers are only a few hundred feet in thickness and the change of N from top to bottom averages about 10 units. Some layers can be traced for tens of miles in horizontal extent while others, particularly the weaker ones, are less than 10 miles in extent. Figure 33 shows an N-profile through an idealized elevated layer. Several parameters of interest are shown; the intensity, ΔN_L, the thickness, Δh, and the heights of the top and bottom of the layer, h_T and h_B, respectively. It will be noted that the N-gradient is shown as being standard below and above the layer. This is usually the case although nominal departures from standard are often found.

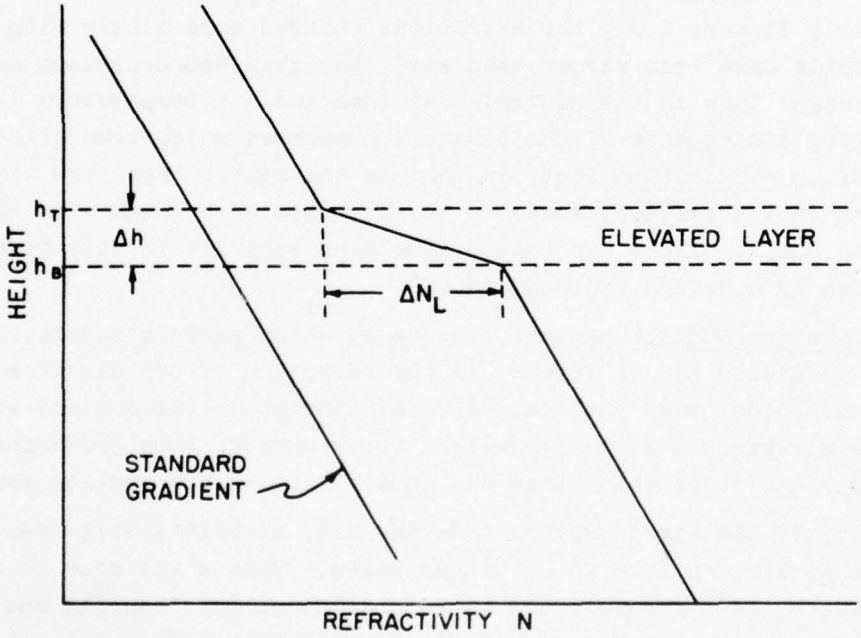

Figure 33. N-Profile—Elevated Layer.

Figure 34, shows the effect of such an elevated layer on rays emanating from a transmitter located well below the layer bottom. The four-thirds earth's radius modification has been used in constructing the earth and layer boundaries. Since (as shown in Figure 33) the N-gradient is standard outside the layer, the ray paths above and below the layer are straight lines. In the

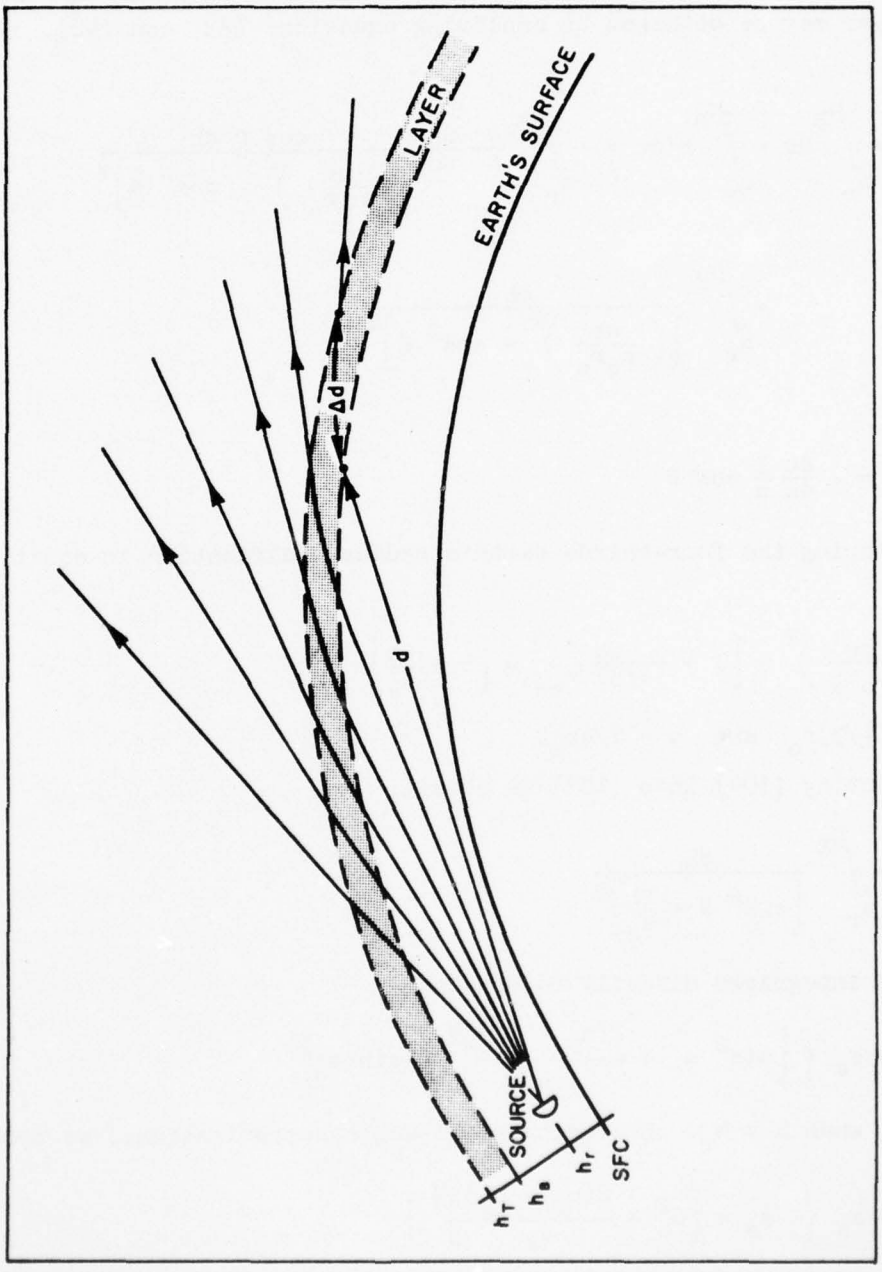

Figure 34. Ray Refraction by an Elevated Layer—Radar Well Below Layer.

layer itself, the N-gradient exceeds standard, therefore, the rays bend downward.

An expression for the distance $\underline{d}$ between the radar and the base of the elevated layer may be obtained by employing equations (33) and (40). We obtain:

$$(103) \qquad d = \int_{h_r}^{h_B} ds = \int_{h_r}^{h_B} r' d\tau = -\int_{h_r}^{h_B} \frac{r'}{n} \frac{dn}{dh} \frac{\cos\theta \, dh}{\left[\left(\frac{nr}{n_o r_o}\right)^2 - \cos^2\theta\right]^{1/2}}$$

$$= \int_{h_r}^{h_B} \frac{dh}{\left[\left(\frac{nr}{n_o r_o}\right)^2 - \cos^2\theta\right]^{1/2}}$$

where

$$\frac{1}{r'} = -\frac{dn}{dh}\frac{1}{n}\cos\theta$$

By employing the four-thirds earth's radius modification in equation (43) we obtain:

$$(104) \qquad \left(\frac{nr}{n_o r_o}\right)^2 \simeq \left[1 + \frac{2h}{(4/3)\, r_o}\right] = \left[1 + \frac{2h}{a_e}\right]$$

where $a_e = (4/3)r_o$ and $\gamma = 1/4r_o$.

Substituting (104) into (103) we obtain:

$$(105) \qquad d = \int_{h_r}^{h_B} \frac{dh}{\left[\sin^2\theta + \frac{2h}{a_e}\right]^{1/2}}$$

which may be integrated directly to obtain

$$(106) \qquad d = a_e \left\{ \left[\sin^2\alpha_o + \frac{2(h_B - h_r)}{a_e}\right]^{1/2} - \sin\alpha_o \right\}$$

where $\theta = \alpha_o$ when $h = h_r$. Employing small-angle approximations, we obtain:

$$(107) \qquad d \cong a_e \left\{ -\alpha_o + \left[\alpha_o^2 + \frac{2(h_B - h_r)}{a_e}\right]^{1/2} \right\}$$

In a similar manner we may obtain the following expression for Δd, the distance the ray travels in the layer.

$$(108) \qquad \Delta d = \int_0^{\Delta h} \frac{dh}{\left[\sin^2\theta + 2h\left(\frac{1-\gamma r}{r}\right)\right]^{1/2}}$$

$$= \frac{r}{1-\gamma r}\left\{\left[(\theta')^2 + 2\Delta h\left(\frac{1-\gamma r}{r}\right)\right]^{1/2} - \theta'\right\}$$

Employing Snell's Law [equation (29)], the approximation $\cos\theta \cong 1 - \theta^2/2$ and the approximation equation (36) and (37), we obtain:

$$(109) \qquad (\theta')^2 = \alpha_o^2 + \frac{2(h_B - h_r)}{a_e}$$

Substituting equation (109) and the expressions

$$\gamma = -\frac{\Delta n_L}{\Delta h} \quad \text{and} \quad r = r_o + (h_B - h_r)$$

into equation (108), we obtain:

$$(110) \qquad \Delta d = \frac{\left[\alpha_o^2 + \frac{2(h_B - h_r)}{a_e} + 2\Delta n_L + \frac{8\Delta h}{3a_e + 4(h_B - h_r)}\right]^{1/2} - \left[\alpha_o^2 + \frac{2(h_B - h_r)}{a_e}\right]^{1/2}}{\frac{4}{3a_e + 4(h_B - h_r)} + \frac{\Delta n_L}{\Delta h}}$$

In the above development a_e is the effective earth's radius, α_o is the inclination angle of the ray as it leaves the transmitter, h_B and h_r are the heights of the layer base and the transmitter respectively, Δh is the layer thickness, and Δn_L (i.e., $\Delta N_L \times 10^{-6}$) is the change in the index of refraction through the layer (see Figures 9 and 34). The distance from the transmitter at which the ray emerges is simply the sum of these two expressions. From this point, the ray proceeds in a straight line as shown in Figure 34. Figure 34 also illustrates the behavior of the rays as the elevation angle, α_o, is changed. For high elevation rays (above 2 degrees) the bending is slight, but as α_o becomes smaller, the rays are deflected more and more from their original direction.

Figure 35, illustrates the effect of raising the transmitter height (or lowering the layer height). The high angle rays still penetrate the layer as before, but now, as α_o is decreased, the rays are bent more and finally (in the third ray from the left) emerge tangent to the layer top. If α_o is decreased even further, the rays do not penetrate the layer at all, but are totally refracted back down toward the surface again. The reason for this will be evident from a consideration of the expression for Δd. If $(h_B - h_r)$ and α_o are sufficiently small, the first radical becomes imaginary, signifying

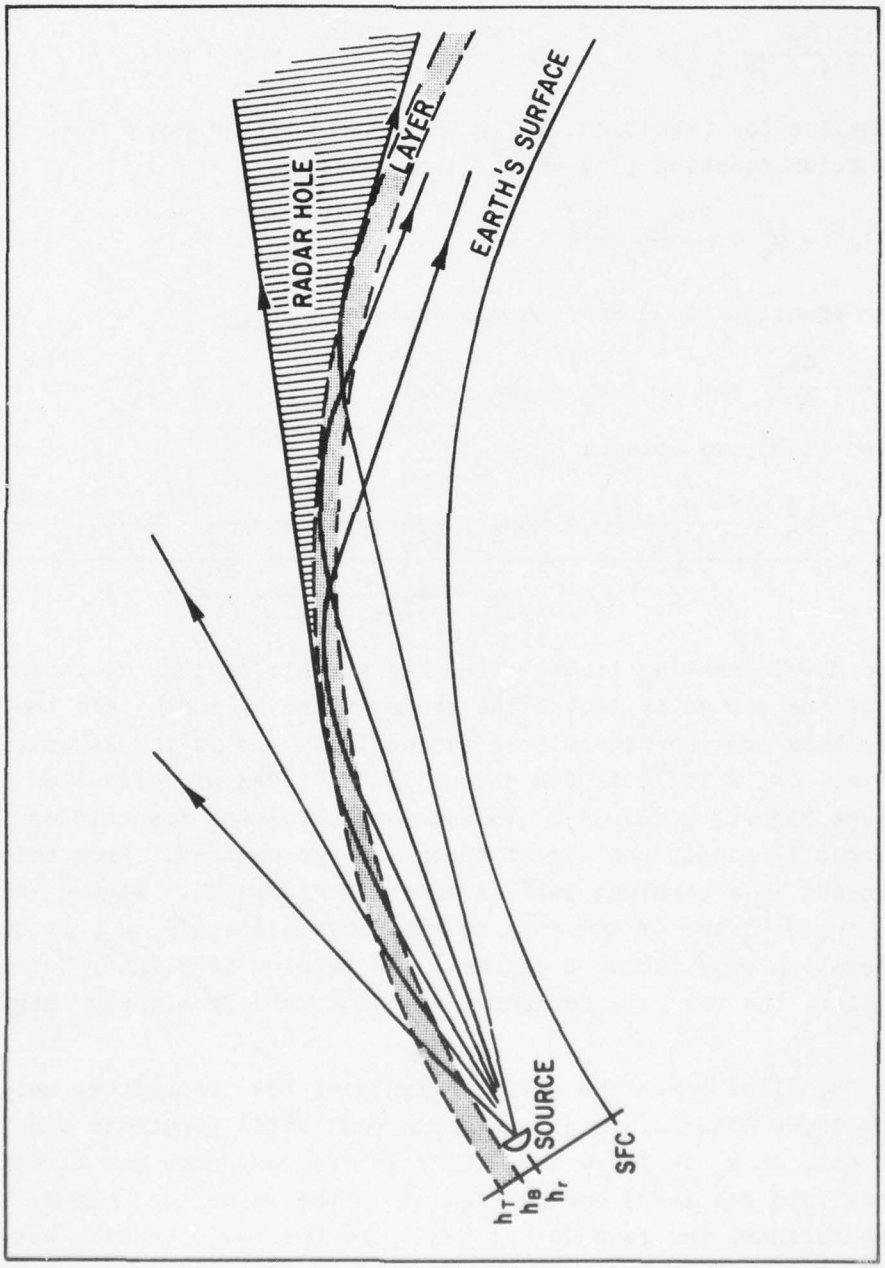

Figure 35. Ray Refraction by an Elevated Layer—Radar Just Below Layer.

AD-A041 877 AIR WEATHER SERVICE SCOTT AFB ILL F/G 17/9
ESTIMATING METEOROLOGICAL EFFECTS ON RADAR PROPAGATION. VOLUME --ETC(U)
DEC 76 W B MORELAND
UNCLASSIFIED AWS-TR-183-VOL-1 NL

2 OF 3
ADA041 877

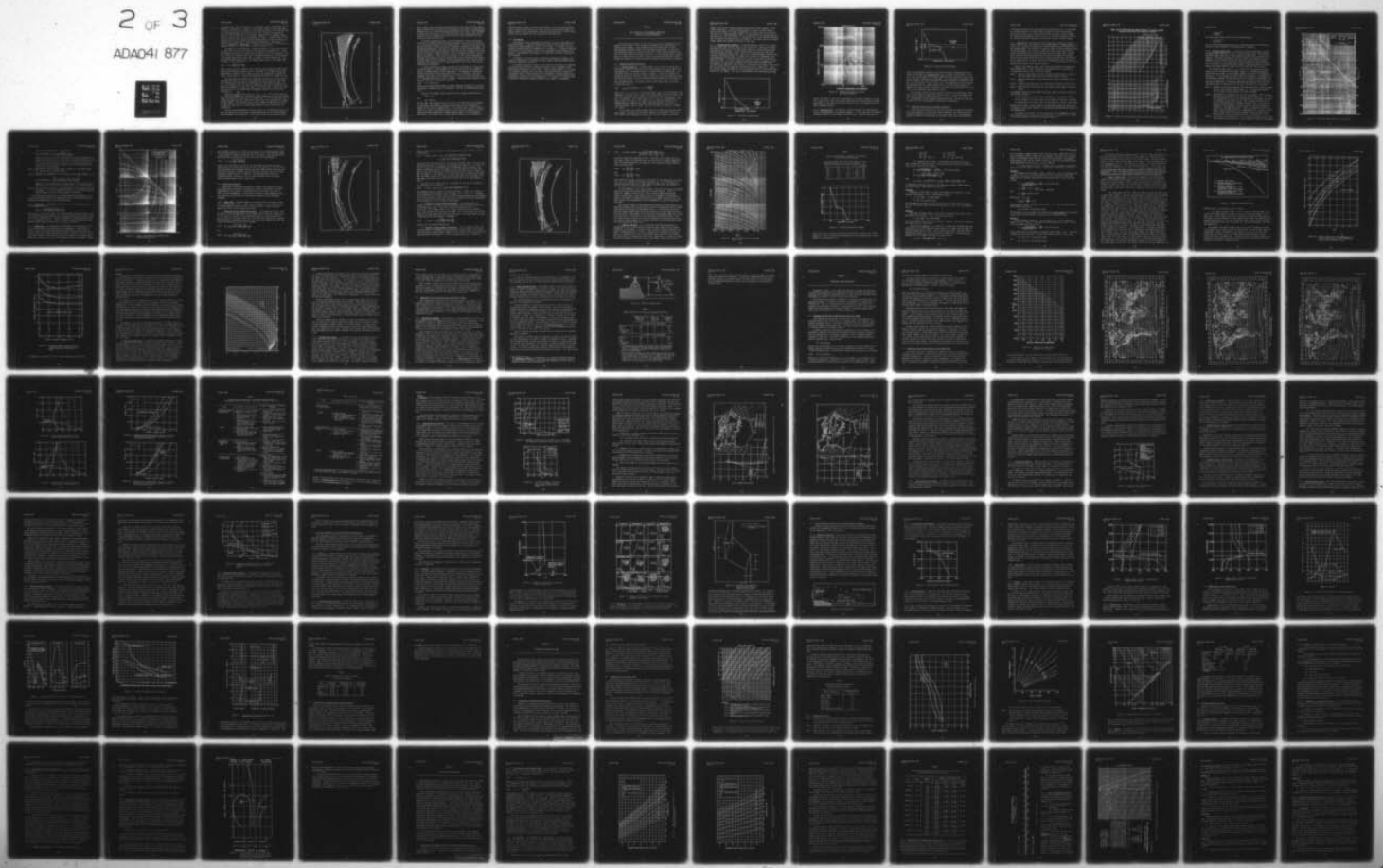

no emergent ray. When this radical is just equal to zero, the emergent ray is tangent to the layer top. However, as α_o becomes negative, there will again be a value of α_o^2, which is larger than the remaining terms in the radical, and rays will again emerge from the layer top. This situation is depicted in Figure 35 by the lowest ray in the bundle. Between the two emerging tangent rays is a region where no energy penetrates the layer. A radar target in this region would not be detected, nor would communications be possible between an airplane in the region and a surface-located transmitter. This region is called a radio hole or radar hole. A discussion of methods for locating these regions, as well as avoiding them, is given in section 6.3.1.

In Figure 36, the transmitter is above the layer. In this case, the upper rays do not intersect the layer at all, and are unaffected by it. There are, however, two rays which again define a radar hole in this situation. The first is the ray tangent to the layer top, and the second is a ray going down at a steeper angle, which comes back up through the layer farther out. The distance from the transmitter to the tangent point (start of the radar hole) is simply: [see equation (5)]

$$(111) \qquad d' = \sqrt{2a_e (h_r - h_T)}$$

where h_T and h_r are the heights of the layer top and transmitter respectively and a_e is the effective earth's radius. The width of the radar hole is more complicated to express in this case, than when the transmitter is below the layer. In section 6.3.1, practical methods are presented for operational use.

The main difference between the transmitter being below the layer and being above the layer, is that in the former case one can eliminate the radar hole completely by lowering the transmitter far enough below the layer. If $h_B - h_r$ is large enough, all rays will emerge from the layer regardless of α_o. When the transmitter is above the layer, on the other hand, raising the transmitter moves the hole further away and gradually narrows it but can never eliminate it.

Substituting 12 units for ΔN_L (i.e., $\Delta n_L = -12 \times 10^{-6}$) and 200 feet for Δh in the expression for Δd, shows that if the transmitter is more than 80 feet below the layer base, there will be no radar hole. It can be seen then that a typical elevated layer will have little effect until the transmitter is nearly at layer height. For the same layer, with the radar 80 feet above the layer, a radar hole would exist at radar height between 22 and 60 miles from the transmitter.

The ray tracing expressions discussed above, are theoretically valid only when the layer is smooth and has a uniform N-profile over a large horizontal area surrounding the transmitter. Even though actual elevated layers rarely

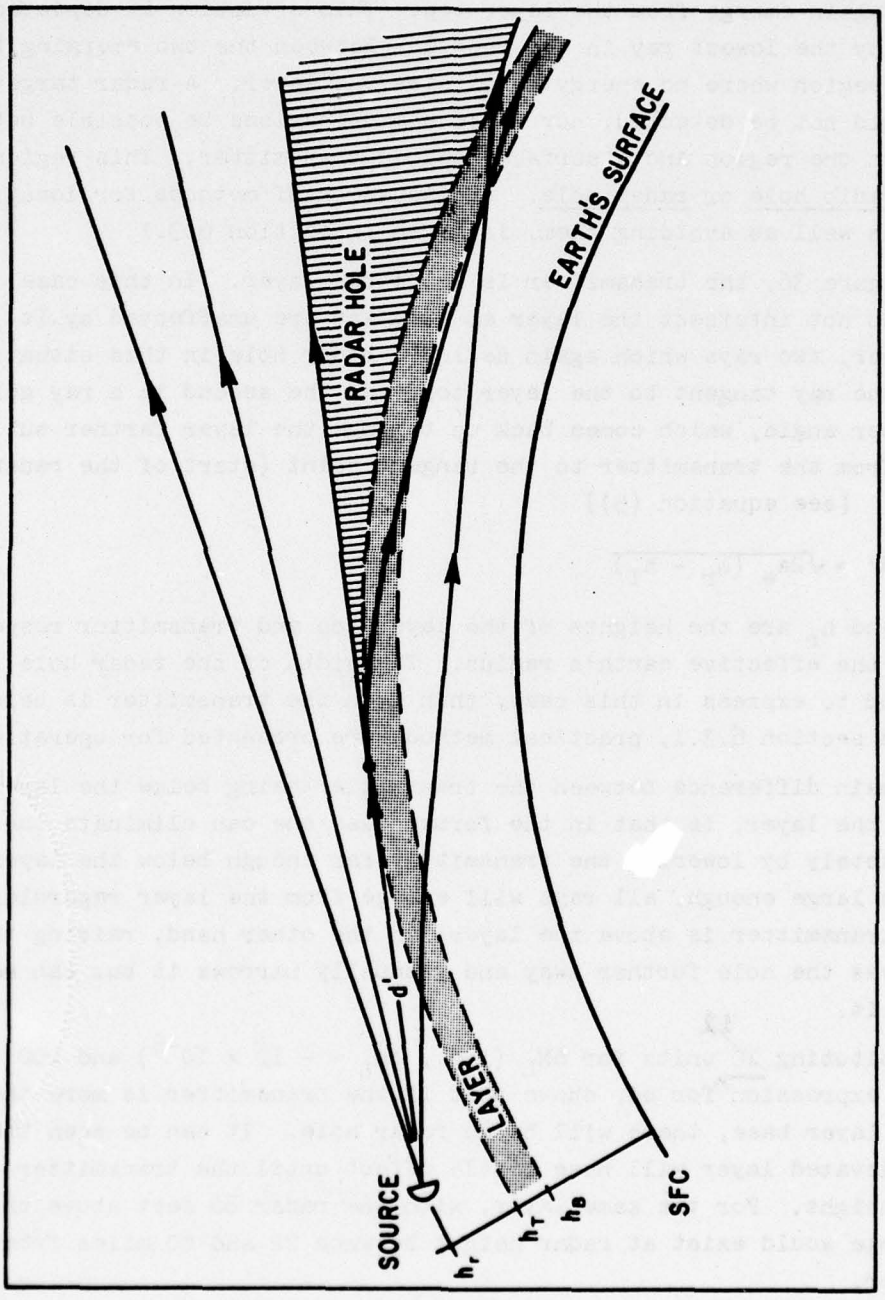

Figure 36. Ray Refraction by an Elevated Layer—Radar Above Layer.

are as smooth as the mathematical model requires, the results of many experimental flights above and below such layers give results which, as indicated by Doherty [16], are in surprisingly good agreement with theory. Field strengths in radar holes are found to be considerably lower than outside them, and the distances to the boundaries agree very well with those calculated from ray theory and measured N-profiles.

In certain geographical areas, strong subsidence of dry air from aloft gives rise to intense elevated inversions (layers) with ΔN's of the order of 40 to 60 units and heights of less than 3000 feet. These areas are near 30°N (and S) latitude in those belts where atmospheric subsidence is strongest. In the Northern Hemisphere, the areas of occurrence of the strongest elevated inversion (layers) are located where the 30°N latitude belt intersects the cold-water west coasts of large continents; namely, southern California, northern Mexico, and Morocco. Little data is available for the Southern Hemisphere, although such evidence as exists indicates that similar areas will be found on the west coasts of the continents in that hemisphere as well. Ducts of this intensity are frequently able to trap energy from surface radar and also at communication wavelengths.

In layers where ΔN_L is large, causing the total refraction of rays with relatively large θ's, the roughness of the layer becomes a very important factor in feeding energy into the radar holes. In experimental studies off southern California, it has been found that in such situations, the field strength in the radar hole is weaker than it is above or below the hole, but it is stronger than when no layer is present. This comes about because of the Rayleigh criterion of roughness, as follows:

(112) $$h < \lambda/(8 \sin \theta)$$

where $\underline{h}$ is the permissible height of random roughness elements for a reflecting surface to appear smooth at wavelength λ and with the grazing angle equal to θ.

Suppose, for example, that a layer has the following characteristics:

$$\Delta N = -50$$

and

$$\Delta h = 200 \text{ feet}$$

We find that total refraction will occur for θ as large as 9.1 milliradians. In this case, the roughness elements must be less than 13 wavelengths in height for the layer to appear smooth. On the other hand, if ΔN is minus 12 units, as it was in our previous layer, θ can only be as large as 2.3 milliradians, giving a permissible roughness-element height of 53 wavelengths. From this, it is evident that a strong elevated layer, which is capable of

trapping energy incident at rather large angles, must also be much smoother than is usually found in Nature in order to give a well-defined radar hole. Weaker layers, which require small ray angles for radar holes to form, can be relatively much rougher and still produce well-defined holes.

5.2. Ray Bending.

The previous section considered the behavior of rays in the presence of steep N-gradients. Of primary concern were those rays which were bent sufficiently to emerge tangent to the top of the layer. In Chapter 2 we considered situations where the bending is not so drastic. It should be realized, of course, that such bending occurs in any atmosphere where N changes with height. If N decreases with height, as it does over the earth, the rays are bent downward.

In Chapter 6, we shall employ the equations developed in Chapter 2 for graphical computations of bending, elevation angle, range and height errors caused by atmospheric refraction.

It should be pointed out that in this report the discussion of radar-ray bending has been confined to refraction caused by the troposphere (—the stratosphere refraction is very small). When the radar target is in or above the ionosphere (heights above 100 miles), additional bending is caused by ionospheric layers. Total bending by the ionosphere is roughly equal to the tropospheric contribution at 100 megacycles (λ = 3 meters). At shorter wavelengths the ionospheric bending decreases as the square of wavelength.

Chapter 6

THE COMPUTATION OF ATMOSPHERIC REFRACTIVE EFFECTS ON RADAR PERFORMANCE

In the previous chapters of this report the various mechanisms were discussed by which radar or radio energy is propagated from a transmitter to a distant point in space. Also considered were the several ways in which meteorological variables affect these propagation mechanisms. It was seen that relatively simple ray-tracing concepts are useful in describing the behavior of radio energy in various situations. In this chapter, these concepts are put to practical use in order to solve the operational problem of determining the variations in radar performance caused by meteorological variables.

6.1. Surface-to-Surface Situations.

6.1.1. "Normal" Detection.

A surface radar, such as those at low shore installations, normally is limited to detecting targets above the horizon line (see Figure 24). Its antenna pattern is characterized by fingers due to interference maxima and minima as shown in Figure 6. Inside the fingers the fields are above the free-space fields, because the direct and reflected waves reinforce one another, and in the regions between fingers the fields are less than free-space fields, because the two waves partially cancel one another. For low radar heights, the vertical angles of the center lines of maximum strength are given by

$$\alpha_{max}\ (\text{milliradians}) = (m - \tfrac{1}{2})\ \frac{1000\ \lambda}{2h_r} \qquad (113)$$

where m is 1, 2, 3, etc., h_r is the radar height, and λ is the wavelength, both expressed in the same units. Thus, for a radar height of 60 meters and a wavelength of 0.3 meters, the interference maxima will occur at 2.5, 7.5, 12.5, etc., milliradians. The minima occur at 5, 10, 15, etc., milliradians. The range at which the tips of the fingers occur is taken arbitrarily as the maximum detection range of the radar; this range depends, of course, on transmitted power, size of target, and other factors not related to propagation itself.

It is evident that surface targets will not be detected unless they are high enough to protrude into the lowest maximum of the pattern. This will occur under normal atmospheric conditions at, or just beyond, the horizon

range for most coastal radar installations and most surface targets. Other things being equal, a short-wavelength radar will detect surface targets farther away because its lowest interference lobe lies closer to the horizon than that of a longer-wavelength radar. In the presence of strong surface or elevated ducts, the lower finger of the pattern may be bent downward considerably as shown by the dashed pattern in Figure 6. The lower side of the bottom finger extends well beyond the horizon in this case.

6.1.2. Advection Ducts (Surface). As was discussed in section 5.1.1, ducts may occur when warm, dry air flows out over a cool sea. They do not extend more than 100 miles or so from land unless there is a strong advection wind carrying the air offshore. Usually these ducts are found over seas lying close to subtropical desert areas, such as in the Mediterranean, Red Sea, Gulf of Arabia, and similar areas. To assess their effects on propagation, one needs radiosonde or other data from which to plot an N-profile to heights of 500 feet or more. In order to determine whether the duct is capable of trapping energy of a particular wavelength (and hence whether extended radar coverage may be expected), the N-profile is plotted and the height of the layer top h_T, and ΔN_L for the layer are determined as shown in Figure 37. Using the criteria curves in Figure 38, one can determine whether a particular wavelength will be trapped. If a point corresponding to the measured h_T and ΔN_L

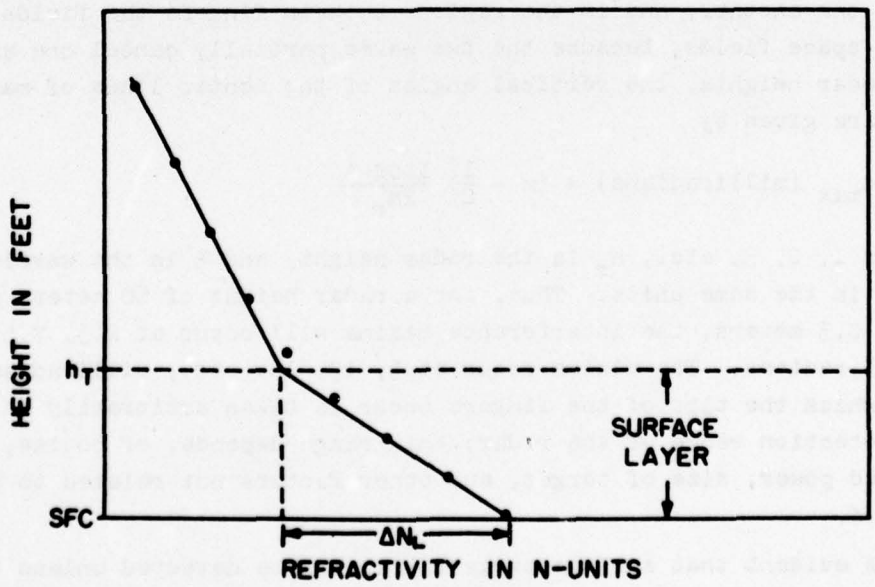

Figure 37. N-Profile—Surface Layer.

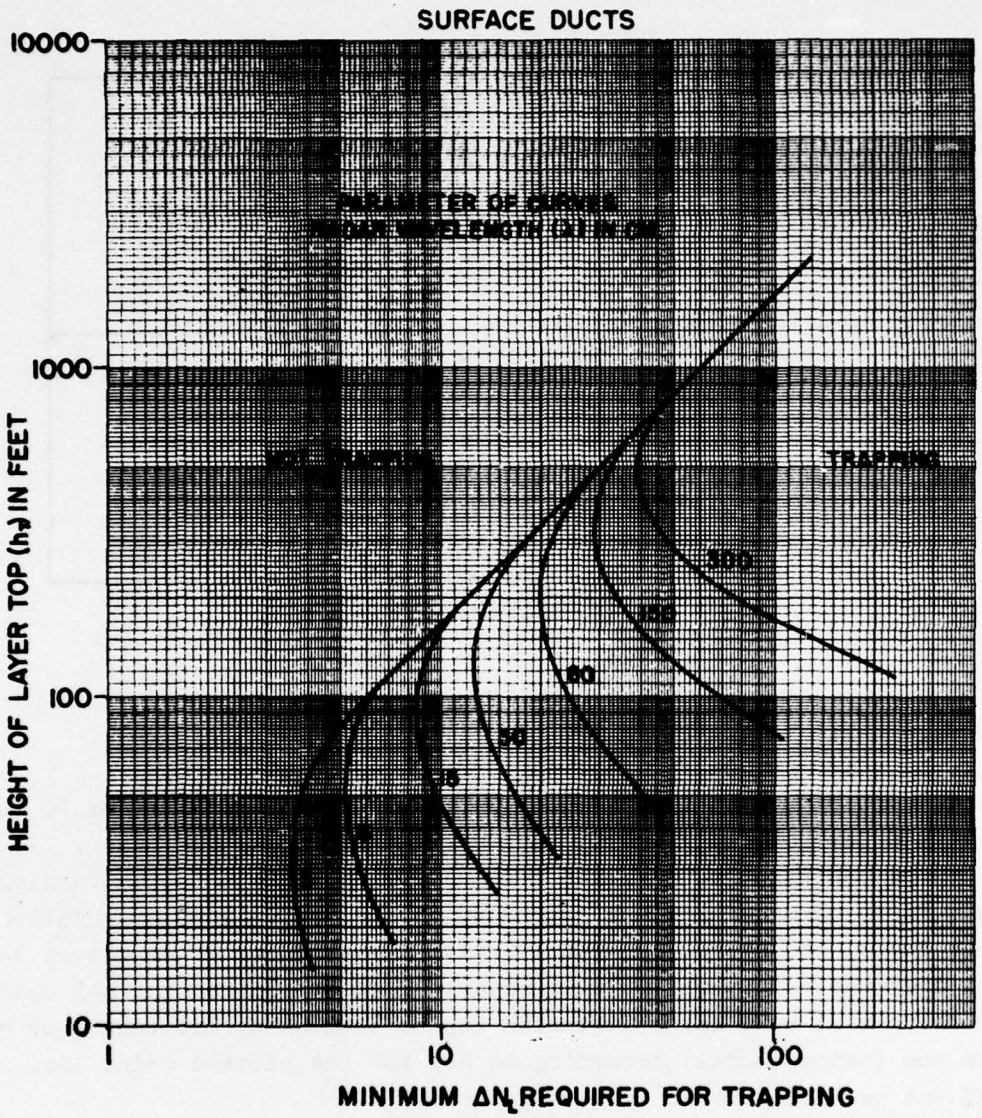

Figure 38. Trapping Criteria for Surface and Elevated Layers.

lies to the right of the curve corresponding to the radar frequency in question, the duct will trap the emitted energy and give extended range coverage. The farther to the right of the curve the point lies, the greater will be the radar coverage extension.

6.1.3. Elevated Ducts. One may use a similar procedure for analyzing the effect of elevated ducts on radar performance. In this case, plot an N-profile as before; Figure 39 illustrates an elevated duct. Figure 38 may again be

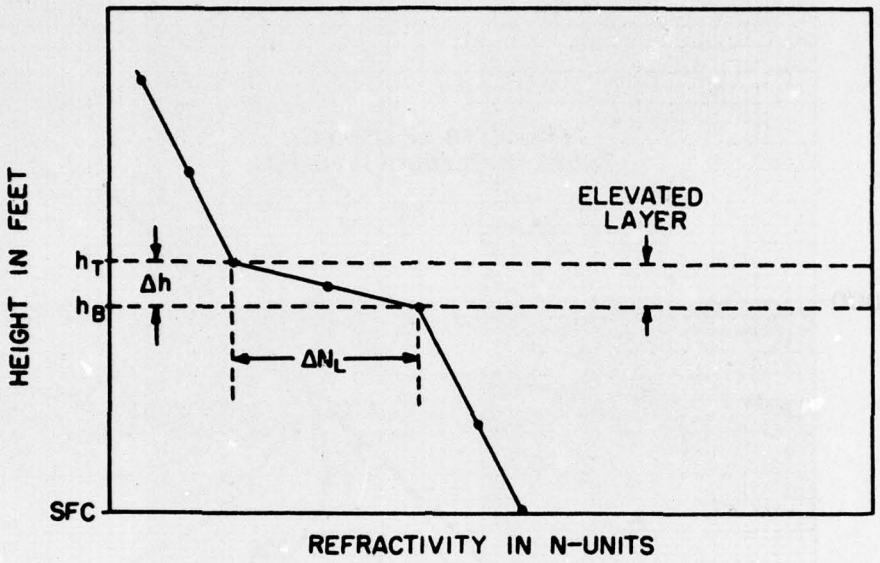

Figure 39. N-Profile—Elevated Layer.

used as the trapping criterion if one plots the point corresponding to the height of the layer top divided by two ($h_T/2$) and ΔN_L for the layer. If the point lies to the right of the radar frequency wave in question, trapping will occur and radar coverage will be extended. As in the case of evaporation and advection ducts, one cannot accurately predict the extent of anomalous coverage, but only whether or not it will occur. With experience one may estimate whether there will be a large extension (up to 5 times normal range) or a moderate one (twice normal) according to how far the plotted point lies to the right of the pertinent radar frequency curve.

The criteria curves shown in Figure 38 are based on a theoretical treatment of the guiding of radio-radar energy by ducts. Numerous attempts have been made to treat the problem theoretically, but this particular method, by S. A. Schelkunoff of Bell Telephone Laboratories [30], has been the only one to stand the test of experimental verification successfully.

6.2. Surface-to-Air and Air-to-Surface Situations.

In the previous discussion it was noted that various types of N-profiles with strong gradients could channel radar energy near the surface and thus illuminate targets which were well below the horizon line. The propagation effects of refractive layers when one terminal is well above the ground are

considerably different from those when both terminals are low. In principle, the coverage pattern of a surface radar looking at a high-flying target, should be the same as that of an airborne radar looking at surface targets. One significant difference, however, is that in the air-to-surface situation sea clutter complicates detection, particularly of small surface targets.

6.2.1. Sea Clutter. The myriad of echoes frequently observed by airborne radars looking over a sea surface is called sea clutter or scope clutter. Its effect is to increase the background of echoes against which one must detect the surface target. Sea clutter is caused by reflection from individual waves. As one would expect, it is worse in heavy seas than in calm ones, and the echoes are stronger for shorter wavelengths than for longer ones. Furthermore, the echo intensity increases as the cube of the angle of incidence. Thus, clutter echoes extend from the sea surface directly under the aircraft out to some distance, as given in Figure 40, depending upon the altitude of the aircraft and the sea state. The presence of strong N-gradients has little effect on the extent of the clutter echoes.

Figure 40 was adapted from a chart originally produced by Lockheed Aircraft Company [34]. It was modified to its present form, on the basis of in-flight sea-clutter data. To use the Figure:

Step 1. Enter at upper right with swell height plus wave height in feet, or with the coded value of H_W, mean maximum height of waves.

Step 2. Proceed horizontally to the appropriate surface wind speed line in knots.

Step 3. Proceed vertically down to the appropriate aircraft altitude curve.

Step 4. Read the sea-clutter radius on the scale at lower right in nautical miles.

For example, suppose the wave height plus swell height is 8 feet and the surface wind is 10 knots:

If the aircraft is at 5000 feet, R (the radius of clutter) = 64 miles.

If the aircraft is at 10,000 feet, R (the radius of clutter) = 93 miles.

If the aircraft is at 20,000 feet, R (the radius of clutter) = 134 miles.

Because of the effect of wave shape on the reflected energy, one should add 15 percent to the clutter radius in the upwind area and subtract 20 percent in the downwind area.

As stated on the chart, the values given are for a 2-megawatt, 10-centimeter radar having an antenna gain of 35 decibels. To obtain clutter ranges for other wavelengths multiply the indicated ranges by

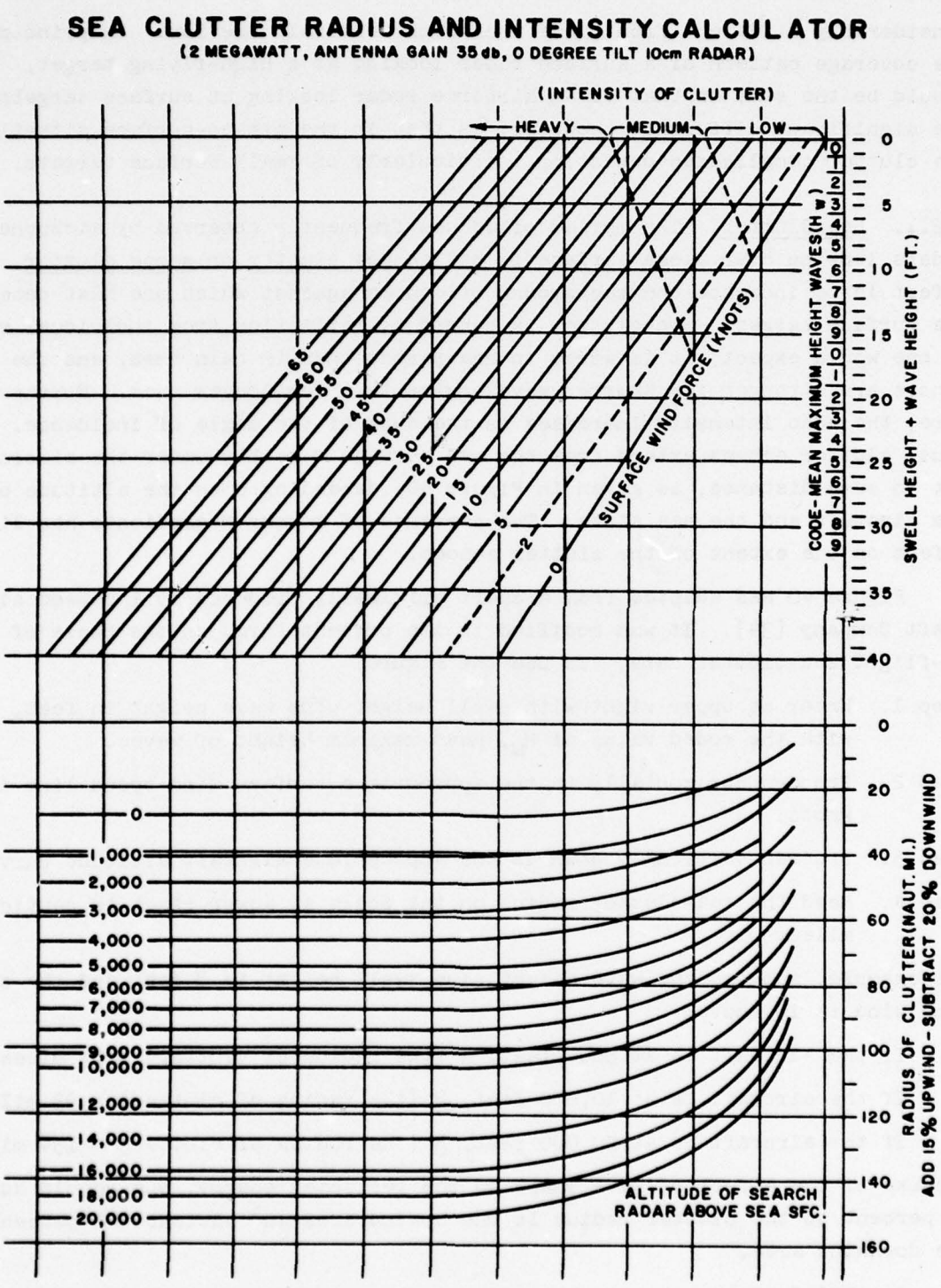

Figure 40. Graph for Estimating the Radius and Intensity of Sea Clutter.

$$\left[\frac{10}{\lambda\ (cm)}\right]^{3/2}$$

for other radar powers multiply the indicated ranges by

$$\left[\frac{P_r\ (mw)}{2}\right]^{1/3}$$

and for other antenna gains multiply the indicated ranges by the antilog of {0.067 [G - 35]}, where G is the antenna gain in decibels.

6.2.2. Elevation-Angle Error. An important problem encountered in surface, air-search radar operation is that of elevation-angle error. The standard N-profile causes radar rays to bend downward as they travel through the troposphere. The total ray bending along the tangent line amounts to about 3/4 degrees as the ray proceeds from the surface up through the stratosphere. About 90 percent of this bending takes place between the surface and 30,000 feet; as a result an air-search radar capable of measuring precise elevation angles will always indicate higher elevation angles than the true ones.

The elevation-angle error, ϵ_a, is a function of the measured elevation angle, α_o, the N-profile and the target height, h_t. Reference atmosphere corrections can be made to take average bending into account (see Appendix A, Volume II). In the presence of layers where the N-gradient is stronger than the reference, however, the bending error can be increased considerably. If one has a refractivity profile, the radar elevation-angle error may be determined quite accurately. According to Weisbrod and Anderson [37], the following method, based on equations (71) and (72) is accurate to 0.06 percent:

Step 1. Subtract all N-values (computed from radiosonde data) from the refractivity at the surface (radar height), N_s. Tabulate the resulting $N_s - N_h$ values for each height, h, above the radar.

Step 2. Using Figure 41, determine 500 tan θ at each height. This is done by entering the left margin of the figure with the proper $N_s - N_h$. Next, move horizontally to the curve corresponding to the height, h, which is expressed in thousands of feet. Now, proceed vertically to the curve corresponding to the measured elevation angle, α_o, which is expressed in milliradians. Finally, read 500 tan θ by moving horizontally to the right-hand scale. This is a graphical solution of Snell's Law [see equation (53)]. Occasionally, $N_s - N_h$ will be negative; in this case enter the left margin with $N_s - N_h$ and use the dashed height curves, proceeding as above to determine 500 tan θ.

Step 3. By dividing the atmosphere into layers whose boundaries are the radiosonde heights tabulated above, the ray bending $\Delta\tau$ caused by each layer

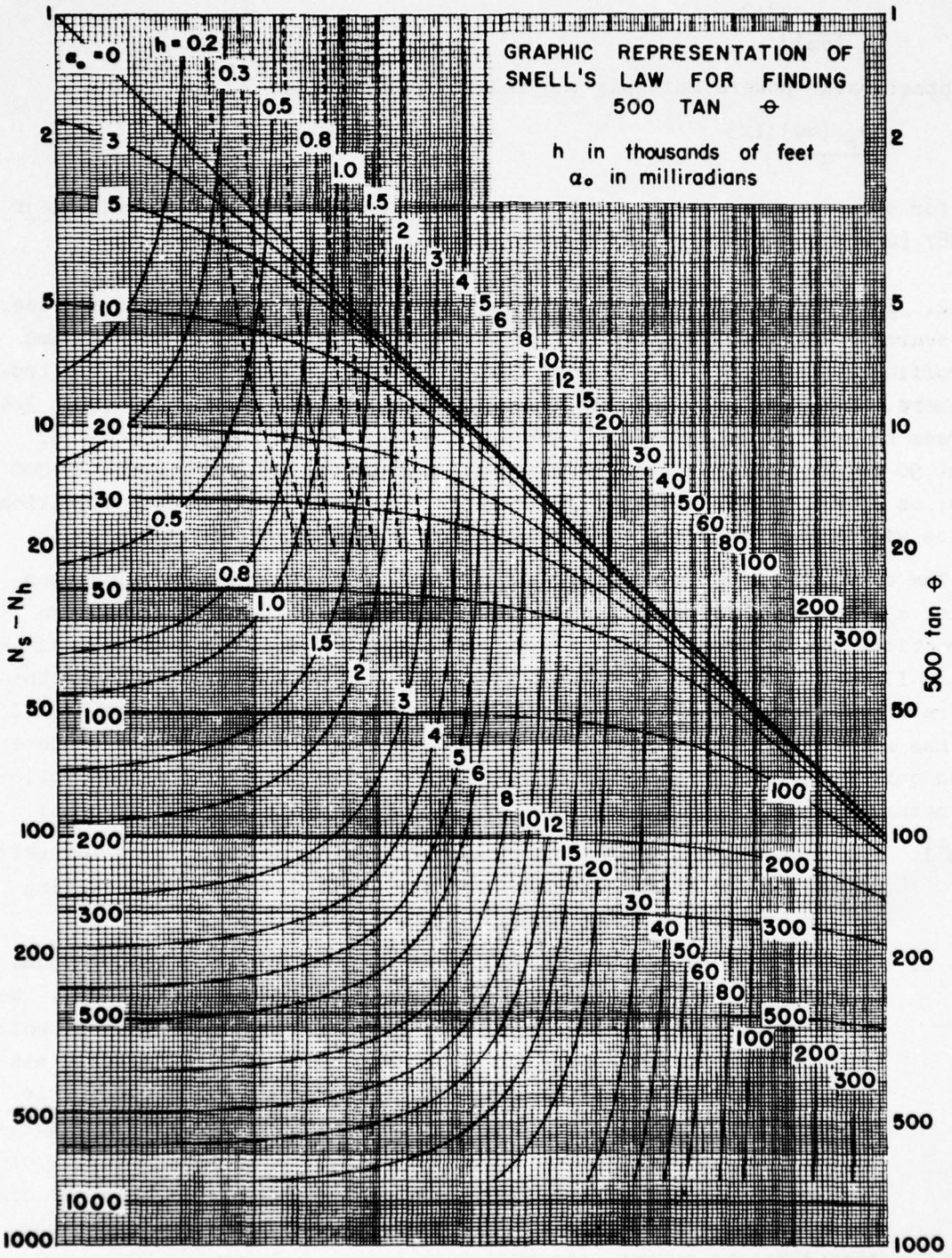

Figure 41. Graphical Representation of Snell's Law.

can now be determined from the expression

$$\Delta\tau \text{ (milliradians)} = \frac{\Delta N_L}{500 \tan \theta_B + 500 \tan \theta_T}$$

where $500 \tan \theta_B$ is the value tabulated at the lower boundary of a given layer and $500 \tan \theta_T$ is the value tabulated for the next higher level; ΔN_L is equal to $\underline{N}$ at the bottom of the layer minus $\underline{N}$ at the top of the layer. For each consecutive pair of heights one gets a value of $\Delta\tau$ in milliradians.

Step 4. Add the $\Delta\tau$'s from the radar height (surface) to the target height, h_t. The sum is τ_t in milliradians.

Step 5. Compute ϵ_a corresponding to the assumed α_o and target height, h_t, by

$$\epsilon_a \text{ (milliradians)} = \frac{1000\,\tau_t \tan \theta_t - (N_s - N_t) + \frac{\tau_t^2}{2}}{\tau_t + 1000 \tan \theta_t - 1000 \tan \alpha_o}$$

where N_t is the refractivity at target height, $1000 \tan \theta_t$ is twice the value of $500 \tan \theta$ at target height, and τ_t is in milliradians.

Step 6. This will give a value of ϵ_a corresponding to the assumed α_o and target height. It must be repeated from Step 2 on, for other α_o's and target heights to cover a useful range of conditions.

The procedure outlined above is straightforward though tedious. It is, however, quite exact, and is the simplest way (short of using an electronic computer) for determining ϵ_a from radiosonde data.

6.2.3. Range Error. Atmospheric retardation in any one layer may be computed from equation (73)

$$\Delta R_{j,j+1} = \frac{(N_j + N_{j+1})\,(h_{j+1} - h_j)}{1000\,(\sin \theta_j + \sin \theta_{j+1})}$$

where $\Delta R_{j,j+1}$ is the range error for one-way passage through the layer. $1000 \sin \theta$ can be obtained from Figure 42 in a manner analogous to that of obtaining $500 \tan \theta$ from Figure 41. Height is expressed in thousands of feet and $\Delta R_{j,j+1}$ is expressed in feet. Values of ΔR for a passage through the troposphere at zero elevation angle are on the order of 350 feet.

6.2.4. Radar Holes. The occurrence of radar holes or blind spots in a surface, air-search radar coverage pattern is infrequent. It was noted in section 5.1.2, that intense elevated layers cause such holes but that the fields in them are stronger than when the layer is absent, so they do not reduce radar coverage. Weak elevated layers are incapable of causing surface radar holes unless they are just a few hundred feet above the radar. Surface

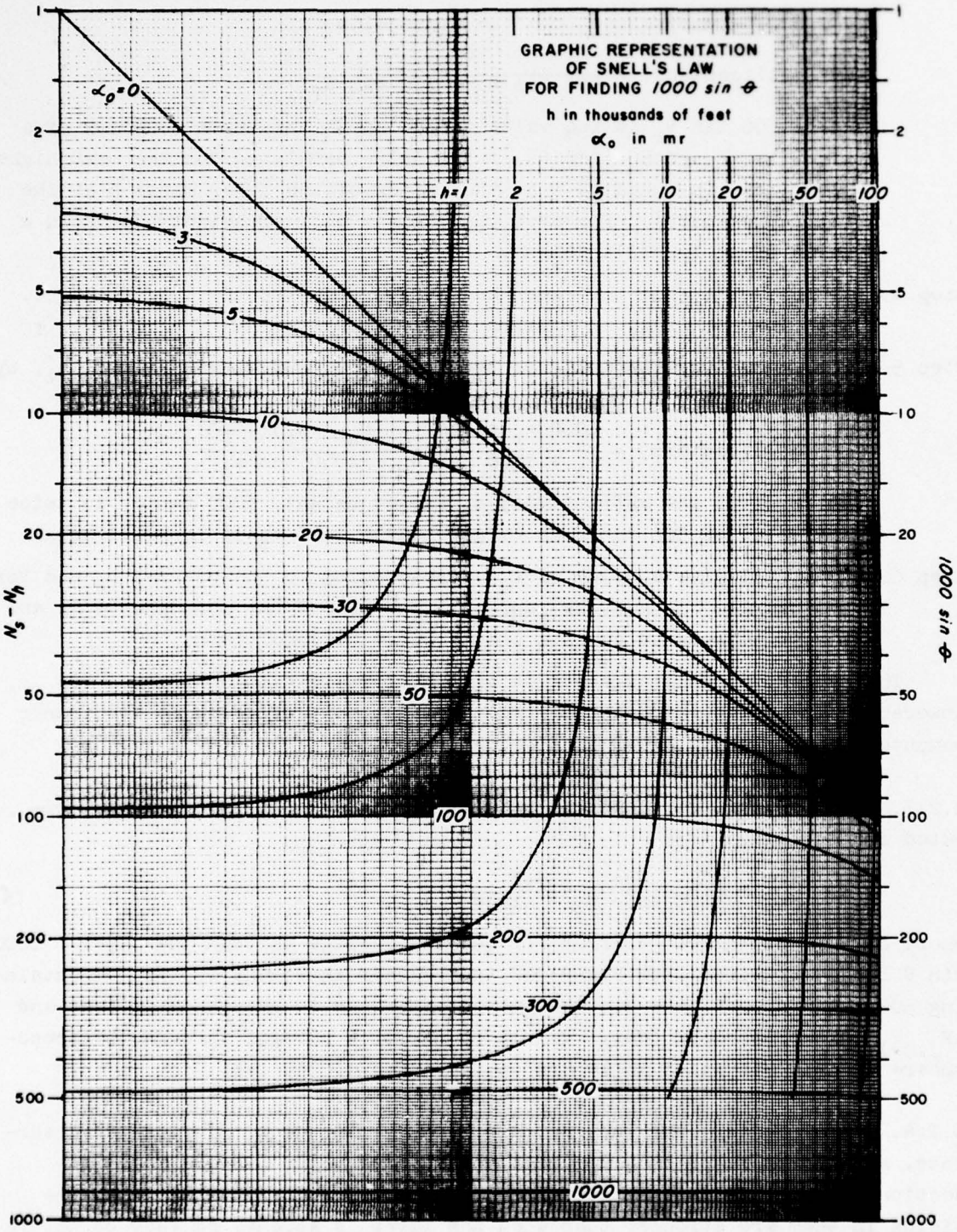

Figure 42. Graphic Representation of Snell's Law for Finding 1000 sin θ.

ducts caused by advection, however, can cause surface, air-search radar holes. The ray-tracing results for this case also apply to low, weak elevated layers. In both cases, the radar is below the top of the layer. The near edge of the radar hole will be located at the top of the layer at the distance

$$(114) \qquad d = h_T \sqrt{\frac{2}{\Delta N_L - 0.048\, h_T}}$$

where h_T is the height of the top of the layer above the surface and ΔN_L is equal to N at the surface minus N at the top of the layer, $N_s - N_T$. It can be seen that unless the N-gradient between the radar antenna height (surface) and the top of the layer is greater than 48 units per 1000 feet, d will be imaginary and no radar hole will be present. The same expression applies to evaporation ducts, although in this case ΔN_L as defined above will almost never be large enough to give a radar hole.

6.3. Air-to-Air Situations.

Since both the radar and the target are usually well above the sea surface, evaporation and advection layers have little, if any effect, on radar performance in this instance. Such layers are too far below the line of sight to affect propagation, and even when the line of sight grazes the horizon, they have little effect for the reasons discussed in the preceeding paragraph.

6.3.1. Radar Holes. Elevated layers, on the other hand, can be quite effective in causing radar holes. It was shown in Chapter 5, that radar rays can be totally refracted when the radar is below the layer, thereby causing a region into which little energy can penetrate.

a. Location of Holes (Radar Below Layer). The distance R' and R", from the radar to the near edge and to the far edge of the radar hole, respectively (at the top of the layer), can be expressed in terms of the refractivities N_r, N_B, and N_T at the radar, layer base, and layer top, respectively, together with the three corresponding heights h_r, h_B, and h_T (see Figure 43). For this purpose two parameters D_1 and D_2 are defined:

$$(115) \qquad D_1 = \frac{0.232\,(h_T - h_B)}{N_B - N_T - 0.048\,(h_T - h_B)}$$

and

$$(116) \qquad D_2 = \frac{0.232\,(h_B - h_r)}{N_r - N_B - 0.048\,(h_B - h_r)}$$

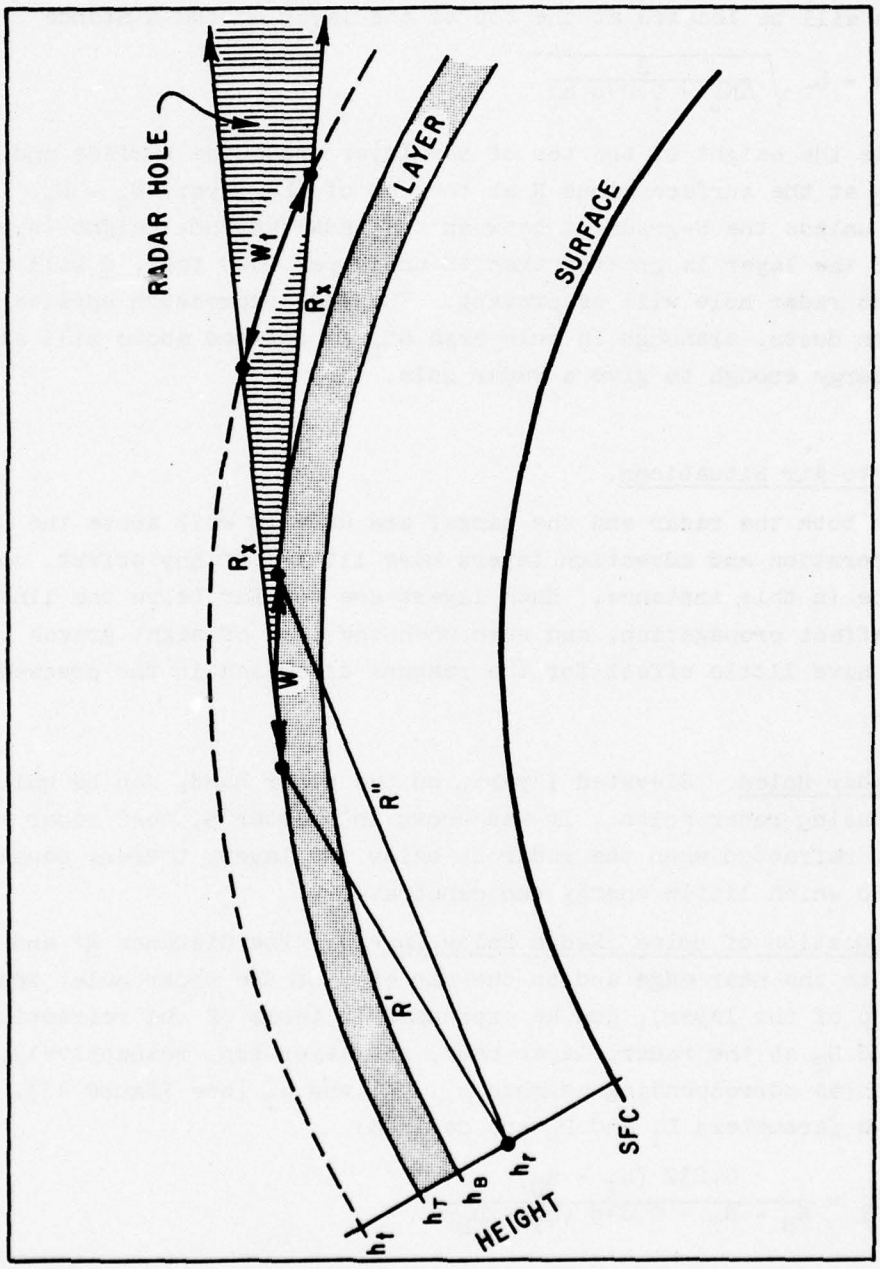

Figure 43. Idealized Radar Hole Geometry—Radar Below Layer.

where D_1 and D_2 are in nautical miles and h_T, h_B, and h_r are in feet. It can be shown that

$$(117) \quad R \text{ (naut. miles)} = (D_1 - D_2)\sqrt{N_B - N_T - 0.048\,(h_T - h_B)} \pm D_2\sqrt{N_r - N_T - 0.048\,(h_T - h_r)}$$

Subtracting the two terms give $\underline{R}'$, the range to the near edge of the hole, and adding them gives $\underline{R}''$, the range to the far edge (see Figure 43). It should be noted that D_2, which is determined by the N-gradient below the layer, will usually be negative, since the gradient will be less than 48 units per 1000 feet; on the other hand, D_1 will always be positive when there is a radar hole. When the radar is at the height of the layer base, the two radicals are equal. When the radar is within the layer, D_1 and D_2 are equal, and the range to the near edge of the radar hole is given by the last term of the range equation (117).

The width of the radar hole, $\underline{W}$, at the level of the top of the layer is approximately given as follows:

$$(118) \quad W \text{ (naut. miles)} \cong 2\,D_2\sqrt{N_r - N_T - 0.048\,(h_T - h_r)}$$

The foregoing equation assumes the radar hole width is equal to the range to the far edge minus the range to the near edge; i.e., $W = R'' - R'$. In Figure 43, we see that this is only strictly true if the angle between $\underline{R}'$ and $\underline{R}''$ equals zero; in all practical cases this angle will be small and the error introduced by the assumption will be entirely insignificant.

b. Avoidance of Holes (Radar Below Layer). It was pointed out in Chapter 5, that if the radar is sufficiently far below the layer, there will be no radar hole at all. This can be seen from equation (118); if $[0.048\,(h_T - h_r)]$ becomes equal to $(N_r - N_T)$, the radical will be equal to zero, and the radar hole will have zero width. For a still lower h_r, the hole width will become imaginary and no hole will exist. The radar height at which a radar hole will first appear is therefore,

$$(119) \quad h_r \text{ (max.)} = h_B\left[\frac{0.048h_T - N_s + N_T}{0.048h_B - N_s + N_B}\right]$$

where N_s is the surface refractivity.

c. Location of Holes (Radar Above Layer). When the radar is above the elevated layer, the distances to the near and to the far edges of the radar hole are given at radar height instead of at the height of the layer top as was done previously (see Figure 44). The near edge distance, $\underline{R}'$, is given by

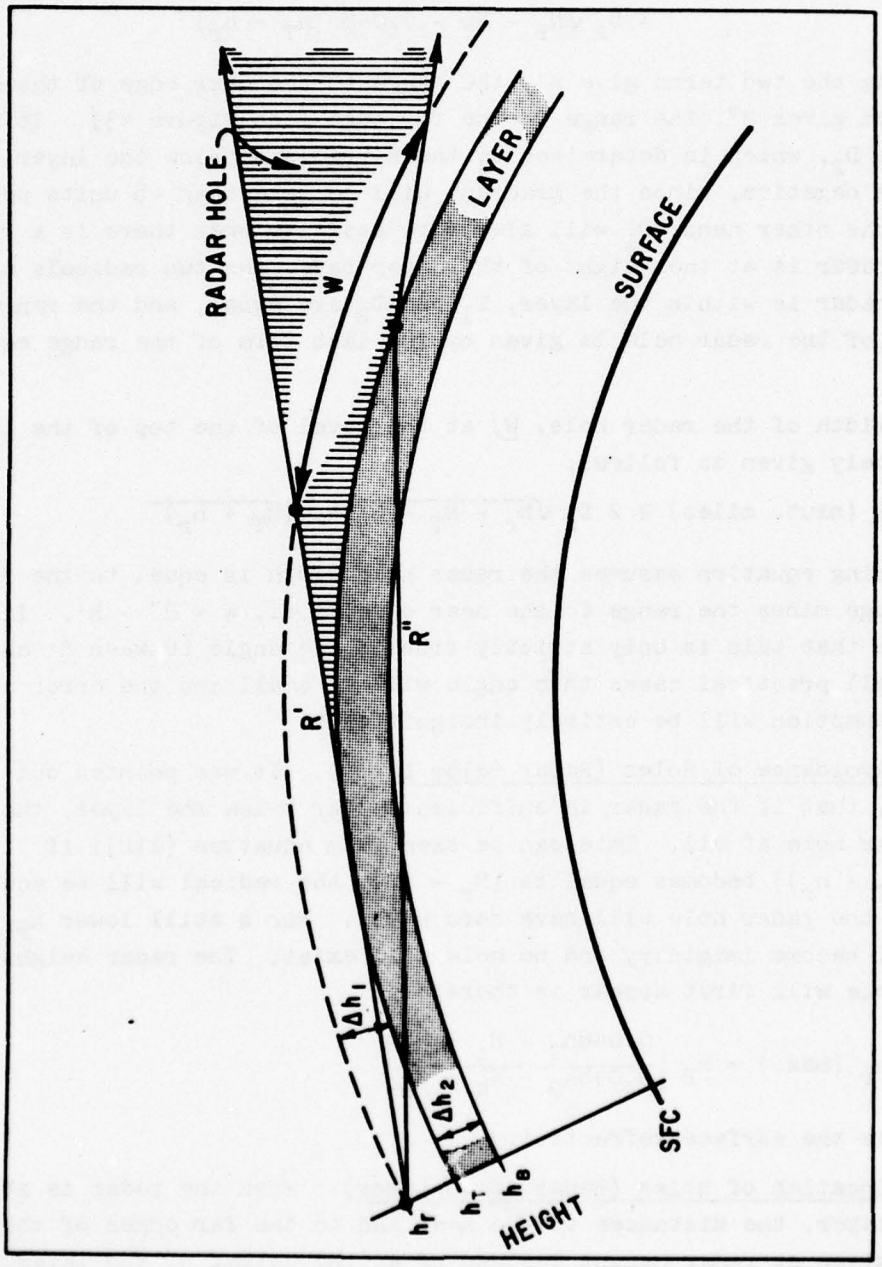

Figure 44. Idealized Radar Hole Geometry—Radar Above Layer.

$$(120) \qquad R' \text{ (naut. miles)} = \frac{0.465\ (h_r - h_T)}{\sqrt{0.048\ (h_r - h_T) - (N_T - N_r)}}$$

where all heights are expressed in feet. The width of the radar hole, when the radar is above the elevated layer, turns out to be a complex expression, which is plotted graphically in Figure 45. The abscissa is C_2/C_1, where C_1 and C_2 are defined as

$$(121) \qquad C_2 = \frac{N_T - N_B}{h_T - h_B} + 0.048$$

and

$$(122) \qquad C_1 = \frac{N_r - N_T}{h_r - h_T} + 0.048$$

The ordinate is $\Delta h_1/\Delta h_2$, where Δh_1 is the height of the radar above the layer top, $(h_r - h_T)$, and Δh_2 is the layer thickness, $(h_T - h_B)$. The family of curves gives hole width, W, at radar height, divided by R', the distance to the near edge of the hole at radar height.

In the expressions for C_1 and C_2 above, it will be seen that C_1 is always positive, but that for strong layers C_2 can become negative. Thus, in Figure 45, negative values of C_2/C_1 refer to strong layers and positive values to weak layers. When C_2/C_1 is zero, the N-gradient in the layer is equal to the earth's curvature, and when C_2/C_1 is equal to positive one, the layer becomes indistinguishable since its N-gradient is equal to that above the layer.

The curves of Figure 45 were adapted from theoretical work carried out at Cornell University [16], and the results have been compared with actual flight data taken by the Wright Air Development Center. It was found that actual elevated layers produce radar holes whose location and width agree quite well with the theory. Furthermore, it was found that appreciable radar holes occur even when C_2/C_1 is as much as 0.9 (as indicated by radiosonde data). Since this value of C_2/C_1 is associated with an N-gradient in the layer only 30 percent greater than standard, it is evident that even very weak elevated layers can cause significant radar holes.

d. Numerical Examples. It is likely that the descriptions given in paragraphs 6.3.1a, b, and c above for locating radar holes involve concepts unfamiliar to the reader. To clarify these concepts, numerical examples are given in subparagraphs d(1) and d(2). Suppose the radiosonde data given in Table 4 is representative over the area where radar holes are to be located. The first step is to compute N at each level, using Chart I or Chart II; these values are tabulated in the last column of the Table. Next plot N versus

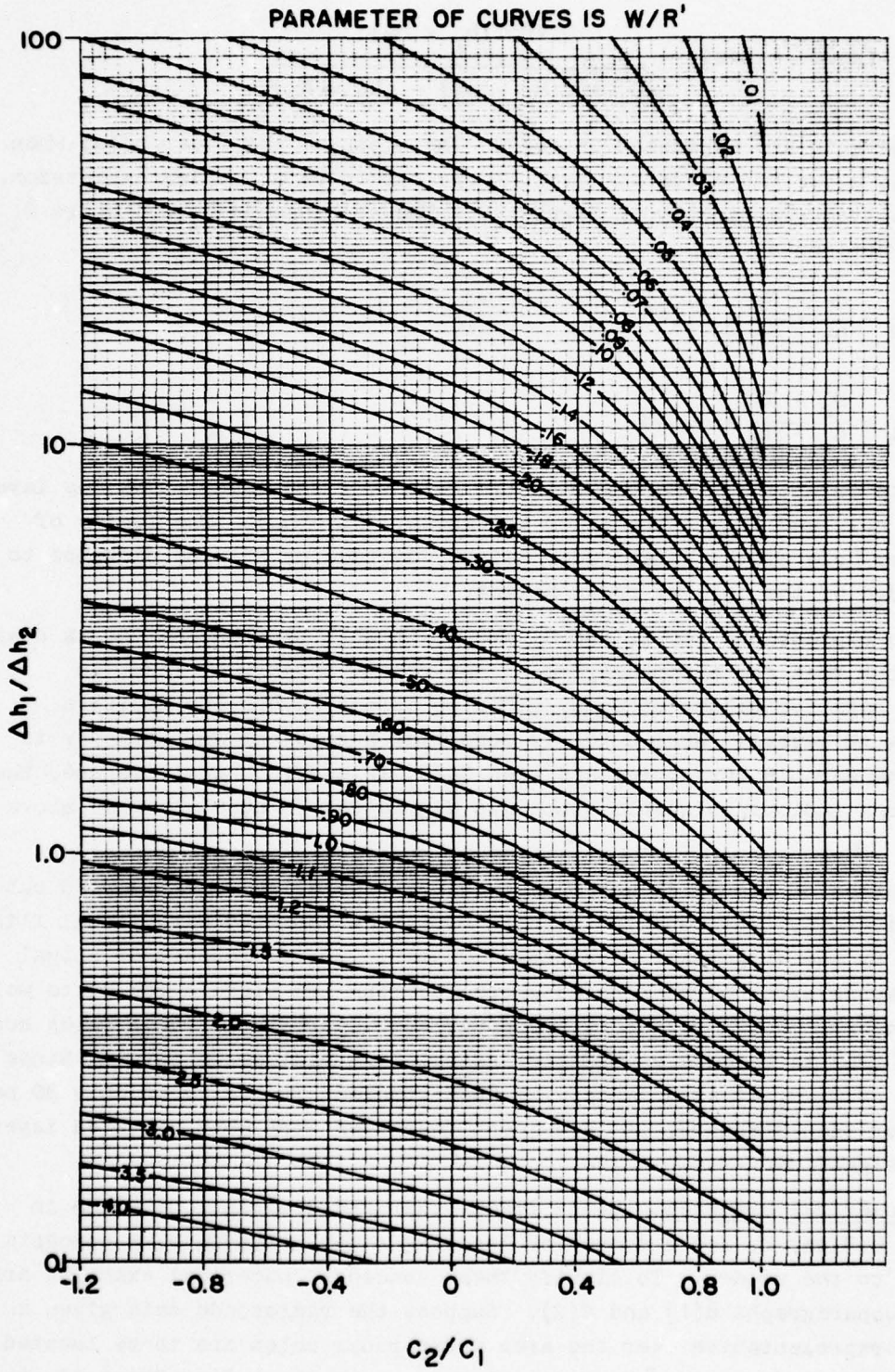

Figure 45. Width of Radar Hole Chart—Radar Above Layer.

TABLE 4

Sample Radiosonde Data, Heights, and N-Values for the Numerical Examples.

Pressure	Temperature	Dew Point	Height	N
mb	°C	°C	ft	N-Units
1013	15.0	12.0	0	336
902	8.4	7.0	3260	296
885	12.2	-13.0	3760	250
850	9.5	-18.0	4900	240
700	-1.3	-35.0	9900	201

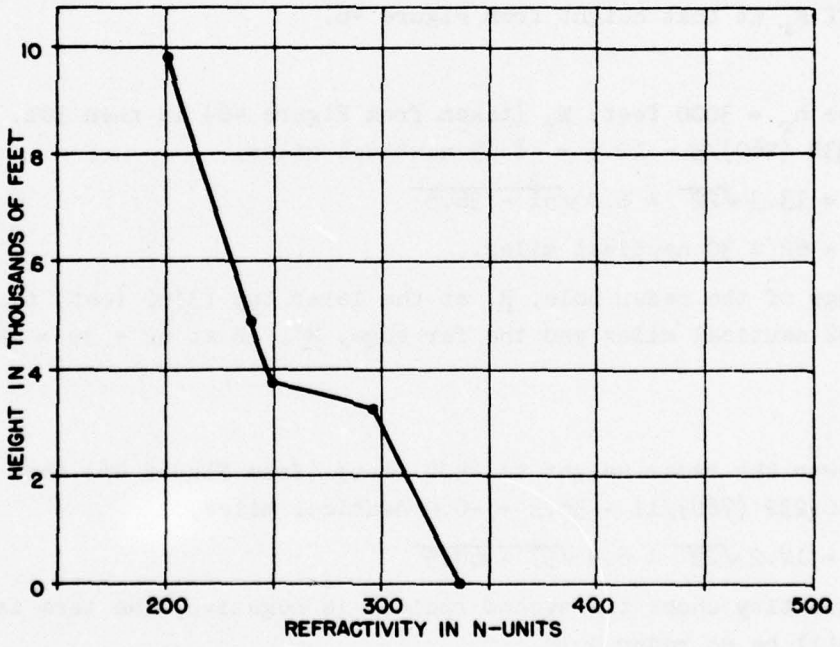

Figure 46. N-Profile—Numerical Example.

height to obtain a refractivity profile as described in section 3.3.3 (see Figure 46). From this profile the parameters of the trapping layer, which is present, are determined to be

$N_B = 296$ $\qquad h_B = 3260$ feet

$N_T = 250$ $\qquad h_T = 3760$ feet

$\Delta N = N_B - N_T = 46$ $\qquad \Delta h = h_T - h_B = 500$ feet

(1) Radar below the layer. To determine the radar hole location when the radar is below the layer, substitute the above values into equations (115), (116), and (117) as follows:

$$D_1 = \frac{0.232\ (500)}{46 - 0.048\ (500)} = \frac{116}{46 - 24} = 5.28 \text{ nautical miles},$$

$$D_2 = \frac{0.232\ (3260 - h_R)}{N_r - 296 - 0.048\ (3260 - h_r)} \quad \leftarrow h_r$$

and

$$R = (5.28 - D_2)\sqrt{46 - 24} \pm D_2\sqrt{N_r - 250 - 0.048\ (3760 - h_r)}$$

To determine the actual location of the radar hole, assume a radar height h_r and read off N_r at that height from Figure 46.

Example 1

Suppose $h_r = 3000$ feet; N_r (taken from Figure 46) is then 301. D_2 now becomes $0.232\ (260)/5 - 12.5 = -8.05$ nautical miles,

$$R = 13.3\sqrt{22} \pm 8.0\sqrt{51 - 36.5}$$

$$R = 62 \pm 30 \text{ nautical miles.}$$

The near edge of the radar hole, R' at the layer top (3760 feet) is thus at $62 - 30 = 32$ nautical miles and the far edge, R", is at $62 + 30 = 92$ nautical miles.

Example 2

Now lower the radar height to 2500 feet; (from Figure 46) then $N_r = 307$. D_2 becomes $0.232\ (760)/11 - 36.5 = -6.9$ nautical miles,

$$R = 12.2\sqrt{22} \pm 6.9\sqrt{57 - 60.5}$$

Since the quantity under the second radical is negative, the term is imaginary, and there will be no radar hole.

From the above examples, it is seen that a radar hole is present when the radar height is not far below the layer base, but is absent when the radar is lowered an additional 500 feet. For this particular layer, one may find the maximum radar height which will not produce a radar hole. Substituting the parameters of the example into equation (119) we have

$$h_r\ (\max) = \frac{3260\ (180 - 86)}{156 - 40} = 2640 \text{ feet}$$

In this example, a radar height of 2640 feet will give a radar hole width of zero; at greater heights a radar hole will appear. This then is the critical height for avoiding a radar hole for the particular profile of the example. Using equation (119) one can readily compute h_r (max) for any elevated layer, using appropriate values of h_B, h_T, N_s, N_B, and N_T.

(2) Radar above the layer. Consider now the problem of locating the radar hole when the radar is above the same layer as specified in Figure 46.

Example 3

For comparison with Example 1 above, assume $(h_r - h_T)$ in the present case is equal to $(h_B - h_r)$ in the previous case, or $h_r = 4020$ feet; then from Figure 46, $N_r = 248$ and substituting into equations (120), (121), and (122) we have

$$R' = \frac{0.465\ (260)}{\sqrt{0.048\ (260) - 2}} = \frac{121}{3.2} = 38 \text{ nautical miles}$$

$$C_2 = \frac{-46}{500} + 0.048 = 0.044$$ ← −0.044

and

$$C_1 = \frac{-2}{260} + 0.048 = 0.040$$

Then $C_2/C_1 = -1.1$, and

$$\Delta h_1/\Delta h_2 = \frac{260}{500} = 0.52$$

Entering these values in Figure 45 gives $W/R' = 1.8$. Thus, the hole width at radar height is given as

$$W = 1.8\ (38) = 68 \text{ nautical miles}$$

The distance to the near edge of the radar hole <u>at radar height</u> is 38 nautical miles, and to the far edge it is 68 plus 38 or 106 nautical miles.

Example 4

In this example, assume $(h_r - h_T)$ is equal to $(h_B - h_r)$ in Example 2, namely 760 feet. Then $h_r = 4520$ feet and from Figure 46, $N_r = 243$. In this case, from equation (120), we have

$$R' = \frac{0.465\ (760)}{\sqrt{0.048\ (760) - 7}} = \frac{354}{5.4} = 66 \text{ nautical miles}$$

and C_1 and C_2 will be the same as in Example 3 above ($C_2/C_1 = 1.1$). The ratio $\Delta h_1/\Delta h_2$ will now be 760/500 = 1.5 and from Figure 45, $W/R' = 0.94$. Thus,

$$W = 0.94\ (66) = 62 \text{ nautical miles}$$

and

$$R'' = 66 + 62 = 128 \text{ nautical miles}$$

The results obtained in Examples 3 and 4 show that, when the radar is not far above the layer top (260 feet), the near edge of the radar hole is 38 nautical miles away and has a width of 68 nautical miles. Raising the radar height 500 feet, moves the near edge of the hole out to 66 nautical miles, but does not remove the hole. When, however, the radar is an equal height below the layer base (Example 2), the hole disappears entirely. This illustrates the statement made previously; namely, if the radar is above the layer, raising its height moves the hole outward and narrows it slightly, but does not eliminate it. When the radar is below the layer, one can eliminate the hole entirely by locating the radar several hundred feet below the layer base.

e. Shape of Radar Holes. The previous paragraphs have discussed the location of the radar hole (1) where it intersects the top of the elevated layer, for the case where the radar is below the layer, and (2) where it intersects the radar altitude, for the case where the radar is above the layer. Since the radar target will rarely be at either of these particular altitudes, one would like to be able to locate the boundaries of the hole at any target height.

(1) Radar below the layer. When the radar is below the layer, this is particularly simple. Since the rays defining both edges of the hole emerge tangent to the layer top, they will remain the same distance apart at all heights above the layer top; in other words, the width of the radar hole above the layer is constant with altitude. This effect is illustrated in Figure 43. At a height, h_t (above the top of the layer), the radar hole width is equal to W_t; comparison will show that $W \cong W_t$. The only problem then is to define the range beyond the layer top, R_x, versus altitude (above the layer top) relationship of one edge of the hole (see Figure 43), and the problem is completely solved. Figure 47 shows various curves defining this relationship for several different refractive conditions. In the Figure, the layer top is shown, together with segments of curves drawn at 10,000-foot increments above the layer top. The range scale, R_x, is in nautical miles beyond the point where the ray emerges from the layer top. The exact trajectory of the ray will depend on the characteristics of the N-profile above the layer. The upper straight line, Curve 1, assumes no change of N with height above the layer, which of course, is unrealistic. The second curve, 2, assumes a reasonably dry atmosphere above the layer, which corresponds to an exponential profile with N_s equal to 250. The next two curves assume a very high surface N of 400. In these cases the amount of atmosphere below the surface is of importance, thus, the third curve, 3, is for a radar height of 1000 feet, and the fourth curve, 4, is for a radar at 5000 feet. An exponential decrease of N with height above the layer, as portrayed in Figure 18, has been assumed in all cases except the top line. The proper curve to use in most cases will lie

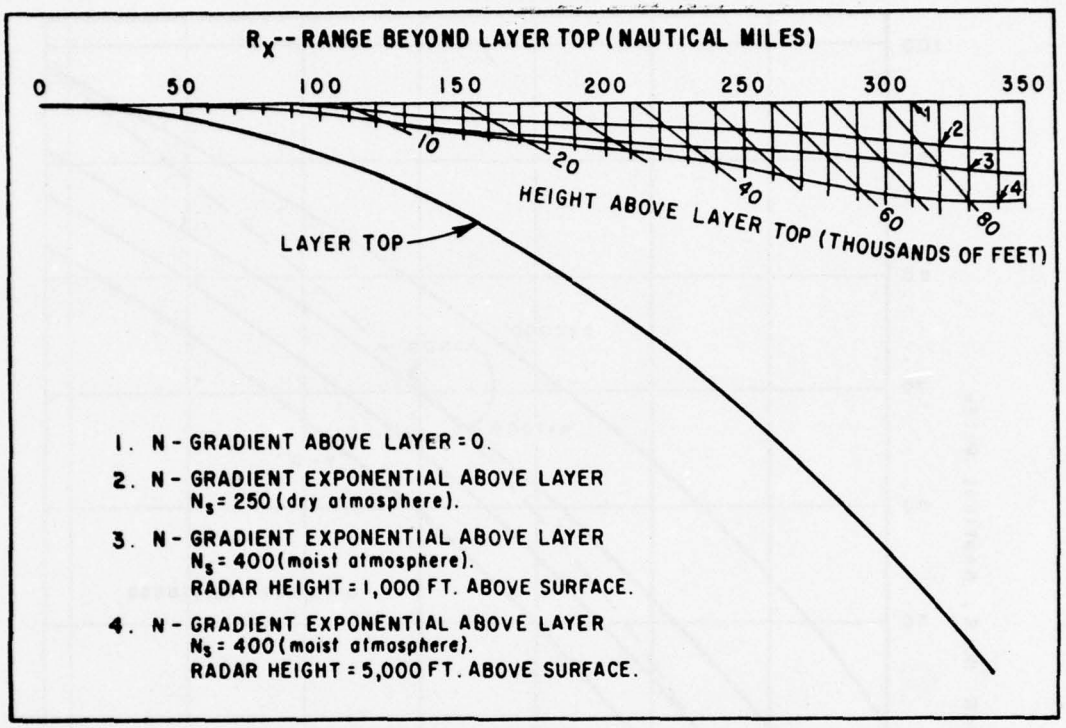

Figure 47. Shape of Radar-Hole Chart.

between 2 and 3, and probably closer to Curve 2.

(2) Radar above the layer. In this situation, the near edge of the radar hole is again defined by Figure 47, since this edge is tangent to the layer top. The far edge of the hole is defined by the next ray emerging from the layer top, which emerges at a small upward angle rather than being exactly tangent (see Figure 44). The hole, therefore, gets narrower (width decreases) with increasing altitude above the layer, at a rate which depends on the layer characteristics.

Two diagrams developed by Fannin [19] may be used to estimate the width of the radar hole at target elevations varying from 0 to 50,000 feet above the transmitter. Figure 48 represents the width of the hole for a radar transmitter 500 feet above the top of a superstandard layer and with a target 10,000 feet above the radar itself. Figure 49 gives a correction factor to be used when the reference conditions used in Figure 49 are modified in terms of distance to the layer or target elevation.

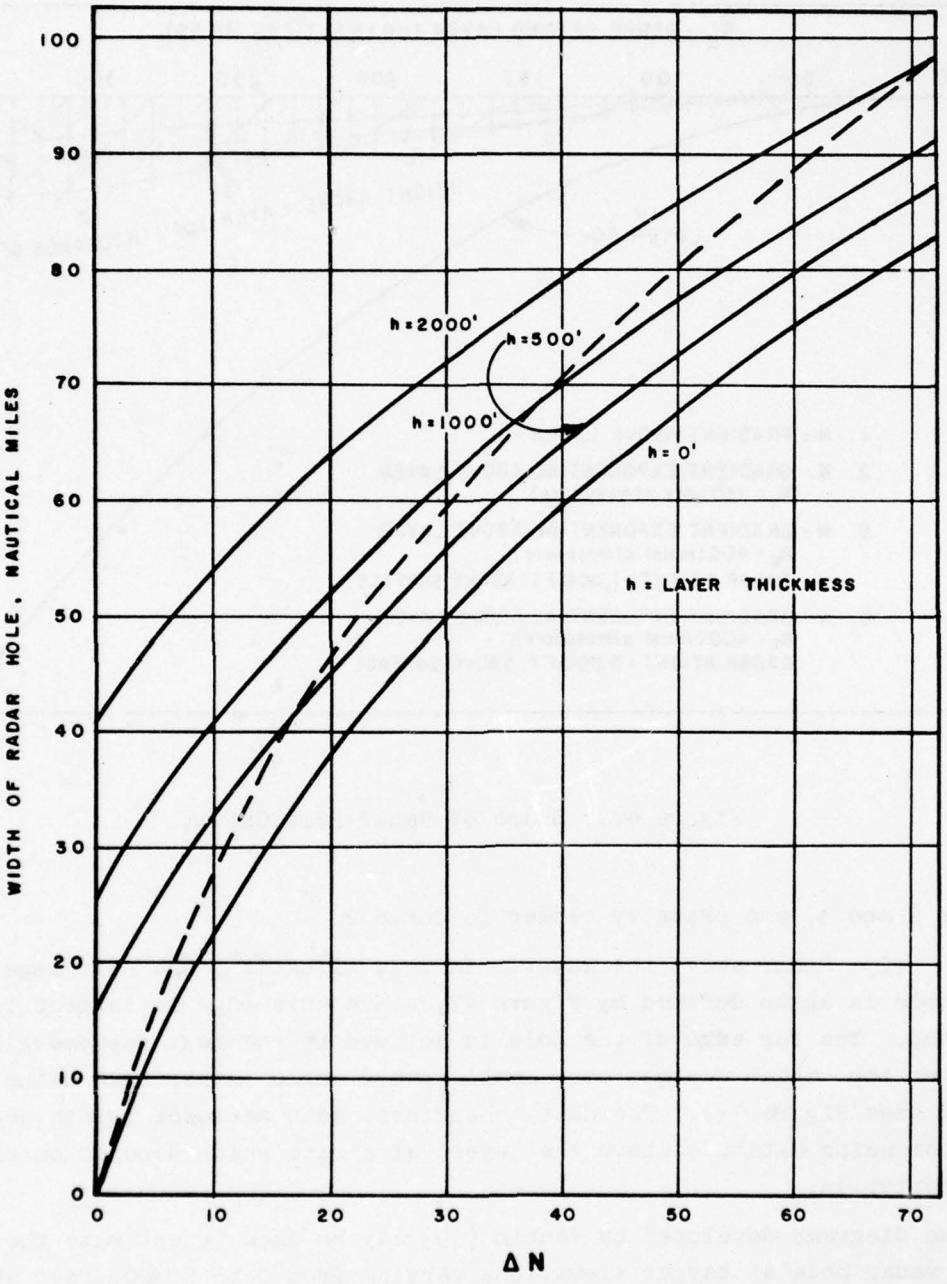

Figure 48. Width of Radar Hole Versus ΔN, ΔN-Deficit for Superstandard Layer 500 Feet Below Transmitter. Second target 10,000 feet above transmitter (after Fanin [19]).

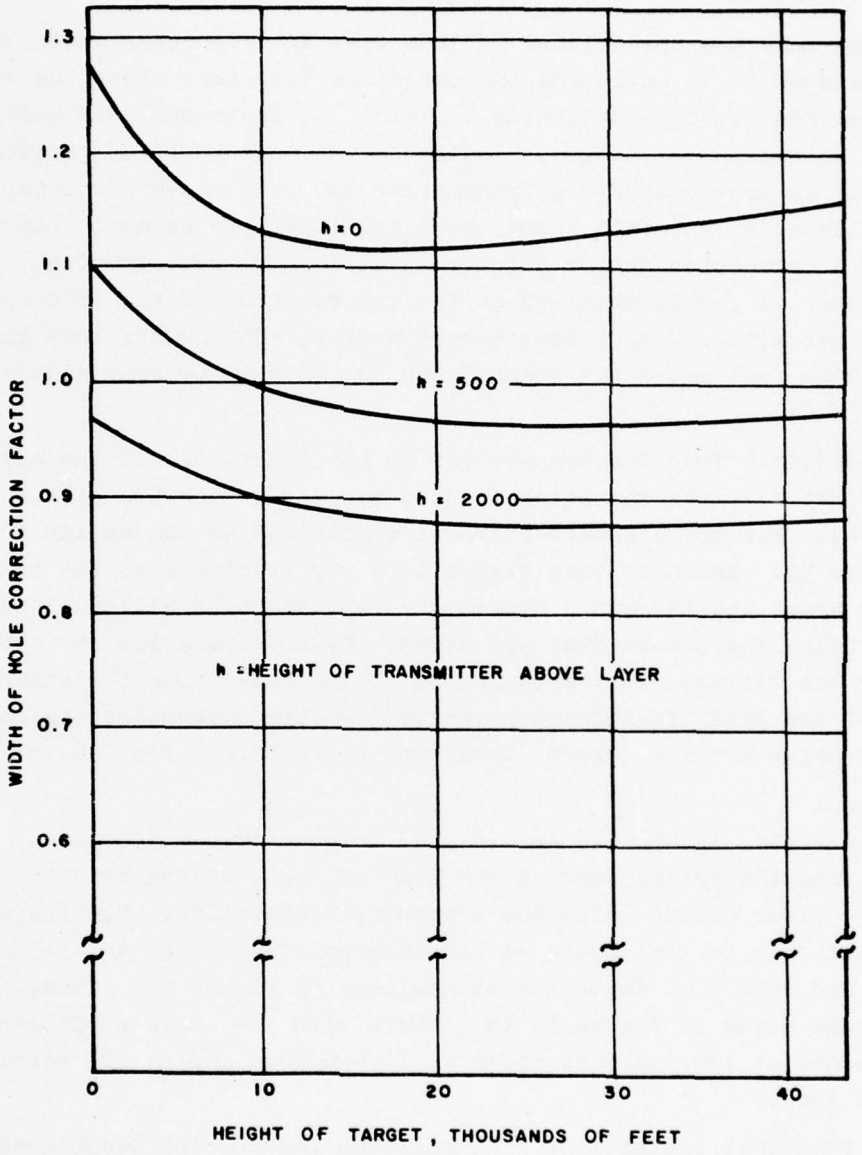

Figure 49. Correction Factor for Variation of Transmitter and/or Target Altitude above Transmitter (after Fannin [19]).

An example to illustrate the use of these diagrams is given below:

Example

Assume that the transmitter is 1000 feet above a layer whose thickness is 500 feet and ΔN is 40 units and the target is 5000 feet above the transmitter. First enter Figure 48 to determine the width of the radar hole under specified reference conditions. The graph indicates the hole to be 65 nautical miles wide. This is true only for a transmitter 500 feet above the layer and at a reference level 10,000 feet above the transmitter, so we must enter Figure 49 to obtain a correction factor for the specific altitudes involved. For this case a factor of .98 is obtained at the intersection of the 1000-foot transmitter height with the 5000-foot target height. This means that the hole width at 5000 feet above the transmitter is $.98 \times 65$ or approximately 64 nautical miles.

The distance from the transmitter to the inner edge of the hole is closely approximated by the ray which is just tangent to the top of the layer (Figure 44). For the standard refractive gradient we can obtain this distance from Figure 50. Shown in this Figure is a ray tracing with the transmitter at 4000 feet above the terrain. Successive rays reaching altitude increments of 500 feet below the transmitter are drawn. By interpolation it is possible to determine the distance to the beginning of the radar hole for cases in which the top of the layer is located anywhere from the transmitter height down to 4000 feet below and for target elevations up to 20,000 feet above the transmitter.

For example, if we have an elevated transmitter at 2000 feet, then the distance from the transmitter to the edge of the hole can be determined easily whenever a layer exists below the transmitter elevation. For instance, if it is 800 feet down to the layer, we can interpolate between the rays passing 500 feet and 1000 feet below the transmitter in Figure 50. Thus, adjusting the altitude scale in Figure 50 to conform with the above conditions, the hole will commence at 150 nautical miles at 10,000 feet and at 203 nautical miles at 20,000 feet.

f. Practical Limitations. In applying ray-tracing techniques to practical propagation problems, several limitations should be kept in mind. First, elevated layers as they occur in Nature are rarely uniform over the 100- to 200-mile ranges called for in the foregoing ray treatment. Even if one had an accurate refractive-index profile at one point along the propagation path, this would not necessarily be representative of the layer characteristics 100 miles, or even 50 miles, away. Usually elevated layers can be regarded as being reasonably uniform, but one must remember that a single radiosonde ascent may not be representative of the layer in question. It is always necessary to consider carefully all available synoptic information.

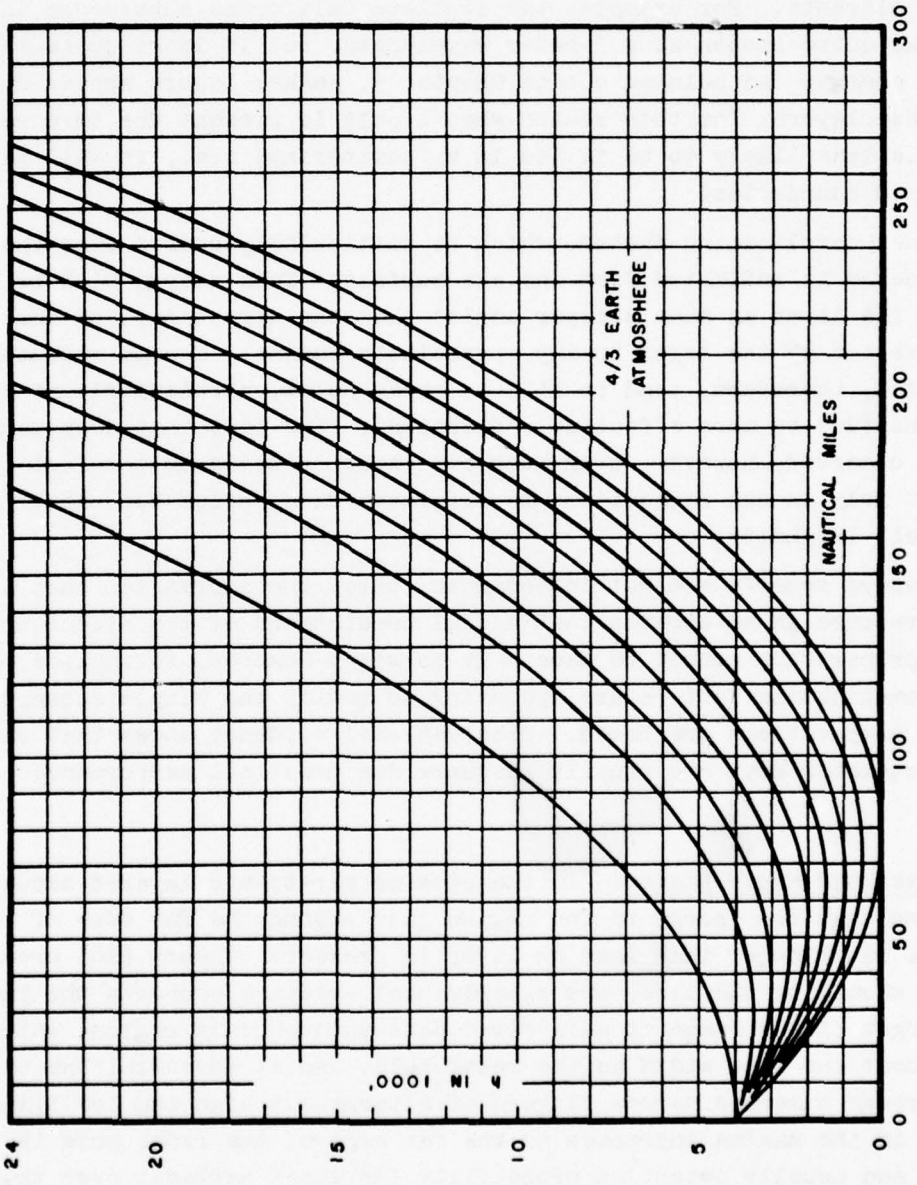

Figure 50. Ray Paths at 500-Foot Intervals Below Transmitter.

Another characteristic of layers is that they have small-scale irregularities which make them more like a ground glass mirror than a smooth mirror in the region of total refraction. This has the effect of scattering energy into the radar hole from adjacent rays. This "filling in" of the theoretical well-defined radar hole is more apparent at the edges of the hole, particularly at shorter wavelengths, since these wavelengths are more affected by small-sized roughness elements. For example, the southern California subsidence inversion layer looks quite smooth at a 3-meter wavelength, but it looks quite rough to 0.5-meter energy. As pointed out in Chapter 5, weaker layers appear smoother than intense layers; for this reason when a hole is present due to a weak layer it is less likely to be filled in by scattering; i.e., it will have more well-defined boundaries.

Another complicating factor, which is particularly common over the sea, is that energy is reflected from the sea surface. This energy will be incident upon the layer at much steeper angles than the direct ray and thus will not be affected by the layer to any appreciable extent. Energy reflected from the sea will, therefore, tend to fill in radar holes, particularly at longer wavelengths (due to more efficient reflection). The fact that deep radar holes are observed, however, even over sea paths, attests to the fact that one should not rely on sea reflections to eliminate radar holes but rather only to reduce their intensity.

The above remarks are not intended to convey the impression that atmospheric structure is so erratic that useful predictions of its effect on radio or radar propagation cannot be made. It is wise, however, to realize that various complicating factors are operating to modify the simple assumptions on which the computations are based. Observational evidence shows that radiosonde and refractometer data are usually adequate for practical performance calculations.

6.3.2. Extended Radar Ranges. In the case of air-to-air layered situations, it is found that the energy in the region just beyond the far edge of the radar hole is stronger than when no layer is present. Theory [16] predicts that this should be the case, and experimental evidence supports the theory. As the target closes range it will first pass through this region, which is usually about the same width as the radar hole. As it moves in, the target passes through numerous narrow fingers of alternately high and low illumination. The field in the maxima increases as the far edge of the radar hole is approached, and usually detection probability increases markedly over that expected if no layer were present. Finally, when the far edge of the radar hole is passed, the target will be lost until it emerges from the near edge of the radar hole at relatively close range. The layer, therefore, serves to

extract radar energy from the region of the radar hole and to concentrate it in the region beyond. As mentioned above, the enhancement is strongest just beyond the radar hole; it decreases gradually through a distance about equal to the hole width, and merges with the free space field beyond.

When a layer is present which causes a radar hole, the best operational procedure is to fly the radar above the layer at a height such that the far edge of the radar hole coincides with the radar's normal detection range. In this way, the enhancement beyond the radar hole will serve to increase the detection range by at least half the width of the radar hole.

6.4. Employment of Ray-Tracing Catalog for Radar Coverage.

Using approximate theoretical ray-tracing procedures, the effects of atmospheric conditions on radar coverage can be estimated. Although this technique suffers from the limitations described in section 2.1.2 and the assumption of horizontal stratification with a standard refractivity-index gradient (-12N/1000 feet) above and below a single layer (see Figure 39), it has been found that many cases encountered in the atmosphere can be treated with good qualitative results.

6.4.1. Ray-Tracing Diagrams. The flat-earth concept described in section 4.3 was employed for the ray-tracing catalog given in Volume II, Appendix B. Since the earth's curvature is added to the curvature of each ray, the patterns shown in the catalog have curvatures which differ from the true ray curvature. However, this transformation of curvature does not matter in the correlations between the ray tracings and the propagation effects they portray.

Each ray pattern shows the direct paths followed by the rays in a given atmosphere. They do not show the reflected paths of downcoming rays which are emitted from the transmitter at negative values of the initial elevation angle, α_o, and which are reflected at the earth's surface. In each ray family the rays are radiated in a series of equal increments of vertical angle from a transmitter at a fixed position. In this way the relative concentration or scarcity of rays in a ray family gives a graphic picture of the relative strength or weakness of radar signals in the region. This interpretation assumes that the reflected rays, which are not considered in this catalog do not give appreciable signals in the areas concerned. This has been found to be true in propagation over land many times, and over the ocean sometimes. The ray-crossing areas gives rise to anti-holes regardless of reflections, as a result of interference of the crossing rays. A radar anti-hole is defined as a region, following a radar hole, in which the field intensity as a function of position in the region fluctuates above and below the corresponding field

intensity in free space.

In this ray family presentation the beam shape is not considered. This does not present a serious limitation since tilt angle of the antenna will vary somewhat from one site to another and with other different conditions.

6.4.2. Radar Coverage Catalog. Considerable value can be derived from reference to a graphic representation of radar coverage. The cases included in Volume II, Parts 1 through 6 (Appendix B) are hypothetical cases which bracket situations frequently occurring in the atmosphere. These cases are indexed by section on the basis of vertical distance from the transmitter with further internal distinctions as to layer thickness and N and B change at the layer.

The following discussion is an illustration of how the information contained in the catalog may be applied.

Figure 51 presents a typical situation in which a radar on top of a coastal peak surveys an adjacent coastal region. A survey of the catalog reveals that Case 15 corresponds closely to the conditions illustrated in the figure. This situation differs from Case 15 by 2 N-units and 250 feet in distance above the layer. These differences can be taken into account by interpolation. In Case 4 the difference is 2 N-units as before, but 750 feet in distance above the layer. The difference in the N value is quite small and can be neglected; however, the height difference is fairly large and will cause an appreciable effect. When each case is evaluated in terms of distance to the radar hole, width of this hole, and refraction horizon[3], it is relatively simple, as a rule, to determine values of these parameters which will apply to the specific case under consideration.

Table 5 contains the values obtained from the catalog for the situation presented in Figure 51.

The effect of a surface duct in producing an extension of ground clutter is well illustrated by the cases in Volume II, Appendix B, Part 6. Increased duct intensity causes the rays to intersect the earth at a larger angle than in cases of lesser intensity. This results in a greater reflection of energy back to the radar and, therefore, a greater amount and intensity of ground clutter. It is also interesting to note the characteristic path length between hops with varying intensity and thickness of the duct. This may in some

[3] The refraction horizon is determined by the farthest distances reached by the appreciable densities of rays from the transmitter. Within this refraction horizon, there may occur large gaps (radar holes) which are not reached by rays from the transmitter.

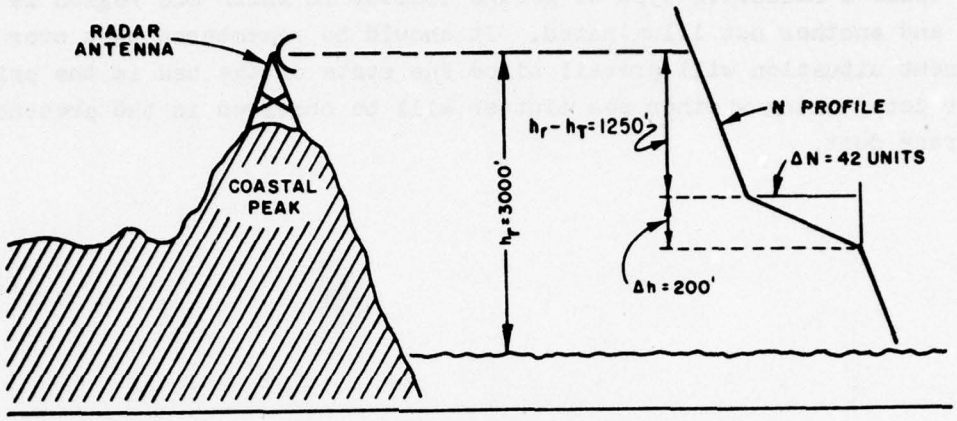

Figure 51. Radar on Coastal Peak.

TABLE 5

Sample Procedure for Evaluating Propagation Effects.

	Beginning of Radar Hole (n.m.)	Width of Radar Hole (n.m.)	Refraction Horizon* (n.m.)
	10,000 Feet Above Transmitter		
Case 15	168	58	233
Case 4	191	55	191
Interpolated Value	174	57	Unk**
	20,000 Feet Above Transmitter		
Case 15	218	56	283
Case 4	240	52	240
Interpolated Value	224	55	Unk**

* In determining the refraction horizon for this particular case, it is assumed that rays passing lower than 3000 feet below the transmitter intersect the earth's surface and should be disregarded.

** The refraction-horizon calculation indicates in Case 15 that some coverage is afforded by the narrow band of rays passing at the outer edge of the radar hole. In Case 4 this does not occur and the initial detection is thus predicted at the inner edge of the hole. It is not feasible to interpolate between the values obtained in the above table.

cases cause a selective type of ground clutter in which one region is illuminated and another not illuminated. It should be remembered that over water a different situation will prevail since the state of the sea is the primary factor determining whether sea clutter will be observed in the presence of a surface duct.

Chapter 7

REFRACTIVE INDEX CLIMATOLOGY

In Chapters 4 and 5 of this report methods were discussed for describing the refractive properties of an atmosphere in terms of various refractivity profiles, and in Chapter 6 procedures were outlined for predicting radio-radar performance in terms of specific refractivity conditions.

In situations where specific information is lacking, and particularly for planning purposes, it is useful to develop a knowledge of the climatology of refractivity. Thus, an understanding of the refractive properties of the synoptic air-mass types is helpful in answering questions as to the horizontal extent and time persistence of refractive layers. For these reasons such a climatology is presented in the following paragraphs.

7.1. Seasonal Distribution of Refractivity Near the Surface.

If we examine the first term, the dry term, on the right-hand side of equations (78) or (79), we see that it is proportional to air density. From typical atmospheric data, it can also be shown that the dry term constitutes at least 60 percent of the value of N. For these reasons the refractivity is strongly affected by pressure changes.

In order to study the distribution of refractivity at the surface, it is desirable to suppress those variations produced solely by surface topography. For this purpose we use a technique analogous to that of reducing station pressures to sea level. Solving the expression for the standard refractivity profile, equation (81), for N_s we have

$$N_s = N_h \exp(c_d h)$$

where N_s is the refractivity at the earth's surface, N_h is the refractivity at height h above the surface, and c_d is the exponential coefficient of a particular standard profile. We then define a datum refractivity, N_o, as follows:

$$N_o = N_s \exp(c_d h_s) \tag{123}$$

where N_s is the surface refractivity, h_s is the height of the surface, and c_d is again the exponential coefficient of a particular standard profile. The datum refractivity is then the value obtained if one extrapolates the surface

value along a standard refractivity profile to zero height.

In order to facilitate the reduction of surface refractivity values to the zero-height datum, Figure 52 has been prepared, using the value of $c_d = 0.1057$ as arbitrarily adopted by Bean and Riggs [7] as being the most representative standard profile. Equation (123) then becomes

$$N_o = N_s \exp(0.1057 h_s)$$

where N_o, N_s, and h_s (in kilometers) are defined as in equation (123). In use, one locates the point on Figure 52 corresponding to the surface refractivity, N_s, and the surface elevation, h_s. By laying a straight edge through the point and parallel to the set of sloping, dashed lines, the datum refractivity, N_o, may be read from the ordinate scale. Other values of the exponential coefficient, c_d, could be represented on Figure 52 by additional sets of sloping, dashed lines of different slopes.

Using the reduction method described above, Horn, Bean, and Riggs [22] have prepared world-wide maps of datum refractivity for various months and seasons. Figures 53 and 54 show these results for the months of February and August. It can be seen that N_o varies from 390 in humid tropical areas to 290 in desert and plateau regions. Continental interiors and mountain chains in middle latitudes are reflected by low values of N_o as compared to coastal areas. Such major climatic details as the Indian monsoon and orographic rain shadows are also indicated by the N_o contours.

Figure 55 illustrates the climatic response of surface refractivity and shows a world-wide analysis of the annual range of monthly mean values of N_s. Climatic controls, such as the prevailing transport of maritime air inland over the west coasts of North America and Europe, are indicated by relatively small annual ranges of N_s (20 to 30 units). On the other hand, a range of 40 to 50 units or more along the east coast of the United States reflects the frequent invasion into this area of such diverse air masses as continental arctic and maritime tropical. The largest annual ranges of N_s (90 units) are observed in the Sudan of Africa and in regions affected by the Indian monsoon.

7.2. Refractive Index Characteristics of Air-Mass Types.

An air-mass type may be defined as an extensive portion of the earth's atmosphere whose properties (principally temperature and moisture) approximate horizontal homogeneity. Since the temperature and moisture distributions determine the refractive properties of the atmosphere, it is evident that certain characteristic refractive distributions may be expected in each air mass. This general dependence of refractive properties on air masses is the

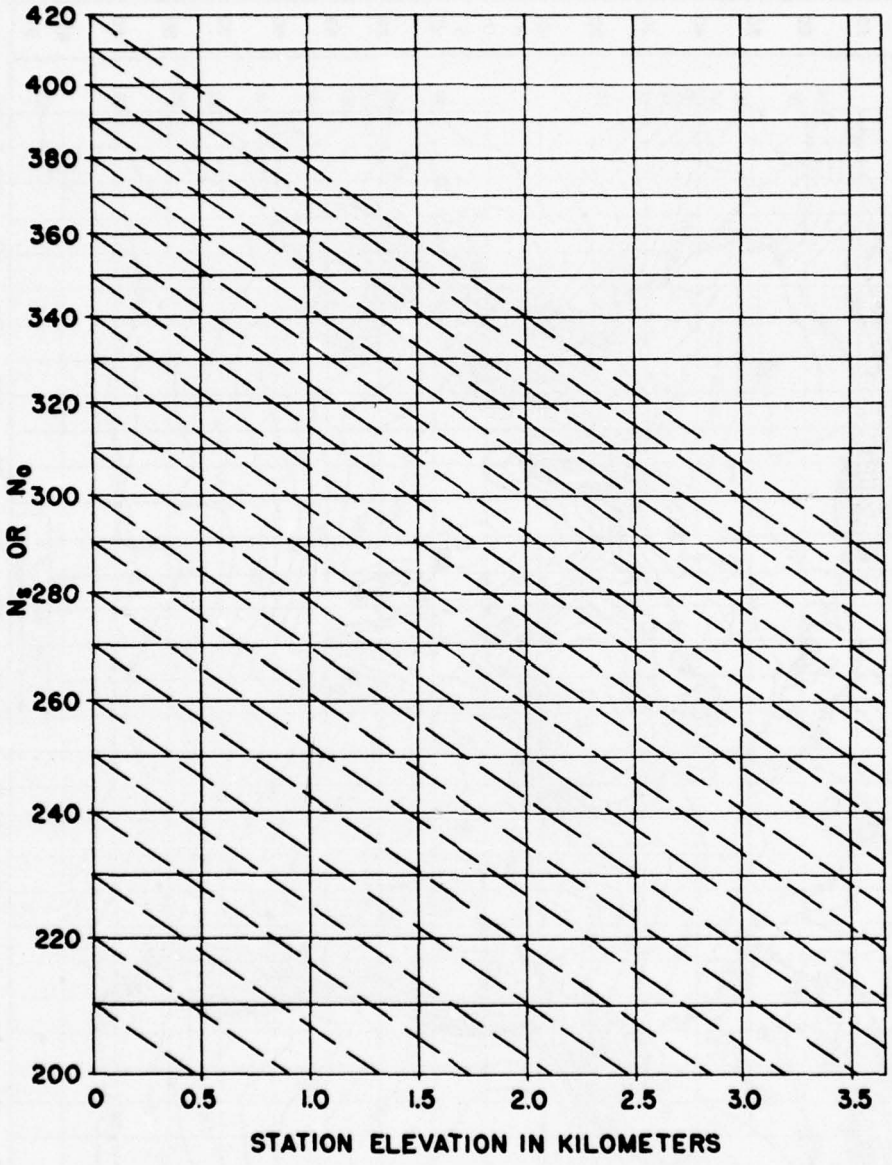

Figure 52. Chart for the Reduction of N_s Values to N_o Values.

initial consideration, and the broad basis, for forecasting refraction.

In this section we will employ, following Plank [29], the B-profiles of refraction index discussed in sections 3.4.1 and 4.2, since we are primarily interested in departures from standard conditions which are exhibited by air

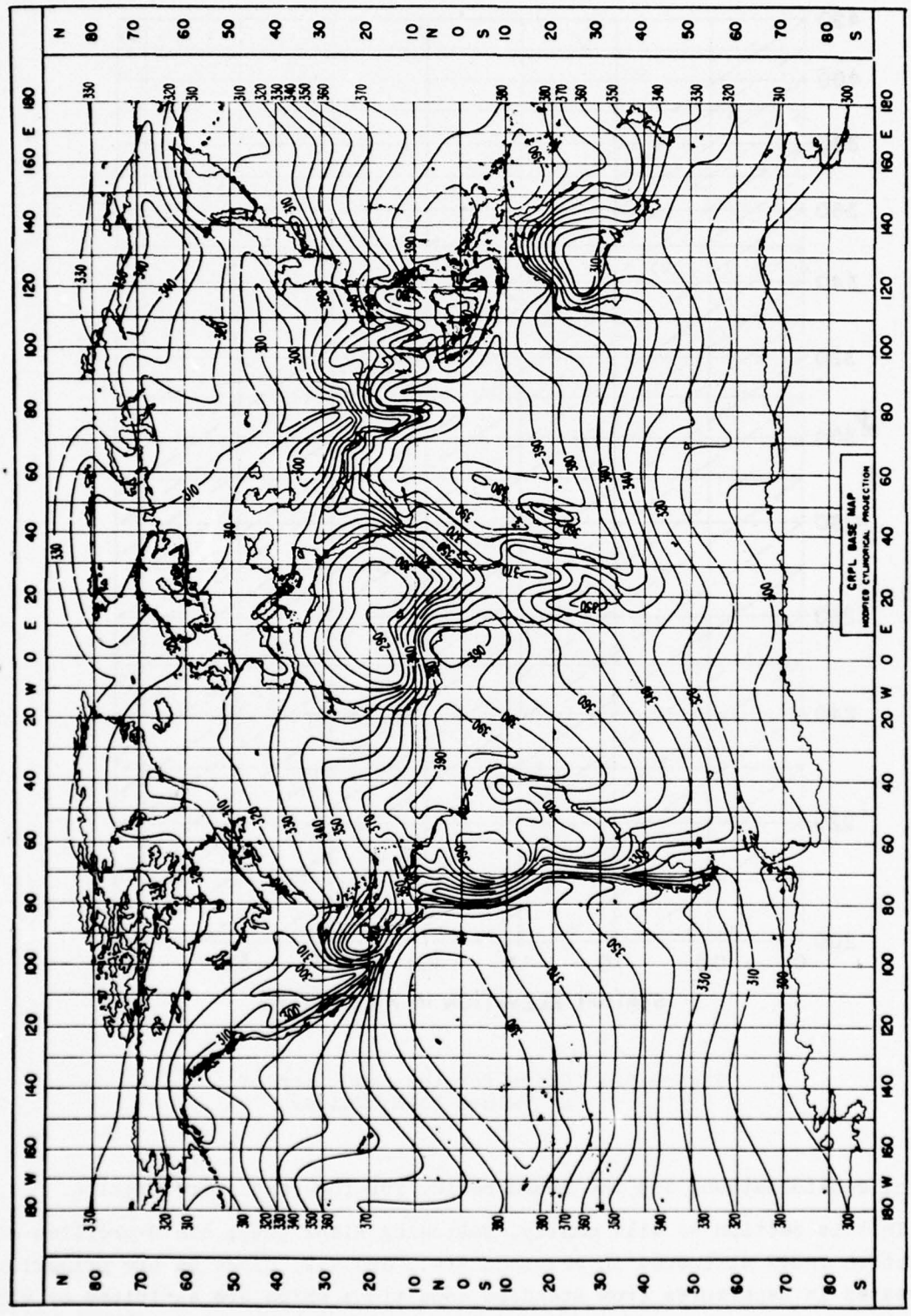

Figure 53. World-Wide Distribution of Datum Refractivity, N_o, for the Month of February.

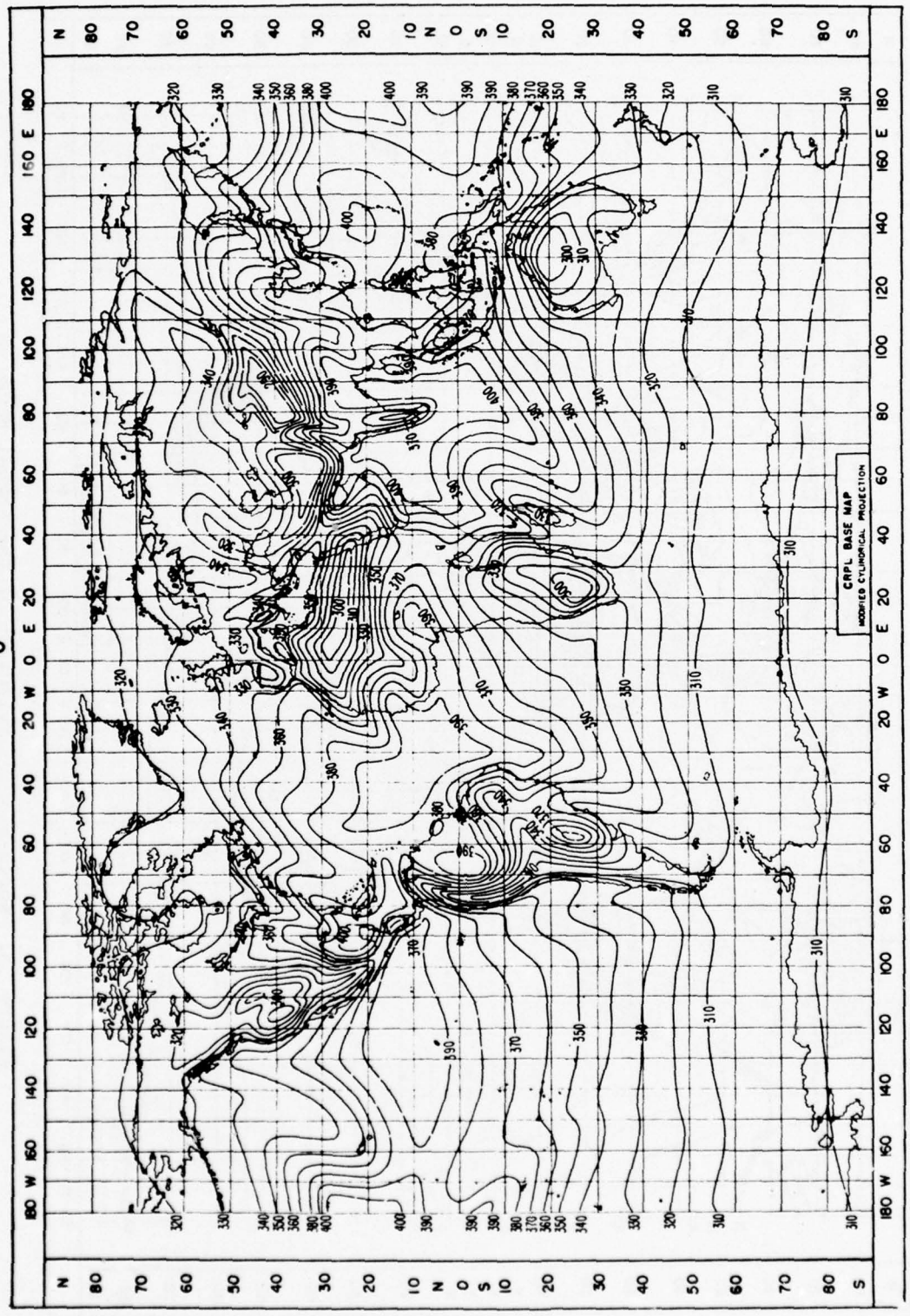

Figure 54. World-Wide Distribution of Datum Refractivity, N_0, for the Month of August.

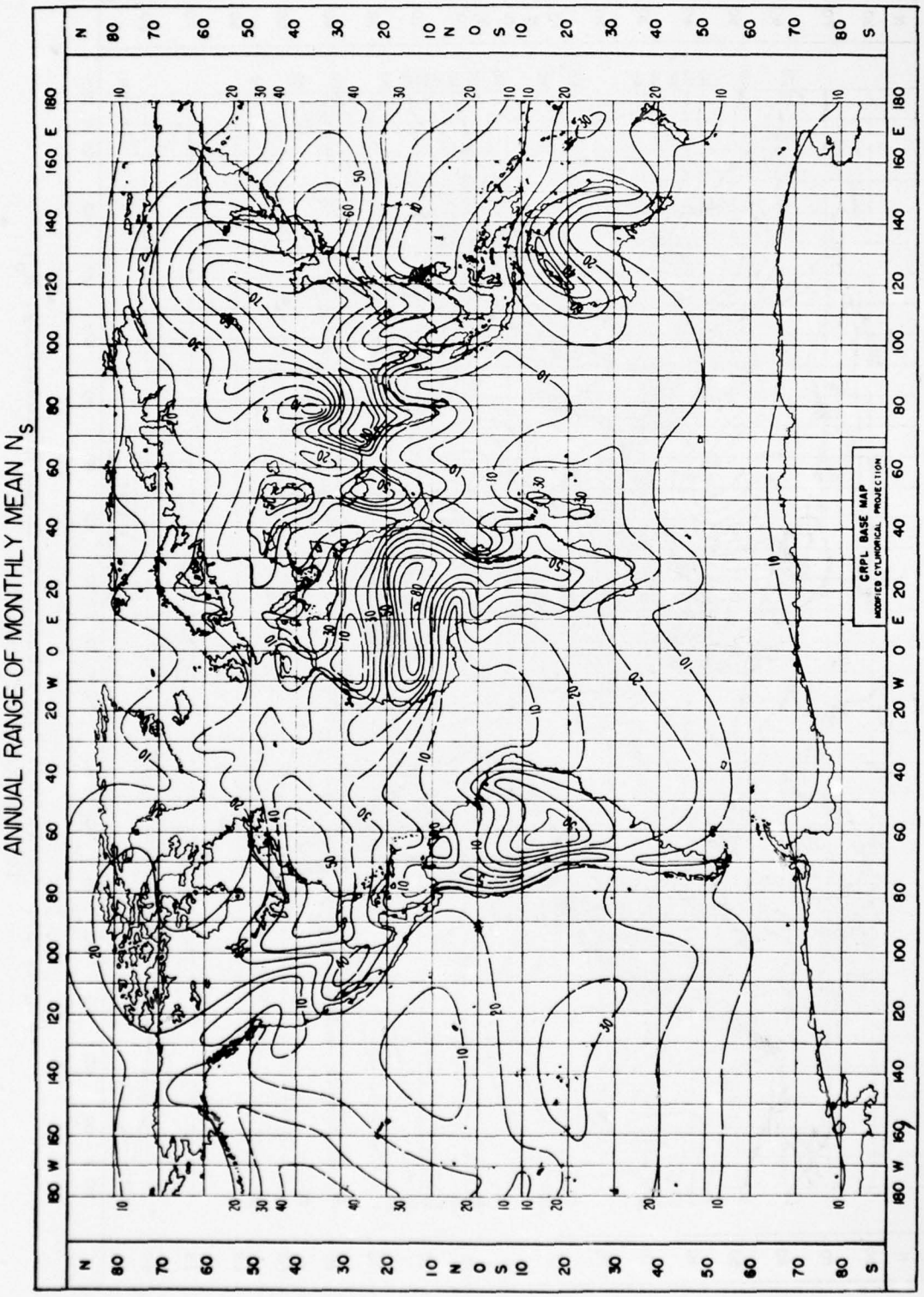

Figure 55. World-Wide Distribution of the Annual Range of Monthly Mean Refractivity at the Surface, N_s.

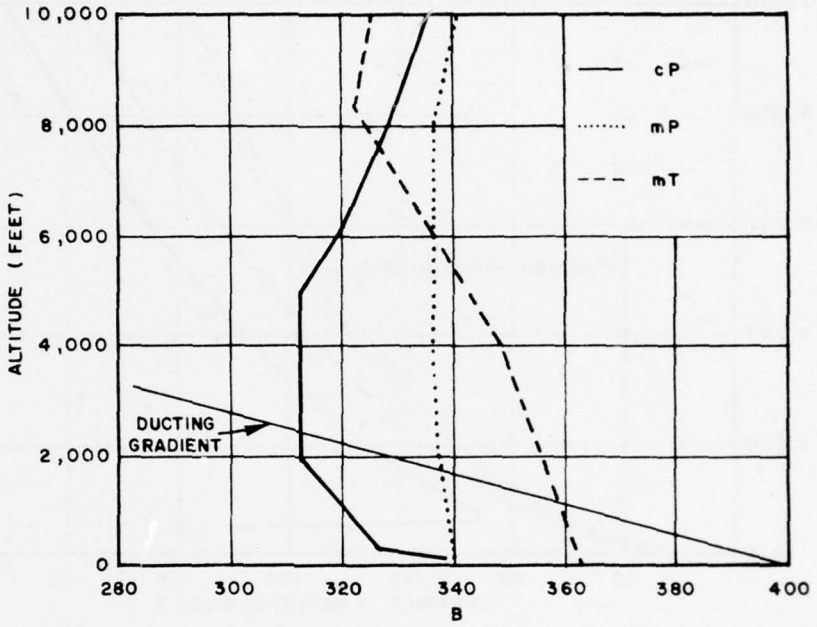

Figure 56. Typical Winter B-Profiles in the Source Region (after Plank [29]).

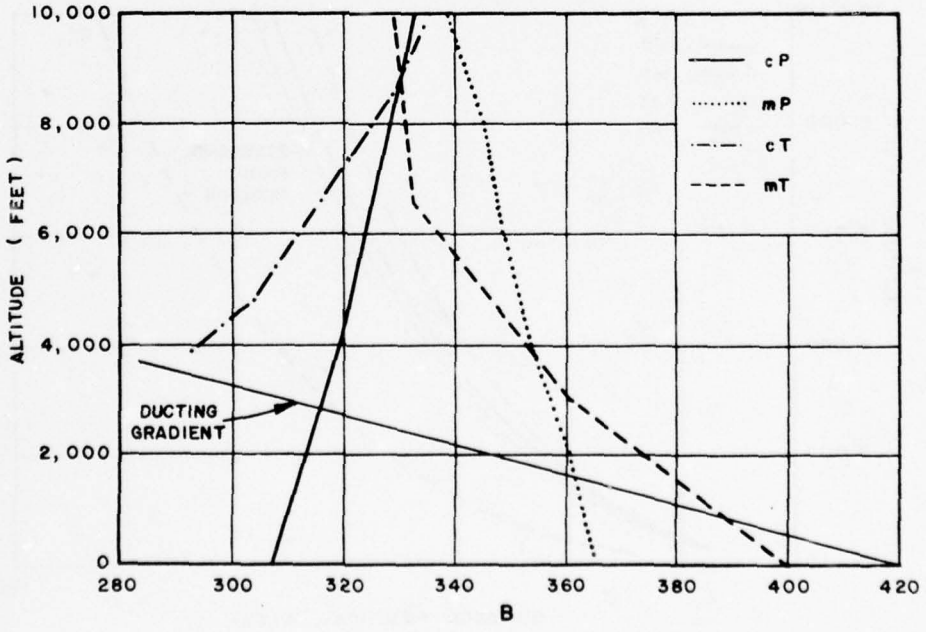

Figure 57. Typical Summer B-Profiles in the Source Region (after Plank [29]).

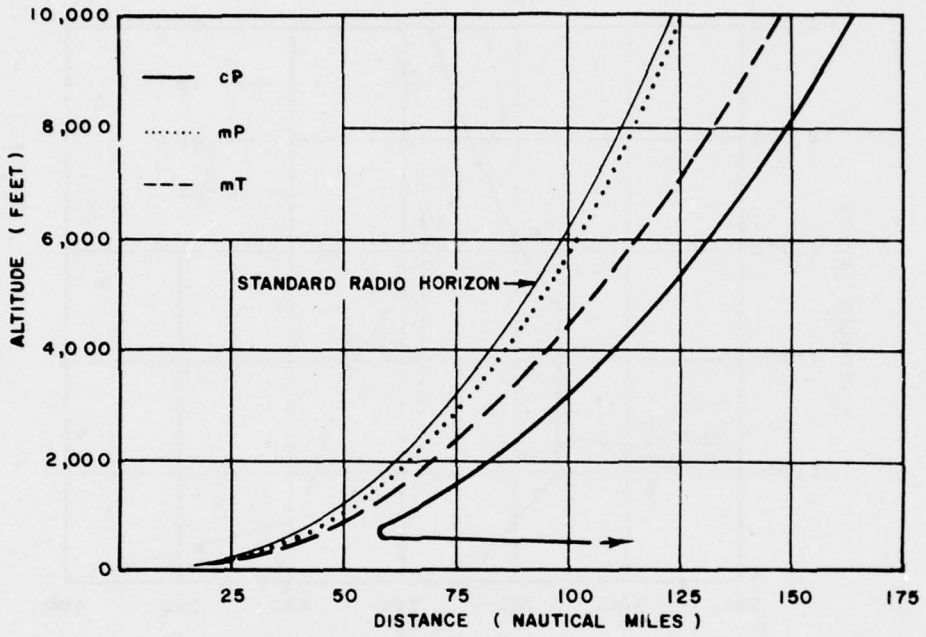

Figure 58. Probable Source Region Radio Horizons in Winter. Transmitting antenna height assumed to be 70 feet (after Plank [29]).

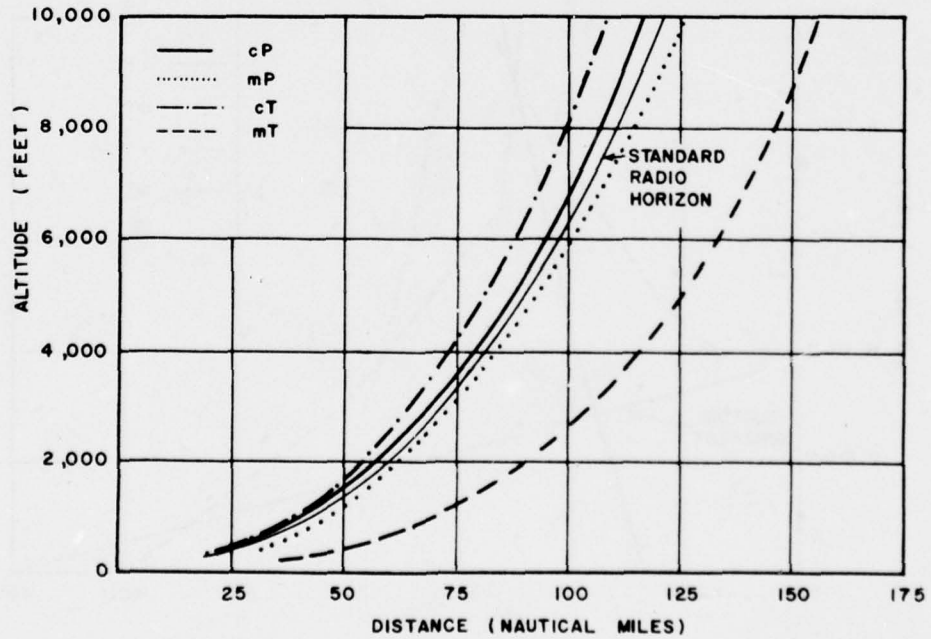

Figure 59. Probable Source Region Radio Horizons in Summer. Transmitting antenna height assumed to be 70 feet (after Plank [29]).

TABLE 6

Meteorological Properties in Air-Mass Source Regions
(Petterssen, 1940 [28]; Willett, 1944 [39]; Anderson, 1951 [1])

Type	Source-Region Characteristics	Air-Mass Properties in Source Region
Continental-Polar Winter (cP)	1. Land, snow, or ice surface 2. Excessive outgoing radiation 3. Average 80% reflection of sun's insolation 4. Low temperature: -25°C to -50°C 5. Average high pressure, with subsiding air aloft and horizontal divergence at the surface	1. Strong surface temperature inversion 2. Isothermal middle layer (no change of temperature with height) 3. Steep temperature lapse rate aloft; approximately 8° C/km 4. Very dry; mixing ratio less than 1 gm/kg
Summer	1. Snow-free land areas 2. Strongly-heated, long days, short nights 3. Relatively dry area, surface moisture available only from vegetation, rivers, lakes, etc.	1. Steep temperature lapse rate in lower levels; approximately 8° C/km 2. Stable aloft 3. Dry; mixing ratio approximately 5-6 gm/kg 4. Large diurnal temperature range
Continental-Tropical* (cT)	1. Dry land area 2. Extreme heating (greater than 35°C during daytime) 3. Thermally created low surface pressure with high-level anti-cyclone aloft	1. Adiabatic lapse rate of temperature to high levels 2. Superadiabatic lower levels in daytime 3. Warmest possible air 4. Mixing ratio of 3-4 gm/kg; very dry at all levels 5. Large diurnal temperature range
Maritime-Polar Winter (mP)	1. Ocean surface 2. Water relatively warm compared with air in western section; in central and eastern sections, air and water temperatures approach equilibrium 3. General low pressure 4. Convergence 5. Rapid moisture lapse near surface	Western Section 1. Steep to superadiabatic temperature lapse rate in the first 50-100 ft above the sea surface 2. Convectively unstable lower levels 3. Steep lapse rate aloft 4. Rapid decrease of moisture in first 50-100 ft 5. Little diurnal temperature variation Eastern Section 1. Convectively unstable lower strata; temperature lapse rate approximately 6-7° C/km 2. Uniform moisture distribution with height; mixing ratio averages 6-8 gm/kg

TABLE 6 (Cont'd)

Type	Source-Region Characteristics	Air-Mass Properties in Source Region
Maritime-Polar Winter (Cont'd)		Eastern Section (Cont'd) 3. Cold and dry above 10,000 ft 4. Little diurnal temperature variation
Summer	1. Ocean surface 2. General moderate pressure with weak gradients 3. Water temperatures which may be warmer or colder than air	1. Convectively unstable lower layers to 6000 or 8000 ft; lapse rate about 8° C/km 2. Uniform moderate decrease of moisture with height 3. Dry aloft, with subsidence above the level of convection 4. Slight diurnal temperature variation
Maritime-Tropical (mT)	1. Ocean surface 2. Water temperature approximately 27-30°C 3. Average high pressure 4. Weak air flow	1. Moderately steep lapse rate, approximately 7-8° C/km 2. Convectively unstable below 6000 to 10,000 ft 3. Very moist air; surface mixing ratios range from 18-24 gm/kg 4. Large moisture gradient to top of convective mixing layer 5. Subsiding air aloft, which tends to cap convective activity 6. Little diurnal temperature variation
Winter	1. Ocean surface 2. Water warmer than adjacent land; water temperature average 21-24°C 3. Average high pressure 4. Weak air flow	1. Moderately steep lapse rate, 7-8° C/km 2. Convectively unstable below, 8000 to 10,000 ft 3. Moist air; surface mixing ratios range from 13-15 gm/kg 4. Moderate uniform decrease of moisture with height 5. Subsidence above level of convection 6. Little diurnal temperature variation

* Because the characteristics and properties of both summer and winter cT air are essentially the same, only summer is covered.

masses. When B-profiles show layers with negative gradients, these layers are defined as ~~superrefractive or~~ superstandard, when they show positive gradients they are termed ~~subrefractive or~~ substandard.

Typical
Tropical winter and summer modified refractive-index profiles for air masses in their source regions are shown in Figures 56 and 57. These B-profiles were computed from typical soundings for the pertinent air-mass type. Also, Figures 58 and 59 show the radio horizon that should be expected for an antenna 70 feet above the ground operating in these air masses. When dealing with air-mass types average conditions are being considered. At any particular station and time the local atmospheric conditions may be much more important in refraction.

For convenience, the characteristic properties of each air-mass type are summarized in Table 6. The air-mass classification is the one in common synoptic use, based on type of surface and latitude of the source region.

7.2.1. Continental-Polar—Winter. The shape of the B-profile for the typical source-region winter cP air in Figure 56 reflects the air-mass properties as outlined in Table 6. The superrefractive lower portion of the profile is due to the temperature inversion, the standard middle portion to the isothermal middle layer, and the subrefracting upper portion to the steep temperature lapse rate aloft. The moisture content of winter cP air is so low that it is not an important factor in determining the shape of the B-profile.

Four actual B-profiles taken in cP air are shown in Figure 60. These profiles show the typical refractive conditions of the air mass even though a considerable distance from the source region. Variation from the typical profiles of Figure 56, although apparent, certainly is not extreme.

When refraction is considered alone, the radio horizon for typical winter cP air in the source region should look like the plot in Figure 58. Surface trapping can occur as a result of the very intense temperature inversion when the layer is sufficiently thick compared with the wavelength. Its presence or absence will be a function of wind speed and turbulence. Low speeds permit the temperature inversion to become intense; higher speeds tend to bring warmer air from aloft down to the surface, thereby destroying or weakening the inversion. The radio horizon above the trapping region should be extended about 25 percent. Because of the low sun angle and the high reflectivity of the snow surface, there is little warming during the day and diurnal temperature variations are small. As a consequence, the refractive properties of winter cP are much the same both day and night; therefore, the refractive-index profile for this air varies but little with time. This profile characteristic will be referred to as conservative.

Figure 61 shows the successive stages of modification in the refractive properties of air resulting from continued stay in a winter cP source region. The original idealized soundings from which refractive-index values were

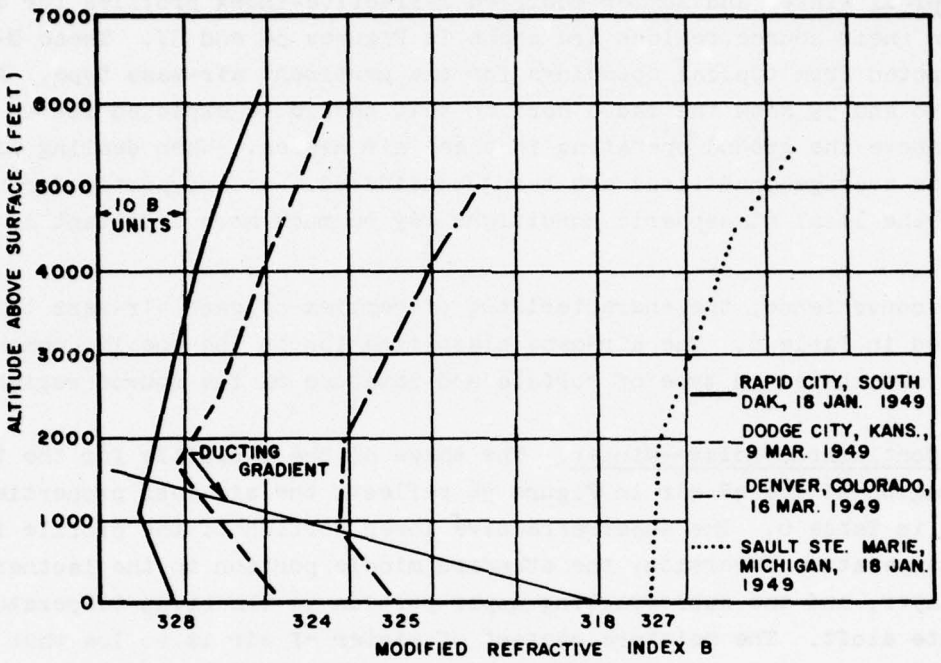

Figure 60. Examples of B-Profiles in Winter cP Air. Profiles are displaced along abscissa as shown (after Plank).

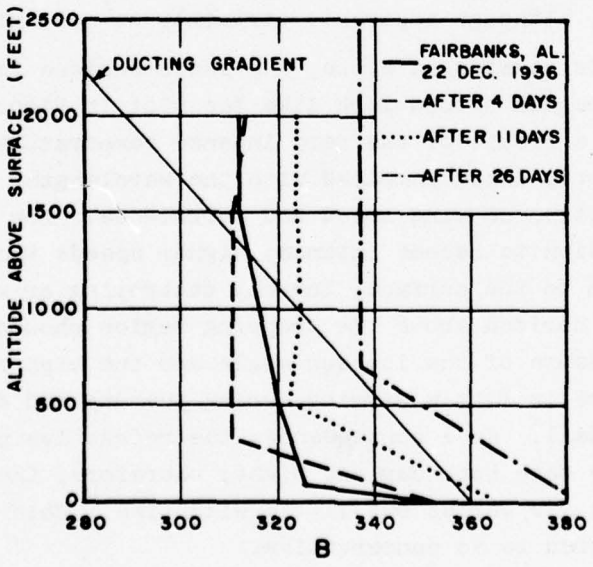

Figure 61. Successive Stages of Modification of a B-Profile in a cP Source Region (after Wexler [38]).

computed were presented by Wexler [38], who assumed ideal radiation conditions. The refractive-index profile for 22 December 1936 at Fairbanks, Alaska, was presented by Lukes [26] in verification of Wexler's deductions. The B-profiles for 4, 11, and 26 days after that date were modified from Lukes' data. It is interesting to note that each of the four B-profiles in Figure 61 has a ground-based superrefractive stratum sufficiently intense for ducting.

When the air mass moves out of the source region, the properties acquired in the source region are carried along with it and are gradually modified by the surface over which the air passes and by the meteorological conditions along the path. Winter cP usually moves out of the source region behind a cold front as a definite mass of air. Normal modification of this moving air results from (a) addition of heat and moisture from the surface, (b) subsidence, and (c) turbulence. The modification processes vary with type and condition of terrain and the synoptic situation, but the usual changes in refractive conditions are:

a. Elimination of surface trapping and surface superrefractive strata to greater or less extent depending on:

(1) Turbulence; when turbulence is strong the strata are wiped out.

(2) Advection over snow-covered land or snow-free land surface; modification is slight over a snow-covered surface and moderate over snow-free surface.

b. Formation of a superrefractive layer to an approximate average height of 50 feet with passage over water. Air above this level slowly becomes more superrefractive with increasing time of passage.

c. Greater diurnal variations of refractive properties as the air mass moves southward; diurnal temperature range becomes greater as the sun angle becomes larger and as less reflecting snow surface is encountered.

d. Day-to-day change of the refractive properties aloft because of subsidence.

The refractive-index profile for winter cP moving over a snow-covered surface should be conservative both day and night. The profile for cP moving over a snow-free surface should be slightly variable during the day and conservative during the night.

Figures 62 and 63 show two different types of refractive modifications associated with the same cP air mass as it moves out of the source region. Figure 62 reveals the refractive changes that occur in a stream of cP air which moved from near Norman Wells on 18 January 1949, to Churchill on the 19th, and thence to Buffalo on the 20th. This air moved along the foreside of

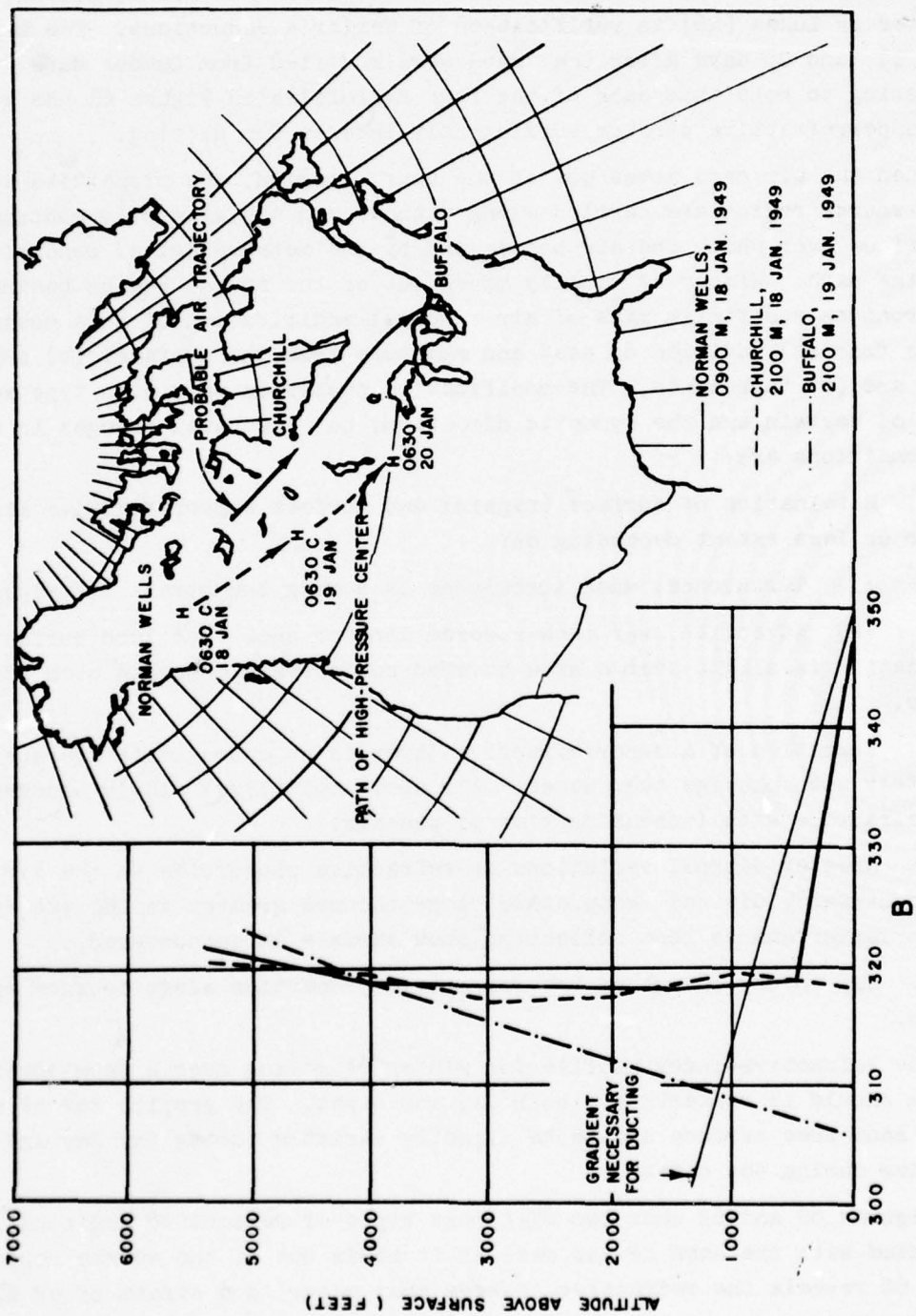

Figure 62. Modification of Air Along the Front Side of a cP High.

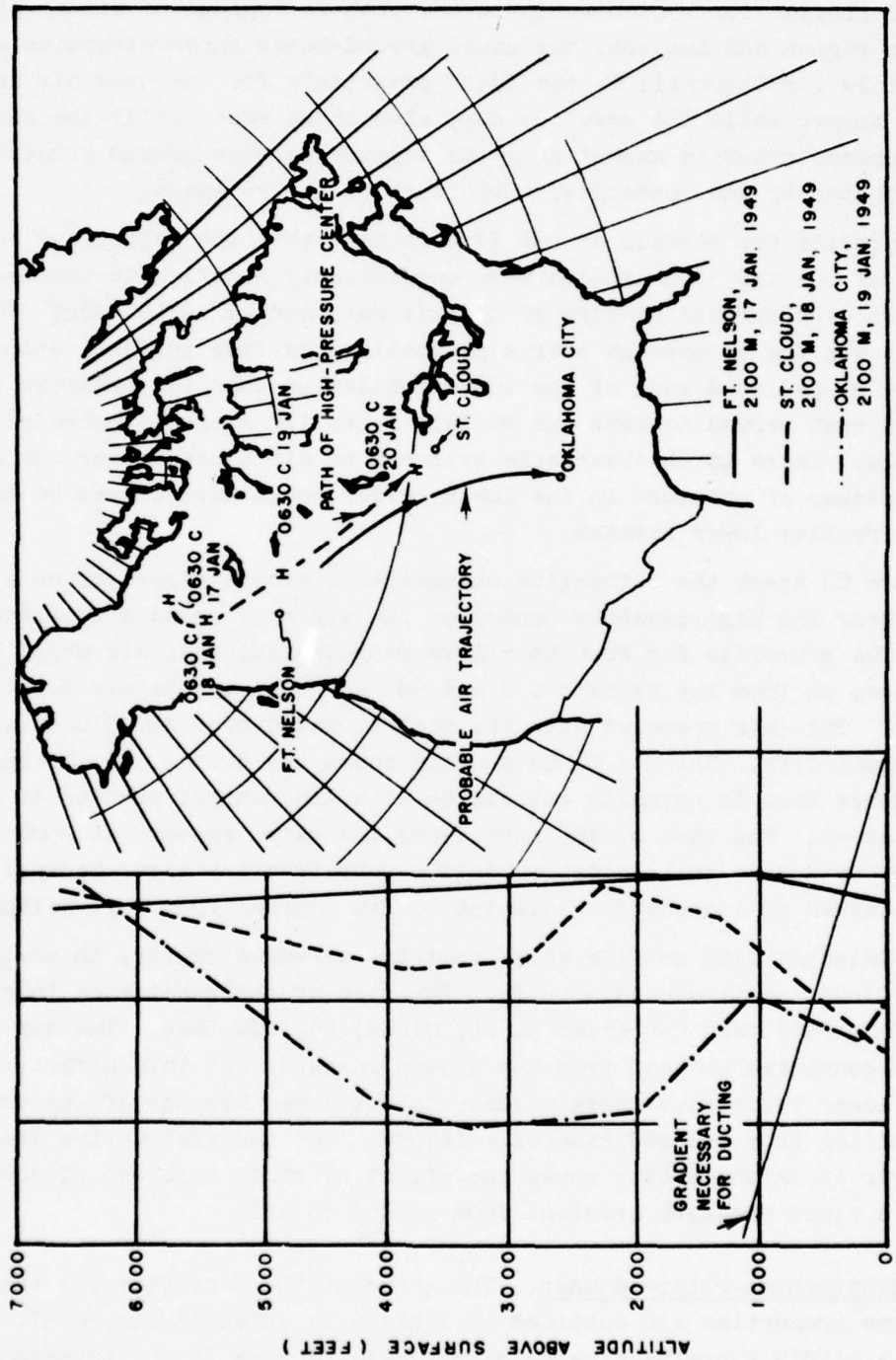

Figure 63. Modification of Air Near Center of a cP High (after Plank).

the air mass under the domination of the clockwise circulation of the associated anticyclone.

The B-profile for Norman Wells on the 18th is typical of winter cP air in the source region and includes the usual ground-based superrefractive stratum. The B-profile for Churchill on the 19th, presumably for the same air as observed at Norman Wells the previous day, also shows essentially the same refractive characteristics except that the superrefractive ground stratum has been eliminated by the mechanical turbulence of air movement.

The profile for Buffalo on the 20th reveals that the refractive characteristics of the air at Churchill were considerably modified in the 24-hour travel period by surface heating of the air mass and by turbulence. The heating effect was due to passage over a partially snow-free surface, which absorbed and re-radiated more of the sun's insolation than the previous terrain. This added heat served to make the Buffalo B-profile slightly subrefractive to high levels. There is no observable evidence of air passage over the Great Lakes; a pickup of moisture in the lower levels would have served to establish a superrefractive lower stratum.

Figure 63 shows the refractive changes in a second stream of cP air which traveled near the high-pressure center as the air mass moved out of the source region. The B-profile for Fort Nelson is representative of air which had recently moved in from the Pacific and had not yet been completely modified to winter cP. This air traveled with the center, moved over St. Cloud, and thence over Oklahoma City. The St. Cloud profile shows the drying and warming effects of subsidence that is normally associated with the central portion of high-pressure areas. The base of the subsidence inversion appears at 2500 feet. The lower portion of the profile reveals a subrefractive layer because the air mass was warmed by increased insolation in its journey from Fort Nelson.

The Oklahoma City profile shows that the air-mass center, in moving from near St. Cloud, continued to subside. The base of the subsidence inversion lowered from 2500 feet (observed at St. Cloud) to 1200 feet. The air also picked up considerable heat from the ground enroute, but this effect, which tends to lower refractive-index values, is not shown because of the compensation resulting from the addition of moisture. The superrefractive ground-based layer at Oklahoma City shows the effect of rapid moisture pickup resulting from a vapor-pressure gradient from ground to air.

7.2.2. Continental-Polar—Summer. The shape of the B-profile for this air mass, whose properties are outlined in Table 6 is shown in Figure 57. The profile is mildly subrefractive to high levels because of the dryness and the large temperature gradient.

The radio horizon for summer cP in the source region as shown in Figure 59 is reduced about 5 percent, but is close enough to standard to be considered as such for most purposes. Source region diurnal effects, primarily due to the large diurnal temperature range of 15 to 25°C, will appreciably extend the radio horizon beyond standard, but trapping should rarely occur only on very calm, clear nights if at all. The refractive-index profile should be variable during the day because convection currents and eddies cause random time variations of refractive-index values. With decreased convection at night, profiles should be less variable.

Summer cP air does not usually move out of the source region as a definite mass, for summer pressure gradients are weak and the frequency of intense frontal activity is low. Rather, the air moves out in isolated streams, either behind weak frontal systems or on the foreside of highs, and is usually quickly modified by addition of heat and moisture from the surface and mixing aloft. As in the source region, the air remains unstable to 8000 or 10,000 feet.

Normal changes in the refractive properties of summer cP air outside the source region are slight, but with addition of heat and moisture the B-profile tends to become standard or slightly superstandard. Diurnal effects will extend the radio horizon but trapping should be rare. Daytime refractive-index profiles should be only moderately variable, because of increased convective activity and the presence of more moist air. The contribution of moisture in determining B exceeds the temperature contribution; consequently, convection currents and eddies in moist air cause greater fluctuations in refractive-index profiles than they do in dry air. Refractive-index profiles during the night are somewhat less variable because of decreased convective activity.

7.2.3. Continental-Tropical. Because winter cT air does not occur except in low latitudes and because, even in these latitudes, it has essentially the same characteristics as summer cT, only summer cT air will be discussed.

The shape of the B-profile in Figure 57 shows the effect of the meteorological properties. The profile is strongly subrefractive to high levels because of the dryness and large temperature gradient. The mixing ratios are so low for these temperatures that they are unimportant in determining the shape of the profile.

The radio horizon for typical cT air is shown in Figure 59. About 10 percent reduction should be normal. Diurnal effects due to the large diurnal temperature variation of 15 to 20°C are significant, but normally will not be very effective in extending the radio horizon beyond standard. With average

nighttime radiation, the radio horizon should become about standard. The refractive-index profile will generally be only moderately variable during the day, because of the extreme convective activity associated with this air mass. The profile will be variable at night.

Ordinarily cT air does not move far from the source region as a surface air mass but may mix with or overrun mT or other summer air masses; cT air is the only common dry air that will overrun moist air. A B-profile through an air mass overrun by cT air shows a superrefractive stratum at the zone of overrunning. This stratum results from the moisture decrease and temperature increase observed in going from the lower air mass to the overrunning cT air mass.

Since any superrefracting stratum associated with this overrunning will be elevated, it is problematic whether the stratum will be low enough to affect propagation appreciably. However, in certain regions it definitely is; for instance, along the southwest Pacific coastal area of the United States cT air occasionally overlies a surface layer of moist maritime air and causes refractive profiles similar to the San Diego B-profile in Figure 64.

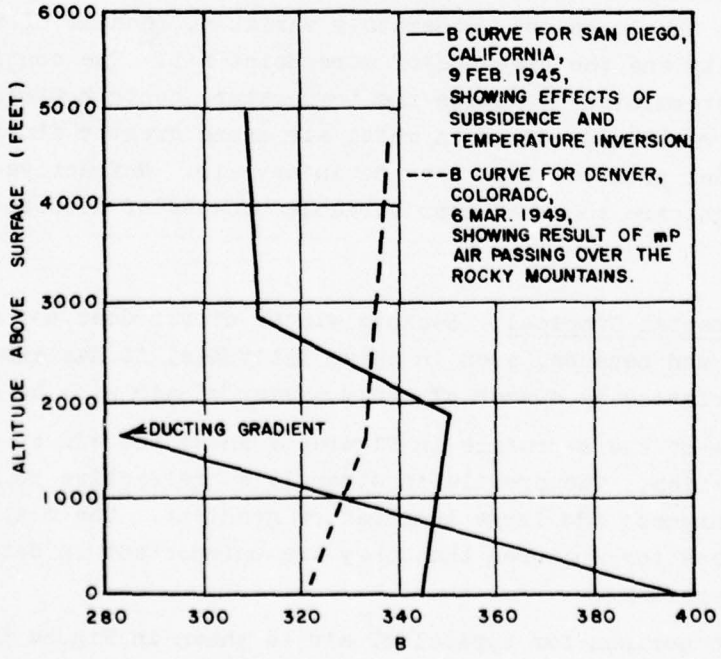

Figure 64. Profiles for Modified Winter mP Air (after Plank).

7.2.4. Maritime-Polar—Winter. Source regions of the mP type create new air masses with uniform properties by rapidly modifying continental air masses which normally enter the western side of the source region and move eastward across extensive water areas. Properties of the air in the western portion of the source region will be those of cP type starting to modify to mP, in the central portion those of a transitional type, and in the eastern portion, those of true mP air in approximate equilibrium with the sea surface. The effect of this modification on the refractive-index profile is discussed in the section on advection. The mP source regions should, therefore, be divided into at least a western and an eastern subsection when the refractive properties of the region are considered.

a. Western Section, Winter mP Air. The properties of air over the western section of the source region will be primarily due to the modification, by a comparatively warm sea surface, of cold continental air entering the source region from the west.

Depending on the wind speed and the gradients of temperature and moisture just above the sea surface, a surface-refracting stratum often exists which is sufficiently intense to trap radio and radar energy of centimeter wavelengths. Effects of the very steep lapse rate of temperature in the lowest levels which tend to create a subrefractive surface layer are overbalanced by the effects of the moisture gradient, yielding the trapping condition.

As this western-section air progresses eastward, the intense moisture and temperature gradients gradually decrease and the refractive properties of the lowest levels tend to become more standard. Over water, diurnal effects in western-section winter mP air are slight. Refractive-index profiles should be only moderately variable because of high winds and convective activity.

b. Eastern Section, Winter mP Air. The shape of the B-profile for the true winter mP air found over the eastern section of the source region is shown in Figure 56. The profile is very close to standard because of the unstable lapse rate of temperature and the low value of moisture gradient. The superrefractive surface layer associated with western-section mP air may still exist, but it is much weaker and less likely to affect propagation greatly because the moisture and temperature lapse rates are less extreme.

The radio horizon for winter mP air is normally standard. Diurnal effects over water are slight. Refractive-index profiles are only moderately variable because of prevailing high winds and convective activity.

As winter mP air moves out of the source region toward the western regions of a continent, refractive conditions should change radically. A number of geographical and meteorological factors may cause these changes, and it is

difficult to consider them all in generalized statements. Each coastal locale should be considered separately. However, some of the normal changes in the refractive properties of winter mP air after moving out of the source region are described below:

(1) An elevated superrefracting stratum will form when mP air moves over a cool coastal water current and air is simultaneously lowered from aloft by subsidence. The water cools the air near the surface and creates a temperature inversion. This inversion becomes elevated because of mechanical turbulence and is intensified by the effect of the warm dry air subsiding over and spreading out along its surface. An intense superrefractive stratum can be created in this manner, since both the temperature inversion and the moisture gradient within the inversion are usually extreme.

(2) Air from an mP source may become trapped in a coastal valley and progressively suffer a daily surface heat loss because the amount of incoming short-wave solar energy received at the ground is less than the energy lost to space by long-wave radiation at the earth's temperature. Such heat loss creates a temperature inversion just below the general level of the mountain crests, which augmented by the normal subsidence effect above causes an intense superrefractive stratum. Situations of this type are prevalent along west coast areas adjacent to source regions. For example, an inversion in the San Joaquin Valley in California, normally associated with a dense fog and smoke accumulation, is common in winter. A B-profile taken through such a valley inversion would appear very similar to the B-profile for San Diego in Figure 64.

(3) When mP air moves over an extensive mountain range, and there is orographic precipitation on the windward slope, it usually arrives on the lee side as a considerably drier air mass with slightly subrefractive properties up to moderate levels. This mP air can be distinguished from winter cP air because of its higher temperature. The Denver B-profile in Figure 64 shows the appearance of mP air on the lee side of the Rocky Mountains.

Diurnal refractive-index variations, which are slight over the ocean source region, become apparent as mP air moves overland, where insolation radiation effects are operative. Where mP air prevails overland, B-profiles should become generally less variable from day to day because of the light winds and stabilizing effects of surface cooling and subsidence.

7.2.5. Maritime-Polar—Summer. With the weaker pressure gradients of summer, air enters mP source regions from a number of locations along the windward periphery. This air may be originally of polar or tropical origin. Therefore, the characteristics of the air over the areas of the windward perimeter are a

function of the types of air entering the area. The shape of the B-profile for summer mP air over the central source region, in which approximate equilibrium conditions prevail, is shown in Figure 57. The profile is mildly superrefractive because of the uniform decrease of moisture with height.

The radio horizon for summer mP in the source region as shown in Figure 59 is normally extended about 5 percent, and for most purposes can be considered standard. Diurnal effects are slight. Owing to convective activity and moderate winds the refractive profiles are only slightly variable.

Summer mP air frequently comes under the domination of a high-pressure area before moving onshore, in which case an elevated subsidence inversion, which may become quite pronounced, usually forms. A temperature inversion of 10°C or more combined with a pronounced moisture decrease of 4 to 6 grams per kg may occur between 2000 and 3000 feet, to produce a superrefractive stratum. Occasionally, warm dry continental air mixing with the mP air above the inversion, and cold coastal waters cooling the air under the inversion, aid the subsidence effect and combine to create one of the most intense superrefractive situations observable. The shape of the resulting B-profile is very similar to the one shown in Figure 64 for winter mP air over San Diego except that summer profiles have more intense superrefractive strata.

Diurnal effects in this air may be large over land near the coast, if the superrefractive stratum is weakened by daytime heating and strengthened again by nighttime radiation. Both these processes are active below the subsidence inversion. Refractive profiles will be moderately variable during periods of sea breeze and in the early afternoon when convective currents are present. Otherwise, the profiles should be generally conservative.

As summer mP air moves far inland, its refractive properties become at first standard, then subrefractive to an extent depending upon surface heating. When the heating is extreme, mP air will become cT; when only moderate, the mP air will become similar to cP.

7.2.6. Maritime-Tropical—Summer. The typical B-profile for summer mT air in the source region is shown in Figure 57. The profile is strongly superrefractive in the lower levels to 7000 feet. This stratum, resulting from moisture decrease with altitude, frequently becomes sufficiently intense to allow trapping. Subsidence effects above the level of convection tend to create more or less standard refractive conditions aloft. This air mass has only a short sea-and-Gulf source region trajectory and could be more precisely classified as tropical-Gulf air.

The radio horizon for summer mT air in the source region is shown in Figure 59. Average extension is about 30 percent. Diurnal effects are

negligible, and the refractive-index profiles should be only moderately variable because of the high moisture content of the air and the convective activity.

Summer mT air usually moves out of the source region over a strongly heated adjacent continent and does not always travel behind a definite warm front. When present over immediate coastal land areas, this air exhibits the refractive properties of the source during the day, while at night radiational cooling frequently serves to strengthen the normal superrefractive lower stratum to trapping intensity. Refractive-index profiles in this situation will be extremely variable during the day and only moderately variable at night.

Summer mT air moving further inland generally becomes drier in the lower levels because of extensive convective mixing of the moist surface air and the drier air aloft, reducing radio ranges because the lower levels become less superrefractive. Diurnal temperature changes gradually increase, but nighttime trapping conditions are much less probable than with mT air over the coastal areas, and profiles are only moderately variable during the day and slightly variable at night.

When the travel of mT air over the continent is associated with thunderstorm activity the lower levels become more moist than normal because rain falls out of the air mass and evaporates into these levels. Therefore, mT air in the vicinity of recent thunderstorm activity exhibits a large decrease of moisture with height. A superrefractive stratum sufficiently intense to cause trapping even during the day is not uncommon in such air. Diurnal temperature effects will be large with nocturnal trapping almost a certainty if trapping existed during the day and a distinct possibility otherwise. Refractive-index profiles should be extremely variable during the day because of high moisture content of the air and the great convective activity. Nighttime profiles should be only moderately variable as a result of reduced convection.

Four sample B-profiles taken in mT air over a land station are shown in Figure 65. Although obtained from widely scattered locations, these profiles demonstrate the typical refractive nature of the air mass. Individual profile variation from the typical profile of Figure 57, however, is extreme. This type of profile variation is also true from moment to moment and day to day within a single air mass. Comparison of the lower portions of individual profiles in Figures 60 and 65 reveals the extreme of refractive-index profile variability that are observable within a single air mass. Figure 60 shows the conditions in cold dry air where profiles are normally conservative, and Figure 65 shows the extremely variable profiles of warm moist air.

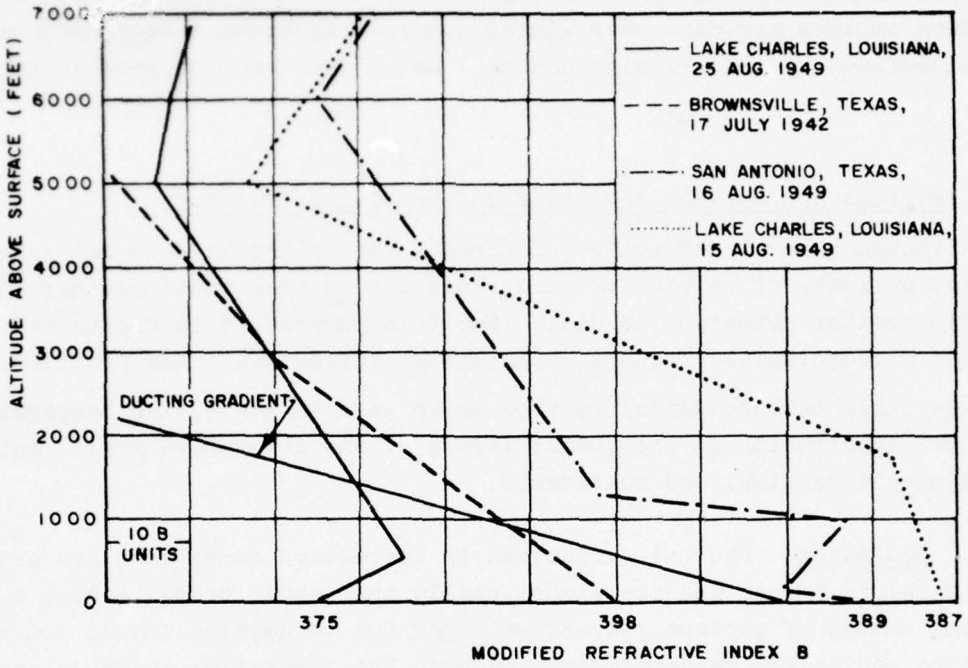

Figure 65. Examples of Summer B-Profiles. Profiles are displaced along abscissa as shown (after Plank).

7.2.7. Maritime-Tropical—Winter. The B-profile for winter mT air in the source region as shown in Figure 56 is moderately superrefractive because of the uniform moisture decrease with height. The effect of subsidence is apparent above 8000 feet.

The radio horizon associated with this air should be extended about 15 percent, as shown in Figure 58. Source-region diurnal effects are negligible. Refractive-index profiles are only moderately variable because of high moisture content and convective activity.

Winter mT air moving onshore out of the source region usually travels as a definite mass behind a warm front, and moves over a progressively colder land surface. Condensation occurs, a temperature inversion is created, and the lower air levels in general become stabilized. Normal subsidence effects intensify the inversion itself and the moisture gradient through the inversion. A superrefractive stratum is thus formed at inversion level. Although generally insufficient for trapping, this elevated stratum may appreciably extend the radio horizon beyond the normal source region horizon.

Stratus clouds, fog, and mist associated with the stabilization and condensation in this air mass over winter continental areas tend to moderate the diurnal refractive index variations because of decreased diurnal temperature range.

7.3. Physical and Dynamic Processes Influencing Refraction.

Although general refractive properties can be ascribed to air masses, a detailed estimate of refractive conditions for an area must consider the specific weather situation as well. For this purpose it is desirable to discuss the meteorological factors which modify refractive-index profiles.

The basic meteorological factors which tend to modify the temperature and moisture distribution in the lowest layers of the atmosphere are: radiation, turbulence, advection, and subsidence.

7.3.1. Radiation. Diurnal variations in refractive conditions are principally continental in nature and are almost wholly the result of decreasing and increasing values of surface refractive index due to daytime insolation and nighttime radiation, respectively. Because the refractive-index values a few thousand feet above the ground surface are not greatly affected by the diurnal range of surface temperature, a refractive-index profile generally shows a subrefractive lower layer during the day, especially at the time of maximum surface temperature near mid-afternoon, and a superrefractive lower layer during the night, especially at the time of minimum surface temperature near daybreak. A given diurnal temperature variation will not cause equal diurnal refractive-index variations in different air masses.

The surface heat loss associated with nighttime radiation will create a surface-based, or perhaps slightly elevated, temperature inversion under proper conditions. Superrefractive strata resulting from this inversion frequently cause trapping. The formation of such strata is favored by clear skies and low wind speeds. Clear skies permit the maximum amount of terrestrial radiation, and low winds insure that the lowest atmospheric levels will have the most heat loss and temperature drop. A method for predicting the nocturnal duct is presented in section 8.2. Such predictions must be made for a rather restricted area, since local weather and drainage effects are of paramount importance.

7.3.2. Turbulence and Convection. Convective turbulence, or convection, is the tendency of strongly heated surface air to rise in eddies through the atmosphere until it cools, adiabatically, to a temperature that is in equilibrium with its surroundings. Convection tends to create uniform vertical

distribution of potential temperature and moisture. However, daytime surface heating, produced by insolation, results in very high surface temperatures and a superadiabatic lapse rate just above the ground. As a result, temperatures decrease superadiabatically just above the ground, then adiabatically to an altitude at which general air-mass effects become the control. This altitude varies with cloud cover, winds, the degree of mechanical turbulence and convection, and the type of roughness of the underlying land surface. In general, within the affected layer the greater the degree of turbulence the closer will refractive-index profiles tend toward the standard profiles.

Moisture also tends to be transported upwards within an air mass by convection, and the resulting moisture profile shows that moisture tends to decrease approximately exponentially with altitude from its surface value to some quasi-constant value aloft.

The appearance of the refractive profiles associated with daytime heating varies from standard to extremely substandard, depending upon the insolation intensity. The general shape of such profiles can be predicted by considering the air mass, the type of absorbing land surface, the expected cloud cover, and winds.

The usual diurnal changes in a B-profile due to insolation and radiation are shown in Figure 66.

7.3.3. Advection. Advection is used to designate the horizontal displacement of air. Sixteen separate classes of temperature and moisture advection can occur. Four types of air (cold dry, cold moist, warm dry, and warm moist) may be advected over four types of surface (cold dry, cold moist, warm dry, and warm moist). These sixteen classes are shown in diagram form in Figure 67. In each case, the refractive conditions normally found in the air type considered are assumed to exist before the advection takes place and are shown by the solid B-profile. The profiles indicating the refracting conditions after a short advection period and after a longer period are shown as dotted and dashed, respectively. Horizontal movement across Figure 67 maintains identical surface conditions, and vertical movement maintains identical air-mass conditions.

The notation "warm" in the figure implies that warm air is at the same temperature as a surface classified as warm. Similarly, the notation "cold" is identical for air and surface. Therefore, for the cases warm air-warm surface and cold air-cold surface there can be no modification with respect to temperature.

However, the notation moist does not carry this implication. As applied to the air masses, moist implies an air mass in which the moisture content is

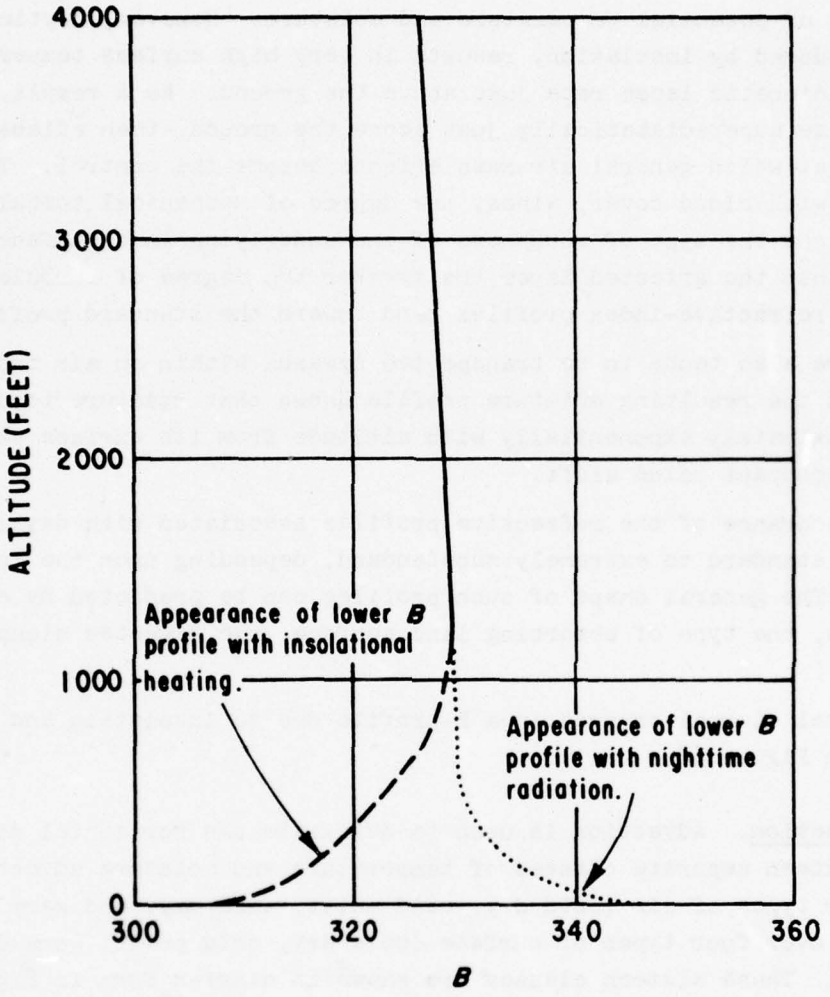

Figure 66. Effects of Radiation and Insolation (adapted after Plank).

high compared to the normal moisture content of other air masses in the same season. Water or a moist land surface implies that air near the surface contains nearly its maximum possible moisture content. Moist air masses traveling over moist surfaces can thus have moisture gradients that are either positive or negative, depending upon the circumstances.

The reasons for the changes in the B-profile are briefly covered for each class in the pertinent square. Height lines indicate the normal effective thickness through which the advection process operates. An attempt to specify each class as favorable or unfavorable for the formation of superrefractive strata is noted.

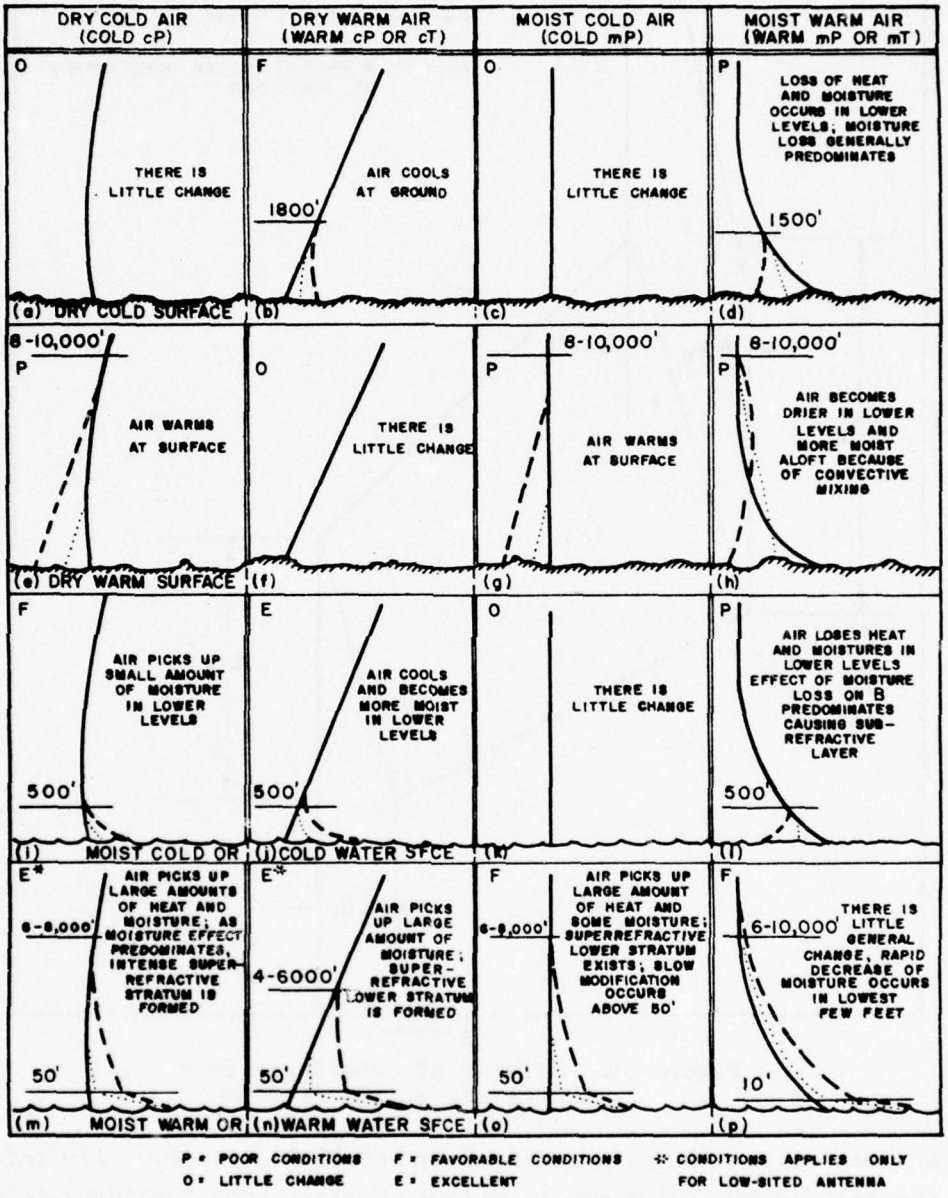

Figure 67. Effects of Advection on the Refractive Index (adapted after Plank).

7.3.4. Subsidence. The slow adiabatic settling of air within an air mass is known as subsidence, and its effect is to make the subsiding air warmer. Its effect on the refractive properties of the atmosphere is to eliminate

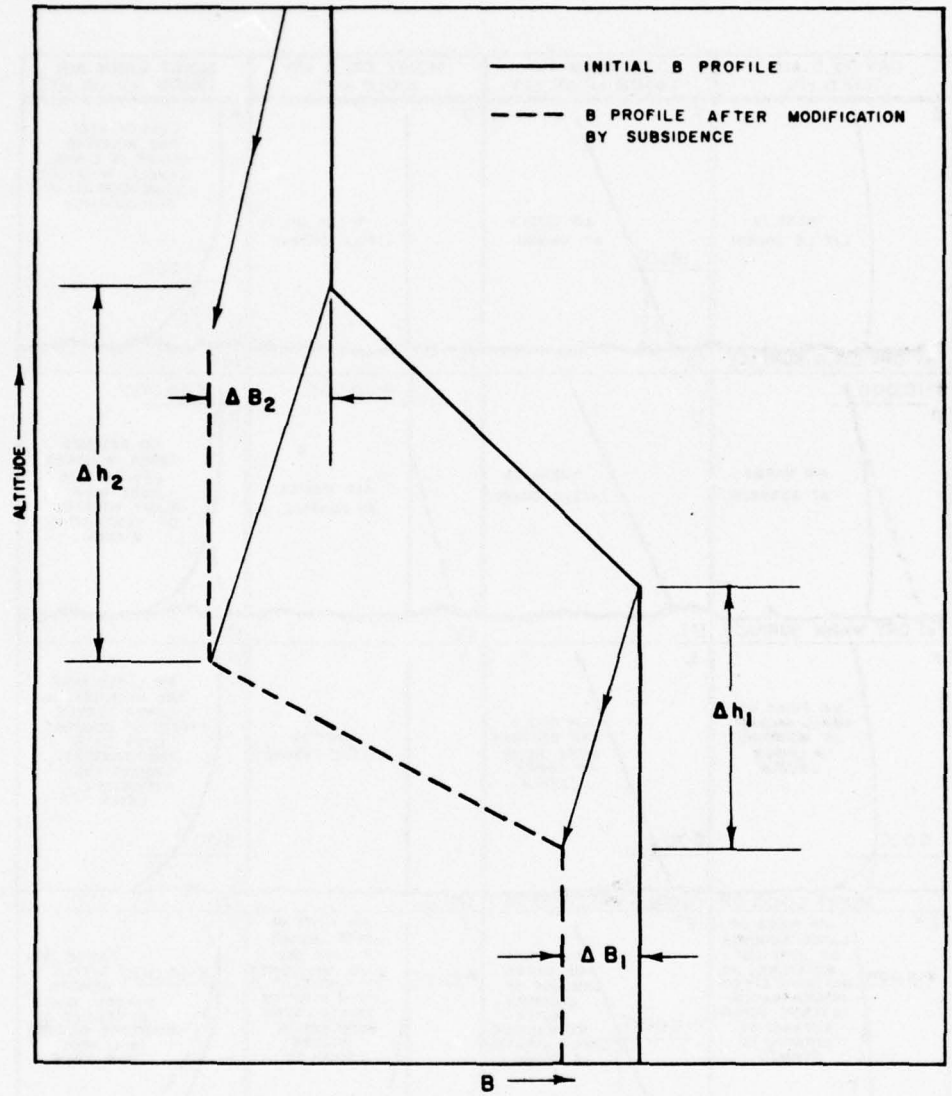

Figure 68. Effects of Subsidence on a Superrefractive Stratum (adapted after Plank).

subrefractive layers and to intensify superrefractive layers. Air initially having the solid B-profile shown in Figure 68 will, upon subsiding adiabatically through a given pressure interval, change its refractive properties to those shown by the dashed B-profile. Air at higher levels both sinks and is warmed more than air at lower altitudes. Consequently, $\Delta h_2 > \Delta h_1$ and $\Delta B_2 > \Delta B_1$. Subsidence is usually most important above 5000 feet but frequently is observable at lower elevations, particularly in the subtropics. As discussed under both winter and summer mP air, elevated superrefractive strata of great intensity are the results of subsidence of air over a moist surface stratum. Subsidence is always accompanied by horizontal divergence, the slow spreading out of air, and its effects are generally associated with high-pressure areas.

7.4. Local Refractive Effects Due to Meteorological Phenomena.

A number of meteorological phenomena are uniquely associated with well-defined local propagation conditions. These are discussed briefly to point up the significance of the relationship.

7.4.1. Land and Sea Breeze. Land and sea breezes often produce ducts near coastal regions. These winds are of thermal origin and are produced by temperature differences between land and sea. The mechanism is illustrated in Figure 69. During the day, when the land gets warmer than the sea the air rises over the land and descends over the sea and causes an air circulation in which the wind blows from sea to land (sea breeze) in the lowest levels. Vice versa, if during the night the land becomes colder than the sea, a circulation in the opposite direction arises. This is the land breeze. As a rule, this type of phenomenon is shallow, and the winds do not extend above a few hundred feet. Often there is a reverse wind in the layer above the land- or sea-breeze layer. A sea breeze may modify the local refractive conditions in various ways, and extremely strong ducts have been observed repeatedly under sea-breeze conditions. The land and sea breezes are of a strictly local nature and in most cases will extend only a few miles from the coast. Nevertheless, this region may be an important part of the trajectory of radio or radar beams. These breezes develop only under fairly calm conditions; under conditions of moderately strong gradient wind, the sea and land breeze will be perceptible only as a slight modification of the existing wind. Because of their limited entent, forecasting these breezes requires a study of the local wind and temperature conditions in relation to favorable or unfavorable general synoptic situations.

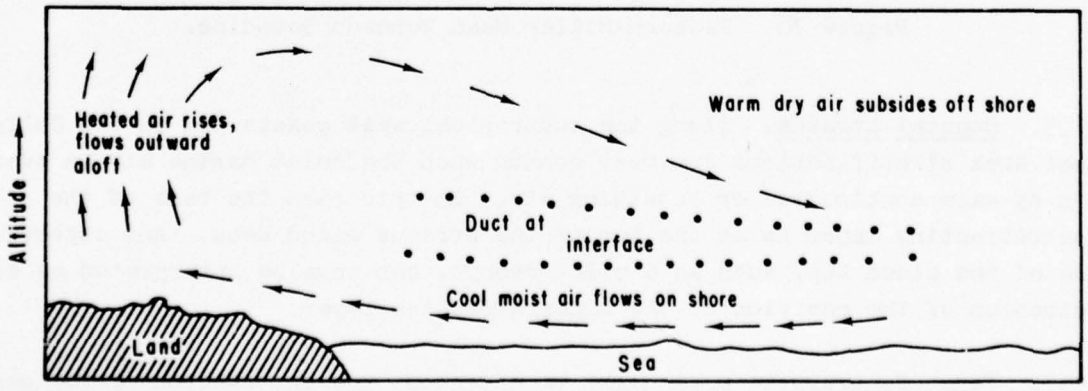

Figure 69. Sea-Breeze Duct.

7.4.2. Thunderstorms and Tornadoes. The conditions which favor the development of thunderstorms and tornadoes are generally those under which an elevated superstandard layer exists. The mean tornado sounding determined by Fawbush and Miller [20] based on 75 cases (mainly central United States) is shown as a B-profile in Figure 70. This stratum is intensified by the evaporation of rain falling through the lower layer. Strong effects on propagation are likely to be extremely local and most pronounced in the region of dissipating thunderstorms.

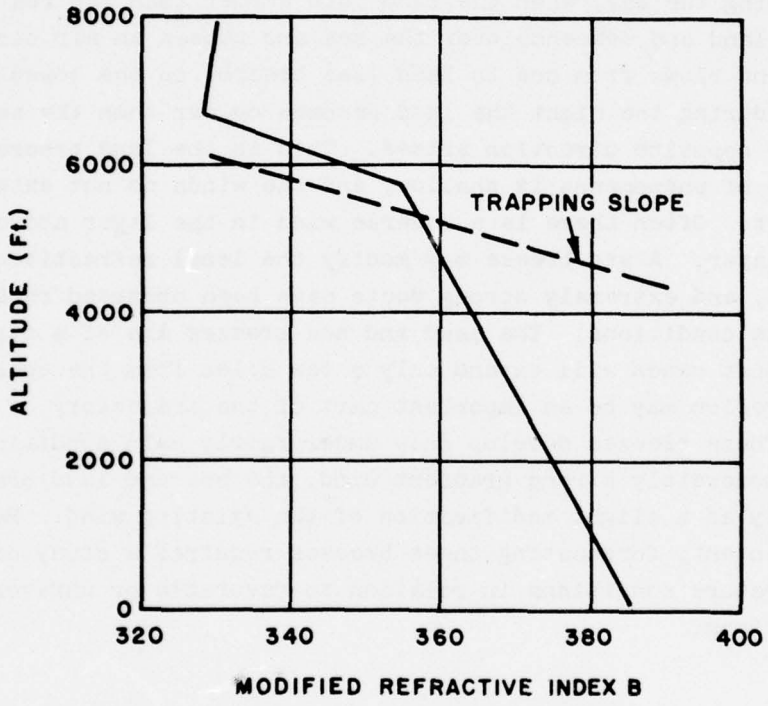

Figure 70. Fawbush-Miller Mean Tornado Sounding.

7.4.3. Coastal Stratus. Along the subtropical west coasts and in the Gulf-coast area stratifications are very common when the moist marine air is overlain by warm continental or subsiding air. In this case the base of the superrefracting layer is at the top of the stratus cloud deck. Any observation of the cloud top, such as a pilot report, can thus be interpreted as an indication of the position of the superrefractive layer.

7.4.4. Fog. Contrary to what might be expected, the information of fog generally results in a decrease of refractive index. When fog forms, e.g., by nocturnal cooling of the ground, the total amount of water in the air remains

substantially unchanged, but part of the water changes from the gaseous to the liquid state. The contribution of a given quantity of water to the refractive index is less when the water is contained in liquid drops than when it exists in the form of vapor. If the temperature increases through the fog layer, the saturation vapor pressure increases with height, and a substandard (negative slope) B-curve frequently results. This occurs with ground fog (caused by nocturnal cooling of the ground) and sometimes also with mixed advective-radiation fog (caused by the advection of warmer air over a cooler surface) if the wind is light.

Fog, however, does not always produce a substandard B-curve, though that is the most common case. In certain other less frequent types of fog, the temperature (and thereby the saturation vapor pressure) may be constant or decrease with height through the fog layer (as in windy tropical air fog, or windy advection stratus). In this event near standard propagation will prevail, or a duct may develop when the negative temperature decrease is strong enough. An example is steam fog, formed when cold air passes over a warm sea. Windy advection fog will likely have a superrefractive layer above the surface standard layer.

7.4.5. Foehn Winds. On the lee side of mountains a special type of advection may cause surface or low elevated superrefractive layers when warm dry air acquires moisture from the surface by evaporation. This effect has been noted in the spring in the upper Great Plains when the sudden onset of a foehn wind caused melting of the snow cover and resulted in the formation of a strong surface duct near the mountains which became slightly elevated farther east.

7.4.6. Fronts. A front may be defined as the discontinuity of the transition zone of density between two air masses. It is usually joined to one or more other fronts as part of the complex air-mass wave pattern associated with extratropical cyclones. Such a wave pattern is called a frontal system.

In every case of frontal activity, less dense air either actively rides over or lies above the more dense air. The refractive condition created by each type of overridding can be shown by using the typical profile for the less dense upper air mass to represent the refractive conditions above the frontal surface and the typical profile of the more dense lower air mass to represent the refractive conditions below the frontal surface. The refractive conditions up through the frontal zone can be inferred by connecting the two profiles, using the meteorological convention that the frontal transition zone occurs in the lower air mass.

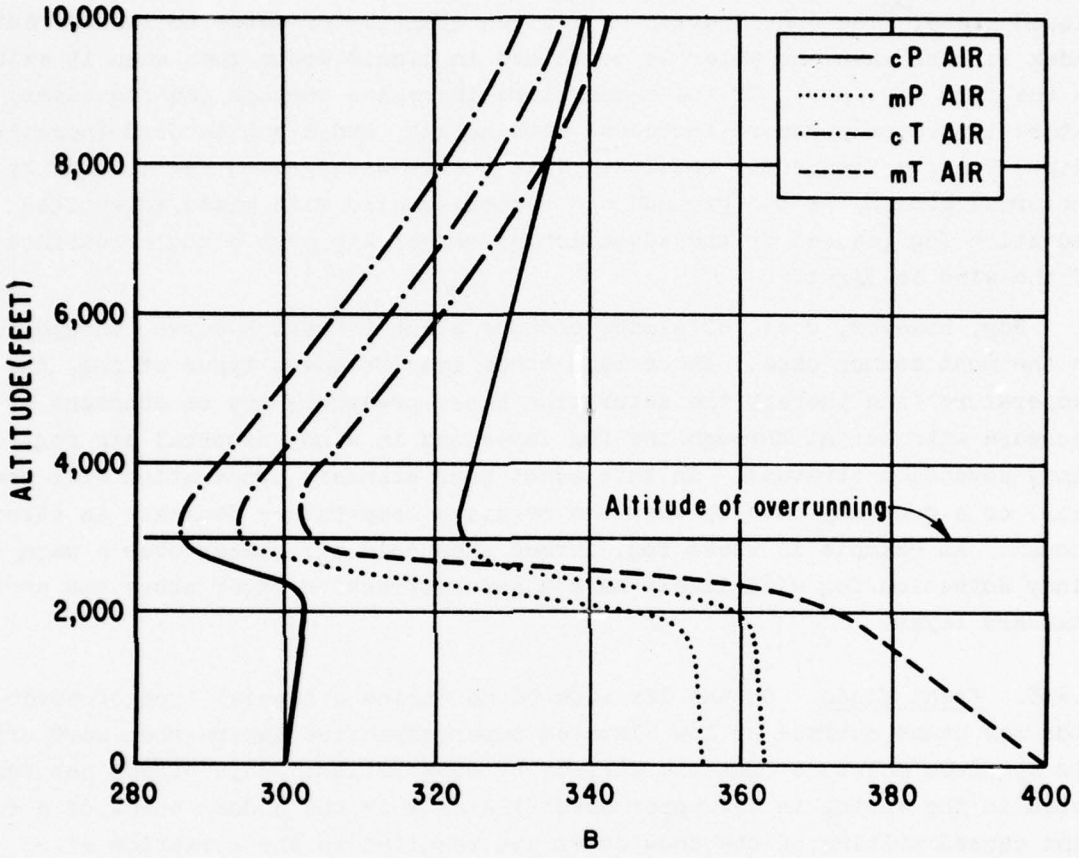

Figure 71. Uncommon Cases of Over- or Underrunning (adapted after Plank).

Figures 71 and 72 show several possible cases of overrunning or underrunning. In each case, the transition is arbitrarily assumed to occur at 3000 feet. When an air mass is shown several times in an over- or underlying position, the air-mass B-profile position is shown slightly displaced for clarity.

Common cases, with the exception of mT/mP which shows little change, tend to create subrefractive layers at inversion level; uncommon cases tend to create superrefractive layers at this level.

7.4.7. Precipitation. The presence of any form of precipitation tends to decrease radio (radar) ranges. This effect is apparently due to increased attenuation. Propagation conditions are usually near standard when precipitation occurs.

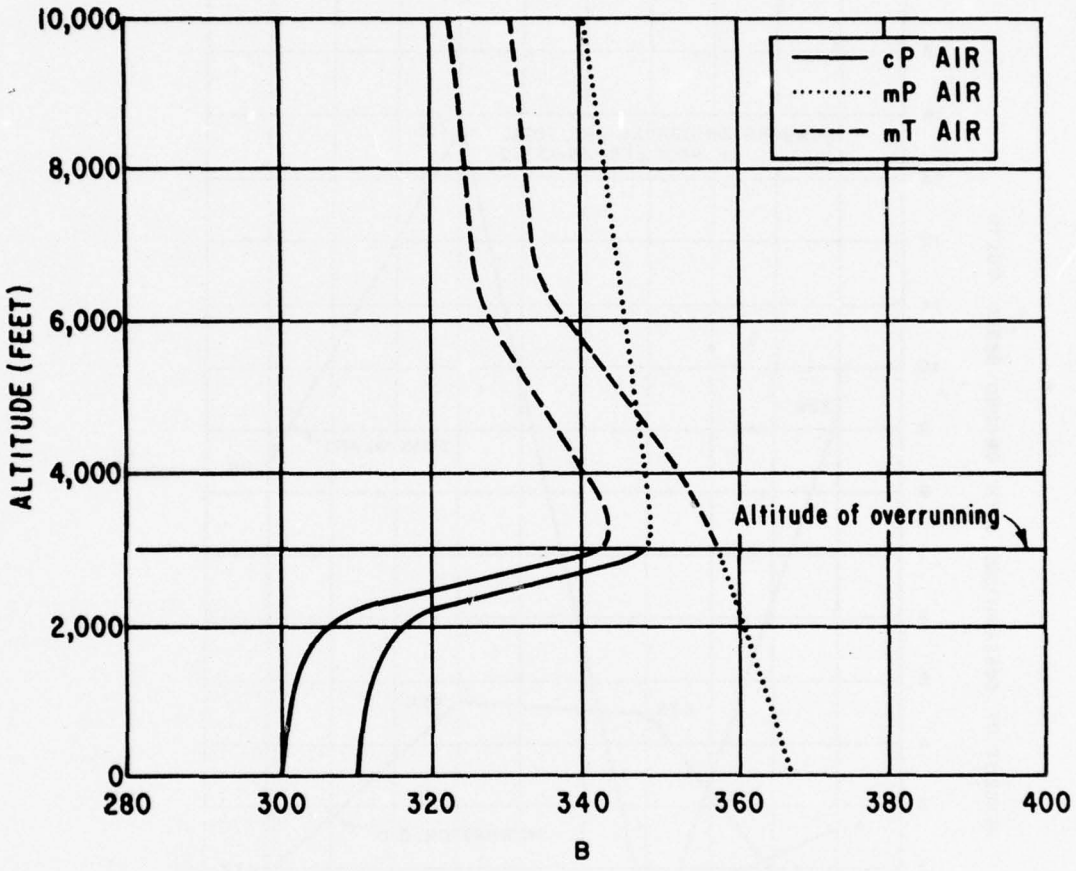

Figure 72. Common Cases of Over- or Underrunning (adapted after Plank).

7.5. Climatology of Ground-Based Ducts.

For the purposes of this section atmospheric ducting (trapping) is defined to occur whenever geometrical optics indicate that a radio ray leaving the earth's surface is sufficiently refracted that it eventually travels back toward or parallel to the earth's surface. This criterion has been applied by Bean [5] to several years of radiosonde observations from stations typical of polar, temperate, and tropical climates, in order to derive estimates of the variation of the occurrence of radio ducts with climatic conditions.

Approximately 3 years of radiosonde data typical of a polar climate (Fairbanks, Alaska), a temperate climate (Washington, D. C.), and a tropical marine climate (Swan Island, W. I.) were examined by means of a digital

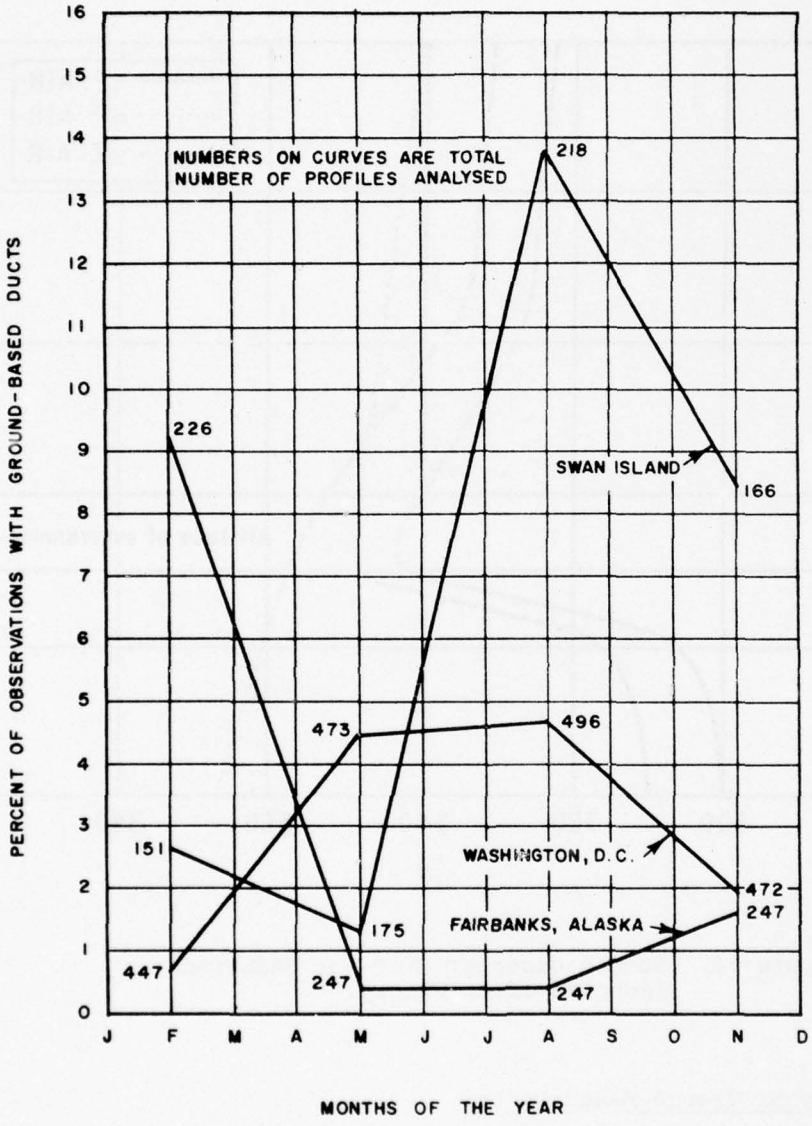

Figure 73. Frequency of Occurrence of Ground-Based Ducts.

computer for the occurrence of ducts during the months of February, May, August, and November. The percentage occurrence of ducts is shown in Figure 73 for these three locations. The maximum occurrences of 13.8 percent for August at Swan Island and 9.2 percent for Fairbanks in February are significantly greater than the values observed at other locations and times of the year. The Washington data display a summertime maximum of 4.6 percent. These data indicate that the tropical zone, maximum incidence occurs in late summer and

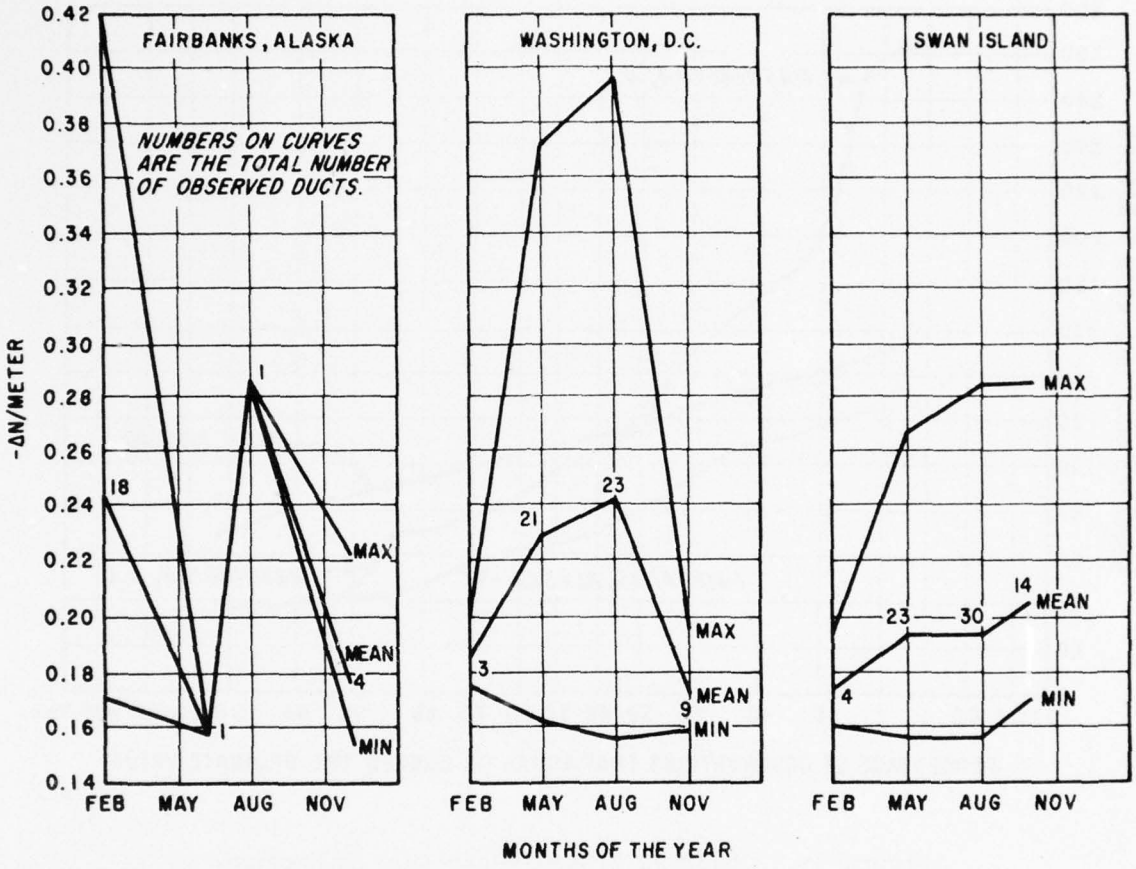

Figure 74. Typical Refractivity Gradients of Ground-Based Ducts.

is nearly three times the temperate zone, summertime maximum; while the arctic zone maximum occurs in midwinter and is about twice as large as the temperate maximum.

The results of an analysis of refractivity gradients observed during ducting are given in Figure 74. The maximum gradient of 420 N-units per kilometer was observed during February at Fairbanks, Alaska; with a value of 396 N-units per kilometer observed during August at Washington, D. C. The gradient observed during ducting at Swan Island, W. I., reached a maximum (285 N-units per km) both during August and November. The annual mean values of N-gradient appear to show a small latitudinal trend from a high value of 230 N-units per kilometer at Fairbanks to a value of 190 N-units per kilometer at Swan Island.

Another property of radio ducts is their thickness; typical thickness

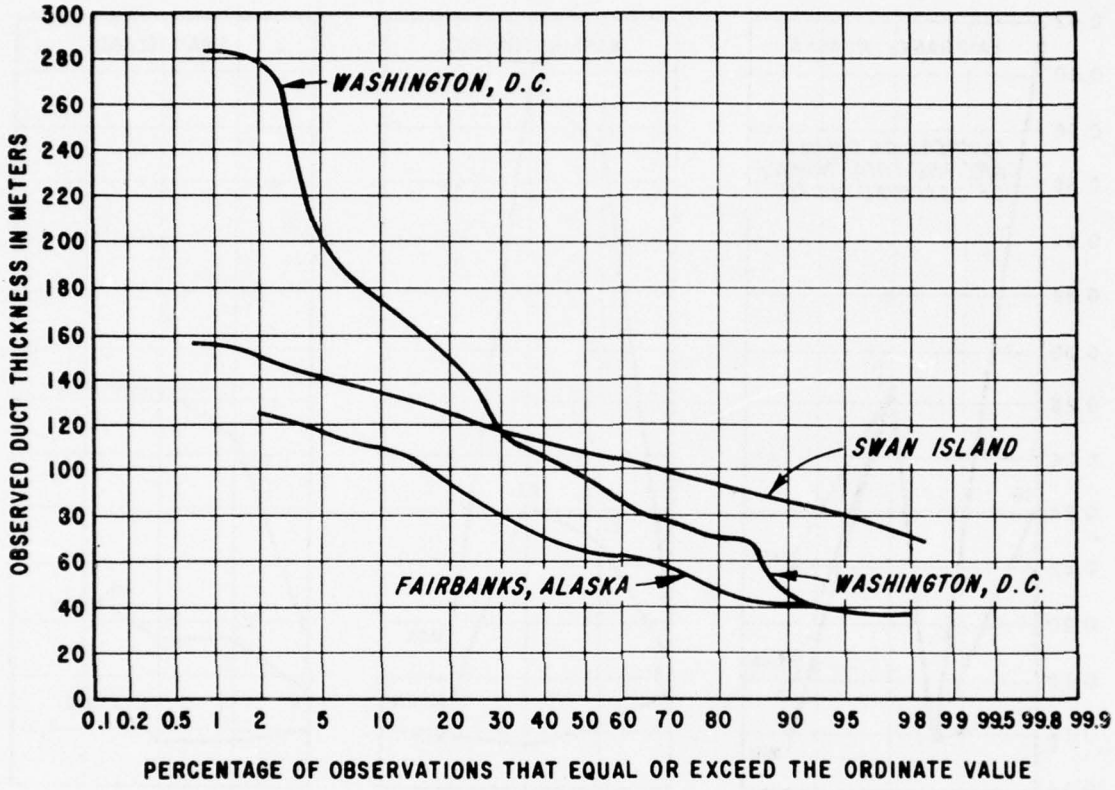

Figure 75. Observed Ground-Based Duct Thickness.

values are shown in Figure 75. Again a small latitudinal trend is observed as the median thickness increases from 66 meters at Fairbanks to 106 meters at Swan Island.

We may summarize the data of Figures 74 and 75 by saying that polar climates (Fairbanks) are characterized by shallow layers with relatively intense gradients, tropical marine climates (Swan Island) are characterized by thick layers with relatively weak gradients, and temperate climates (Washington, D. C.) lie in between.

It is interesting to consider the temperature and humidity distribution that accompanies a radio duct. An example typical of each station is given in Figure 76. The polar duct illustrated was accompanied by a surface temperature of -25°C with a strong temperature inversion and a slight humidity lapse, indicating an inversion associated with wintertime cooling of the air next to the ground. The temperature example appears to be typical of a temperate-zone

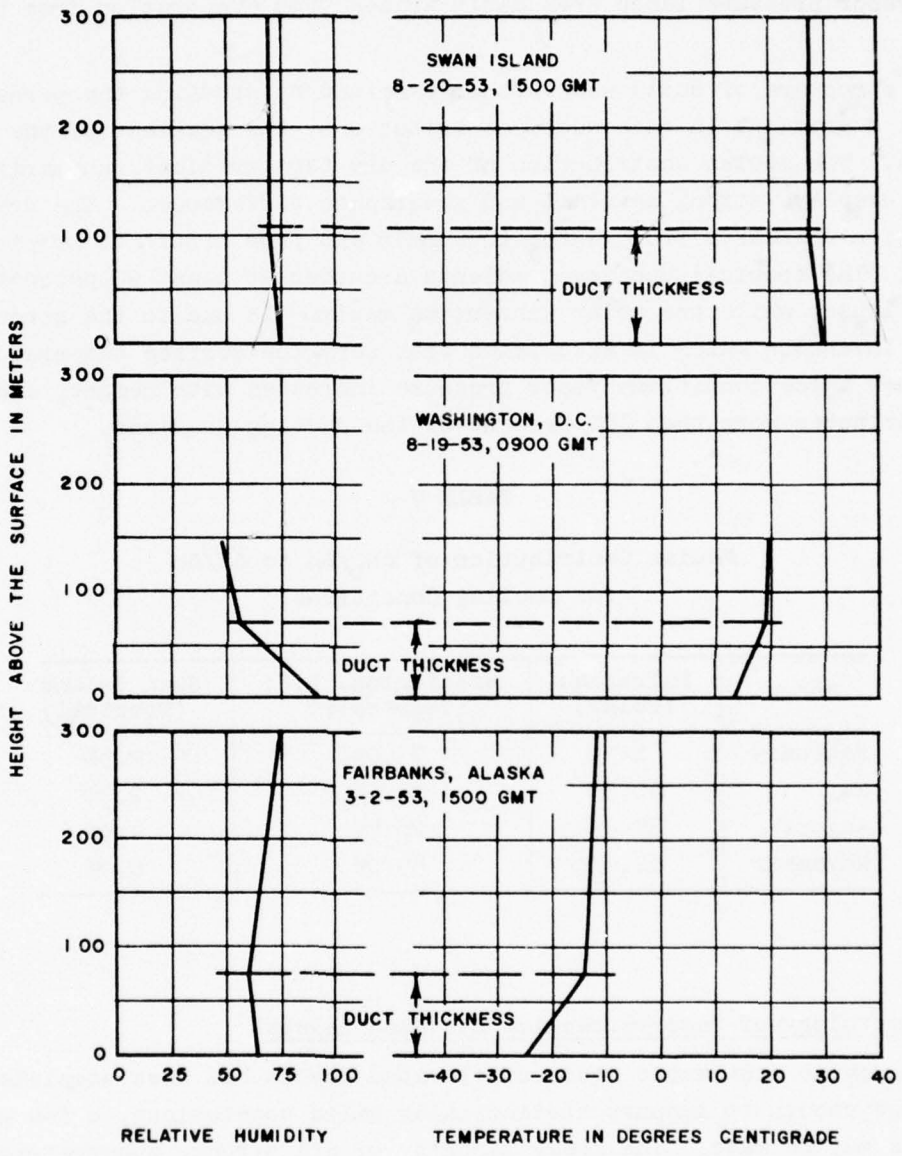

Figure 76. Temperature and Humidity Profiles for Typical Ground-Based Ducts.

temperature inversion. The tropical profile, however, shows a moderate lapse of both temperature and humidity. This apparent inconsistency is explained by the strong lapse in vapor pressure which is associated with a moderate lapse in temperature and humidity when the surface temperature is near 30°C. This

strong, vapor pressure lapse presumably arises from evaporation from the sea surface.

The structure of ducts was further examined by studying the percentage of the total N-gradient in each duct, contributed by the gradient of the dry and wet terms. The median contribution of the dry term gradient, summarized in Table 7, displays strong seasonal and geographic differences. The dry-term contribution decreases from winter to summer and from arctic to tropical climates. The tropical ducting gradients are then at least 90 percent due to humidity lapse, while the polar wintertime maximum is due to the strong temperature inversion which is associated with very low surface temperatures. In fact, under these conditions vapor pressure increases with height, and the dry term contributes more than 100 percent of the ducting gradient.

TABLE 7

Median Contribution of $\Delta N_D/\Delta h$ to $\Delta N/\Delta h$
for Ducting Conditions.

Month	Fairbanks (Polar)	Washington, D.C. (Temperate)	Swan Island (Tropical)
February	103%	73.0%	9.5%
May	40.5%	33.5%	2.0%
August	37.0%	26.5%	4.5%
November	62.0%	55.0%	6.0%

7.6. Climatology of Superrefractive Elevated Layers.

Although no systematic study of elevated layers has been completed on a scale large enough to support statistically valid conclusions, a few general statements may be made. The great majority of all strong, superrefractive, elevated layers are associated with subsidence in the atmosphere. Since subsidence involves an adiabatic process, a given layer may, therefore, be associated with a certain, constant potential temperature. In other words, the layer is in an isentropic surface. This concept may be used operationally to estimate the horizontal extent of strong superrefractive layers by indicating the particular heights most likely for layer occurrence at points removed horizontally from the known sounding. It must be remembered, however, that the existence of the "same" potential temperature alone is not sufficient evidence for extending an elevated layer horizontally into "unknown" areas; other

considerations must also indicate a "good" probability for its existence.

In maritime-polar air masses over the western Atlantic and North Pacific, the boundary between the moist, lower, mixed layer and the unmodified, dry, upper layer can frequently become an elevated superrefractive layer. When the existence of such a layer has been established by measurement, the tops of the convective clouds in the mixed lower layer can be assumed to be at the height of the layer base.

Chapter 8

FORECASTING REFRACTIVE INDEX

Forecasting for radio meteorological purposes differs from routine forecasting only in that one's interest is centered on a specialized application. In a given area the general meteorological principles can be organized into a system of standard procedures for predicting propagation effects. No attempt is made here to establish any standard system since wide variations are to be expected in differing climatic regimes.

A logical approach to the problem would be to consider first the large-scale features of the synoptic pattern and modify these to incorporate smaller-scale processes and phenomena. In many cases it will be found that a particular process is the primary one to be considered. Specific forecasting methods are discussed later which apply to forecasting advective and nocturnal ducts.

The meteorologist must use ordinary forecasting techniques to predict refractivity values or elevated layers. Due to the number of parameters involved in determining refractive-index values or elevated layers as well as the importance of local effects, such as an evaporating surface, forecasts can be only of qualitative nature inasmuch as the individual parameters are predicted subjectively.

8.1. Limitations of Radiosonde Observations.

Forecasts of refractive-index profiles must of necessity be based to a large extent on data obtained from radiosonde measurements. The limitations in the measurement of these data were discussed in sections 3.2.2 and 3.3.4, and must be recognized by the meteorologist so that he will consider what adjustments of reported data may reasonably be or should be made.

For measurements of the change of index through a layer and the height of the base of a layer, the error in radiosonde data does not usually prevent its use. The computed change of index may be slightly less than the true value and the base of the layer slightly higher than indicated but this error will not exceed the measuring interval (approximately 200 feet). The thickness of the layers may be over-estimated by a maximum amount of two measuring intervals (400 feet) but on the average may be expected to be approximately 200 feet too large. For the thick and most intense layers this error will generally be less

than in the case of the relatively thin layers.

In this connection too, it has been found inconvenient to compute the thickness of layers as reported from radiosonde data. To aid in this computation, a simple computer based on the hydrostatic equation is illustrated in Figure 77. Few radar sites are co-located with a radiosonde observation station. Care must be exercised when using radiosonde data to determine refraction conditions for a distant radar site. Radiosonde measurements may not be representative of conditions producing refraction in radar transmissions, depending on the horizontal and/or vertical separation between the site and observation point. Conditions measured by the radiosonde are transient; and for analysis of a sounding with refraction in mind, one should seek understanding of the causes of the atmospheric structure before judging the representativity of the measurements.

8.2. Forecasting the Nocturnal Duct.

The meteorological processes underlying diurnally varying propagation effects are nocturnal radiation, turbulent transport of heat, and heat conduction, since the temperature profile is a result of the interaction of these processes. Resulting refractive-index profiles normally show a tendency for radio (radar) duct to begin to form about sunset. It develops rapidly in the early evening hours, more slowly in early morning, and dissipates rapidly after sunrise. A forecasting method which applies to this situation is described here [3].

If we are interested in determining the maximum intensity of the nocturnal duct, we can specify with a fair accuracy the times for which the surface B-values should be determined. It has been found that the B-profile is generally about vertical, that is standard conditions exist, one hour before sunset; therefore, the surface B-value at this time is representative of the values which will exist later aloft where nocturnal modification will not be active. Further, the surface B-value increases rapidly at first during the evening but more slowly later as a near-equilibrium condition is obtained. Generally, by nine hours after sunset the B-value is close to the maximum for the night. Accordingly, the B-value nine hours after sunset minus the B-value at one hour before sunset expresses rather closely the magnitude of the B-change through the modified layer at its maximum intensity.

Next, the maximum depth (or thickness) of this modified layer must be determined. As before, we can assume the time at which it first appears to be nine hours after sunset. Assuming average values for soil conditions and humidity as well as generally clear skies and stable lapse rate, one can represent this thickness as a function of wind speed and surface roughness. The

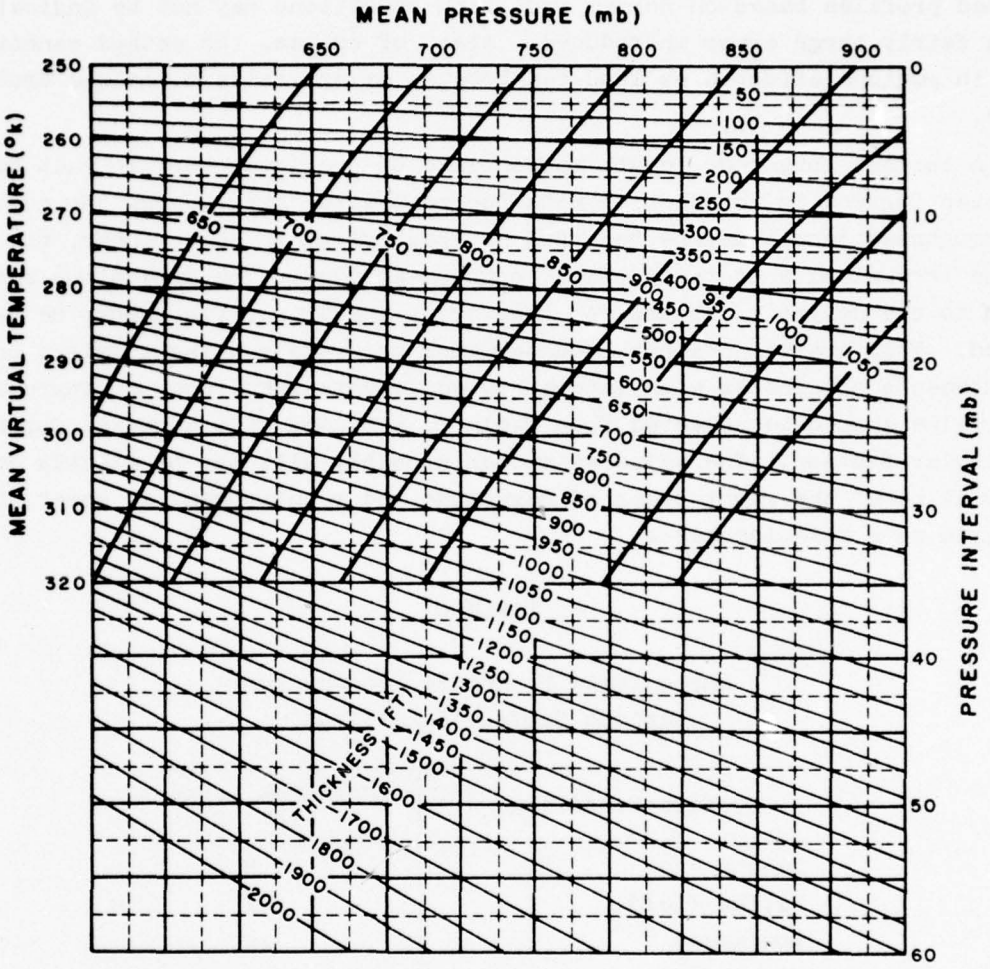

METHOD:

STEP 1 - DETERMINE MEAN TEMPERATURE (°C) PRESSURE INTERVAL (mb) AND MEAN PRESSURE (mb) OF LAYER.

STEP 2 - ADD 273°, THE MEAN TEMPERATURE AND 1/6 OF THE MEAN MIXING RATIO TO OBTAIN MEAN VIRTUAL TEMPERATURE (°k).

STEP 3 - ENTER GRAPH ALONG MEAN VIRTUAL TEMPERATURE TO THE MEAN PRESSURE VALUE.

STEP 4 - MOVE VERTICALLY TO INTERSECT APPROPRIATE PRESSURE INTERVAL VALUE.

STEP 5 - READ LAYER THICKNESS AT THIS POINT (FROM FAMILY OF LINES SLOPING DOWNWARD TO RIGHT.)

Figure 77. Layer Thickness Calculator.

errors resulting from these assumptions should be minor even when some cloudiness prevails. One effect which may indicate appreciable error, however, is condensation. If condensation (fog or dew) occurs early in the night, the

assumed profiles based on normal radiation conditions may not be indicative, and a fairly large error introduced. Also, of course, the method cannot be used in regions affected by land-sea breezes or excessive downslope drainage winds.

A surface roughness length appropriate to the local terrain must be selected for use in conjunction with the mean wind speed during the evening. The roughness length may be regarded as specifying, in some manner, the effect of the irregularity of the surface in the mean flow. The dimensions are related to the height of obstacles; however, a specific ratio cannot be reliably stated. This quantity cannot be determined accurately without fairly precise measurements obtainable with laboratory equipment; therefore, an appropriate mean value should be selected from Table 8, and used as a constant for a particular station. The value so chosen probably will not be exactly correct but will be of the right order of magnitude and results can, at worst, be compared on a relative basis.

TABLE 8

Approximate Roughness Lengths for
Various Surface Conditions.

Surface Conditions	Roughness Length (cm)
Smooth snow	0.5
Fallow field	2.1
Low grass	3.2
High grass	3.9
Wheat field	4.5
Low bushes	10.0
Tall trees and buildings	50.0

8.2.1. Forecasting Method:

Step 1. Using measured temperature and dew point (instrument shelter observation) one hour before sunset, compute the refractive-index (B-units) value representative of the air-mass profile.

Step 2. Prepare a forecast of the minimum temperature, mean wind speed (at 25 feet) and dew point to be expected during the night.

Step 3. Enter Figure 78 with the forecasted wind speed and, at the intersection with the curve representing the predetermined roughness length

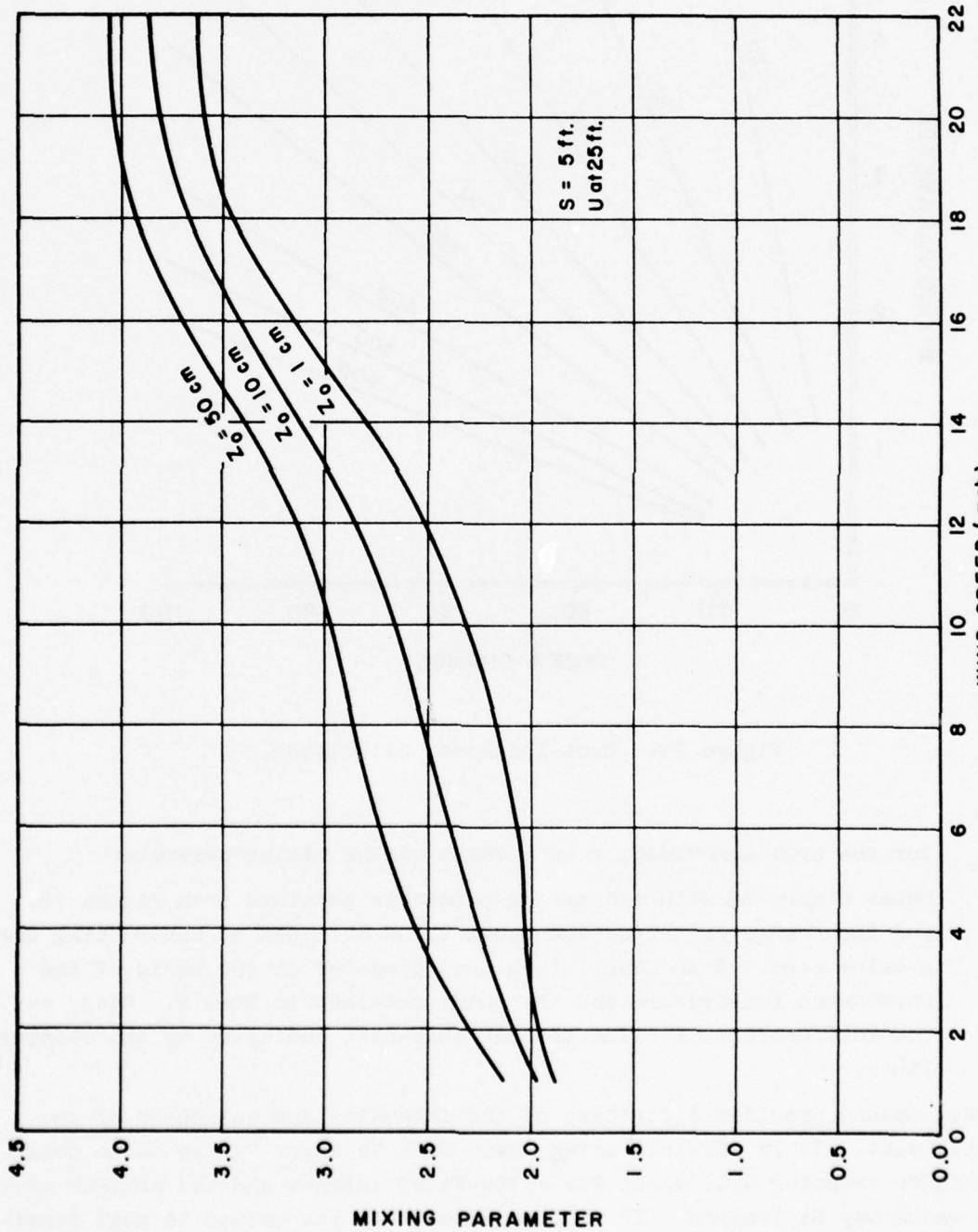

Figure 78. Mixing-Parameter Graph.

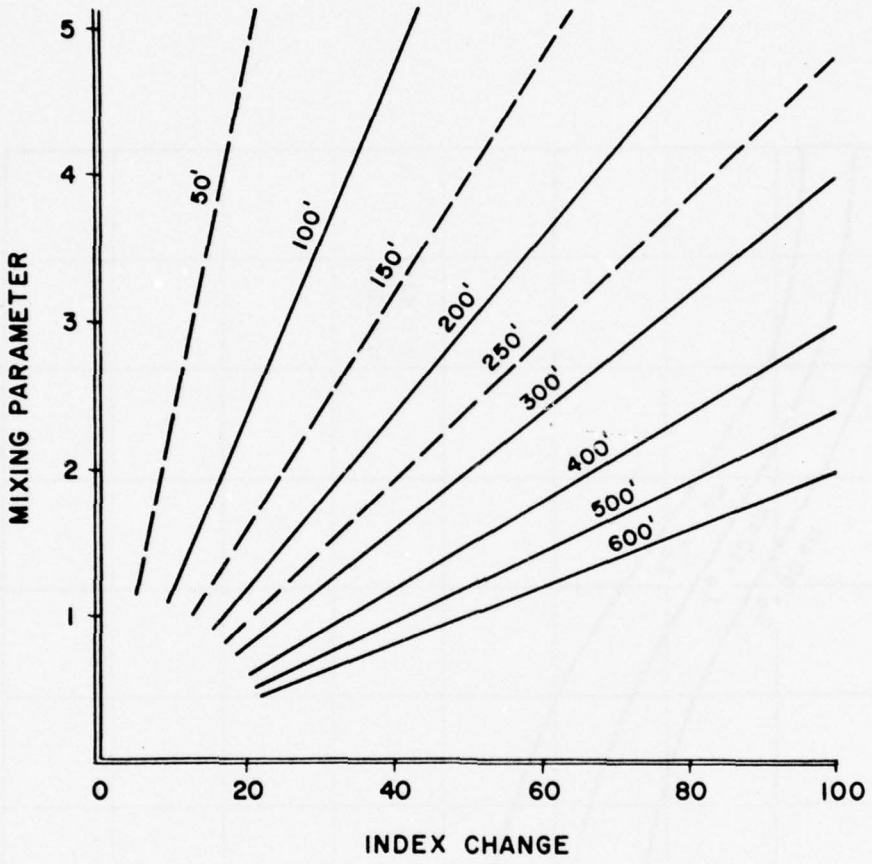

Figure 79. Duct-Thickness Calculator.

for the area concerned, read a value of the mixing parameter.

Step 4. Enter Figure 79 with the mixing parameter obtained from Figure 78, and the change of refractive-index value obtained by subtracting the B-value computed in Step 1 from that computed on the basis of the forecasted temperature and dew point obtained in Step 2. Read, at the intersection, a value of duct thickness indicated by the sloping lines.

This method provides a forecast of the intensity and thickness of the nocturnal duct. It is possible using these data to enter Figure 80 to determine whether trapping will occur for a low-sited antenna and the maximum wavelength which may be trapped. It will be noted that the method is most sensitive to the variation of refractive index and less sensitive to wind speed.

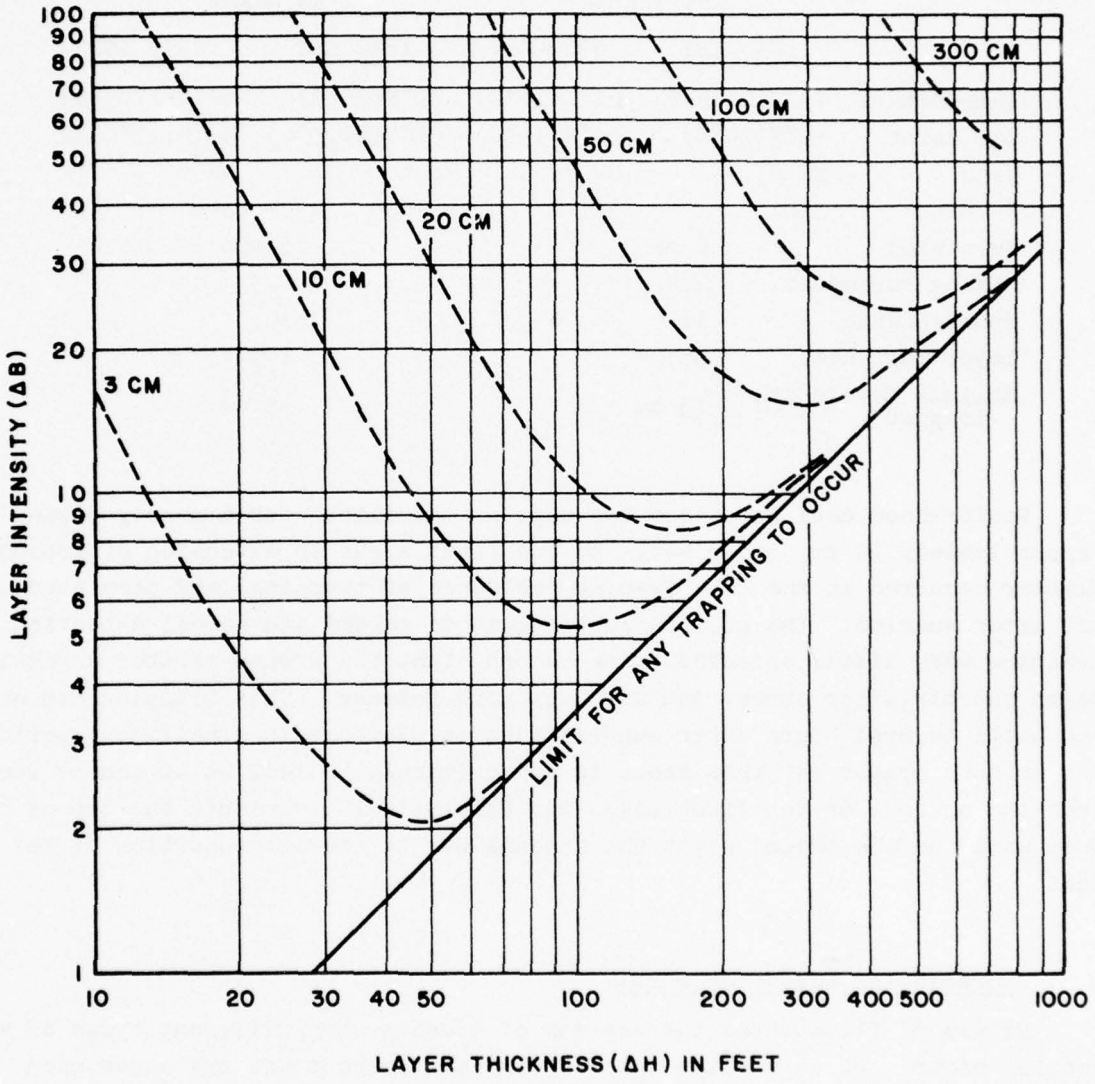

Figure 80. Maximum Wavelength Trapped in a Simple Duct.

This is fortunate because the forecasting of wind speed at a point to the nearest mile per hour is virtually impossible although a forecast of mean wind within broader limits and areas is feasible.

8.2.2. Example: The analysis of specific data for a location in the central United States for two consecutive nights during July 1953, with surface roughness of 10.0 cm, gave the following results:

	1st Night		2d Night	
	1830 LST	0330 LST	1830 LST	0330 LST
Temperature	73°F(22.5°C)	61°F(16°C)	79°F(26°C)	64°F(17.5°C)
Dew Point	49°F(10°C)	50°F(10°C)	51°F(10.5°C)	59°F(15°C)
Wind	SE 5	SW 7	S 6	NW 4
B-Value	318	329	316	346
Mean Wind	6 mph		5 mph	
Mixing Parameter	2.4		2.3	
Index Change	11		30	
Layer Thickness	55'		155'	
Maximum Wavelength Trapped	13 cm		55 cm	

Performance data for these two days are available for a nearby S-band (approximately 10 cm) radar set. On the first night an extension of ground clutter occurred in the late evening (evidence of trapping) and persisted until after sunrise. The ground clutter was not severe and normal detection and tracking were little affected. The second night the ground-clutter extension began shortly after sunset and was much more intense. This trapping did not end until several hours after sunrise when it vanished in a half-hour period. The antenna height for this radar is approximately 50 feet so it can be seen that the antenna on the first night was barely included within the top of the duct while on the second night the antenna was in the lower portion of the duct.

8.3. Forecasting Advection Ducts.

Figure 67 illustrates the variety of effects when different types of advection occur. Of particular interest in this respect are the cases when continental air moves off the east coast onto the Atlantic Ocean. A systematic method of forecasting the formation of these surface ducts is presented here [27].

8.3.1. General Procedure. In essence the method consists of an analysis of the modification that air undergoes in the lower 1000 feet as it moves from a large land mass out over the ocean. The study was carried out in the vicinity of Cape Cod, but indications are that the numerical factors entering into the procedure are much more generally applicable. In the modification of the air moving over the sea, the following assumptions are made:

a. The air initially (before moving off the land mass) is well mixed,

i.e., it exhibits conditions close to neutral equilibrium.

b. The stability conditions of the air as it moves out over water are determined by its initial temperature (over land) relative to that of the sea surface.

c. The modified air at the sea surface rapidly acquires the same temperature as the sea.

d. In the modified air at the sea surface the moisture content becomes that corresponding to saturation at the sea-surface temperature, except for a minor correction owing to the salinity of the sea.

e. The resulting B-curve is determined by the quantities:

(1) Temperature excess

(2) B-deficit

(3) Wind speed and direction

(4) Distance of over-sea travel (in some cases).

Thus, the method attempts to relate duct formation to a limited number of easily determined meteorological factors. It involves a simplified consideration of the upward diffusion of heat and moisture. It turns out, however, that the simplified assumptions yield results which in practical application are of sufficient accuracy to be of definite use in forecasting the existence of nonstandard conditions. It should also be mentioned that, although the method is designed primarily for situations in which air over land moves out over the sea, it can also be satisfactorily applied to situations in which the air has a purely over-sea trajectory.

8.3.1.1. Observation of Initial Conditions. The necessary meteorological measurements to be taken should be as representative as possible, i.e., uninfluenced by purely local effects. Measurements are:

a. Surface air temperature (of the unmodified air over land, in the case of air moving off a land mass);

b. Surface air humidity (also of the unmodified air which can be expressed in terms of relative humidity, specific humidity, dew point, wet-bulb temperature, or vapor pressure);

c. Sea-surface temperature;

d. Wind speed and direction (preferably at 1000-ft elevation); and sometimes

e. Distance from land (of primary importance only in the case of stable air, when the air is warmer than the sea surface).

All these data may, of course, be profitably supplemented by aerological soundings, weather maps, and any other pertinent information available.

8.3.1.2. Modification of Air by Sea Surface. As a qualitative description of the modification that the air undergoes in moving over water, three cases may be distinguished:

a. Neutral equilibrium (resulting when the initial surface air temperature is the same as the sea temperature). The temperature structure of the air remains unchanged; however, since the air is usually not completely saturated, moisture is supplied to the lower layers by evaporation from the sea surface, in this way causing a greater decrease of humidity with height, which tends to establish a B-distribution such that the modified refractive index is decreasing with height. In the case in which the air is initially completely saturated no modification takes place.

b. Unstable equilibrium (resulting when the initial surface air temperature is less than the sea-surface temperature). In this case the moisture content of the air is always less than that corresponding to saturation at the sea-surface temperature, so that the lower layers of air increase with time in humidity as well as in temperature. Owing to the greater sensitivity of B to humidity than to temperature this tends to bring about a decrease of B with height in a layer of air adjacent to the sea surface, while the unstable conditions give rise to vertical mixing which keeps the B-distribution close to standard above this layer so that the duct is confined to lower levels than in the case of neutral equilibrium.

c. Stable equilibrium (resulting when the initial surface air temperature is greater than the sea-surface temperature). If, in addition, the air is initially quite dry, i.e., has a moisture content less than that corresponding to saturation at the sea-surface temperature, then the resulting rapid decrease of moisture with height plus the stable temperature distribution leads to a tendency to surface duct formation. On the other hand, if the initial moisture content of the air is relatively large, moisture may be condensed out of the surface layers of air thus tending to give rise to an increase in humidity with elevation (if wind is light) which when sufficiently marked may counteract the effect of the stable temperature distribution and so prevent the formation of a duct or even produce substandard conditions. In either case, the stable structure of the air tends to hinder vertical mixing so that modification from the surface upward proceeds slowly and hence is highly dependent on the distance traveled by the air over the water.

8.3.1.3. Necessary Calculations. To determine quantitatively the

possibilities of duct formation, the following items can be readily calculated from any particular observed set of initial conditions [12].

a. Temperature excess, which is merely the representative surface-air temperature (before modification) minus the sea-surface temperature.

b. B-deficit, defined as the value of B corresponding to the sea-surface temperature minus the value of B determined from the representative surface-air temperature and humidity (before modification). The vapor-pressure correction due to the salinity of sea water is neglected (approximately 2 percent error).

c. Ratio of duct width to B-deficit, determined from the chart in Figure 81 for a given temperature excess and wind speed as measured at the 1000-foot level.

d. Duct width, found by multiplying the above ratio (c) by the B-deficit.

8.3.2. Applicability of the Method. Since the procedure is designed to take into account only the surface modification of the air over water, its application is restricted to the prediction of standard, substandard, and simple surface trapping conditions. Standard conditions can be presumed to occur when the calculations indicate a duct width of zero, which is the case when the B-deficit is zero. If the B-deficit is negative, then the calculated duct width will be negative, and substandard conditions are to be inferred. A positive B-deficit indicates duct formation (simple surface trapping), and the calculations of the duct width given an estimate of the height to which the duct extends. Once the duct width is calculated, a complete picture of the distribution of B with height can be approximated by assuming that standard conditions prevail above the duct and that the B-deficit is the difference between the actual B-value at the sea surface and the B-value that exists above the duct.

The method is not applicable to conditions over land.

In the case of air with a purely sea trajectory, it turns out that the procedure is closely valid if, in place of the air temperature and humidity measurements made over land, these measurements are taken in the air at a few feet elevation above the sea surface, for example, at bridge level on a large ship.

In practical application results will be most reliable when the assumptions listed under "General Procedure" are satisfied. However, this does not mean that the method is useless under other circumstances. Figure 81, which is the crux of the method, is largely empirical and is based on relationships

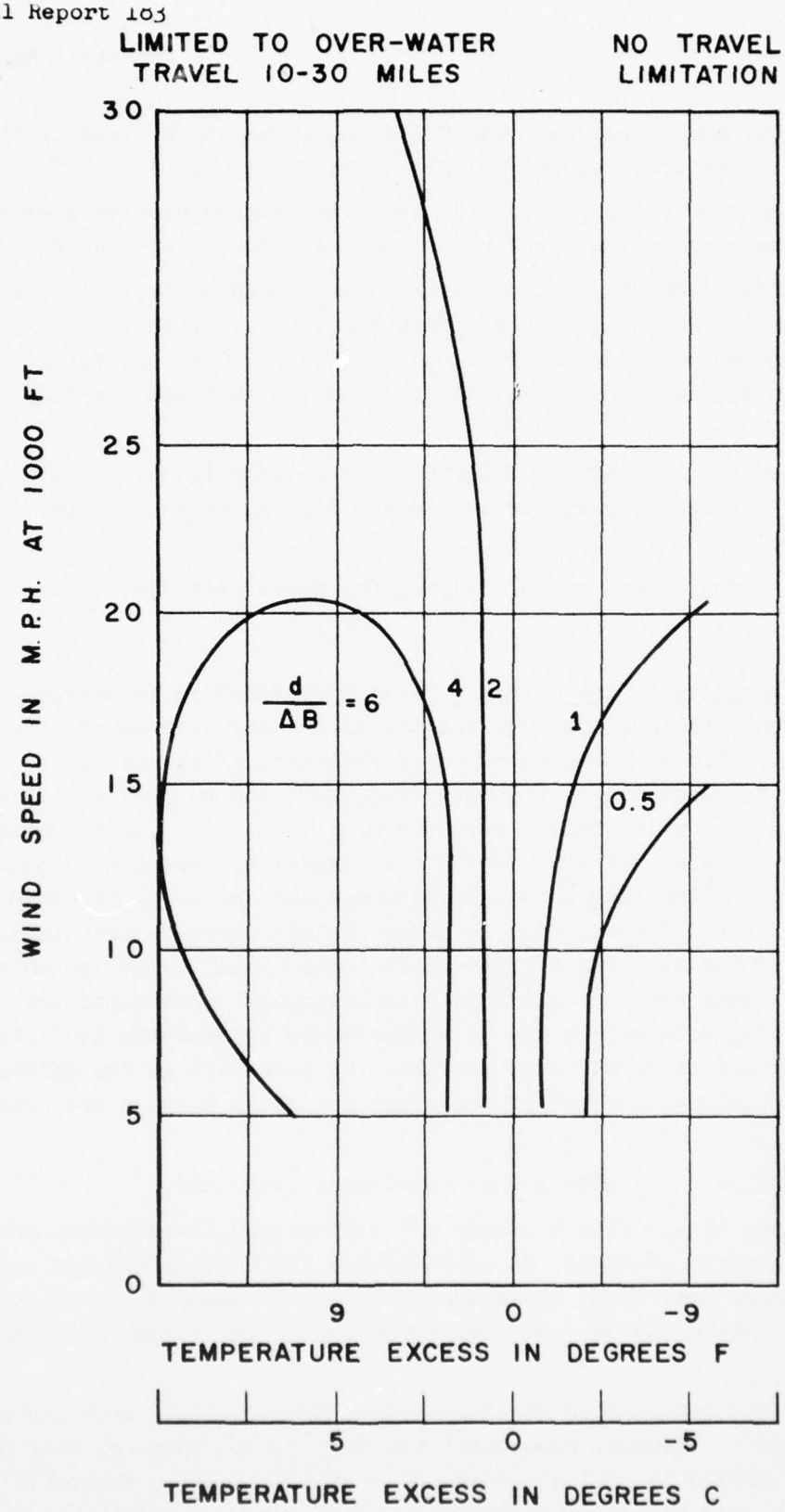

Figure 81. Graph Showing the Value of the Ratio of Duct Width to the B-Deficit, ΔB, for Values of Temperature Excess and Winds at the 1000-Foot Level [12].

which have been observed to hold under various meteorological conditions. Consequently, reasonably accurate results are not limited to only a few idealized situations.

It should be mentioned also that use of the method in a literal manner can be improved upon if the calculated results are modified by the judgment of someone trained or experienced in boundary-layer meteorology, as well as by experience. Complicating factors such as variations in the initial stability conditions, variability of the sea-surface temperature, effects of convergence, divergence, and subsidence, and presence of fronts can best be taken into account by one familiar with their effects.

Chapter 9

OPERATIONAL APPLICATIONS

The optimum utilization of radio and radar for the many and varied phases of US Air Force operations is of paramount importance at all times. High-precision tracking of missiles and satellites, early detection of enemy aircraft or missiles, and new electronic navigation and geodetic mapping have resulted in new and more stringent demands on radio and radar performance.

Basic meteorological responsibilities in the field of radio-radar propagation are to provide the information necessary for the evaluation of the effects of atmospheric conditions on radar performance. The preceding chapters of this report have indicated the general procedures for providing this information, but it will be necessary for the meteorologist to effect liaison with the cognizant radar personnel to insure continuing and optimum dissemination of the meteorological information for its specific purpose. Specifically, the meteorologist should advise cognizant radar personnel daily of the refractive conditions expected for the day. Dependent on the amount of meteorological data he has available, he can provide information based on the procedures outlined in Chapters 3 through 8 which translate the meteorological data into usable and useful radar propagation criteria. Although much of this information will be qualitative, many apparent failures of the meteorological data in describing radar propagation conditions can be attributed to deficiencies in the operating condition of the equipment. In this connection, it will be necessary to maintain liaison with the cognizant radar personnel to determine more adequately these radar-meteorological relations in the course of daily forecasting and verification.

The following sections will be devoted to describing a few suggested operational procedures for supporting Air Defense Command Radar operations, Hiran and Shoran Electronic Mapping Operations and a brief discussion of the meteorological requirements for support of the high-precision radar employed on the missile ranges.

9.1. Meteorological Support for the Air Defense Command (ADC) Radars.

Currently, there are two major types of height-finding radars in use in the Air Defense Command. These are the older AN/FPS-6 and the recently integrated AN/FPS-26.

9.1.1. The AN/FPS-26 Radar-Height Finder. In the AN/FPS-26, the correction for atmospheric refraction is introduced electronically as a function of range, antenna elevation angle and surface refractivity. The target height above mean sea level is computed by the equation

$$h = K(\alpha_o N_s)\, h_a + h_s \tag{124}$$

where h_s is the radar-site height above mean sea level and $K(\alpha_o, N_s)$ = refractive correction factor (K-function). The K-function may be related to the height-error correction ϵ_h by employing equations (62) and (69) to obtain

$$K = 1 - \frac{(R^2 - h_a^2)}{2R\, h_a}\,\tau \tag{125}$$

From equation (125) we see that the K-function corrects the radar height for atmospheric bending τ. In order to obtain τ the CRPL Exponential Reference Atmosphere described in section 4.4 is employed. Since τ is a function of the initial elevation angle α_o, the K-potentiometer, which electronically determines the height correction, is driven by the antenna-nod axis. Although only one "K-pot" is used with each radar, 20 separate refraction-correction profiles are made available by changing the "K-pot" reference. These 20 profiles, shown in Figures 82 and 83 are indexed or selected by a specific range of surface refractivity (N_s) values. CRPL ray-tracing results were employed in the design of the output of the K-potentiometer.

The value of N_s must represent the actual radar-site value. For those sites not instrumented with meteorological sensors of pressure, temperature, and dew-point temperature, the forecast of these three parameters must be accurate. The value of N_s will undergo a diurnal variation as discussed in sections 7.3.1 and 7.3.2. During stable synoptic conditions, determination of N_s should be done at 6-hourly intervals, with greater frequency during changing synoptic situations. It is the responsibility of weather personnel supporting ADC radar units to provide sufficiently accurate meteorological data for peak precision in radar search and height finding.

9.1.2. The AN/FPS-6. The AN/FPS-6 type height finders lack the refraction correction versatility of the AN/FPS-26. The AN/FPS-26, as previously indicated, is capable of approximating 20 different exponential refractive-index profiles. The AN/FPS-6 can only be calibrated to a single equivalent earth's radius profile at any given time. Originally, a 4/3 earth concept was used. More recently a 1.21 equivalent earth's radius factor has been used. Actually, the AN/FPS-6 can be calibrated to any equivalent earth's radius factor from 1.1 to 1.75.

Experience with this height finder has demonstrated that no single

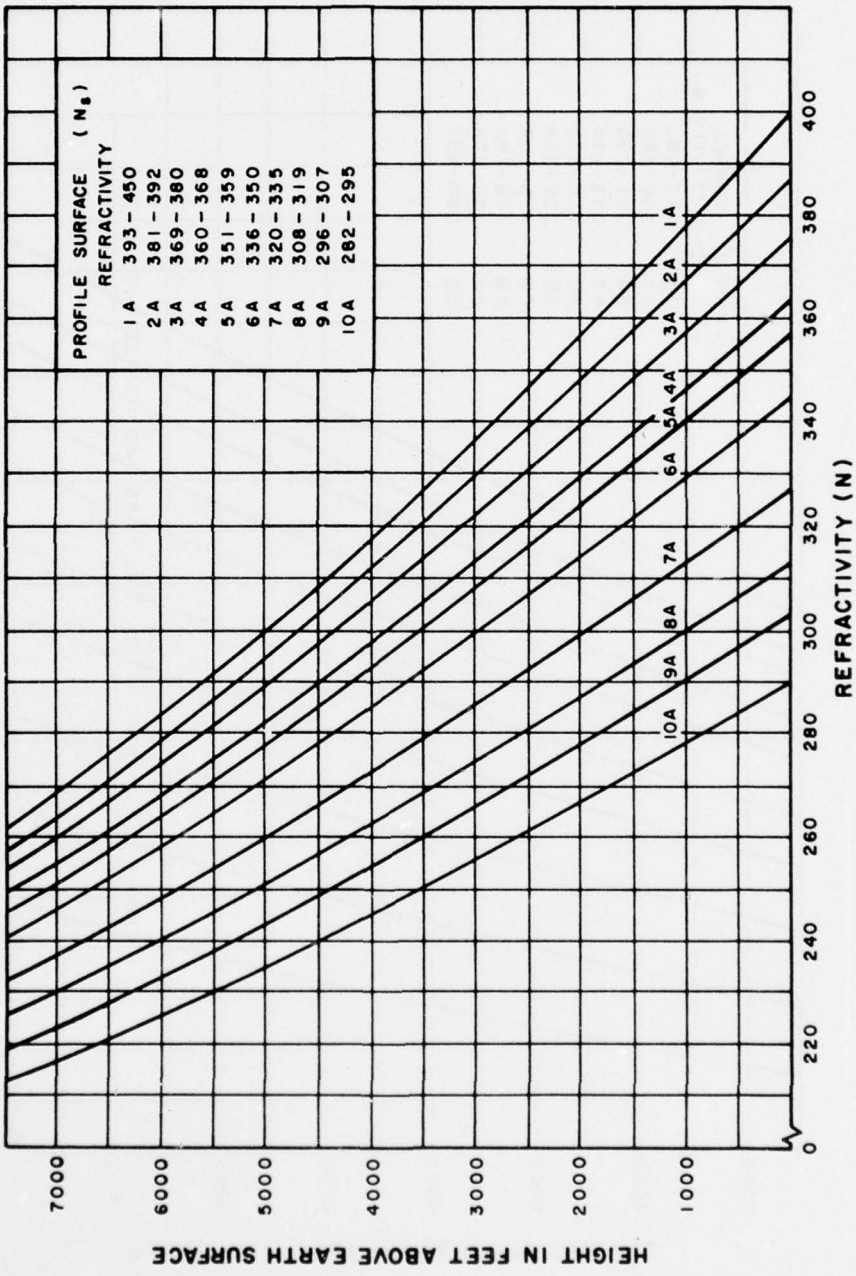

Figure 82. "CRPL Exponential Reference Atmosphere" for Profiles 1A through 10A.

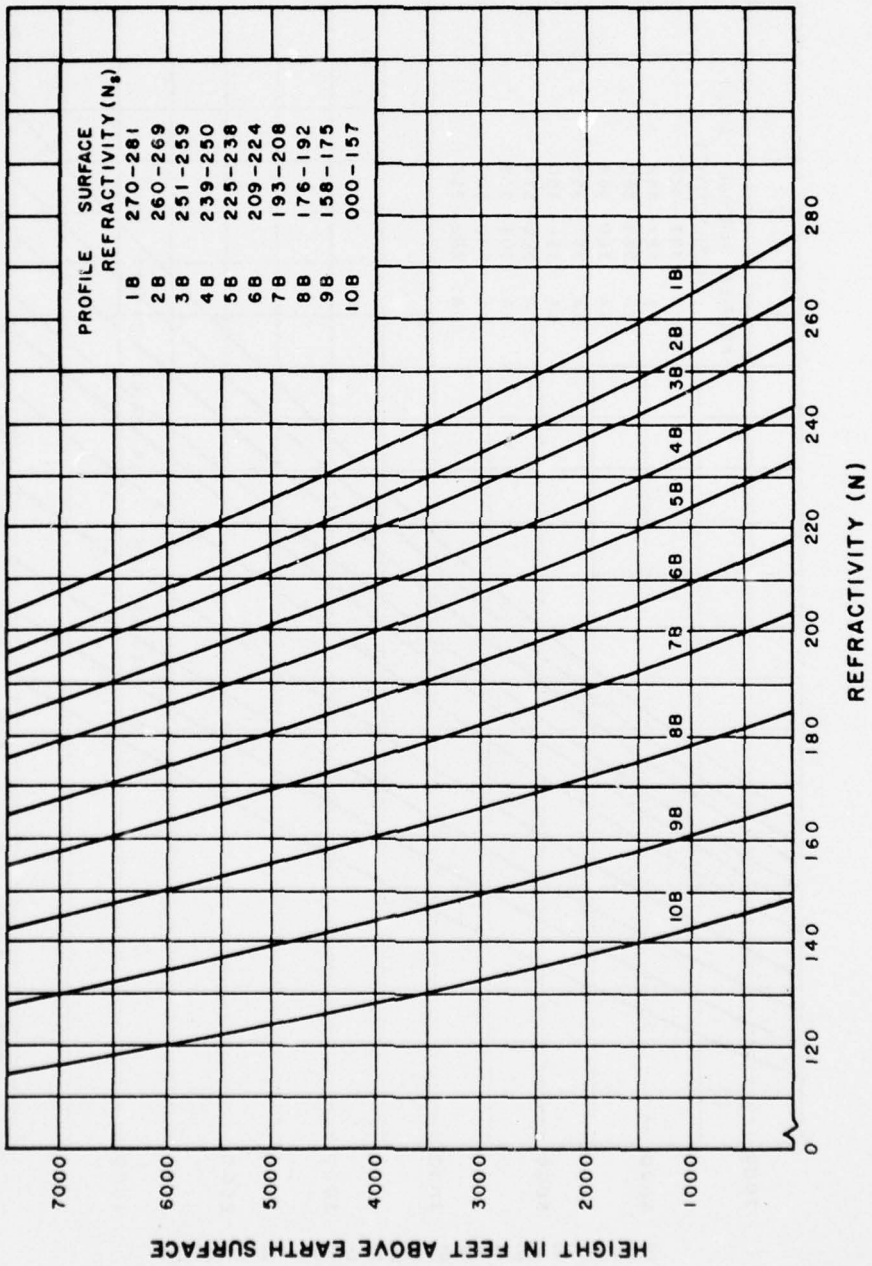

Figure 83. "CRPL Exponential Reference Atmosphere" for Profiles 1B through 10B.

equivalent earth's radius refraction correction can be expected to produce accurate height information throughout the wide range of climatological and geographical conditions in which these radars are located. In fact, at most sites the variations in refractive conditions with season or even month to month are too great to permit the use of a single profile with accurate results. As a consequence of this situation it may be necessary for weather personnel to work with radar personnel to select approximate equivalent earth's radius factors for the AN/FPS-6 which will produce best accuracy on a seasonal or perhaps monthly basis. Three methods of determining the refraction correction for the AN/FPS-6 are given below.

One method consists of determining an immediate correction by comparing a known target's true height with the radar-indicated height.

Another method is based on a manual computation of the path traced by the zero-degree ray through some model atmosphere. This atmosphere is derived from climatic data for 50-mb intervals for specific sites. A seasonal profile is determined and the ray path computed. An equivalent earth radius factor can then be inserted which best approximates the computed path.

A third method involves the use of ray tracings determined for specific exponential refractivity profiles. The Central Radio Propagation Laboratory ray tracings for some 8 exponential profiles presented in Appendix B may be employed for this purpose.

Carvill and Von Hellens [13] selected 10 equivalent factors which would produce ray paths within the boundaries of the 200 N_s and 450 N_s tables. Each equivalent factor is applicable for a specific interval of N_s. Table 9 gives the N_s range for each $\underline{k}$- (effective earth's radius) factor and the calibration check points.

The mean monthly surface refractive-index values of a radar site can be determined and used to identify the k-factor. Some radar sites will find that a particular factor is applicable for longer periods than a month due to small changes in the mean value. In most cases the diurnal changes in N_s will be greater than the mean monthly. Extreme changes in N_s will require a change in the k-factor setting if accuracy is to be maintained. One must bear in mind that an equivalent earth factor may give a good approximation of the zero-degree elevation ray path but cause serious errors with higher antenna-elevation angles, and vice-versa.

Future possibilities for correcting height errors may be the installation of a switch to insert k-factors or the use of computers which would accept raw data and determine the necessary correction prior to data display.

TABLE 9

Range Versus Altitude for Different Correction Factors and Varying Elevation for the FPS-6.

N_s	k-Factor	Elevation Angle	Range in Nautical Miles			
			50 nm	100 nm	150 nm	200 nm
			Feet	Feet	Feet	Feet
< 223	1.11	0.0°	1,990	7,960	17,910	31,850
		5.0°	28,490	60,950	97,400	
		10.0°	54,800			
223-245	1.14	0.0°	1,938	7,752	17,440	31,010
		5.0°	28,430	60,750	96,930	
		10.0°	54,740			
246-268	1.18	0.0°	1,872	7,489	16,850	29,960
		5.0°	28,370	60,480	96,340	
		10.0°	54,680			
269-291	1.21	0.0°	1,826	7,303	16,430	29,210
		5.0°	28,320	60,300	95,920	
		10.0°	54,630			
292-314	1.25	0.0°	1,767	7,070	15,910	28,280
		5.0°	28,260	60,060	95,400	
		10.0°	54,570			
315-337	1.28	0.0°	1,726	6,904	15,530	27,620
		5.0°	28,220	59,900	95,020	
		10.0°	54,530			
338-360	1.32	0.0°	1,674	6,695	15,060	27,780
		5.0°	28,170	59,690	95,550	
		10.0°	54,480			
361-383	1.38	0.0°	1,601	6,404	14,410	25,620
		5.0°	28,100	59,400	93,900	
		10.0°	53,410			
384-406	1.48	0.0°	1,493	5,971	13,440	23,880
		5.0°	27,990	58,960	92,930	
		10.0°	54,300			
> 406	1.57	0.0°	1,407	5,629	12,660	22,520
		5.0°	27,900	58,620	92,150	
		10.0°	54,210			

9.1.3. Constructing the B-Refractive Index Profile. In section 3.3.3 a procedure for plotting the N-profile was described. At times it is more convenient to plot the B-profile in order to determine quickly the regions the atmospheric refractive profile differs from standard conditions, i.e., from the 4/3 earth radius concept. The following procedure for constructing the B-profile has been recommended by the 4th Weather Wing.

Using the N-values and height values, compute the B-value using the chart

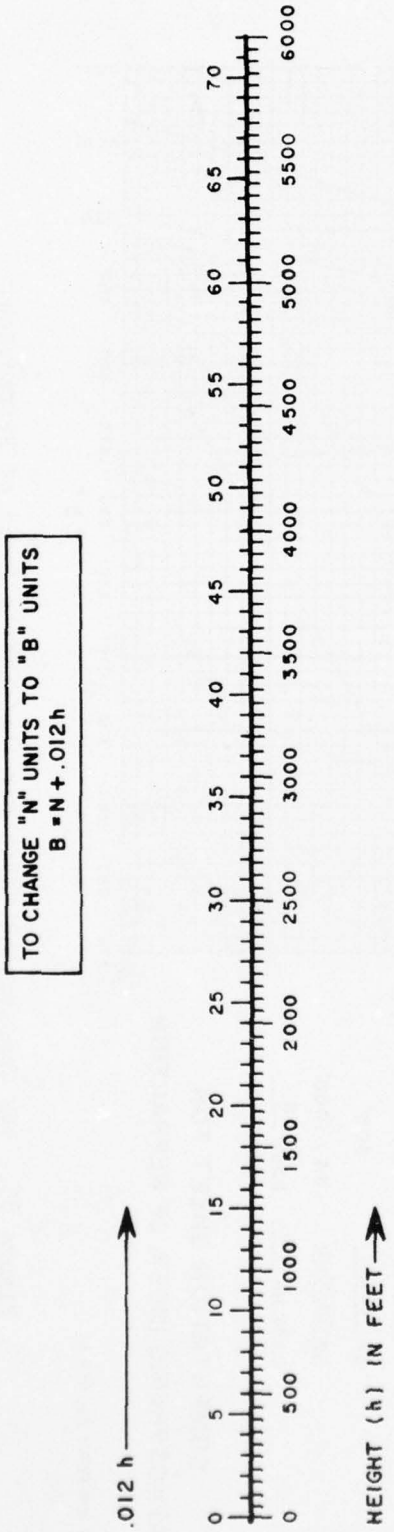

Figure 84. B-Unit Nomogram.

to change N-units to B-units, see Figure 84. Enter the B-value in the appropriate block on the left side of 4WW Form 29 (Figure 85).

On the center section of 4WW Form 29, construct a refractive-index (B) profile by plotting the B-values versus height and connect the points by a straight line. An example of a completed 4WW Form is contained in Figure 85.

9.1.4. Radar Propagation Analysis. The following procedures should be followed in interpreting the refractive-index profiles constructed on 4WW Form 29:

a. Scan the refractive-index profile for negative gradients.

b. Record the

(1) Height (in feet) of the base of the strongest gradient in block "hl."

(2) The thickness (in feet) of the layer with the strongest gradient and enter in block "Δh."

(3) If there are other weaker, significant negative gradients, enter these values also in the appropriate blocks.

c. If B is more positive than -12 -24B/1000 feet, enter the word "normal" immediately after "Case No."

d. If B is between -12 -24B/1000 feet and -36B/1000 feet, abnormal refraction and possible trapping is indicated. If B is equal to or more negative than -36B/1000 feet, trapping is indicated. In these cases refer to the appropriate ray-tracing diagram in the Appendix B in Volume II

RADAR SITE 475th
RAOB STATION OAK
DATE 15 SEP 61 TIME 1200 Z
FORECASTER Lt. Guesser

P	T	Td	Ht	B	N
1000	20.0	16.5	500	351	345
850	15.0	2.5	5150	323	261
1016	20.0	16.8	0	350	350
983	25.0	14.8	1000	337	325
870	15.0	10.8	4500	345	291

	A	B
hi	500'	4500'
Δh	500'	600'
ΔB	-28/1000'	-34 / 1000'

CASE No. 6 PAGE 8

COMPUTATION SHEET FOR
ATMOSPHERIC INDEX OF REFRACTION

4 WW FORM 29, SEP 61

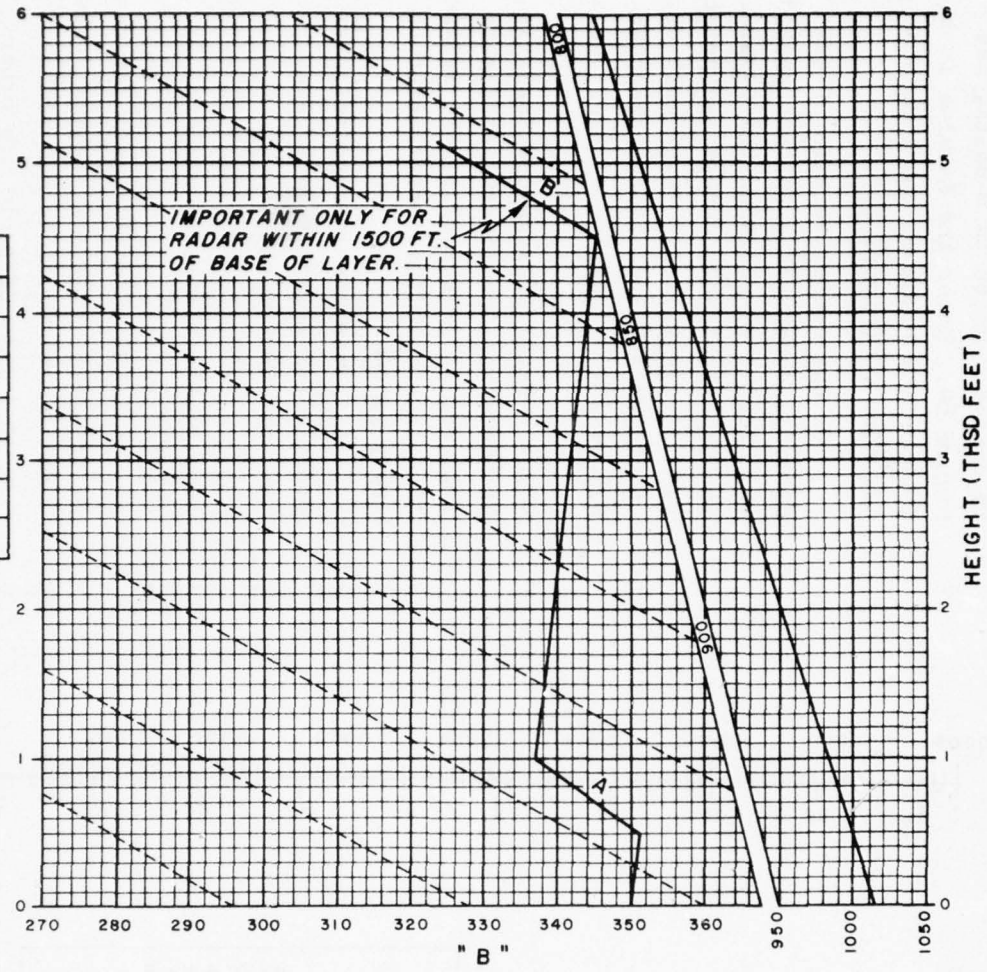

Figure 85. 4WW Computation Sheet for Atmospheric Index of Refraction.

and, knowing the height of the layer relative to the radar, record the "Case No." and "Page" best describing the situation.

The following examples show the format that should be employed by ADC meteorological-support personnel in transmitting radar-propagation analyses:

Example 1.

"Radar propagation analysis for 475th Radar Squadron based upon 1200Z data. Abnormal refraction or possible trapping indicated. Gradient -28B/1000 feet, base of layer 500 feet, thickness 500 feet. Reference Case No. 6, page 68, Appendix B."

a. Figure 85 indicates the completed 4WW Form 29 for this particular example.

b. Radar height 3000 feet (known and used in the analysis). Distance to top of layer (radar above layer) 2000 feet.

c. Case No. 6, page 68, illustrates this situation. In this case, the radar is 2000 feet above the layer (the height scale is relative and may be translated as desired) and the gradient and thickness of layer meet the observational criteria of this particular case.

d. It can be seen that the radar hole at 5000 feet above the radar site begins at 168 nm and ends at 207 nm. At 10,000 feet above the radar site the radar hole begins at 202 nm and ends at 243 nm.

Example 2.

"Radar propagation analysis for 475th Radar Squadron based upon 0000Z data. Trapping indicated. Gradient -75B/1000 feet, base of layer 500 feet, thickness 180 feet. Reference Case No. 25, page 93, Appendix B."

a. Radar height 500 feet, radar in base of layer.

b. Case No. 25 most nearly approximates these conditions. The radar hole at 5000 feet above the radar site begins at 95 nm and ends at 130 nm. At 10,000 feet above the radar site the radar hole begins at 130 nm and ends at 168 nm. Strong, beyond-the-horizon propagation is present at the level of the trapping layer.

Example 3.

"Radar propagation analysis for 475th Radar Squadron based upon 1200Z data. Trapping indicated. Gradient -48B/1000 feet, base of layer 1000 feet, thickness 500 feet. Reference Cases No. 39 and 40, pages 110 and 111, Appendix B."

a. Height of radar 500 feet, distance to base of layer 500 feet.

b. This situation is between Cases 39 and 40 so both are referenced. An interpolation between the two cases is necessary. Case No. 39 shows nearly standard coverage while Case No. 40 shows a weak radar hole. An interpolation of these two cases would indicate a possible, weak radar hole as indicated in Case No. 40 with probable weak beyond-the-horizon propagation as indicated in Case No. 40.

Example 4.

"Radar propagation analysis for 475th Radar Squadron based upon 0000Z data. Trapping indicated. Gradient -68B/1000 feet, base of layer 1000 feet, thickness 500 feet. Reference Case No. 51, page 125, Appendix B."

a. Height of radar 0 feet, distance to base of layer 1000 feet.

b. Case No. 51 illustrates this situation. Although a trapping gradient is present, the ray tracing reveals that normal propagation would be expected.

9.1.5. Altimeter-Height-Correction Factor. When an aircraft is vectored for the interception of a radar target, it is frequently necessary to apply a height-correction factor (HCF) to the interceptor's altimeter in order to position properly the interceptor at true altitude. The following discussion describes techniques that may be employed to obtain the altimeter HCF.

a. Altimeters. The pressure altimeter used on aircraft for height determination is simply a barometer which measures atmospheric pressure and a gearing mechanism which converts the sensed pressure to altitude. The conversion from pressure to altitude is based on a fixed set of values established as the Standard Atmosphere.

This standard atmosphere represents a hypothetical vertical distribution of atmospheric temperature, pressure, and density which by international agreement is taken to be representative of the atmosphere for purposes of pressure altimeter calibrations. A standard unit of atmospheric pressure, "one atmosphere," is defined as that pressure exerted by a 760-mm column of mercury (Hg). Thus, "one atmosphere" is equivalent to 760 mm Hg or 29.92 inches Hg or 1013.2 mb. The temperature at 1013.2 mb, considered as mean sea level, is 15°C and the temperature lapse rate through the troposphere is -6.5°C/km.

By having the standard atmosphere pressure of 1013.2 correspond to a zero pressure altitude (the altitude, in the standard atmosphere, at which a given pressure will be observed), inserting the physical constants into mathematical formulas and making certain assumptions, the height of any pressure surface can be determined.

The height-indicating dial of the aircraft pressure altimeter originates from the calculations of the preceding paragraph. Rather than having the dial

AD-A041 877 AIR WEATHER SERVICE SCOTT AFB ILL F/G 17/9
ESTIMATING METEOROLOGICAL EFFECTS ON RADAR PROPAGATION. VOLUME --ETC(U)
DEC 76 W B MORELAND
UNCLASSIFIED AWS-TR-183-VOL-1 NL

3 OF 3
ADA041 877

END
DATE FILMED
8-77

of the altimeter indicate pressure, it indicates altitude, the height calculated for each pressure surface in a standard atmosphere. The altimeter indicates zero height when the aneroid barometer senses 1013.2 mb (the dial having been set for 29.92). A perfect altimeter will indicate 4781 feet when the aneroid senses 850 mb, 9882 feet when the aneroid senses 700 mb, and the calculated height values for any pressure surface when 29.92 is inserted in the altimeter.

That
The standard atmospheric conditions are rarely observed is a well-known fact to meteorologists. A pressure surface of 1013 is not always at mean sea level, the 850-mb and 700-mb pressure surfaces are not always at 4781 and 9882, respectively. In actuality the height departure of constant-pressure surfaces from standard atmosphere altitudes of these surfaces varies with altitude. An aircraft flying at a constant-pressure altitude will trace the undulations of the pressure surface corresponding to that pressure altitude. The indicated altitude of an aircraft can be corrected for temperature variations, for variations of surface pressure and also for sensing errors due to aircraft speed. For safety of flight all aircraft operating above 24,000 feet must fly with the altimeter set at 29.92 (this assumes sensing errors less than ±500).

b. D-Values. The true altitude of an aircraft is the aircraft's height above mean sea level. A term used to denote the difference between an aircraft's pressure altitude and true altitude is known as a D-value. The sign of the D-value is determined by subtracting the pressure altitude of the point in question from the true altitude of that point. This D-value can vary from point to point both vertically and horizontally as well as varying with time at a specific point in space. It should be understood that D-values have no connection with refraction errors.

The D-value must be taken into account for proper positioning between a target and interceptor. Consider a nonstandard atmosphere where the 300-mb surface (at a specific point) may have a true altitude greater or less than the standard atmosphere's calculated height. One must bear in mind that an altimeter set at 29.92 will indicate 30,000 feet at 300 mb whether that surface is at 25,000 feet or at 45,000 feet.

Assume an aircraft is flying at an indicated altitude of 30,000 feet (pressure altitude of the 300-mb surface). Raob analysis shows the 300-mb surface to be at a true altitude of 32,000 feet. The aircraft, even though indicating 30,000, is actually at 32,000 feet. The D-value is +2000 feet. Here the D-value is a correction applied to the aircraft altimeter to get true altitude.

If the above aircraft is an interceptor, the fact that his altimeter will read 2000 feet less than his true altitude must be considered. For an

intercept the indicated height of an aggressor would be unknown but radar can show the true height, providing atmospheric bending has been taken into account. Knowing the target's true height and the D-value at the target's altitude and Height Correction Factor (HCF) can be given the interceptor to account for the altimeter error (2000 feet in the above case). Here the HCF is applied to the true target altitude. The HCF is the D-value with opposite sign. Using the above case the HCF is -2000 feet. If the radar altitude was 32,000 feet the intercept would be at 30,000 feet indicated.

Note that in the case just illustrated the HCF was applicable only for interceptor correction and not radar- or target-height correction. To illustrate a case where the D-value is applicable to the radar, consider the condition where a radar indicates a target at 27,400 feet but no allowance has been made for atmospheric refraction. Contact is made with the target who states his pressure altitude is 26,500 feet (his aneroid is sensing 352 mb). Analysis of the latest radiosonde ascent reveals the true height of the 352-mb surface to be at 26,000 feet. The D-value is -500 feet (true height 26,000 minus pressure altitude 26,500) and the HCF is +500 feet.

The radar operator is given the target's pressure altitude of 26,500 feet, the weather forecaster gives the operator the D-value of -500 feet. The operator now knows the target's true altitude is 26,000 feet and he can take corrective action which will cause the radar set to indicate the target's true altitude of 26,000 feet.

Appendix C, Volume II, gives methods for determining existing or forecast D-values as well as climatic charts of D-value on a seasonal basis.

9.2. Aerial Electronic Surveying.

Mankind for generations has used a method utilizing observation of the stars to locate points on the surface of the earth to some agreed frame of reference. However, during World War II, several electronic (time-distance) systems were developed to determine the position of a point in space, but not all of them were capable of the precision required for geodetic surveying. A study of these systems was made and the results indicated that SHORAN was the best suited. SHORAN is a pulse radar system which includes both airborne and ground equipment. A pulse is transmitted by the airborne set to a ground station which receives and retransmits to the airborne equipment. The time for a pulse to travel between the aircraft and the ground station is measured and converted to distance. A system was later developed which incorporated the SHORAN principles but achieved higher precision. This system was called HIRAN, a name denoting High Precision SHORAN. A still more accurate SHORAN

system, called SHIRAN, is now under development and will soon be employed for geodetic surveys.

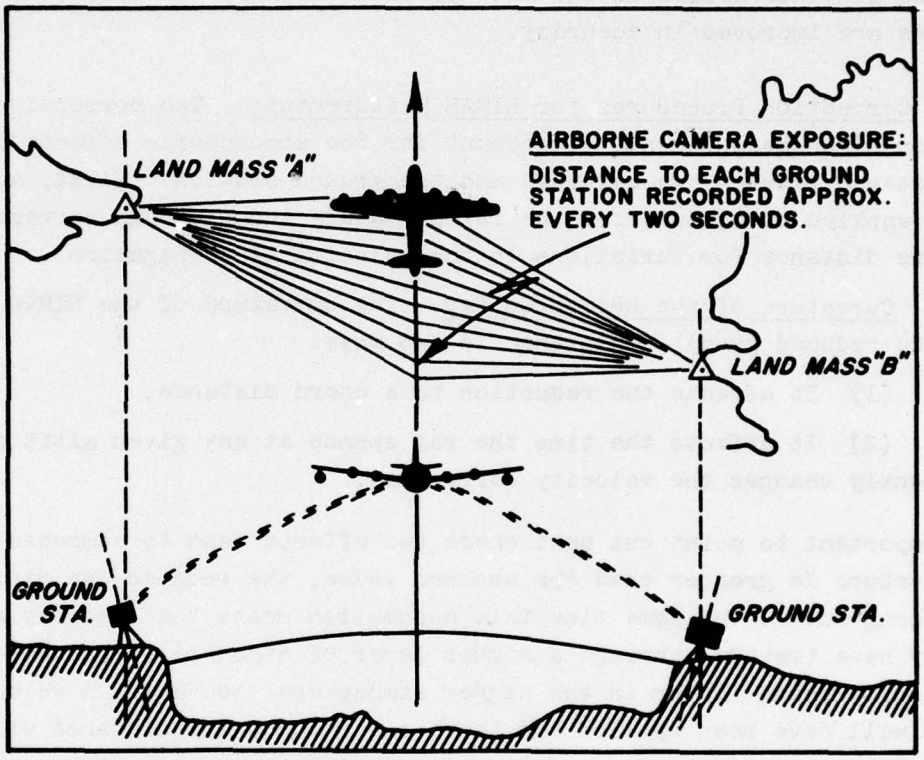

Figure 86. Single HIRAN Line Crossing.

9.2.1. HIRAN Geodetic Surveying. By flying an aircraft between two ground stations as illustrated in Figure 86, and simultaneously recording the distance to each station the minimum sum distance between the ground stations via the aircraft may be determined. This minimum sum, after application of corrections, very nearly equals the geodetic distance between the ground stations. The applicable corrections are: (a) Correction for the true velocity of propagation of the radio waves as compared to the design velocity of the instrument; (b) correction for the change in path length caused by the bending or refraction of the ray along its path; (c) correction of the air-to-ground distance to reduce to the sea-level arc distance; and (d) correction for instrumental errors as determined by calibration.

The accuracy of the position determination is dependent on the accuracy of the individual line measurements. Distances measured in HIRAN projects are

expected to have a probable error not to exceed ±12 feet with the maximum error of any distance measured for a HIRAN net not to exceed ±30 feet. These are errors in observed distances. A trilateration network adjustment distributes the distance errors in the most probable manner; therefore, the adjusted distances are improved in accuracy.

9.2.2. Correction Procedures for HIRAN Measurements. Two corrections are required on HIRAN measurements to account for the atmospheric effects on the ray-path distance between the aircraft and the ground station. First, a correction must be applied to account for the ray curvature and a second correction adjusts the distance for variations in the velocity of propagation.

a. Curvature of the Refracted Ray. The curvature of the HIRAN ray affects the reduced geodetic distance in two ways:

(1) It affects the reduction to a chord distance.

(2) It affects the time the ray spends at any given altitude and consequently changes the velocity correction.

It is important to point out that these two effects tend to compensate. When the curvature is greater than the assumed value, the reduced map distance will be too long but at the same time this assumption means that the ray will actually have traveled through a higher layer of atmosphere than was assumed. The velocity being faster in the higher atmosphere, too small a velocity correction will have been applied and hence the reduced map distance will be too short. It is this feature of compensation which permits the use of approximate methods with a relatively small error in the reduced distance.

The method employed by 1370th Photo-Mapping Wing, USAF, is simple in principle and sufficiently accurate at the present time, considering present instrumental accuracy and the approximations in determining the vertical profile of the refractivity. This method consists of determining the height of the ray between the ground station and the aircraft at 5-mile intervals. The radius of curvature of the ray is assumed to be four times the earth's (4/3 earth-radius concept). The equation employed in this computation may be obtained by employing the law of cosines to the geometry shown in Figure 87. We obtain:

$$(126) \quad h_o = \frac{R_1^2}{2a_e} + R_1 \sin \alpha_o$$

$$(127) \quad H = \frac{R_o^2}{2a_e} + R_H \sin \alpha_o$$

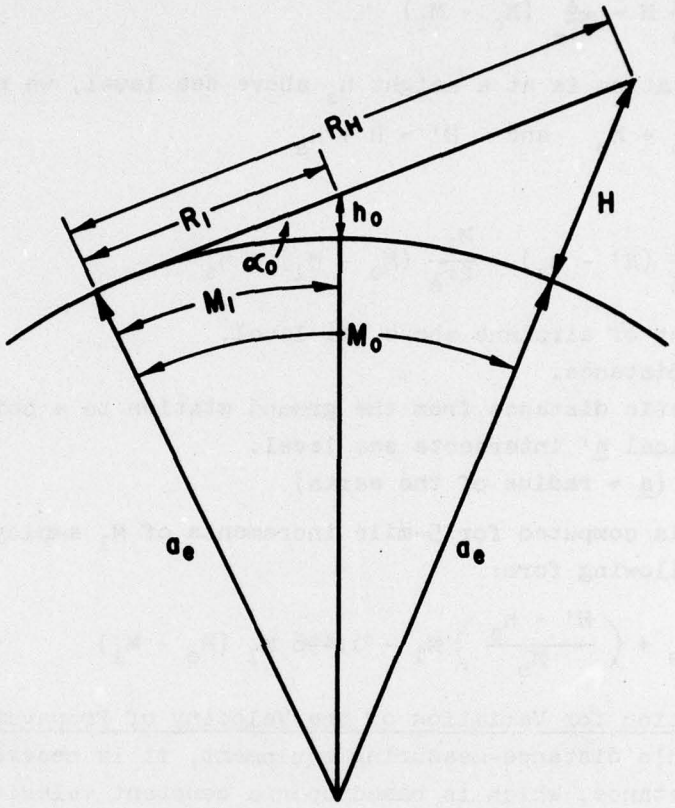

Figure 87. Geometry of Height Computation Employing 4/3 Earth's-Radius Concept ($a_e = 4/3a$).

Upon eliminating sin α_o from (126) and (127), we have:

$$(128) \quad h_o = \frac{R_1^2}{2a_e} + \frac{R_1}{2a\ R_H}\left[2H\ a_e - R_H^2\right]$$

Using the relationships

$$R_1^2 = M_1^2 + h_o^2 \quad \text{and} \quad R_H^2 = M_o^2 + H^2$$

in equation (128), we obtain:

$$(129) \quad h_o = \frac{M_1}{M_o} H - \frac{M_1}{M_o}\left[\frac{M_o - M_1}{M_o}\right]\left[\frac{M_o^2 + H^2}{2r_e}\right]$$

Employing the approximation $\frac{H^2}{2r_e} \ll \frac{M_o^2}{2r_e}$, we obtain

$$(130) \qquad h_o = \frac{M_1}{M_o} H - \frac{M_1}{2r_e} (M_o - M_1)$$

If the ground station is at a height h_s above sea level, we have

$$h' = h_o + h_s \quad \text{and} \quad H' = H + h_s$$

and

$$(131) \qquad h' = \frac{M_1}{M_o} (H' - h_s) - \frac{M_1}{2r_e} (M_o - M_1) + h_s$$

where H' = height of airplane above sea level.
M_o = map distance.
M_1 = geodetic distance from the ground station to a point where the vertical $\underline{h}'$ intersects sea level.
$a_e = 4/3a$ ($\underline{a}$ = radius of the earth).

In practice $\underline{h}'$ is computed for 5-mile increments of M_1 employing equation (131) in the following form:

$$(132) \qquad h' = h_s + \left(\frac{H' - h_s}{M_o} \right) M_1 - 0.496 M_1 (M_o - M_1)$$

b. Correction for Variation of the Velocity of Propagation. With all present electronic distance-measuring equipment, it is necessary to correct the observed distance, which is based upon a constant velocity, for the varying velocity caused by the changes in the meteorological conditions along the ray path. In section 2.4, a formula was developed for evaluating the distance correction when the initial elevation angle α_o is known. However, this parameter is not measured in HIRAN, so a different procedure is required.

In the HIRAN transmitters the design velocity is 186,219.14 mi/sec, the speed of propagation in a vacuum corrected to standard conditions (760 mm pressure, 0°C). Since the actual velocity deviates from this value while the ray travels through the atmosphere, a distance correction must be obtained.

Knowing the altitude $\underline{h}'$ [from equation (132)] of the ray path at the end of each 5-mile increment, an index of refraction is selected from the altitude refractivity profile graph (section 3.3.3) for each increment. Numerical integration is then made along the ray path and the mean index of refraction $\overline{n}$ is computed from

$$(133) \qquad \overline{n} = \frac{\sum_{j=1}^{j=m} \overline{n}_j \, \Delta M_j}{M_o}$$

where $\bar{n}_j$ = the average value of n in the layer j,
ΔM_j = the distance the ray travels in layer j (5 miles except for last increment which will be less than 5 miles), and
m = number of layers involved.

Knowing the mean index of refraction along the ray path the mean velocity may be computed from

$$\bar{v} = \frac{c}{\bar{n}} \tag{134}$$

where c is the vacuum velocity, 186,282.05 mi/sec. The correction to the ray-path length may be computed as

$$\Delta R = M_o \left[\frac{\bar{v} - v_h}{v_h} \right]$$

where v_h is the design velocity of the HIRAN equipment.

9.3. Air Force Missile Test Centers.

At a Missile Test Center, the basic meteorological support for radio-radar propagation consists of obtaining the necessary pressure, temperature, and humidity data to compute the vertical profile of refractive index. The computations for the range and height corrections, employing the basic equations discussed in Chapter 2, are accomplished on the Test Center computers. However, a brief discussion of the tracking system accuracies will give the meteorologist some insight into the problem of the tropospheric refraction as related to high-precision tracking.

9.3.1. Tropospheric Refraction Errors for Missile Tracking Systems. First, there is evidence to support the hypothesis that, in many cases the uncertainties associated with the tropospheric refraction errors are larger than the other uncorrectable errors in high-precision tracking systems.

A study of the refraction problem made for the Air Force by the National Academy of Sciences [40] came to the following conclusions:

a. Tropospheric bias errors are highly predictable using radiosonde or refractometer profiles; residual errors from 1 percent to 3 percent of the refraction correction are commonly attained. Data to within one-half foot in range and 20 to 70 μ-radians in angle can be expected at elevation angles above 5 degrees.

b. Tropospheric fluctuation errors are not correctable using any known procedure, and will amount to a few tenths of a foot in range and 10 to 50 μ-radians in angle (depending on the baseline or aperture used for measurement),

under normal weather conditions.

c. The lowest atmospheric errors are found in trilateration systems using very long baselines. Total position and velocity errors for a typical track (660 miles range, 100 miles altitude) through average weather conditions, are shown in Table 10.

TABLE 10

Position and Velocity Errors for Missile Track.

	mcps	RMS Position Error (feet)	RMS Velocity Error (ft/sec)
Range-Angle Tracker	6,000	310	16
Interferometer	10,000	100	2.4
Trilateration System	2,000	19	0.9
	6,000	2.5	0.15

The error shown in the table may be increased or decreased by a factor of two or three for different weather conditions. The trilateration errors shown are dependent upon perfect survey of station location, as well as instrumental errors below one-half foot in range and 0.02 ft/sec in range rate.

9.3.2. Optimum Methods for Refractive Correction. There are three basic approaches to the refraction problem. One of these is basically meteorological and assumes that the atmosphere is a complex and unpredictable quantity. Hence, one must make meteorological measurements as near to the time of track and as nearly over the whole ray path as possible to determine the index of refraction profile. When this is done, standard ray-tracing techniques, as described in previous chapters, are used to compute the refraction correction. Refractometers, rawinsonde, wiresonde, or ground-level index of refraction may be used to estimate the index of refraction profile. The ultimate success of this approach lies in getting more and better measurements of the atmospheric data.

A second approach to refraction correction is what may be termed the statistical approach. It assumes that there are fluctuations of the index of refraction with time, but that one can construct a model of the atmosphere or what is equivalent to this and predict the refraction correction on a statistical basis, using certain easy to measure parameters. The advocates of this method suggest that one can predict the atmosphere better than it can be

estimated from insufficient measurements.

A third method which combines some of the elements of both of the above methods is used on the Atlantic Missile Range. In this method, the best correction using available meteorological data and ray-tracing methods is used to correct the data before it is entered into a least-squares solution. Then in the least-squares solution, in which one has a mathematical model for the residual part of the refraction correction with undetermined parameters, an adjustment is made for the uncorrected residuals. Hopefully, this would allow one to combine some of the best features of both of the previous methods.

Several mathematical models of uncorrected residuals have been developed for application to a specific refractive correction procedure. However, regardless of the model assumed, its approximate nature should be kept in mind. For it is the error in the refraction correction model rather than just in measured quantities, which is generally responsible for most of the residual refractive error in the first place.

9.3.3. Estimate of Uncorrectable Residuals. In estimating the uncorrectable residuals after the best available refractive correction has been applied, it has been common practice to measure or estimate the vertical profile and make the stratification assumption.

Essentially, all workers in the field have attacked the problem of estimating refraction effects due to a mean static refractive-index profile in more or less similar manner, and the results have been in reasonable agreement with each other. The method of attack has been to estimate either the mean static profile or the mean refraction effects, utilizing a model of the atmosphere which is based on previous atmospheric data. Such data normally included measured vertical refractive-index profiles or reasonable analytical approximations to such profiles, and either the profiles or resultant refraction effects were correlated with certain more readily obtainable parameters such as surface index of refraction and surface index gradient.

In general, there has been good agreement between different investigators of refraction as to the magnitude of the residual error which remains after the best correction for the static profile has been made. For a target altitude greater than about 30,000 feet, the residual errors are estimated to be on the order of 1.4 to 1.6 percent of the total refraction correction. In addition, the residual error in range correction, ΔR, appears to be rather insensitive to elevation angle so that it has been estimated that the residual of ΔR is

$$\delta(\Delta R) \cong 1.6 \times 10^{-2} \Delta R$$

Unfortunately, many of the studies upon which the above estimates have been made have been based on correlation of meteorological data which may have been unreliable or unrepresentative. Predictions of refraction corrections by different investigators for the same geographic locations based on data for that area may differ by four times the standard deviation of the individual predictions. Discrepancies of 5 percent or more between refraction predictions by different computation methods have been reported.

9.3.4. Error Analyses. If refraction corrections computed for average spherically symmetric atmospheres by different, but reasonable, methods do not show very good agreement, then near perfect prediction of corrections for actual ray paths for missile flights should not be expected. The lack of agreement between the true correction and that based on the horizontal stratification approximation with a vertically measured profile may be attributed to three different sources:

a. Errors in the vertical profile measurement,

b. Horizontal inhomogeneity of the atmospheric refraction index, and

c. Rapid changes in the atmosphere with time (scintillation).

Errors in the vertical profile might typically amount to 1 percent when the refractive-index profile is obtained from radiosonde data. This figure can be improved by about a factor of three by the use of expendable balloon-borne refractormeters.

The effect of horizontal inhomogeneities may be considered from two different aspects. Strong departures from horizontal homogeneity can lead to elevation-angle errors of 10 percent if predictions are based on vertical profiles. At the other end of the scale, horizontal inhomogeneities again become important in setting lower limits on residual elevation-angle errors. This comes about because the effects of horizontal inhomogeneities, although small at higher elevation angles, do not become necessarily negligible. In addition, such inhomogeneities contribute to azimuthal bending which is generally completely neglected in analyses of ray paths. Investigations have shown that for elevation angles above 5 degrees, the effects of horizontal inhomogeneities are greater than the residual error in the predictable (on the basis of surface refractive index) vertical bending.

It is only possible to make an educated estimate of the residual errors after the best refraction corrections have been made. Considering the lack of agreement between the different range corrections, the residual error in the range refraction correction may be estimated at about 5 percent of the total correction.

As yet little data has been obtained on the residual scintillation refraction error caused by atmospheric turbulence. However, experiments have been proposed which should provide the necessary data to give an answer to the problem in the near future.

REFERENCES

[1] Anderson, L. J.: "Prediction of Extended Coverage of Submarine Radars," NEL Rept. No. 228, US Navy Electronics Laboratory, San Diego, Calif., February 1951, 42 pp.

[2] Anderson, L. J. and Gossard, E. E.: "The Effect of the Oceanic Duct on Microwave Propagation," Trans. Am. Geophys. Union, Vol. 34, No. 5, October 1953, pp. 695-700.

[3] Anderson, L. J. and Gossard, E. E.: "Prediction of the Nocturnal Duct and Its Effects on UHF," Proc. IRE, Vol. 41, No. 1, January 1953, pp. 135-139.

[4] Air Weather Service: "Use of the Skew T, Log P Diagram in Analysis and Forecasting, Vol. I, Radiosonde Analysis," AWSM 105-124, Vol. I, 15 March 1961.

[5] Bean, B. R.: "Climatology of Ground-Based Radio Ducts," J. Res. NBS, Vol. 63D, No. 1, July-August 1959, pp. 29-34.

[6] Bean, B. R. and Cahoon, B. A.: "Effect of Atmospheric Horizontal Inhomogeneity Upon Ray Tracing," J. Res. NBS, Vol. 63D, No. 3, November-December 1959, pp. 287-292.

[7] Bean, B. R. and Riggs, L. P.: "Synoptic Variation of the Radio Refractive Index," J. Res. NBS, Vol. 63D, No. 1, July-August 1959, pp. 91-97.

[8] Bean, B. R., Riggs, L. P., and Horn, J. D.: "Synoptic Study of the Vertical Distribution of the Radio Refractive Index," J. Res. NBS, Vol. 63D, No. 2, September-October 1959, pp. 249-254.

[9] Bean, B. R. and Thayer, G. D.: "Models of the Atmospheric Radio Refractive Index," Proc. IRE, Vol. 47, No. 5, Part I, May 1959, pp. 740-755.

[10] Birnbaum, G.: "Fluctuations in the Refractive Index of the Atmosphere at Microwave Frequencies," Phys. Rev., Vol. 82, April 1951, pp. 110-111.

[11] Born, M. and Wolf, E.: Principles of Optics, Pergamon Press, Inc., New York, 1959.

[12] Burrows, C. R. and Attwood, S. S.: Radio Wave Propagation, Academic Press, Inc., New York, 1949.

[13]

[14] Crain, C. M. and Deam, A. P.: "An Airborne Microwave Refractometer," Rev. Sci. Instr., Vol. 23, No. 4, April 1952, pp. 149-151.

[15] Day, J. P. and Trolese, L. G.: "Propagation of Short Waves Over Desert Terrain," Proc. IRE, Vol. 38, No. 2, February 1950, pp. 165-175.

[16] Doherty, L. H.: "Geometrical Optics and the Field at a Caustic, with Applications to Radiowave Propagation Between Aircraft," Part V of Final Report on Contract AF 33(038)-1091, School of Electrical Engineering, Cornell University, Ithaca, New York, 10 September 1952, 148 pp.

[17] Domb, C. and Pryce, M. H. L.: "The Calculation of Field Strengths Over a Spherical Earth," J. IEE, Vol. 94, Part III, September 1947, pp. 325-336.

[18] Durst, C. S.: "Radio Climatology," in Meteorological Factors in Radio-Wave Propagation, Report of 1947 Radio Climatology Conference Held 8 April 1946 at Royal Institution, London. Physical Society London and Royal Meteorological Society, 1947, pp. 193-212.

[19] Fannin, B. M.: "Field Strength Determination by Ray Tracing Techniques for Horizontally Stratified Layers," Rept. No. 6-04 under Contract AF 19(604)-494, Electrical Engineering Research Laboratory, University of Texas, 15 August 1953, 29 pp. with 6 Appendices.

[20] Fawbush, E. J. and Miller, R. C.: "The Types of Airmasses in Which North American Tornadoes Form," Bull. Am. Meteorol. Soc., Vol. 35, No. 4, April 1954, pp. 154-165.

[21] Heaviside, O.: "Telegraphy," Encyclopaedia Britannica, London and Edinburgh, 10th edition, Vol. 9 (i.e., Vol. 33 of 9th edition), 1902, pp. 213-235.

[22] Horn, J. D., Bean, B. R., and Riggs, L. P.: "Some Meteorological Aspects of the Radio Refractive Index," NBS Rept. 6066, National Bureau of Standards, Boulder, Colorado, 31 August 1959, 14 pp.

[23] Jehn, K. H.: "The Use of Potential Refractive Index in Synoptic-Scale Radio Meteorology," Rept. No. 6-29 under Contract AF 19(604)-2249, Electrical Engineering Laboratory, University of Texas, Austin, Texas, 15 September 1959, 10 pp.

[24] Kennelly, A. E.: "On the Elevation of the Electrically Conducting Strata of the Earth's Atmosphere," Electrical World and Engineer, Vol. 39, No. 11, March 15, 1902, p. 473.

[25] Kerr, D. E.: Propagation of Short Radio Waves, McGraw-Hill Book Company, Inc., New York, 1951, 728 pp.

[26] Lukes, G.: "Arctic Radio Meteorology," in "Symposium on Tropospheric Wave Propagation, 25-29 July 1949," NEL Rept. No. 173, US Navy Electronics Laboratory, San Diego, California, June 1950, pp. 83-89.

[27] National Defense Research Committee: Radio Wave Propagation Experiments, Summary Technical Report of the Committee on Propagation, NDRC, Washington, D. C., Vol. 2, 1946, pp. 123-125.

[28] Petterssen, S.: Weather Analysis and Forecasting, 1st edition, McGraw-Hill Book Company, Inc., New York, 1940, pp. 138-204.

[29] Plank, V. G.: "Refractive Properties of Air Masses," NEL Rept. No. 243, US Navy Electronics Laboratory, San Diego, California, February 1952, 28 pp.

[30] Schelkunoff, S. A.: "Microwave Transmission of a Non-Homogeneous Atmosphere," MM-44-110-53, Bell Telephone Laboratory, July 1944.

[31] Schelleng, J. C., Burrows, C. R., and Ferrell, E. B.: "Ultra-Short-Wave Propagation," Proc. IRE, Vol. 21, No. 3, March 1933, pp. 427-263.

[32] Schulkin, M.: "Average Radio-Ray Refraction in the Lower Atmosphere," Proc. IRE, Vol. 40, No. 5, May 1952, pp. 554-561.

[33] Smith, E. K. and Weintraub, S.: "The Constants in the Equation for Atmospheric Refractive Index at Radio Frequencies," Proc. IRE, Vol. 41, No. 8, August 1953, pp. 1035-1037.

[34]

[35] Sweezy, W. B. and Bean, B. R.: "Correction of Atmospheric Refraction Errors in Radio Height Finding," NBS Rept. 7977, 25 October 1963, 53 pp. Also in: J. Res. NBS, Vol. 67D, No. 2, March-April 1963, pp. 139-151.

[36] Watson, G. N.: "The Diffraction of Electrical Waves by the Earth," Proc. Roy. Soc. London, Vol. 95, 1919, pp. 83-99.

[37] Weisbrod, S. and Anderson, L. J.: "Simple Methods for Computing Tropospheric and Ionospheric Refractive Effects on Radio Waves," Proc. IRE, Vol. 47, No. 10, October 1959, pp. 1770-1777.

[38] Wexler, H.: "Formation of Polar Anticyclones," Monthly Weather Rev., Vol. 65, No. 6, June 1937, pp. 229-236.

[39] Willett, H. C.: Descriptive Meteorology, Academic Press, Inc., New York, 1944, pp. 183-224.

[40] [Woodring, M. J. (Editor)]: "A Compilation of Papers Presented at the Fifth Joint AFMTC/Range User Data Conference," MTC-TDR-64-5, AF Missile Test Center, Patrick AFB Florida, 15 April 1964, 494 pp.

ADDITIONAL BIBLIOGRAPHY

Anderson, L. J.: "Tropospheric Bending of Radio Waves," Trans. Am. Geophys. Union, Vol. 39, No. 2, April 1958, pp. 208-212.

Anderson, W. L. and Fannin, B. M.: "Discussion of Radar Errors Due to Propagation Effects," Tech. Rept. EE-16 under Contract DA-29-040-ORD-1238, Engineering Experiment Station, University of New Mexico for White Sands Proving Ground, August 1958.

Aslakson, C. I. and Fickeissen, O. O.: "The Effect of Meteorological Conditions on the Measurement of Long Distances by Electronics," Trans. Am. Geophys. Union, Vol. 31, No. 6, December 1950, pp. 816-826.

Atlas, D.: "Meteorological 'Angel' Echoes," J. Meteorol., Vol. 16, No. 1, February 1959, pp. 6-11.

Bailin, B. and Colin, L.: "Tropospheric Refraction Effects on Height-Finding Radars," RADC-TN-59-1, Rome Air Development Center, Griffis AFB New York, February 1959, 43 pp.

Bankston, L. T. and Meeker, D. B.: "Correction of Near-Horizontal Radar Elevation Angles for Atmospheric Refraction," Tech. Memo. No. PMR-TM-64-6, Pacific Missile Range, Point Mugu, California, 6 July 1964, 26 pp.

Barnett, K. M., Bomba, S. J., Heil, T. W., and Kirchner, E. K.: "A Review of the Calculation of Radar Refraction Errors," USAERDAA-MET-7-64, US Army Research and Development Activity, Ft. Huachuca, Arizona, June 1964, 55 pp.

Bean, B. R.: "Attenuation of Radio Waves in the Troposphere," Advances of Radio Research, Academic Press, Inc., New York, June 1964, Vol. I, pp. 121-156.

Bean, B. R.: "Tropospheric Refraction," Advances of Radio Research, Academic Press, Inc., New York, June 1964, Vol. I, pp. 53-120.

Bean, B. R. and Cahoon, B. A.: "The Use of Surface Weather Observations to Predict the Total Atmospheric Bending of Radio Rays at Small Elevation Angles," Proc. IRE, Vol. 45, No. 11, November 1957, pp. 1545-1546.

Bean, B. R. and Dutton, E. J.: "On the Calculation of the Departures of Radio Wave Bending from Normal," J. Res. NBS, Vol. 64D, No. 3, May-June 1960, pp. 259-263.

Bean, B. R. and Horn, J. D.: "On the Average Atmospheric Radio Refractive Index Structure Over North America," NBS Rept. 6756, National Bureau of Standards, Boulder, Colorado, March 20, 1961, 35 pp.

Bean, B. R. and Horn, J. D.: "On the Climatology of the Surface Values of Radio Refractivity of the Earth's Atmosphere," NBS Rept. 5559, National Bureau of Standards, Boulder, Colorado, March 3, 1958, 17 pp.

Bean, B. R. and Horn, J. D.: "Radio-Refractive-Index Climate Near the Ground," J. Res. NBS, Vol. 63D, No. 3, November-December 1959, pp. 259-271.

Bean, B. R., Horn, J. D., and Ozanich, A. M., Jr.: "Climatic Charts and Data of the Radio Refractive Index for the United States and the World," NBS Monogr. No. 22, November 1960, 178 pp.

Bean, B. R. and Thayer, G. D.: "Central Radio Propagation Laboratory Exponential Reference Atmosphere," J. Res. NBS, Vol. 63D, No. 3, November-December 1959, pp. 315-317.

Bean, B. R. and Thayer, G. D.: "A Model Radio Refractivity Atmosphere," NBS Rept. 5576, National Bureau of Standards, Boulder, Colorado, June 9, 1958, 88 pp.

Bean, B. R., Thayer, G. D., and Cahoon, B. A.: "Methods of Predicting the Atmospheric Bending of Radio Rays," J. Res. NBS, Vol. 64D, No. 5, September-October 1960, pp. 487-492.

Bellamy, J. C.: "The Use of Pressure Altitude and Altimeter Corrections in Meteorology," J. Meteorol., Vol. 2, No. 1, March 1945, pp. 1-79.

Berry, F. A., Bollay, E., and Beers, N. F.: Handbook of Meteorology, McGraw-Hill Book Company, Inc., New York, 1945, pp. 604-621.

Campen, C. F. and Cole, A. E.: "Tropospheric Variations of Refractive Index at Microwave Frequencies," AF Surv. Geophys. No. 79, October 1955, 76 pp.

[Cowan, L. W.]: "Computing the Index of Refraction of the Atmosphere," Tech. Paper No. 1, 3d Weather Group (now 4th Weather Wing), Ent AFB Colorado, May 1952, 17 pp.

Cowan, L. W.: "Forecasting Refractive Index Profiles in the Atmosphere," Tech. Paper No. 2, 3d Weather Group (now 4th Weather Wint), Ent AFB Colorado, September 1953, 80 pp.

Cowan, L. W.: "Interpreting Refractive Index Profiles in Terms of Radar Coverage," Tech. Paper No. 3, 3d Weather Group (now 4th Weather Wing), Ent AFB Colorado, October 1953, 99 pp.

Cramond, W. R., Leeman, J. E., and Thorn, D. C.: "Radar Elevation Angle Errors and Refraction Corrections," Tech. Rept. EE-79 under Contract DA-29-040-ORD-1238, Engineering Experiment Station, University of New Mexico for White Sands Missile Range, September 1962, 46 pp.

Cunningham, R. M.: "Cumulus Climatology and Refractive Index Cloud Refractive Index Studies, II," Geophys. Res. Papers No. 51, January 1962, 109 pp.

Cunningham, R. M., Plank, V. G., and Campen, C. F.: "Cloud Refractive Index Studies," Geophys. Res. Papers No. 51, October 1956, 106 pp.

Fannin, B. M.: "A Review and Evaluation of the Radar Propagation Error Problem," Rept. No. 7-03 under Contract DA-23-072-ORD-763, Electrical Engineering Research Laboratory, University of Texas, 15 November 1954.

Fannin, B. M. and Jehn, K. H.: "A Study of Radar Elevation-Angle Error Due to Atmospheric Refraction," Trans. IRE, Vol. AP-5, No. 1, January 1957, pp. 71-77.

Freeman, J. J.: "Range-Error Compensation for a Troposphere with Exponentially Varying Refractivity," J. Res. NBS, Vol. 66D, No. 6, November-December 1962, pp. 695-697.

Freeman, J. J.: "Real-Time Compensation for Tropospheric Radio Refractive Effects on Range Measurements," NASA CR-109, October 1964, 18 pp.

Gerson, N. C.: "Variations in the Index of Refraction of the Atmosphere," Geofis. Pura Appl., Vol. 13, Nos. 3-4, September-October 1948, pp. 88-101.

Gilmer, R. O., Cramond, W. R., and Byrd, M. R.: "Survey of Papers on Tropospheric Refraction," Tech. Rept. EE-86 under Contract DA-29-040-ORD-1238, Engineering Experiment Station, University of New Mexico for White Sands Missile Range, February 1963, 116 pp.

[Gordon, W. E. et al.]: "Investigation of Air-to-Air and Air-to-Ground Experimental Data," Final Report, Part III, to Contract AF 33(038)-1091, School of Electrical Engineering, Cornell University, Ithaca, New York, 10 December 1951, 182 pp.

[Gordon, W. E. et al.]: "Summary Report, Air-to-Air and Air-to-Ground Electromagnetic Propagation," Final Report, Part II to Contract AF 33(038)-1091, School of Electrical Engineering, Cornell University, Ithaca, New York, 1 June 1951, 109 pp.

Gossard, E. E. and Anderson, L. J.: "The Effect of Superrefractive Layers on 50-5,000 mc. Non-Optical Fields," IRE Trans., PGAP AP-4, April 1956, pp. 175-178.

Holden, D. B., Gossard, E. E., and Hopkins, R. U. F.: "Radio Meteorology and Climatology of the Eastern North Pacific," NEL Rept No. 966, US Navy Electronics Laboratories Research and Development, San Diego, California, 25 April 1960, 24 pp.

[Jones, D. R.]: "Meteorological Refractive Effects Upon Radar Wave Propagation," NAVAER 50-1P-527, Chief of Naval Operations, Washington, D. C., 1 July 1954, 34 pp.

Kroll, C. W.: "A Rigorous Method for Computing Geodetic Distance from SHORAN Observations," Trans. Am. Geophys. Union, Vol. 30, No. 1, February 1949, pp. 1-4.

Landry, P. M. and Parks, L. D.: "Atmospheric Refraction Effects on Tracking System Data," APGC-TDR-63-28, Air Proving Ground Center, Eglin AFB Florida, September 1963, 37 pp.

Martin, C. F. and Carroll, C. L., Jr.: "Tropospheric Refraction Corrections and Their Residual Errors," MTC-TDR-64-3, AF Missile Test Center, Patrick AFB Florida, 15 February 1964, 85 pp.

Martin, F. L. and Wright, F. E.: "Radar-Ray Refraction Associated with Horizontal Variations in the Refractivity," J. Geophys. Res., Vol. 68, No. 7, April 1, 1963, pp. 1861-1869.

Michaelis, J. and Gossard, E.: "Distribution of Refractive Layers Over the North Pacific and Arctic," NEL Rept. No. 841, US Navy Electronics Laboratories Research and Development, San Diego, California, 18 April 1958, 12 pp.

Millman, G. H.: "An Analysis of Tropospheric, Ionospheric and Extra-Terrestrial Effects on VHF and UHF Propagation," Electronics Division, Technical Information Series No. R56EMH31, General Electric, Syracuse, New York, 6 October 1956, 138 pp.

The Mitre Corporation: "Proceedings of the Second Tropospheric Refraction Effects Technical Review Meeting (3 volumes)," ESD-TDR-64-103 under Contract AF 19(628)-2390, March 1964.

Moler, W. F. and Gossard, E. E.: "Atmospheric Refraction Error in Radar Elevation Angles," NEL Rept. No. 795, US Navy Electronics Laboratory, San Diego, California, July 1957, 24 pp.

Moyer, V. E. and Gerhardt, J. R.: "Survey of Microwave Refractive Index Analysis and Forecasting Techniques," Rept. No. 6-18 under Contract AF 19(604)-494, Electrical Engineering Research Laboratory, University of Texas, 25 March 1957, 16 pp.

Naito, K.: "A Method of Forecasting the Refractive Index of the Elevated Layer," Res. Rept. EE-280 under Contract AF 33(616)-3236, School of Electrical Engineering, Cornell University, 30 January 1956.

Nupen, W.: "Checklist of References to Literature on Tropospheric Propagation of UHF, VHF, and SHF Radio Waves (1929-1959)," NBS Rept. 6005, National Bureau of Standards, Boulder, Colorado, July 1959, 53 pp.

Nupen, W. and Thuronyi, G.: "Checklist of References on Tropospheric Propagation of UHF, VHF, and SHF Radio Waves (1918-1957)," NBS Rept. 6001, National Bureau of Standards, Boulder, Colorado, August 26, 1958, 174 pp.

Pappas, C. F., Volger, L. E., and Rice, P. L.: "Graphical Determination of Radio Ray Bending in an Exponential Atmosphere," J. Res. NBS, Vol. 65D, No. 2, March-April 1961, pp. 175-179.

Petterssen, S., Sheppard, P. A., Priestly, C. H. B., and Johannessen, K. R.: "Report on an Investigation of Subsidence in the Free Atmosphere," M.R.P. 207, Air Ministry, Meteorological Research Committee, 29 September 1944. (Also in: Geophys. Publ., Vol. 16, No. 10, 1946.)

Physical Society London and Royal Meteorological Society: Meteorological Factors in Radio-Wave Propagation. Report of a Conference held on 8 April 1946 at the Royal Institution, London, 1947, 325 pp.

Plank, V. G.: "A Meteorological Study of Radar Angels," Geophys. Res. Papers No. 52, July 1956, 117 pp.

Plank, V. G.: "Spurious Echoes on Radar, A Survey," Geophys. Res. Papers No. 62, May 1959, 51 pp.

Rainey, R. J. and Thorn, D. C.: "A Radar Refraction Correction for Symmetric and Nonsymmetric Tropospheric Index Distributions," Tech. Rept. EE-43 under Contract DA-29-040-ORD-1238, Engineering Experiment Station, University of New Mexico for White Sands Missile Range, February 1961.

Sinclair, J. G.: "Temperatures of the Soil and Air in a Desert," Monthly Weather Rev, Vol. 50, No. 3, March 1922, pp. 142-153.

Taylor, P. B. and Engler, N. A.: "Charts of Corrections to Radar Observations for Refraction by Terrestrial Atmospheres," WADC Tech. Rept. 59-619, Aerial Reconnaissance Laboratory, Wright-Patterson AFB Ohio, February 1960, 139 pp.

Thayer, G. D.: "A Formula for Radio Ray Refraction in an Exponential Atmosphere," J. Res. NBS, Vol. 65D, No. 2, March-April 1961, pp. 181-182.

US Navy Weather Research Facility: "Meteorological Aspects of Radio-Radar Propagation," NAVWEPS 50-1P-550, Chief of Naval Operations, Washington, D. C., June 1960.

Wagner, N. K.: "The Effect of Radiosonde Time Lag on Index of Refraction Layer Height, Thickness and Gradient," Rept. No. 6-33 under Contract AF 19(604)-2249, Electrical Engineering Research Laboratory, University of Texas, 10 April 1960, 12 pp.

Wait, J. R.: "Radio Wave Propagation in an Inhomogeneous Atmosphere," NBS Tech. Note No. 24 (formerly NBS Report 6035), Boulder Labs, September 10, 1959, 20 pp.

Wong, M. S.: "Ray-Tracing Picture of Radio-Wave Propagation in Arbitrary Atmosphere," AF Tech. Rept. No. 6631, WADC, Wright-Patterson AFB Ohio, July 1951, 60 pp.

Wong, M. S.: "Refraction Anomalies in Airborne Propagation," Proc. IRE, Vol. 46, No. 9, September 1958, pp. 1628-1638.